FINAL REPORT

TASK I

SOLAR ENERGY THERMIONIC (SET)

PROGRAM

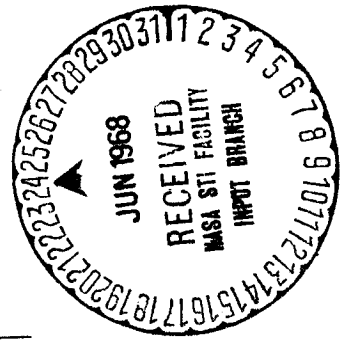

THERMO ELECTRON

ENGINEERING CORPORATION

Contract No. 950671 Report No. TE 4034-73-67

Thermo Electron Corporation, 85 First Avenue, Waltham, Massachusetts 02154

FINAL REPORT

TASK I

SOLAR ENERGY THERMIONIC (SET) PROGRAM

March 1968

by

P. G. Pantazelos
S. Merra
P. Brosens
B. Gunther

Prepared for

Jet Propulsion Laboratory
Pasadena, California

TABLE OF CONTENTS

TABLE OF CONTENTS (continued)

TABLE OF CONTENTS (continued)

CHAPTER 1

INTRODUCTION

Described in this report are the results of a program to develop an improved solar thermionic converter and solar thermionic generator. The work was performed by the Thermo Electron Corporation for the Jet Propulsion Laboratory of the National Aeronautics and Space Administration.

The objectives of this task were the development of a solar thermionic generator incorporating converters with rhenium emitters. The design of the converters was to emphasize power output and mechanical ease of attachment to a generator structure. The generator was to include thermal shielding between the converters and the support structure in order to maximize efficiency. Also, the generator design was to be capable of meeting certain prescribed environmental conditions of shock, vibration, and acceleration.

Both the converter and generator designs were to be logical extensions of prior developments as exemplified by the Series I through VII solar converters and the JG2 generator which had been constructed and tested earlier.

The program consisted of the sequential design, construction and test of three prototype converters. The design of the third prototype was used in the generator. Concurrently, the generator support structure shielding and electron-bombardment heater were designed and constructed. Finally the generator was assembled and tested.

CHAPTER 2

SUMMARY

The first converter prototype, VIII-P-1, employed a pyrolytically deposited rhenium emitter and a molybdenum collector. A method was developed for electron-beam welding the emitter cavity piece to its thin support sleeve. A seal and diode support-flange structure was designed which allowed precise jigging of the diodes during assembly so that they could be installed interchangeably in the generator while maintaining close emitter-to-emitter clearances to minimize heat losses. A support structure was developed to restrain the thin cesium tubulation during vibration and shock, and a new output lead attachment technique was used to ensure a tight joint. Impurities were observed in the pyrolytically deposited rhenium emitter material and in the tantalum substrate, and of five pieces procured only one was used. This converter was tested extensively to establish the optimum collector temperature and thus provide the basis for the radiator design of the next prototype. Collector work function measurements correlated well with prior rhenium-molybdenum data, as did the diode's performance.

The second prototype, VIII-P-2, included a redesigned radiator based on the results of VIII-P-1. Procurement of several pyrolytically deposited emitters failed to produce one of equal quality to that used in the first prototype. The best available was chosen and used in a converter, VIII-P-2b, and concurrently pressure-bonded samples were procured. Emitters manufactured with these appeared cleaner and more uniform, and a converter, VIII-P-2a, was assembled with such an emitter. VIII-P-2a with the pressure-bonded emitter performed significantly better than VIII-P-2b, and this emitter manufacturing technique was

chosen for subsequent converters. Test results of VIII-P-2a reproduced those of VIII-P-1 and confirmed the validity of the radiator design.

The third prototype, VIII-P-3, employed a pressure-bonded emitter. Its radiator was trimmed in size to match the operating condition established in the generator design. The VIII-P-2 series was designed to achieve maximum power output at 0.7 volt and thus required a large heavy radiator to reject the necessary heat. Generator calculations indicated that optimum generator efficiency occurred at a diode voltage of 0.9 volt. Thus the radiator of subsequent diodes was designed to optimize at this point. The cesium reservoir temperature distribution of VIII-P-3 was improved by the addition of a thin radiation shield between the radiator and the reservoir. Its test results were satisfactory, and the design was frozen.

Six converters using the VIII-P-3 design were manufactured without incident. The four with the best performance were used in a generator, and two were kept as spares.

A four-converter generator, JG-3, was designed incorporating thermal shielding between the diodes and the generator block. Thermal shielding tests were conducted with several shielding arrangements, and the best was chosen. A dummy generator, including simulated diodes but otherwise complete, was subjected to a series of environmental tests. The results indicated the need for the addition of thread inserts in the block. The changes were made, and the generator was re-tested successfully. An electron-bombardment gun was also designed, constructed and tested in the dummy generator.

Finally a complete 4-diode generator was assembled and tested. The electron-bombardment gun was found to be very unstable in heating an operating generator. The instability manifested itself in a rapid increase in emission current which the operator could not control, and the generator was severely overheated. Subsequent examination indicated several emitter cavity pieces had tack-welded. The generator was disassembled, and new diodes were inserted. Concurrently, the electron-bombardment gun design was changed from a single filament for all diodes to individual filaments for each diode. Generator testing was resumed and completed without further difficulty.

CHAPTER 3

PROTOTYPE VIII-P-1

3.1 DESIGN

3.1.1 Introduction

Diode VIII-P-1 was the first of three prototype iterations in the development of a rhenium diode for use in an improved solar-powered thermionic generator. In the design of the diode, power output and mechanical ease of attachment to a generator structure were emphasized. Furthermore, additional support was provided for the cesium reservoir tubulation, radiator, and collector of the diode to improve its resistance to shock and vibration.

Research results prior to the program's initiation indicated that better performance could be obtained by using rhenium rather than tantalum as the emitter material. To take advantage of rhenium as an emitter material, it was necessary to redesign the previous series of SET diodes. The principal differences between the SET VIII and the redesigned SET VIII type are summarized in Table 3-1.

TABLE 3-1

COMPARISON BETWEEN SET VII and VIII CONVERTERS

	SET VII	SET VIII
Emitter	Ta	Re
Collector	Ta	Mo
Emitter Sleeve	One Piece	Two Pieces
Support Flange	One Piece	Two Pieces
Cs Reservoir Support	No	Yes
Radiator Support	No	Yes

Because the techniques for attaching a monolithic rhenium emitter to the tantalum emitter support were not available at the start of this program, thin rhenium sheet was attached to a tantalum substrate which was then welded to a tantalum support sleeve. Thus the emitter-sleeve structure became three pieces rather than one.

To position the emitter head within a generator cavity, it was also necessary to make the support flange of two pieces separated by a slip joint. This joint eliminates cumulative errors in machining and brazing. New jigging and fixtures were required to implement this change.

Finally the radiator surface area was increased over the SET VII design to accommodate a larger heat flux, and the radiator and cesium reservoir were strengthened by the addition of bolts and rods.

3.1.2 Emitter Structure

The first method chosen for incorporating a rhenium emitter in the SET-type diode was to deposit rhenium pyrolytically on a tantalum substrate and then electron-beam weld the tantalum substrate to the thin tantalum support sleeve. Figure 3.1, a layout drawing of the diode VIII-P-1, shows the rhenium emitter, the tantalum substrate (which also acts as one generator cavity piece) and the support sleeve.

The design of the emitter structure was severely constrained in two ways. The mass of the emitter should be as small as possible to minimize creep in the sleeve at operating temperatures, and the weld should protrude as little as possible beyond the envelope defined by the diameter of the cavity piece and the sleeve. A protruding weld was undesirable because thermal shielding around the hot emitter sleeve

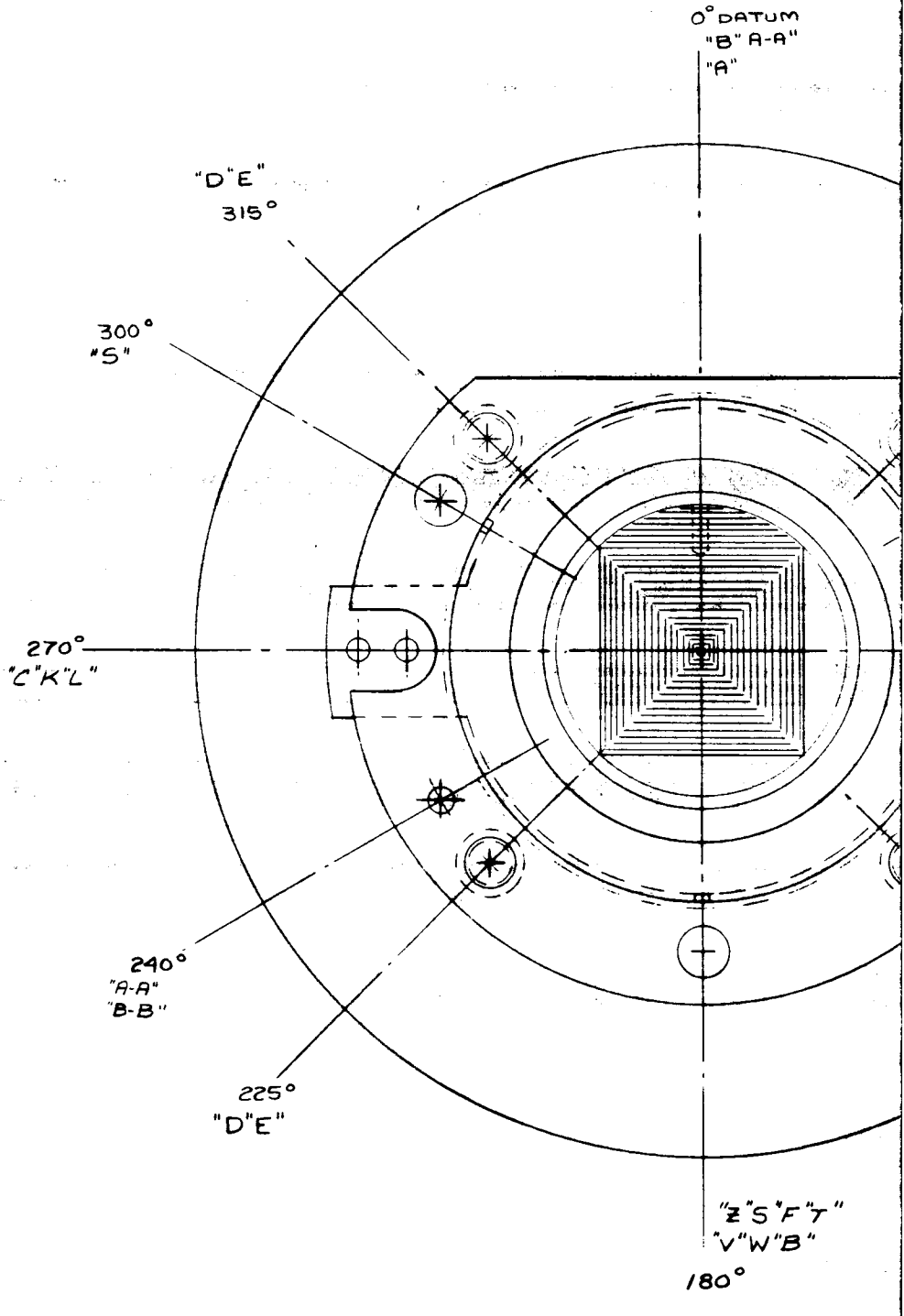

FOLDOUT FRAME 1

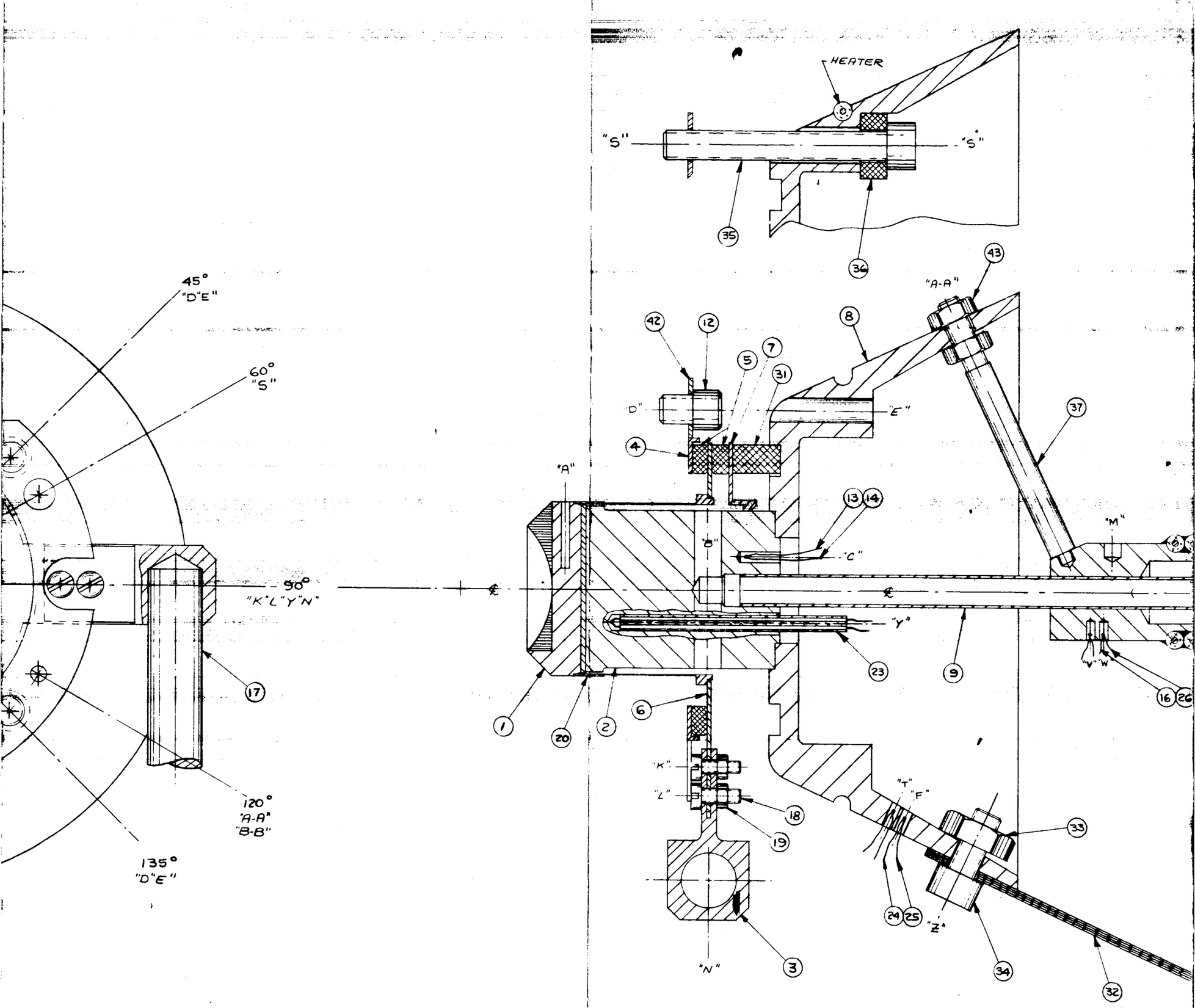

FOLDOUT FRAME 2

FOLDOUT FRAME 3

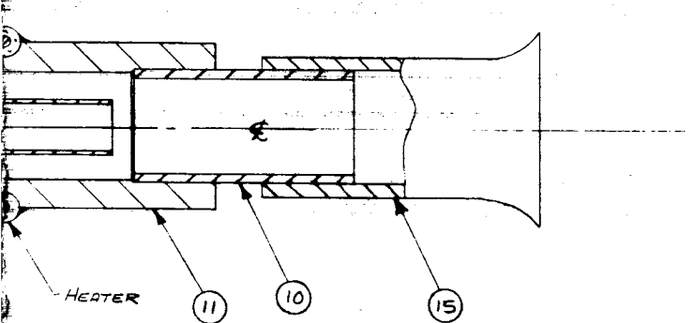

"R"

43	ND		6	SS	#2-56 HEX NUT
42	C		1		
41					
40					
39					
38					
37	B		3		
36	A			Al_2O_3	
35	ND			S.S.	#4-40 x .840 LG S.H.C.S.
34	ND		1	S.S.	#4-40 HEX NUT
33	ND		1	S.S.	#4-40 x .25 LG S.H.C.S.
32	B		4	Cu	
31	B		1	Al_2O_3	
30					
29					
28					
27					
26	ND		AS REQ'D	Chromel	
25	ND			Alumel	
24	ND			Chromel	
23	ND		1	Al_2O_3	
22					
21					
20	C		1	Ta	
19	B		2	Ti	#CC-96 NUT
18	B		2	Ti	#CC-96 x .25 LG
17	ND		1	Cu	#4-(.2043) DIA WIRE
16	ND		AS REQ'D	Alumel	
15	C		1	Cu	
14	ND		1	ALUMEL	
13	ND		1	CHROMEL	
12	A		4	S.S.	#4-40 x 125 LG (TOO.F.ED)
11	C/C		1	Ni	
10	C		1	Ni	
9	C		1	Ni	
8	D		1	Cu	
7	C		1	Nb	
6	C		1	Nb	
5	B		2	Al_2O_3	
4	B		1	ND	
3	C		1	ND	
2	C		1	Mo	
1	C		1	Ta	

PART	SIZE	REV	REQ	MAT'L	NOTES

THERMO ELECTRON

DRAWN	CHECKED	ENGINEER	
MN			

TITLE: VIII-P-1 LAYOUT

SIZE	DRAWING NUMBER	SHEET	REV
H	479-1000	1	B

FOLDOUT FRAME 4

FIGURE 3.1

was planned, and it should be as close to the cavity piece and to the sleeve as possible to minimize radiation losses to the generator block.

In general, a weld between a thin and a thick section is difficult to perform successfully. The heat transferred away from the weld area under these conditions is much higher for the thick section, and it becomes difficult to melt the thick section in the weld area without distortion. This problem is usually overcome by machining a lip in the thicker piece, which in turn is welded to the thin section. The lip then reduces the heat flow. The use of such a lip, however, would require at least 35 mils additional material, and thus would increase the thickness of the cavity piece. Experimental butt welds were made, therefore, on several test pieces, and by very careful control of the fit between the cavity piece and the sleeve, leak-tight, distortion-free welds were achieved. Figure 3.2 shows an assembly after welding, and Figure 3.3 shows the weld being performed.

After the technique for making the weld had been perfected, a sample assembly was subjected to temperature cycling to test its strength. The welded sample was heated in three minutes by electron-bombardment to 1650°C, as observed on the surface of the cavity piece. Then heating was terminated and the sample cooled for three minutes to an estimated temperature of 400° to 450°C, and the power was turned on again. After 35, 70, and 100 cycles the sample assembly was leak-checked and found leak-tight. A visual inspection revealed no damage.

The emitters used at the outset of this program consisted of 20 mils of rhenium pyrolytically deposited from rhenium pentachloride on the flat face of a rod of high-purity tantalum. Initially three emitters

were purchased from an outside vendor. After vapor-depositing the rhenium on the tantalum substrate, grinding and electro-discharge machining were performed by the vendor on the rhenium surface prior to delivery. When the emitters were received at Thermo Electron, no additional surface machining of the rhenium was required. In the following discussions these pieces are identified as No. 1, No. 2, and No. 3.

The overall visual appearance of No. 1 was good. The rhenium exhibited homogeneity, uniformity, and the characteristic color of rhenium. In the No. 2 piece, deep voids approximately 0.001" in diameter were noticeable in the emitter face. These voids were present over a small percentage of the area. In other respects specimen No. 2 was the same as No. 1. The No. 3 piece was similar to No. 1 and No. 2 except that it had fewer apparent voids and had some grinding wheel marks which were not considered serious.

These pieces were then machined into final form so as to mate with emitter spacers. During machining the tantalum was found more difficult to cut than ordinary annealed tantalum. Consequently, hardness readings were taken across the face of the tantalum rod which remained after machining. The material at the center of the rod was found to have the characteristic hardness of annealed tantalum, while the outer edges were approximately four times harder. Photomicrographs similar to that shown in Figure 3.4 were made to investigate this effect, and showed the presence of a second phase not usually found in high-purity tantalum. Hardness measurements and photomicrographs carried out on a control sample of tantalum rod revealed normal hardness values and no precipitate particles. From these results, it was

5205

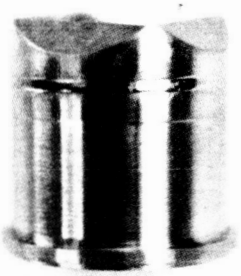

Figure 3.2 Tantalum-Tantalum Beam Weld

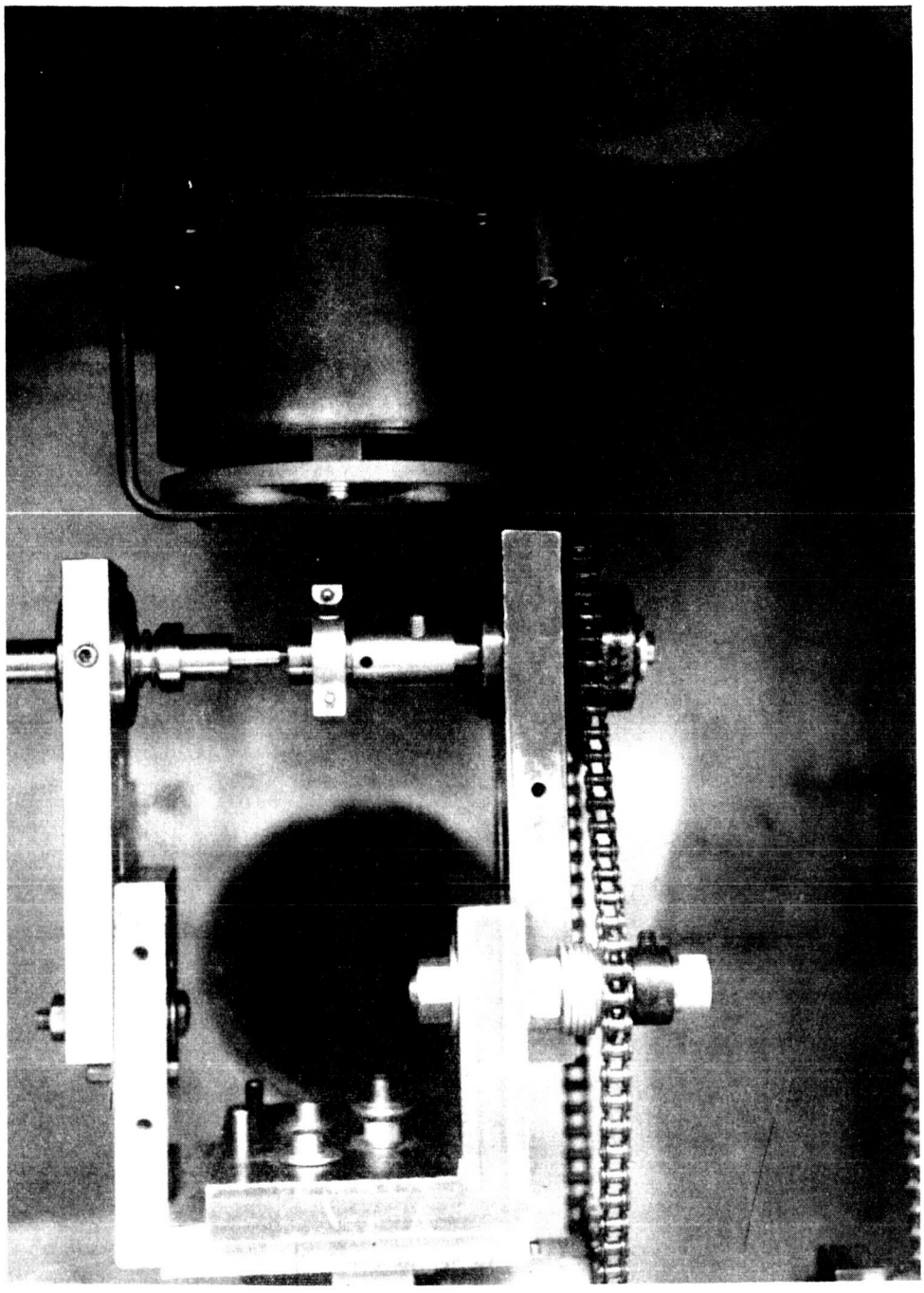

Figure 3.3 Electron Beam Welding of an Emitter to a Sleeve

5210

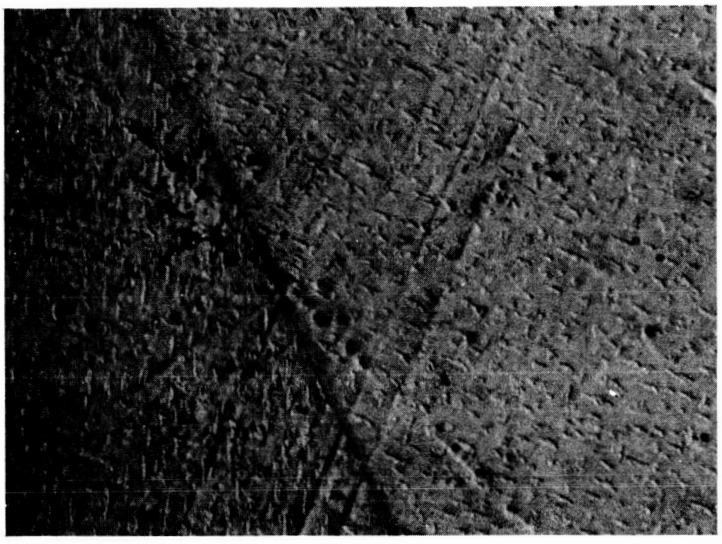

Figure 3.4 Precipitate Particles in Tantalum, Magnified 560X

quite clear that some contaminant was penetrating the tantalum during the pyrolytic deposition process.

The No. 1 emitter was successfully welded to the tantalum spacer. During thermal firing to clean the piece the No. 2 emitter discolored, and upon subsequent firing the rhenium began to separate from the substrate. Emitter No. 3 exhibited non-uniform melting during electron-beam welding to the emitter sleeve, probably due to the same contamination of the tantalum mentioned above.

In an attempt to obtain more satisfactory emitters, two additional pieces, No. 4 and No. 5, were purchased from the same vendor without having been ground or electro-discharge machined. During the first step of electro-discharge machining at Thermo Electron, the rhenium on the No. 5 emitter completely separated from the substrate and visual examination showed no evidence of a bond. The No. 4 piece proceeded through electro-discharge, grinding, and final machining. At the end, it looked clean and adherent. However, after thermal firing small dark spots a few mils in diameter were visible on the surface.

In summary, the yield of emitters was low, and the quality was variable. Emitter No. 1 was deemed the best and was incorporated in diode VIII-P-1.

3.1.3 Collector

Prior data[1] showing the performance of a rhenium emitter to be superior to one of tantalum had been gathered in a thermionic converter incorporating a molybdenum collector. Therefore a molybdenum collector was also chosen here.

Having chosen the collector material, the heat path that this presented was then considered. Because this diode was expected to be operated at lower voltage and higher current than prior series, it was deemed particularly necessary to minimize the temperature drop from the collector to the radiator, thus also minimizing radiator size. During the testing of the first prototype the optimum collector temperature could be determined and the radiator subsequently adjusted in size. The emitter sleeve internal diameter constrains the collector diameter. As can be seen in Figure 3.1, two thermocouples, one near the top and the other at the bottom of the collector structure, were inserted to measure both the collector temperature and the heat flow.

3.1.4 Cesium Reservoir

In previous SET diodes the cesium reservoir had been supported only by the tubulation that connects the reservoir to the collector. The tubulation was made thin to minimize conductive heat flow from the collector, and thus achieve the required low equilibrium temperature in the reservoir in a reasonable length of tubulation. Furthermore, the reservoir was normally constructed similar to an ink bottle to allow operation of the diode in any attitude. It also carried an electrical heater. These added mass to the unsupported end. The reservoir assembly was therefore very susceptible to bending, and consequently steps were taken to add support to the free end of the reservoir.

The principal constraints that limited the types of supports that could be considered were the following:

1. The overall length of the reservoir assembly should not be greatly increased.

2. The reservoir should be able to achieve its proper operating temperature without the use of a heater.

3. The support should present as little shielding as possible to radiation from the inside of the radiator to space and must allow more radiator area to be added if found necessary after testing diode VIII-P-1.

4. The supports should not stress the brazed joint between the collector base and the radiator when the diode is cold, hot or in a transient thermal condition.

5. The support must not unduly complicate the construction of the diode.

The rod-support method shown in Figure 3.1 met the above conditions and was incorporated in the diode. The thermal expansions of the rods, the tubulation, and the radiator were calculated, and the resulting stresses on the parts and the brazes were compared with published strength data and found compatible. The heat flow to the reservoir through the tubulation and through the rods was balanced with the required rejected heat by coating a part of the surface of the reservoir with chrome oxide.

3.1.5 Interelectrode Spacing

The change from a tantalum emitter to a rhenium emitter involved changes in the emitter and seal structure. In this diode, as in previous series, the spacing was achieved by the difference in expansion of the collector compared with that of the emitter, the emitter support sleeve, and the seal structure. When cold, the diode's emitter and collector touch. The spacing at operating temperatures was calculated to be 2.15 mils.

3.1.6 Output Leads

The Series VIII diode was designed to operate at lower voltages and higher currents than earlier series. Therefore, a method of attaching the emitter output lead was designed to provide secure attachment for a large copper lead which in turn could carry heavy currents with small voltage drops.

Another important consideration in the lead design was its ability to accept thermal cycling without becoming loose. Because it was desirable for the emitter lead to be easily removable, brazing or welding was not considered. The method chosen to make this removable connection that was subject to temperature cycling was by choosing materials with the same thermal expansion. Thus stresses in the joints were kept to a minimum. Therefore, the bottom of the emitter spacer was joined to a niobium flange. This flange was designed with tabs to which leads could be attached. A niobium adapter was used to attach to the niobium flange, and this niobium adapter had a copper rod brazed to it, to which was attached the copper output lead. Originally titanium bolts and nuts were used to clamp the two niobium pieces. These were chosen because of availability and because their expansion was similar to that of niobium. Figure 3.5 shows the expansion of niobium and titanium versus temperature.*

To test the joint a niobium piece of the same design as that to be used on the diode was attached to a niobium flange with titanium bolts and nuts. It was cycled two times to 700°C. After the first cycle the niobium clamp had slightly cold-welded to the flange. The nuts were

* Handbook of Thermophysical Properties of Solid Materials, Armour Research Foundation, Pergamon Press (1961).

about a half turn loose. After the nuts were tightened again, the assembly was heated and cooled. The niobium pieces again had slightly cold-welded, but the nuts remained tight. The screws were then easily removed. However, after 20 additional cycles at 700°C, the joint was no longer tight, and the titanium screws and nuts were not easily removed. A lead-attachment scheme using niobium tabs, a niobium adapter, and niobium screws was tested next and did not loosen, nor did the screws bind.

The collector lead of the diode, which was subjected to much smaller temperature differences, had not in the past shown a tendency to loosen. Consequently, in this diode the same attachment scheme was used, namely, a stainless nut and bolt holding the copper lead directly to a clean flat surface on the lower end of the copper radiator.

3.1.7 Diode Mounting in the Generator

The technique for mounting the diode in the generator had to fulfill the following conditions:

1. Hold the diode securely to the generator block.
2. Position the diode accurately in the depth, side-to-side, and angular relationships in order to allow close spacing of adjacent emitters and minimize heat losses between emitters.
3. Allow easy removal and remounting of the diode.
4. Be compatible with a reliable diode seal structure.

Several mounting schemes were considered, and the one shown in Figure 3.1 was chosen for use in diode VIII-P-1. A mounting flange (part 42) was brazed to the top flange (part 4) of the seal. Basically

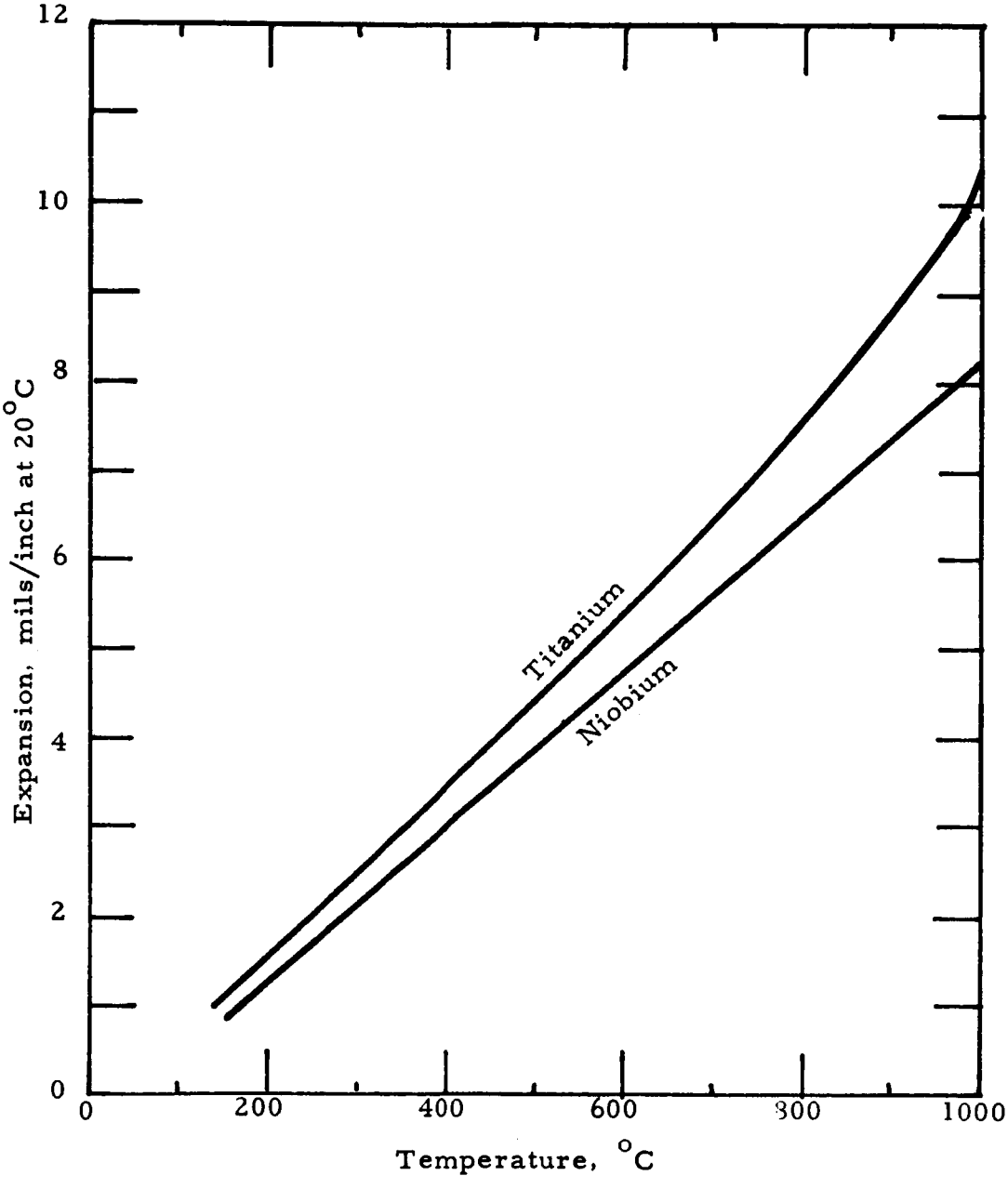

Figure 3.5 Thermal Expansion versus Temperature for Niobium and Titanium

the same seal as used in the earlier Series VII diodes was used here because it had proven to be long-lived and could be constructed with good yield.

The mounting flange, prior to being brazed to the seal, could slide with respect to the seal. The diode emitter assembly could therefore be carefully positioned with respect to the flats on the cavity piece, and the mounting flange could be brazed in such a position as to accurately hold the diode in the generator. Thus the proper depth and angular positions of the diode were established with respect to the mounting flange. Side-by-side positioning was accomplished by carefully jigging the emitter assembly before brazing the top flange (part 4) to the ceramic. With this mounting arrangement any diode could be quickly positioned in a generator and held in place with bolts.

The choice of the bolt material was critical because it was desirable to be able to remove diodes after a generator test. Thermo Electron's past experience indicated that stainless steel bolts did not seize when used in molybdenum. This experience was confirmed when two Series VII diodes, held in molybdenum mounts with stainless steel bolts, were easily removed after more than 3000 hours of operation. Stainless steel was therefore chosen for the mounting bolts.

In addition to positioning the diode in the generator, it was considered desirable to incorporate in the diode some means of securing the heavy parts of the diode directly to the block. Such additional support would aid the diode in withstanding the vibration and shock that it will eventually encounter in a launch vehicle. Again, various schemes of holding the diode were considered. For example, the diode might be held

and positioned from the radiator alone. This method had the advantage of securing the principal mass, but it would result in lower generator efficiency because the emitter cavity pieces could not be accurately positioned. Constraining both the seal and the radiator presented a severe problem in differential expansions. The method finally chosen was to bolt both the seal and the radiator to the block, but the radiator bolts were designed to expand and release their restraint on the radiator as the diode and generator rose in temperature.

3.2 FABRICATION

The final design of diode VIII-P-1 is shown in Figure 3.1. During fabrication of the diode the braze joint between the collector, part 2, and the collector flange, part 7, developed a leak. This necessitated removal of the radiator by machining, remelting of the braze with additional braze material, and the addition of a new cesium reservoir.

Figure 3.6 shows an overall view of VIII-P-1, Figure 3.7 shows a close-up of the emitter portion of the converter, Figure 3.8 shows the top view, and Figure 3.9 shows the rear view. The slip-joint braze of parts 4 and 42 is visible in Figure 3.8 while Figure 3.9 shows the support rod, part 37, from the radiator to the cesium reservoir.

3.3 TESTING

One hundred hours of testing were accumulated on converter VIII-P-1. Also, through normal starting and shut-down procedures, about 40 thermal cycles, consisting of gradual heating and cooling, were performed. Of the total test time, 37 hours were required for static and dynamic testing, 10 hours for work function data, and 53 hours of steady-state operation at 0.7 volt and 54 amperes. There was no evidence of

degradation during testing. During steady-state testing, due to a cesium heater failure, the emitter temperature rose to approximately 2100°C and remained there for ten minutes before shut-down was effected. A rerun of the converter, after heater replacement, showed no apparent damage to the diode or decrease in its performance. The rerun consisted in taking one stabilized static data point.

Because the proper radiator size is critically dependent on the required collector temperature, it was decided to use a size for VIII-P-1 similar to that used in previous SET converters but with external heating and cooling, and to determine experimentally the optimum collector temperature. By using a radiator of this size, an existing water-cooled and electrically heated strap could be used. With knowledge of the required collector temperature, the radiator of the next diode, VIII-P-2, could be designed accordingly. Therefore, all data taken on VIII-P-1 were taken with such a strap attached to the radiator.

During testing of VIII-P-1 all recorded readings of the various thermocouples were made with a room-temperature reference junction, to allow the convenient use of a multi-point recorder in observing the variation of the various measured characteristics. In addition, one thin tantalum radiation shield, supported from a ceramic, was placed around the emitter to minimize bombardment of the seal and to roughly simulate the generator environment.

Three types of testing were performed, namely, the static and dynamic measurement of output current and voltage, and the measurement of collector work function.

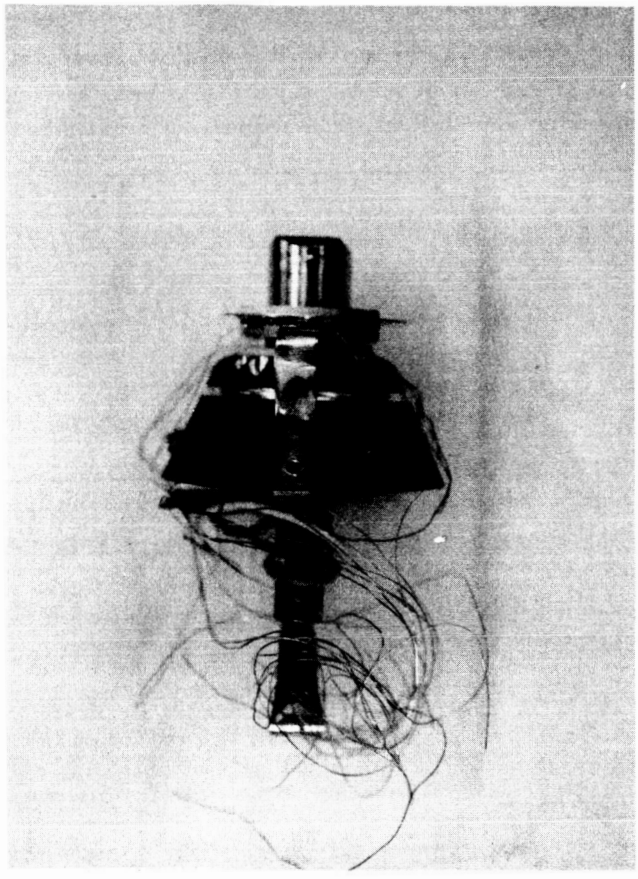

Figure 3.6 Converter VIII-P-1

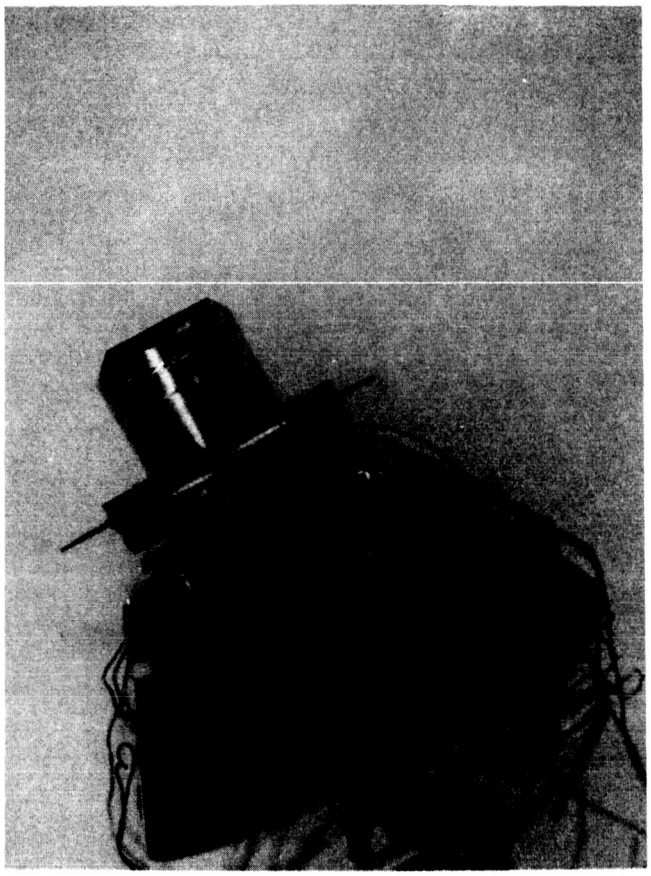

Figure 3.7 Close-Up of Emitter Portion of Converter VIII-P-1

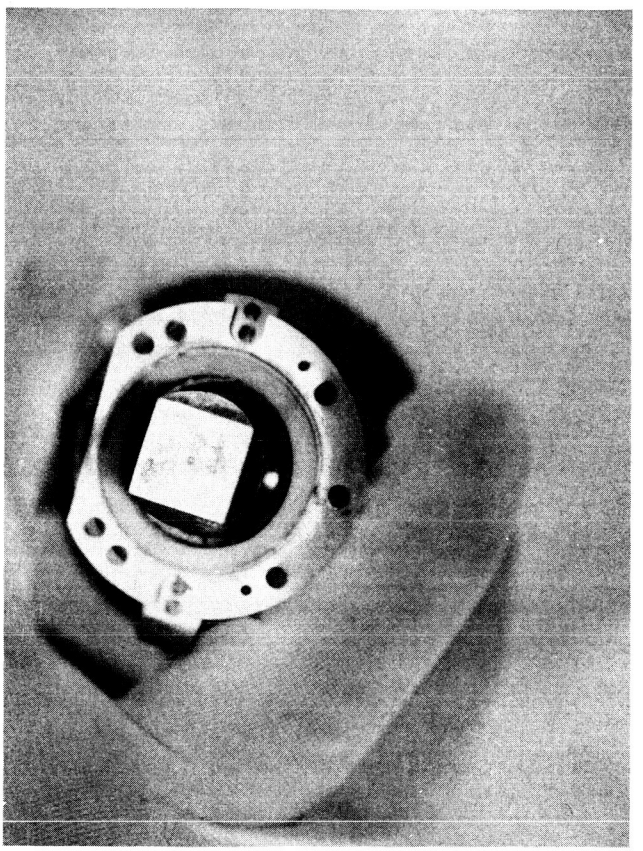

Figure 3.8 Top View of Converter VIII-P-1

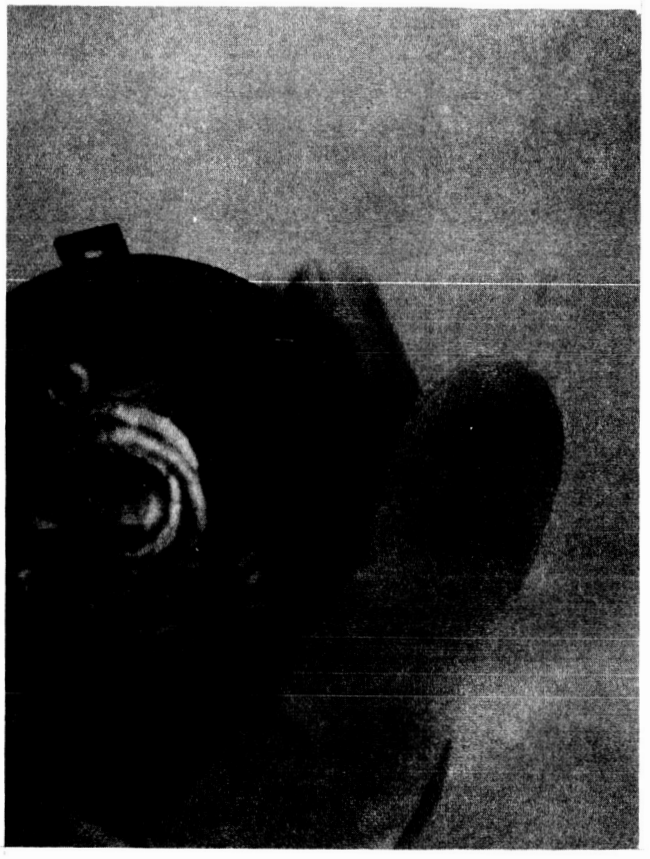

Figure 3.9 Rear View of Converter VIII-P-1

During static testing, which was conducted first, it became evident that the cooling strap attached to the radiator was incapable of cooling the collector sufficiently to allow optimization of the collector temperature in the range of output voltages below 1 volt. More contact surface area between the radiator and the cooling strap was needed. To avoid redesigning the cooling arrangement, static testing was limited to the lowest collector temperature achievable with the existing strap. The bulk of the useful data was obtained by testing dynamically.

In dynamic testing a 60-Hz sine-wave voltage source was placed in series with the diode and the load resistor. The resulting diode current and voltage were observed on an oscilloscope. By sampling these signals at a low frequency (< 1 Hz), the voltage and current were also permanently recorded on an X-Y plotter.

The average current through the diode during dynamic testing was only a fraction of the peak measured currents. This average current, furthermore, was adjustable either by varying the load resistance or by varying the magnitude of the 60-Hz voltage source. Collector heating is strongly dependent on the average diode current, and thus could be varied over a sufficient range to achieve the optimum collector temperature.

Figures 3.10 through 3.14 are dynamic performance data taken at collector temperatures between 569 and 718°C, and Figure 3.15 shows how current density varies with collector temperature at different voltages. Table 3.2 shows the optimum collector temperature at output voltages between 0.6 and 1.0 volt.

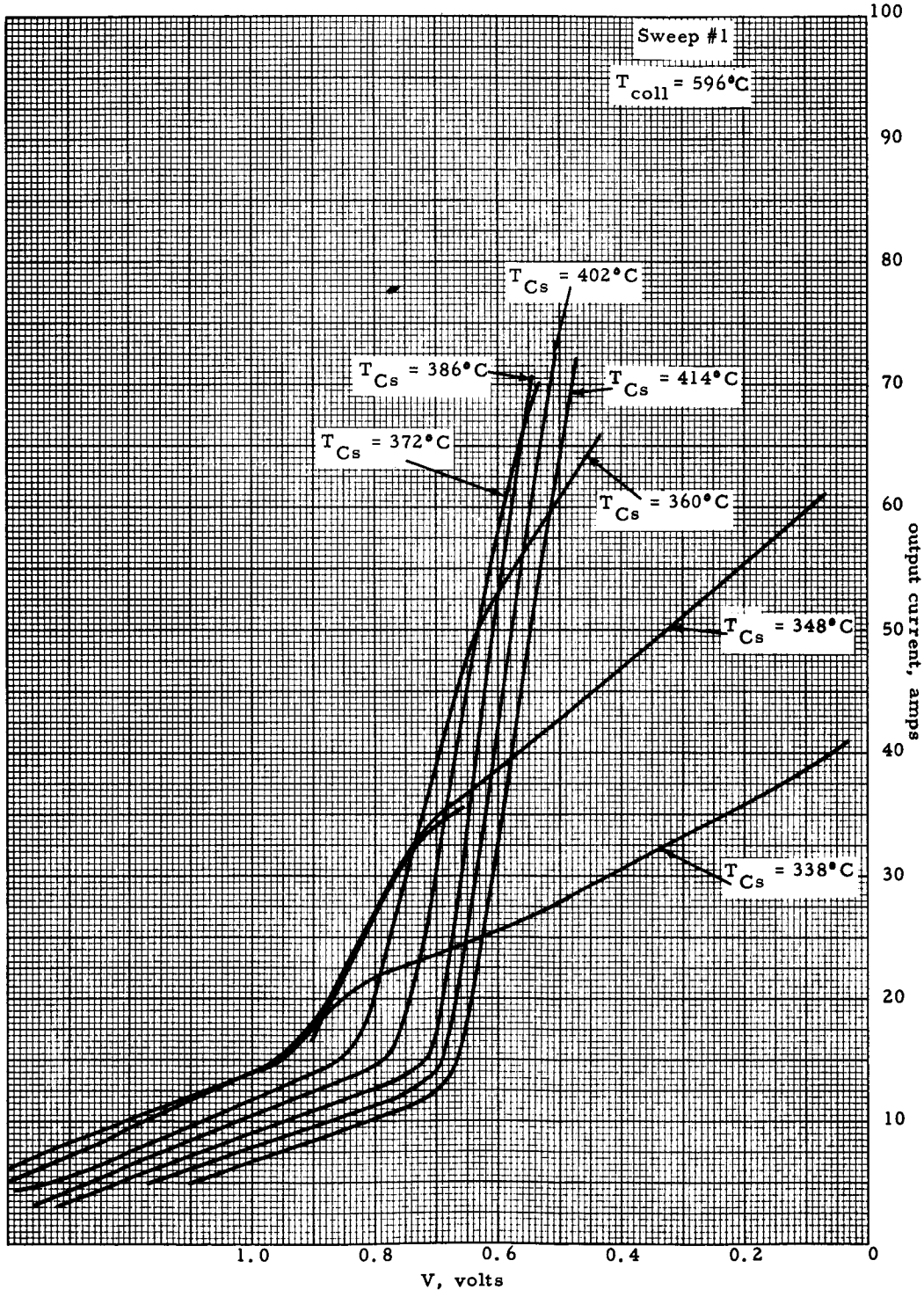

Figure 3.10 Sweep Data at T_E = 1700°C (Obs.) and T_{Coll} = 569°C

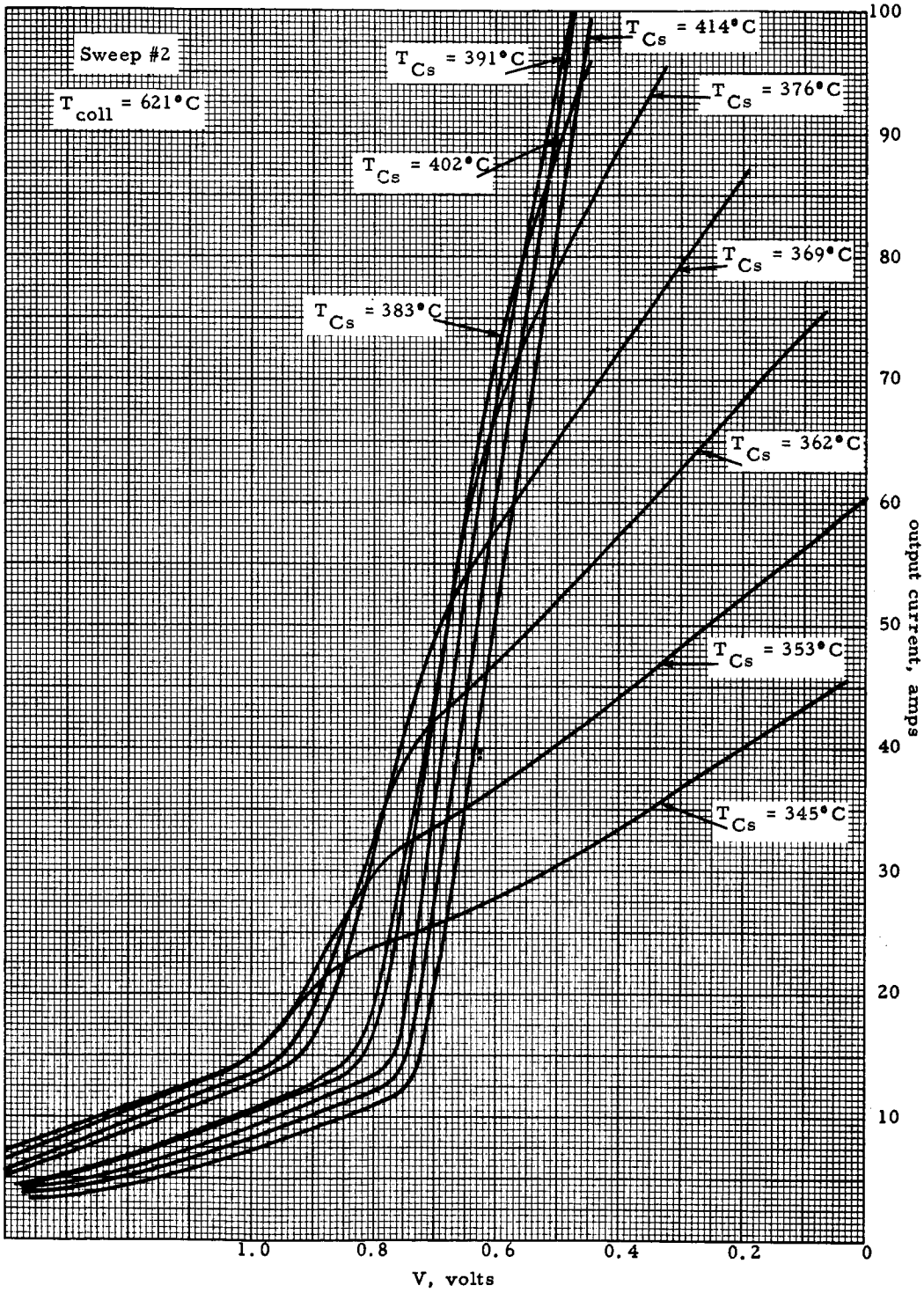

Figure 3.11 Sweep Data at T_E = 1700°C (Obs.) and T_{Coll} = 621°C

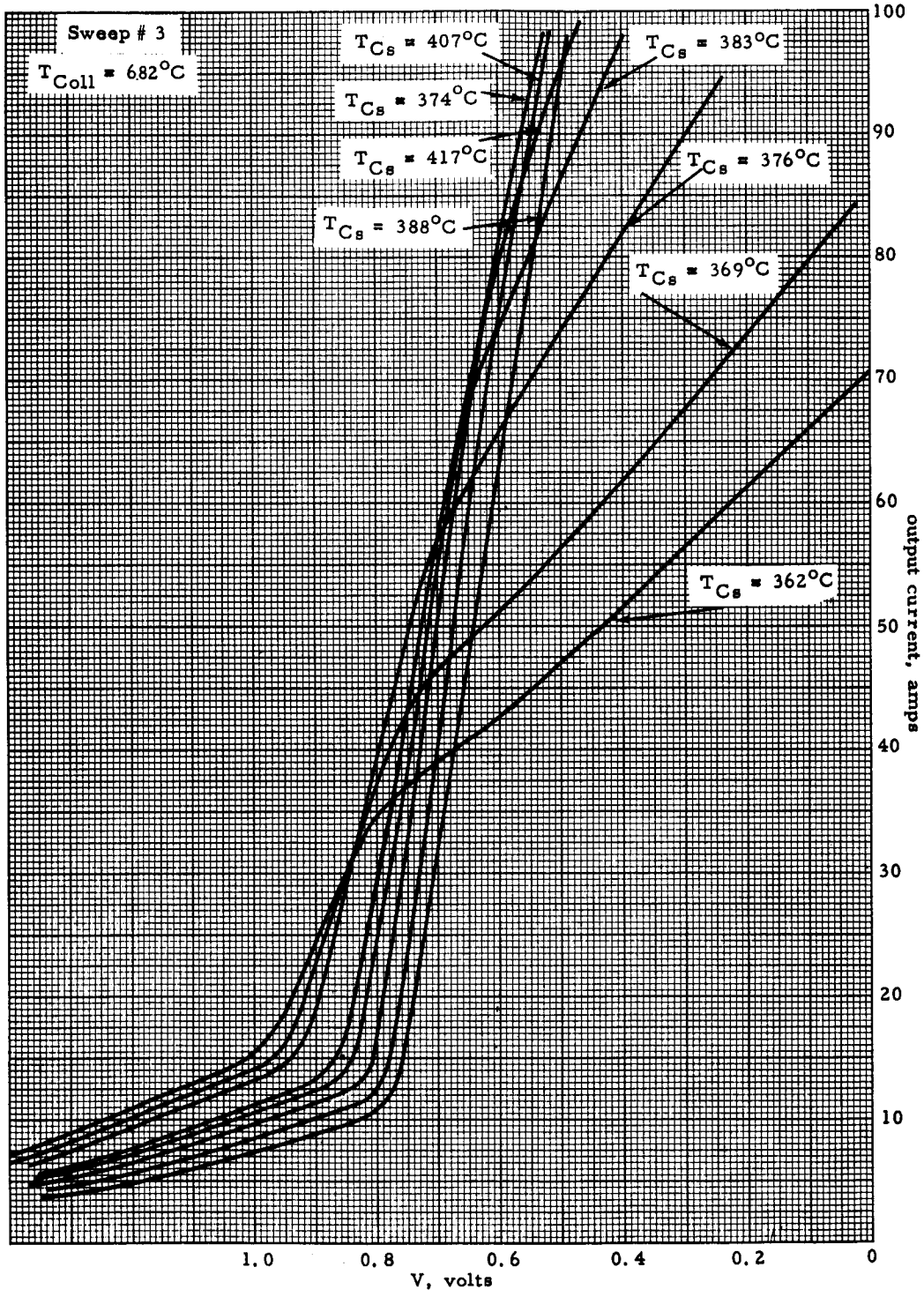

Figure 3.12 Sweep Data at T_E = 1700°C (Obs.) and T_{Coll} = 682°C

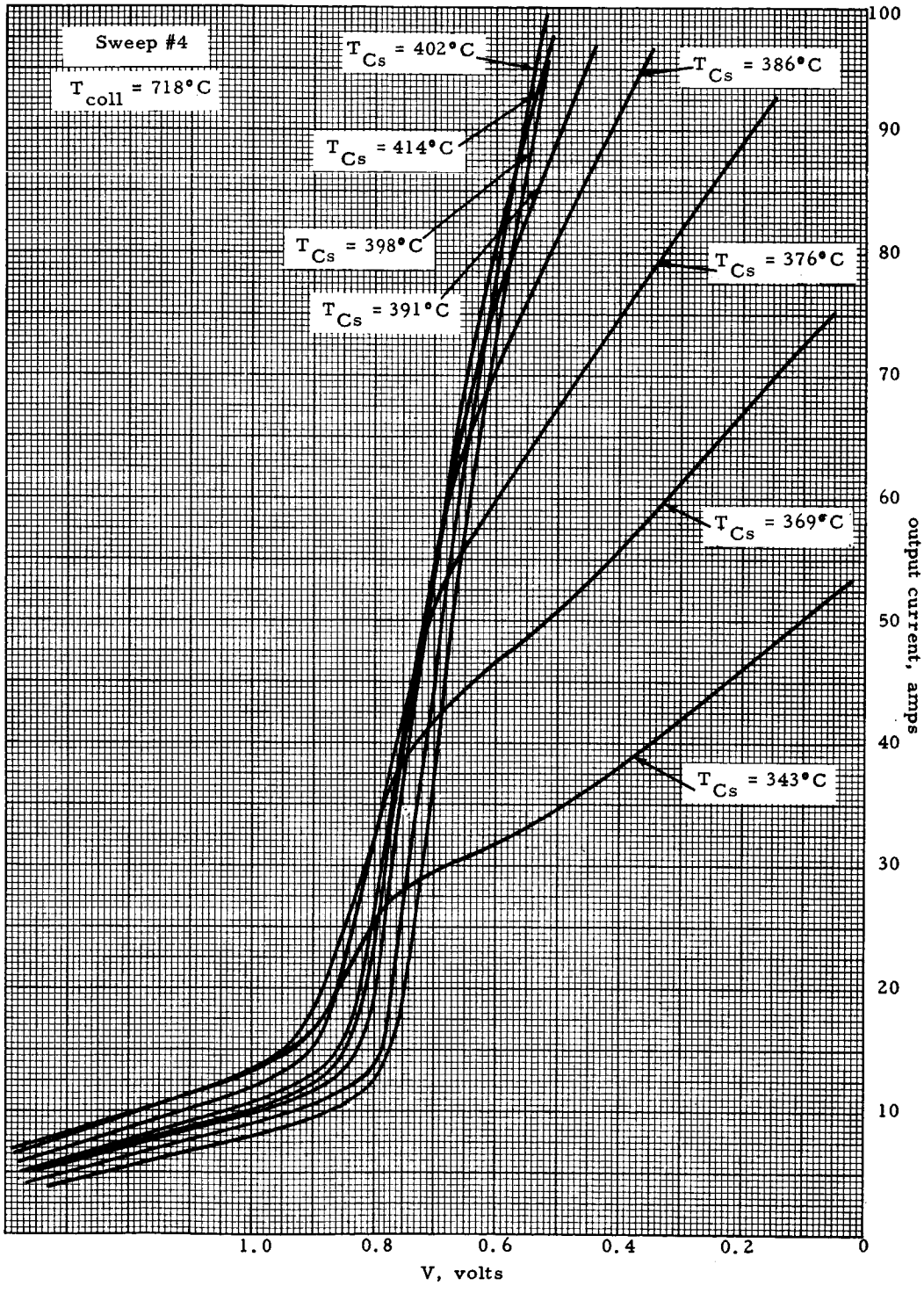

Figure 3.13 Sweep Data at T_E = 1700°C (Obs.) and T_{Coll} = 718°C

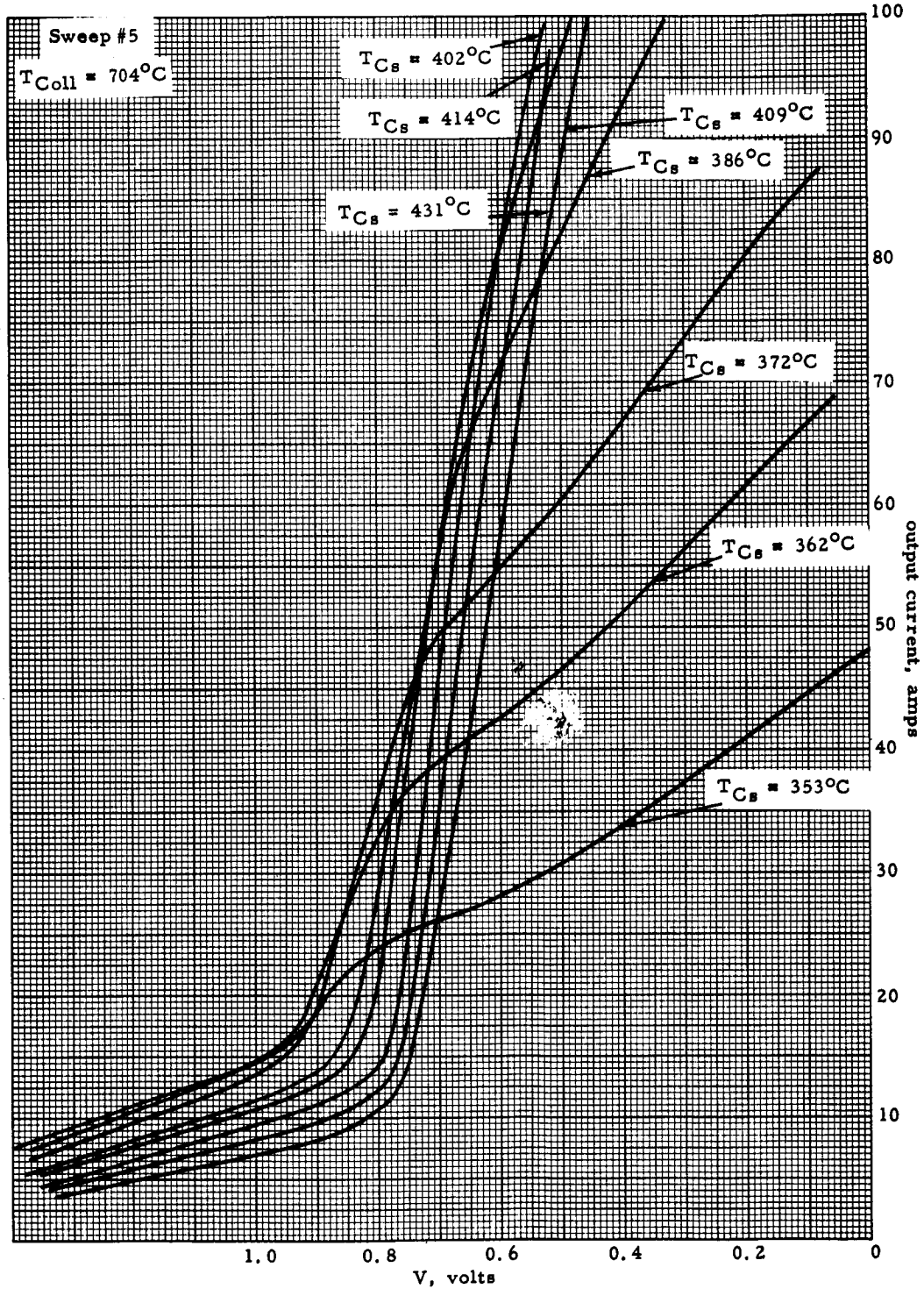

Figure 3.14 Sweep Data at T_E = 1700° C (Obs.) and T_{Coll} = 704° C

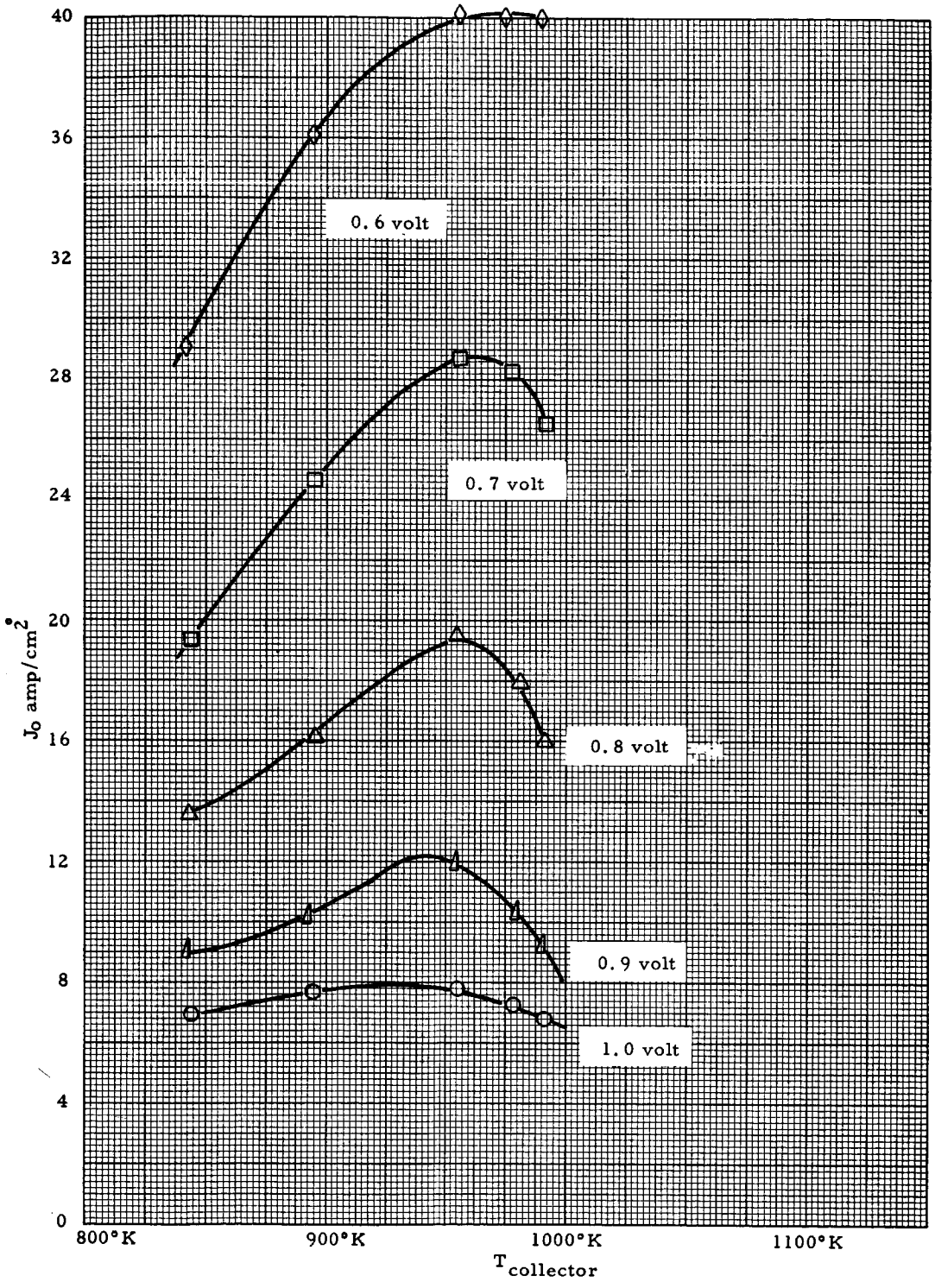

Figure 3.15 Current Density (J_o) versus Collector Temperature at Different Voltages

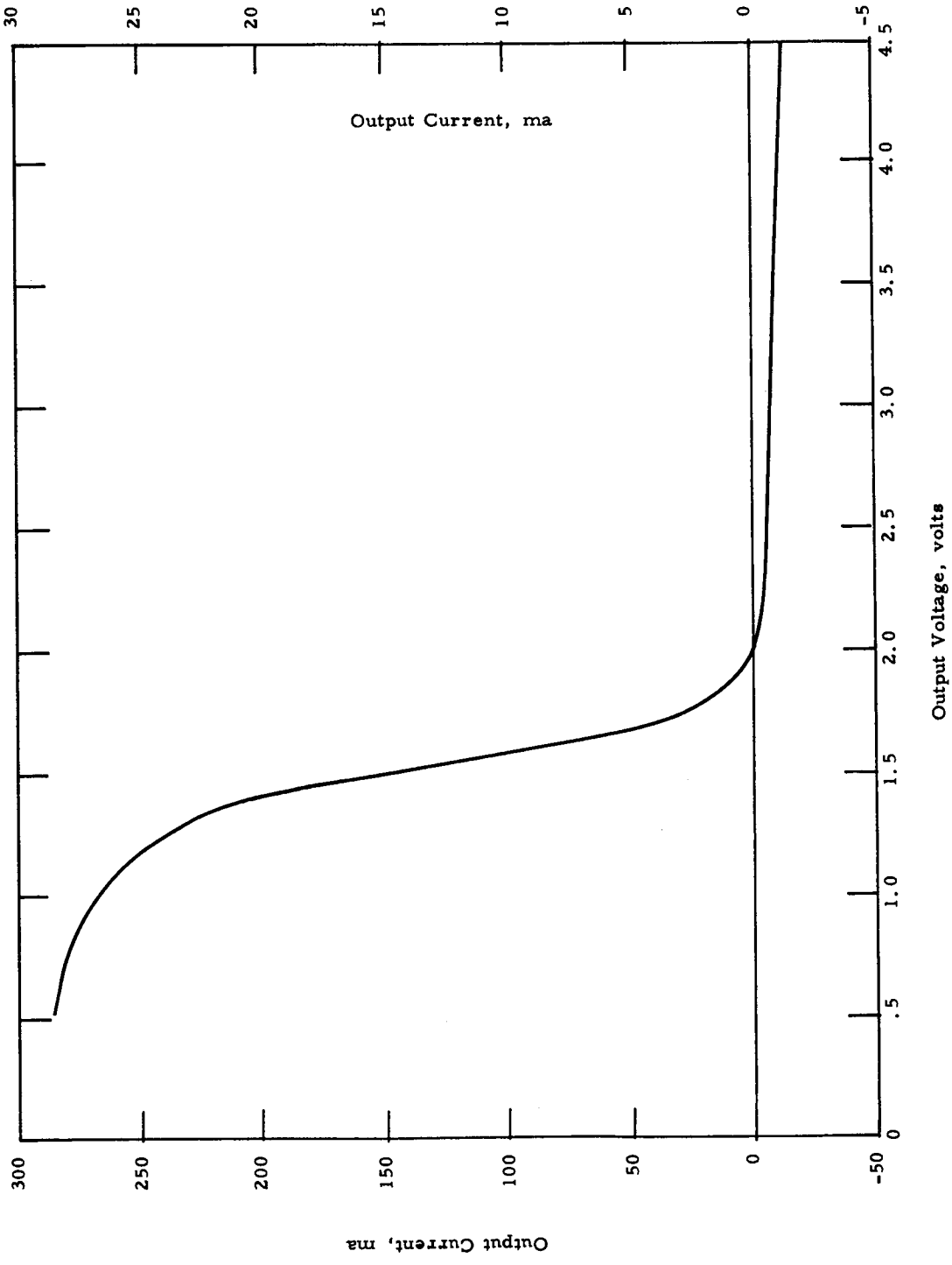

Figure 3.16(a) IV Curve Produced by an X-Y Plotter (Run #2)

VIII-P-1

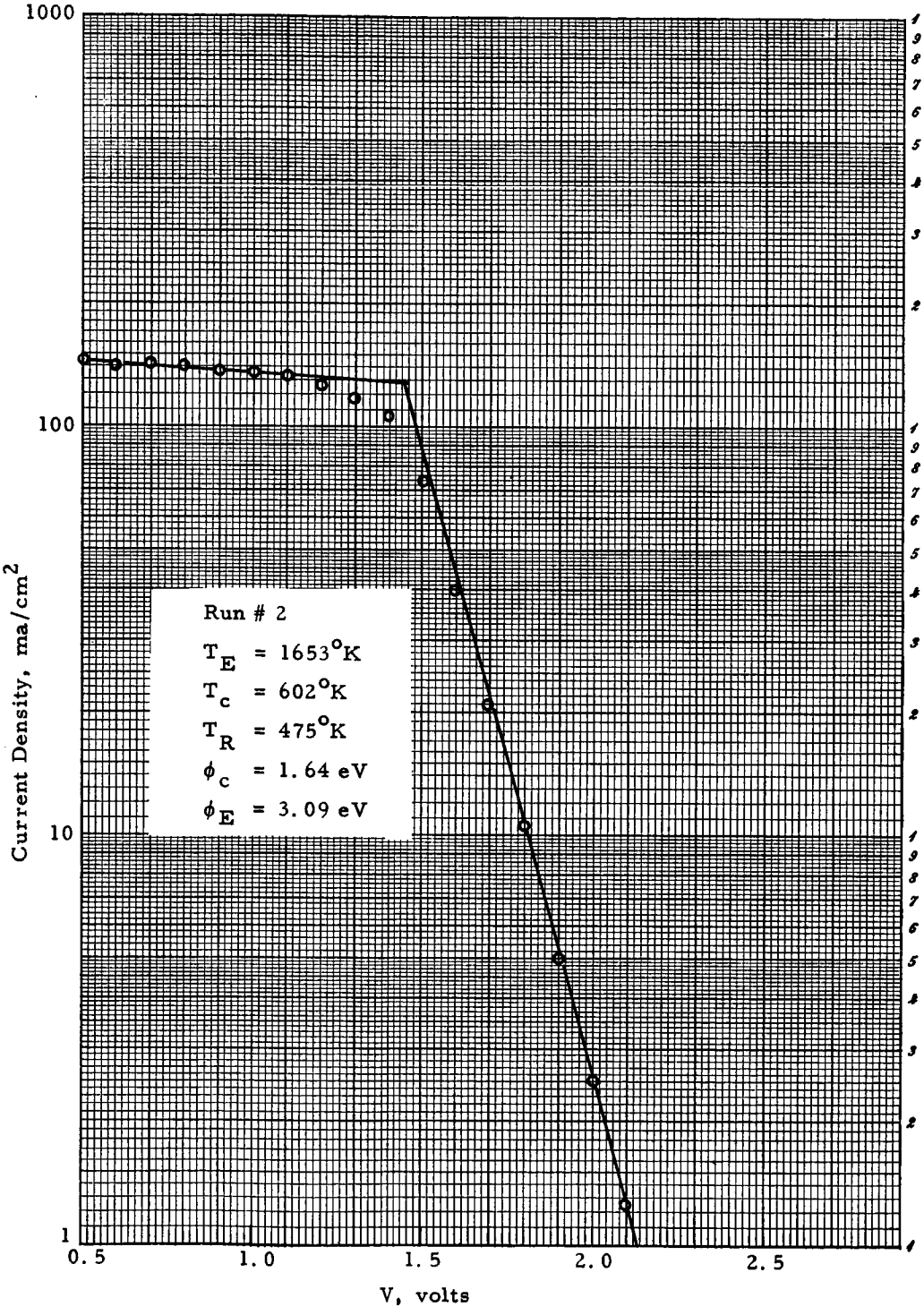

Figure 3.16(b) IV Characteristics (Run #2)

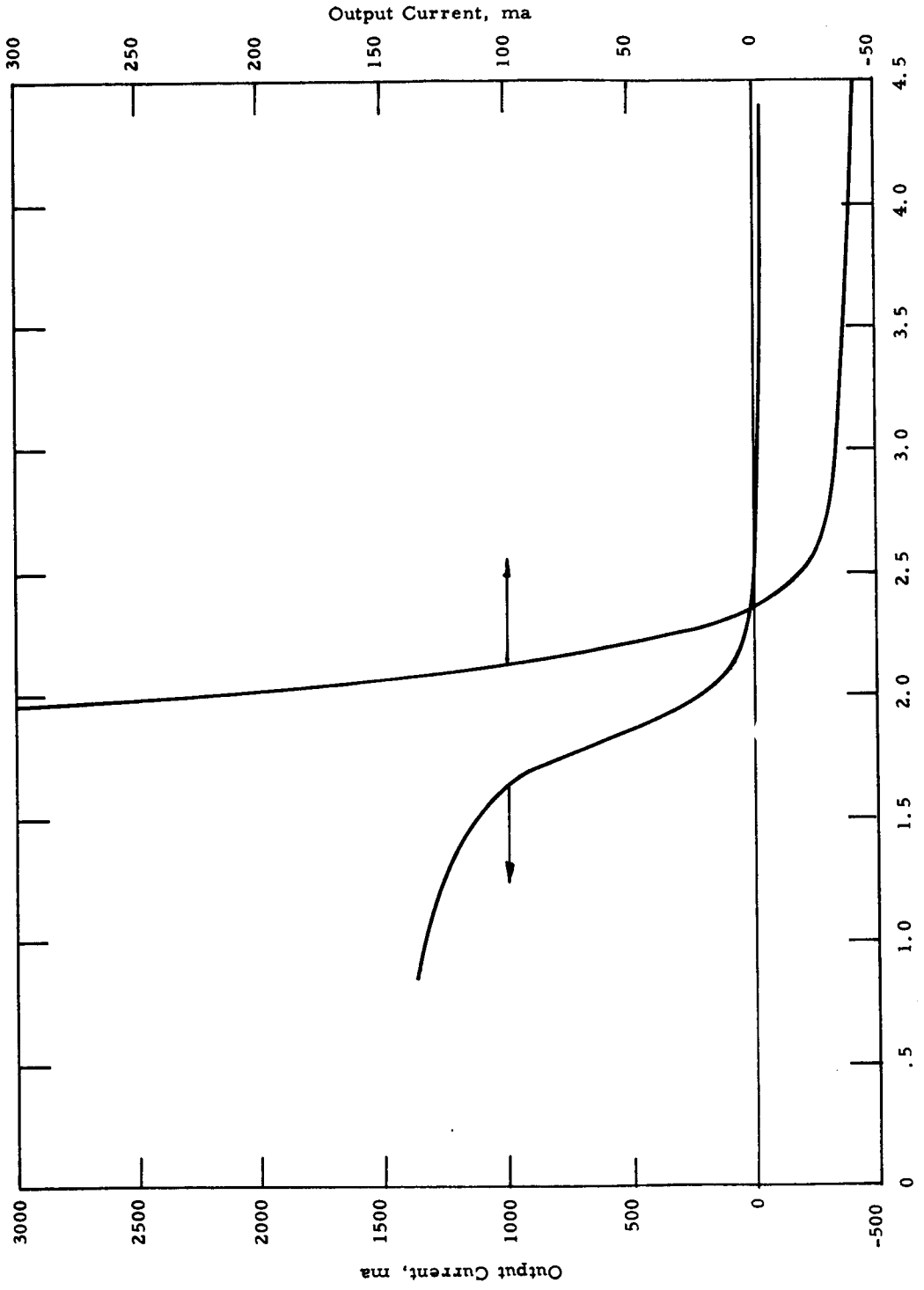

Figure 3.17(a) IV Curve Produced by an X-Y Plotter (Run #3)

VIII-P-1

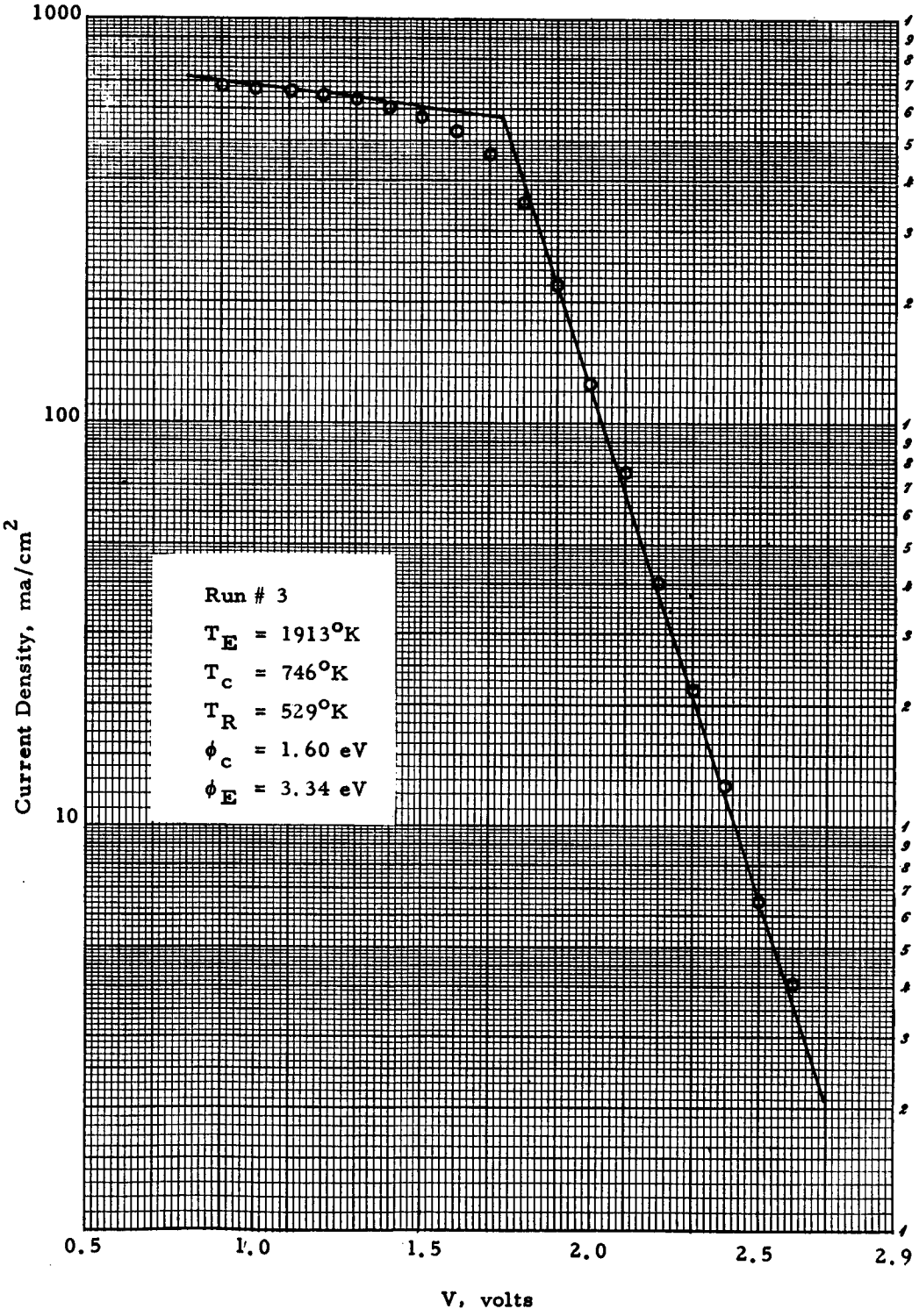

Figure 3.17(b) IV Characteristics (Run #3)

VIII-P-1

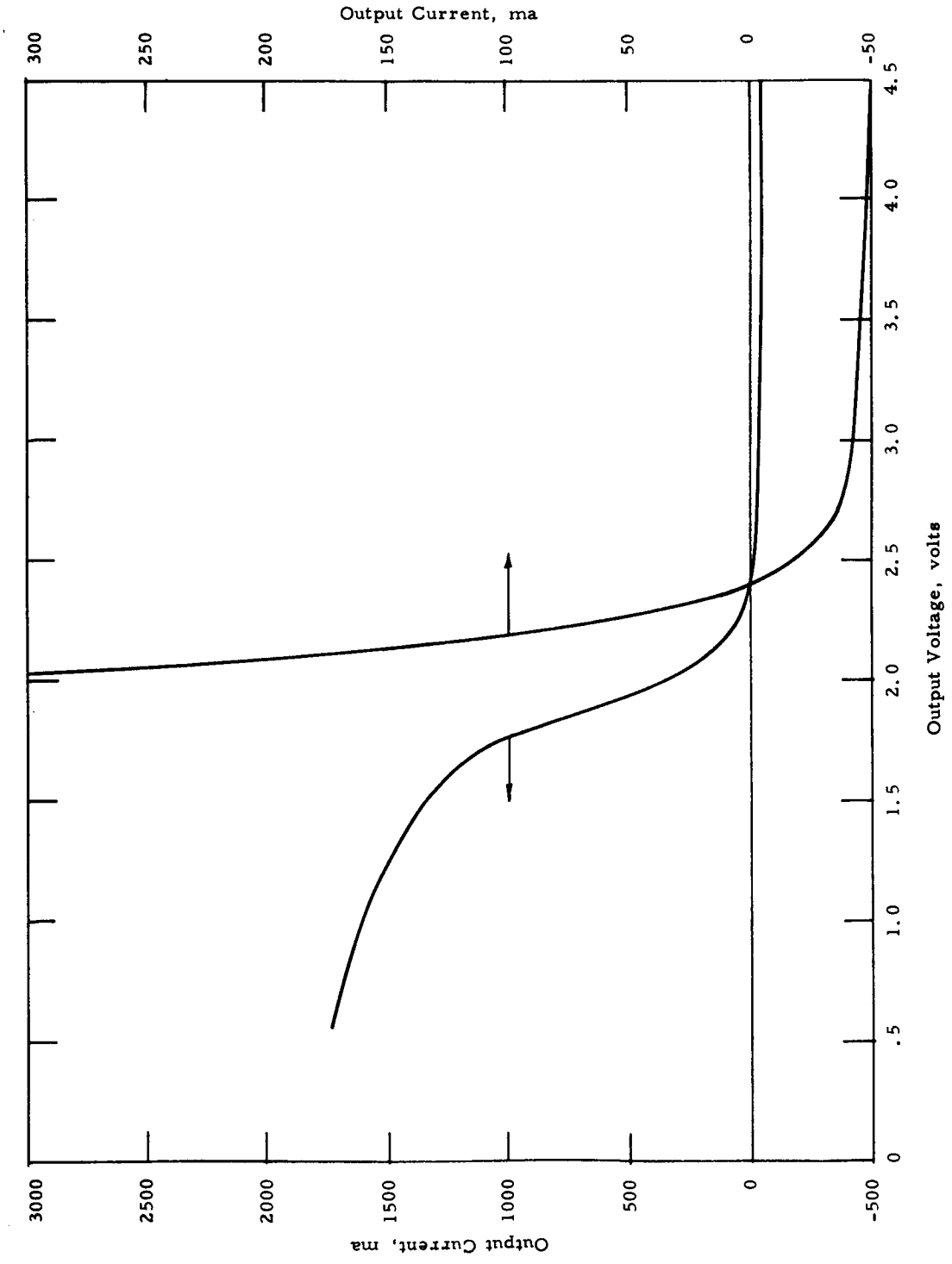

Figure 3.18(a) IV Curve Produced by an X-Y Plotter (run #4)

VIII-P-1

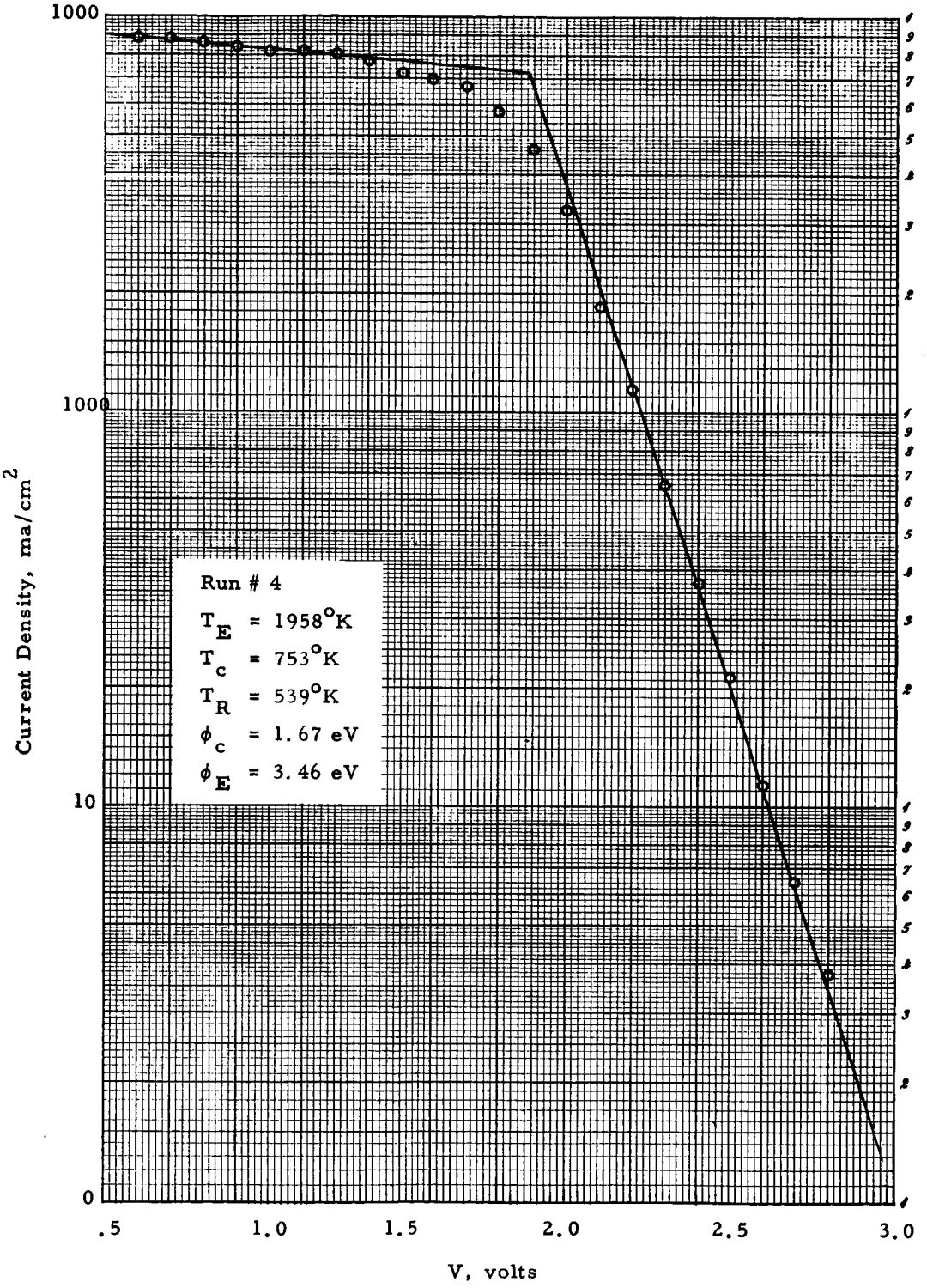

Figure 3.18(b) IV Characteristics (Run #4)

VIII-P-1

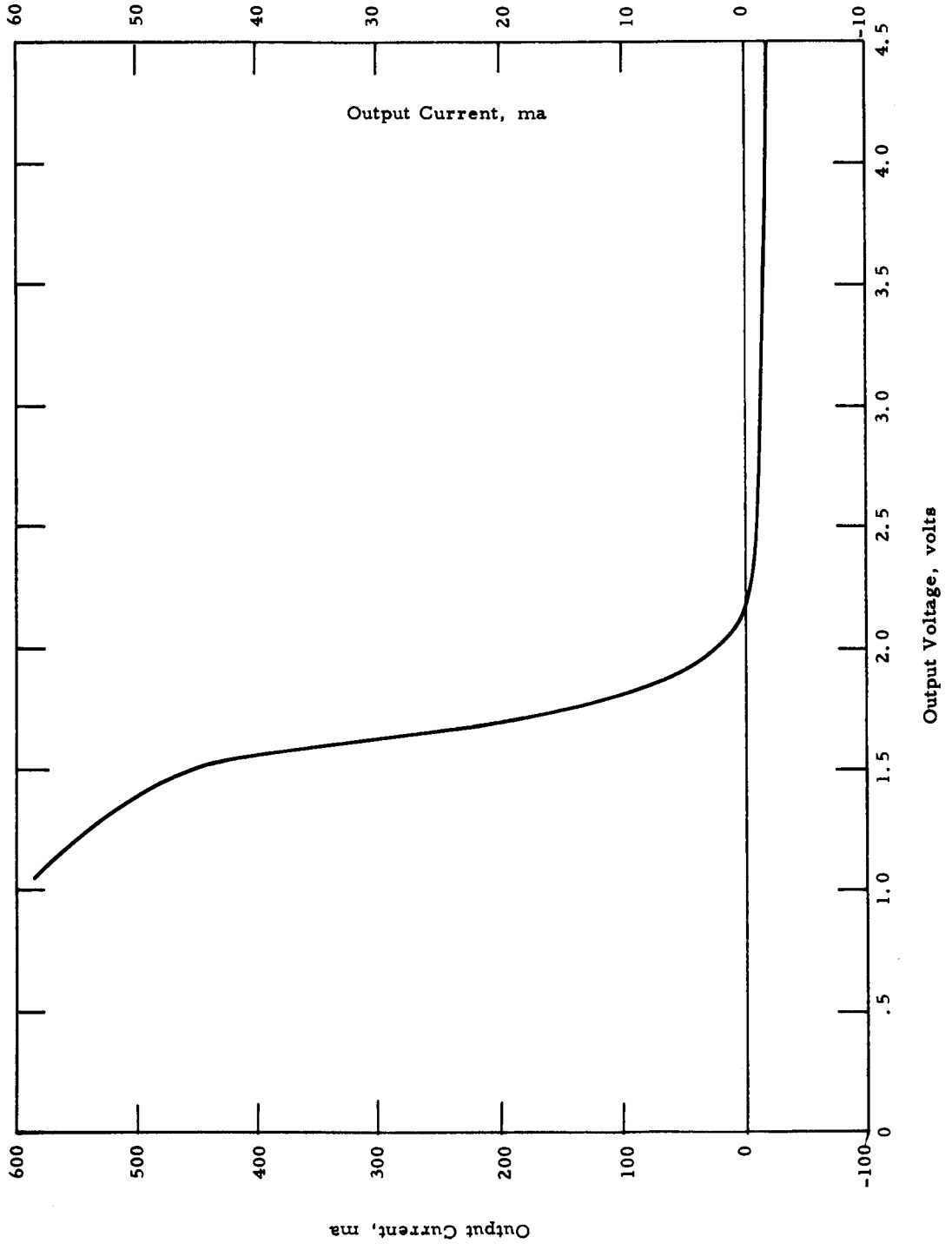

Figure 3.19(a) IV Curve Produced by an X-Y Plotter (Run #5)
VIII-P-1

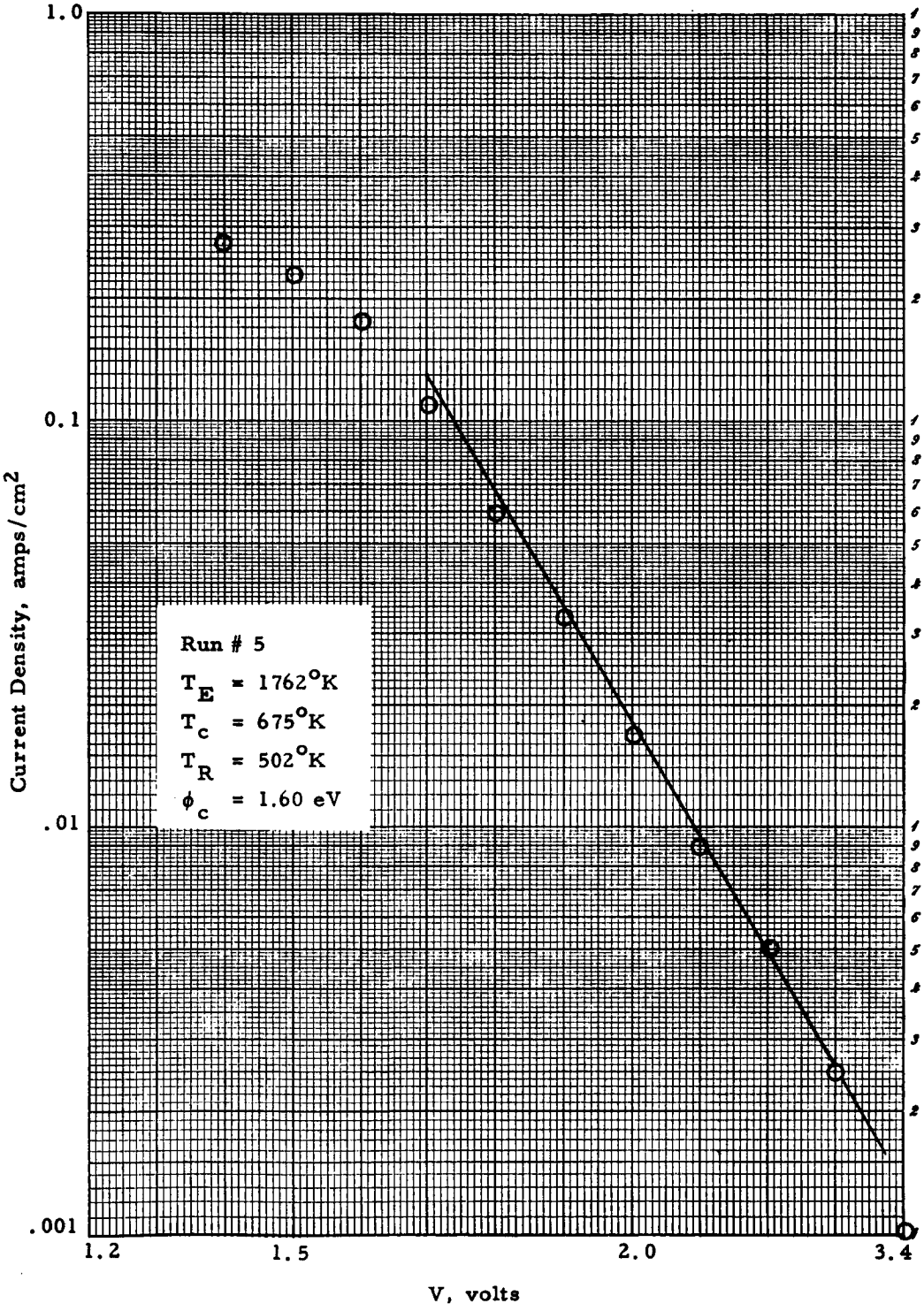

Figure 3.19(b) IV Characteristics (Run #5)

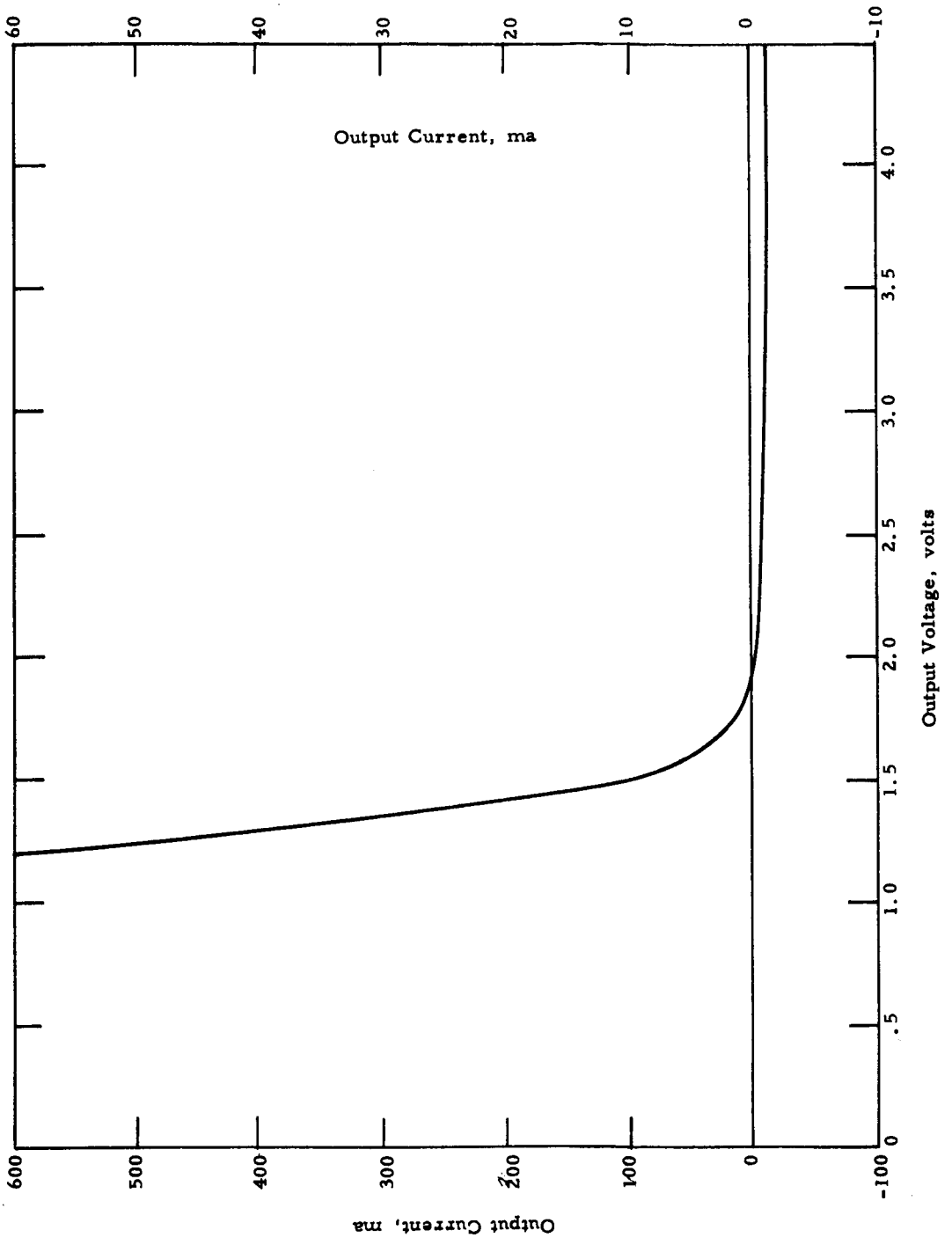

Figure 3.20(a) IV Curve Produced by an X-Y Plotter (Run #6)

VIII-P-1

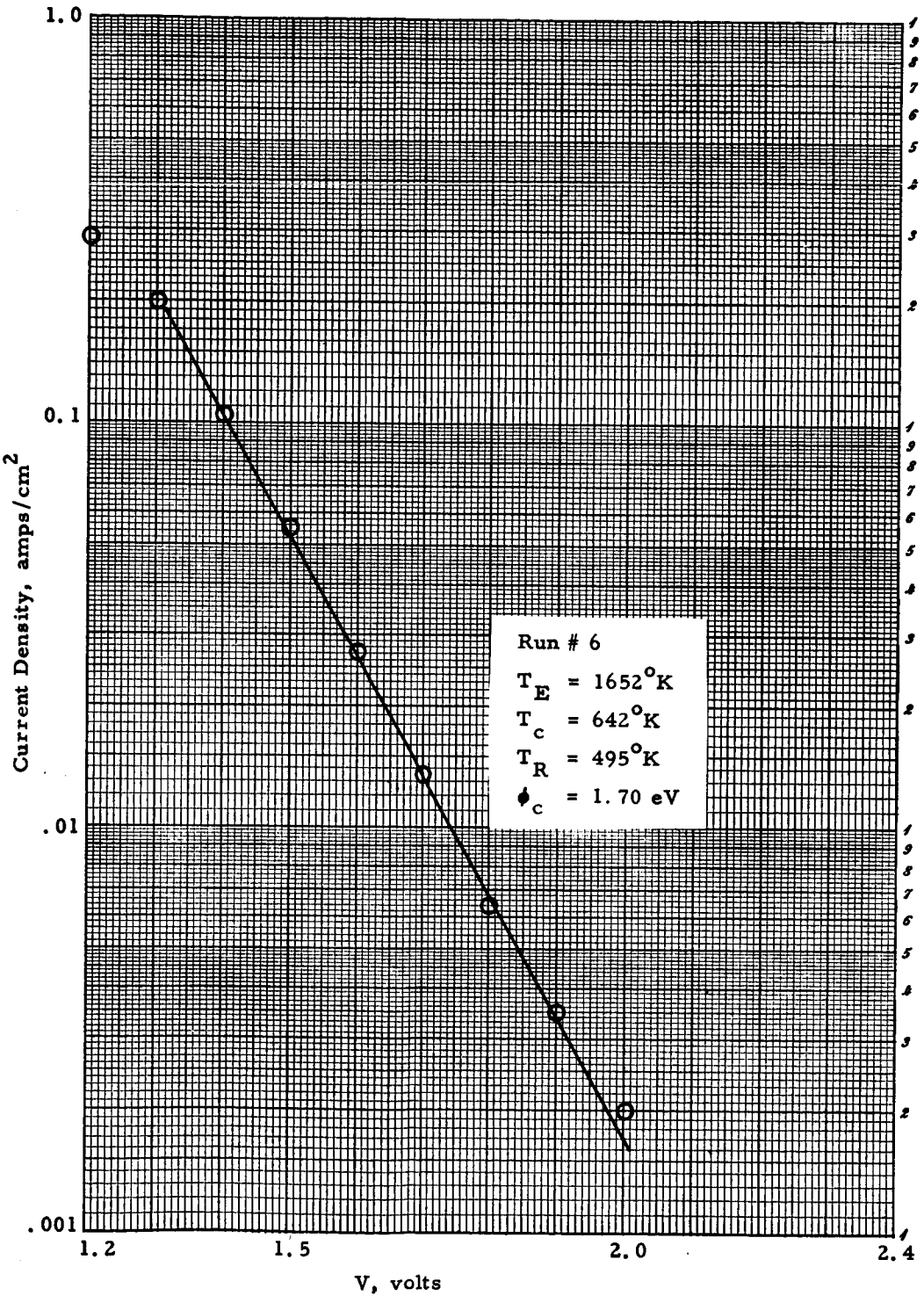

Figure 3.20(b) IV Characteristics (Run #6)

VIII-P-1

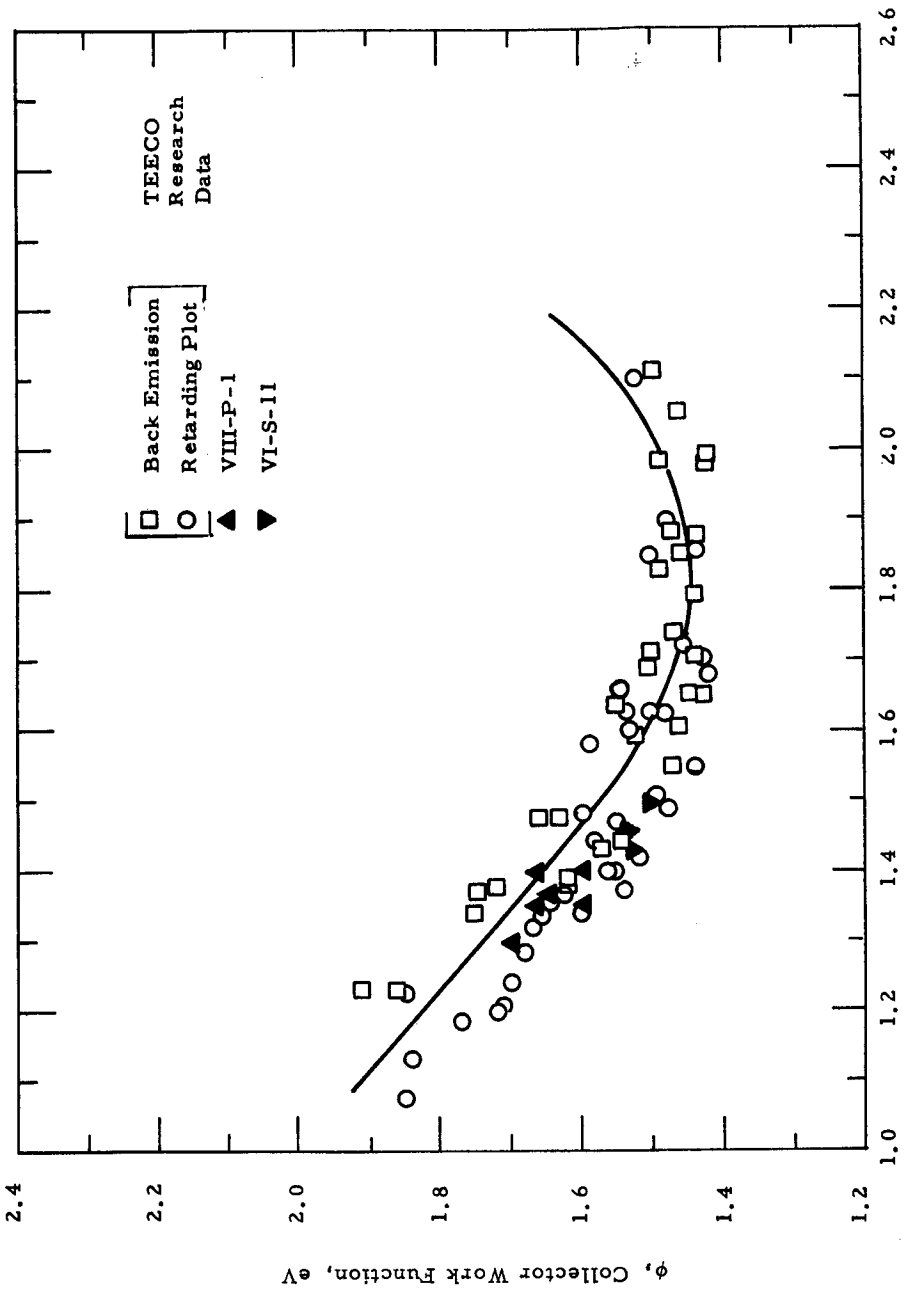

Figure 3.21 Molybdenum Collector Work Function versus T_C/T_R

TABLE 3-2

Output Voltage (volts)	Optimum Collector Temperature (°K)
1.0	925
0.9	940
0.8	950
0.7	960
0.6	975

Collector work function measurements were also made on this diode. These were computed from the current-voltage characteristics shown in Figures 3.16 through 3-20. The computed values are shown in Table 3-3.

TABLE 3-3

COLLECTOR WORK FUNCTION VALUES OF VIII-P-1

Run	T_E(°K)	T_R(°K)	T_c(°K)	T_c/T_R	ϕ_c (eV)
1	1961	517	697	1.35	1.67
2	1653	475	652	1.37	1.64
3	1913	529	746	1.40	1.60
4	1958	539	753	1.40	1.67
5	1762	502	675	1.35	1.60
6	1652	495	642	1.30	1.70

Figure 3.21 shows this data plotted with data taken by Thermo Electron's Research Department, as reported at the 24th Annual M.I.T. Physical Electronics Conference, and data taken on an earlier Series VI converter.

All the data taken from the retarding plot (Boltzmann line) showed good agreement. Therefore, the molybdenum collector work function of VIII-P-1 seemed to be typical of that of a high-performance converter.

Following collector work function tests, Converter VIII-P-1 was operated for 53 hours at constant power input. During this time the emitter temperature, as well as the output, remained constant at 1700°C and 54 amperes at 0.7 volt. This was judged adequate evidence that severe performance degradiation would not occur during electrical and solar testing of a generator made with similar diodes. During these tests an excessive heat transfer to the cesium reservoir was also noted, indicating the need for an adjustment in subsequent diodes.

CHAPTER 4
PROTOTYPE VIII-P-2

4.1 DESIGN

Based on the performance of diode VIII-P-1, an improved prototype, VIII-P-2, was designed. Changes were made in the radiator, the cesium reservoir support, and the emitter structure.

The performance tests of VIII-P-1 showed the optimum collector temperature at maximum power to be about 975°K. Maximum power occurred at 0.6 volt and 40 A/cm^2 of output. The radiator of VIII-P-2 was designed oversized to allow a collector temperature of 900°K at an output current of 40 A/cm^2. The required radiating surface area was calculated by dividing the radiator into seven sections and iterating the heat balance of each section. Based on the temperature measured at the base of the collector of VIII-P-1, the root of the radiator was estimated to operate at 750°K. The required surface area was calculated to be 161 cm^2. This compares with 51 cm^2 for VIII-P-1. Figure 4.1 shows VIII-P-2.

With the longer radiator, the cesium tubulation had to be lengthened to move the reservoir out of the shadow of the radiator and give it a view to space to radiate heat. The tubulation was made 1.76 inches long. The overall length of the reservoir and the tubulation is 3.55 inches. The 1/8-inch nickel tubulation used in VIII-P-1 was replaced with 3/16-inch tantalum with 10-mil walls. Two such tubulations, brazed to molybdenum pieces, had earlier been extensively cycle-tested on an Air Force solar thermionic program and remained sound after 1300 cycles. Tantalum, in addition to being stronger than nickel, is also available

in purer form. Its thermal properties are similar to those of nickel. Electron-beam-melted tantalum drawn into 3/16-inch tubing was used.

With the larger radiator and longer tubulation, the rod support of the reservoir used in VIII-P-1 was not practical with VIII-P-2. Assembly of the diode became inordinately difficult with the rods because the jigs had to maintain the same tolerances for larger diameters and lengths. Therefore, to support the longer tubulation, a stainless steel spider was used. An end view of the spider is shown in Figure 4.1. When made of thin but wide sections, such a spider is stiff in both the transverse and axial directions, and light in weight. The use of a slide fit between the inner support ring of the spider and the reservoir prevented the spider from constraining changes in length of the reservoir and tubulation, thus avoiding difficulties from thermal expansion mismatches. An additional attribute of the spider is that it strengthened the thinner end of the radiator.

4.2 FABRICATION

Because the use of pyrolytically deposited rhenium on tantalum resulted in visual evidence of contamination and in poor adherence between the rhenium and tantalum, an alternate course of fabricating rhenium-tantalum emitters, namely, pressure-bonding by the isostatic and the hot-pressing methods, was also pursued.

Eight 1"-diameter by 3/4"-long pieces of pyrolytically deposited rhenium on tantalum were procured. An EDM cut between the 1" diameter and the final dimension of 0.641" was used to remove the hardened outer shell. In addition to these eight pieces two 3/4"-diameter by 3/4"-long samples were also procured to evaluate the possibility of

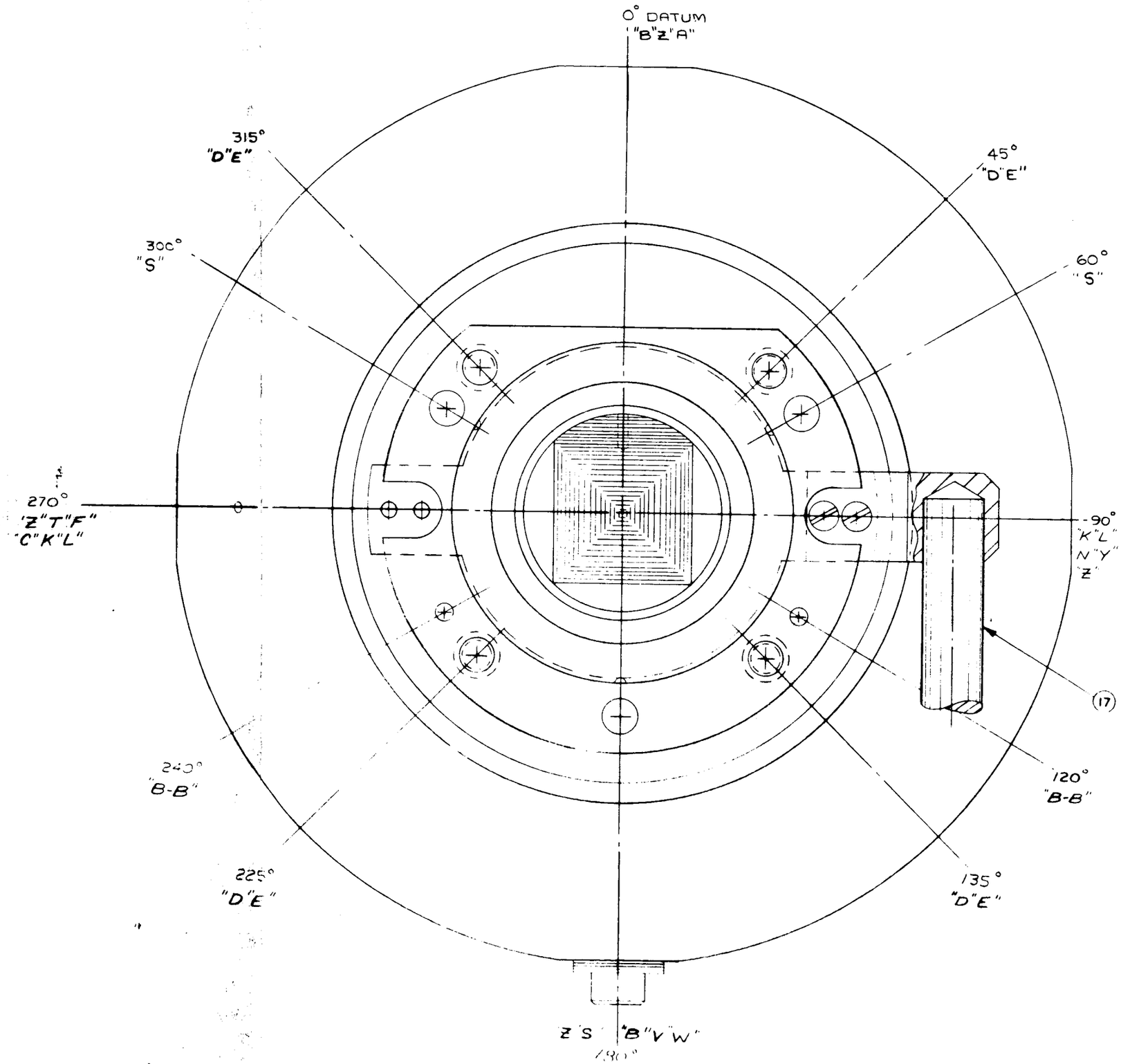

FOLDOUT FRAME 1

FOLDOUT FRAME 2

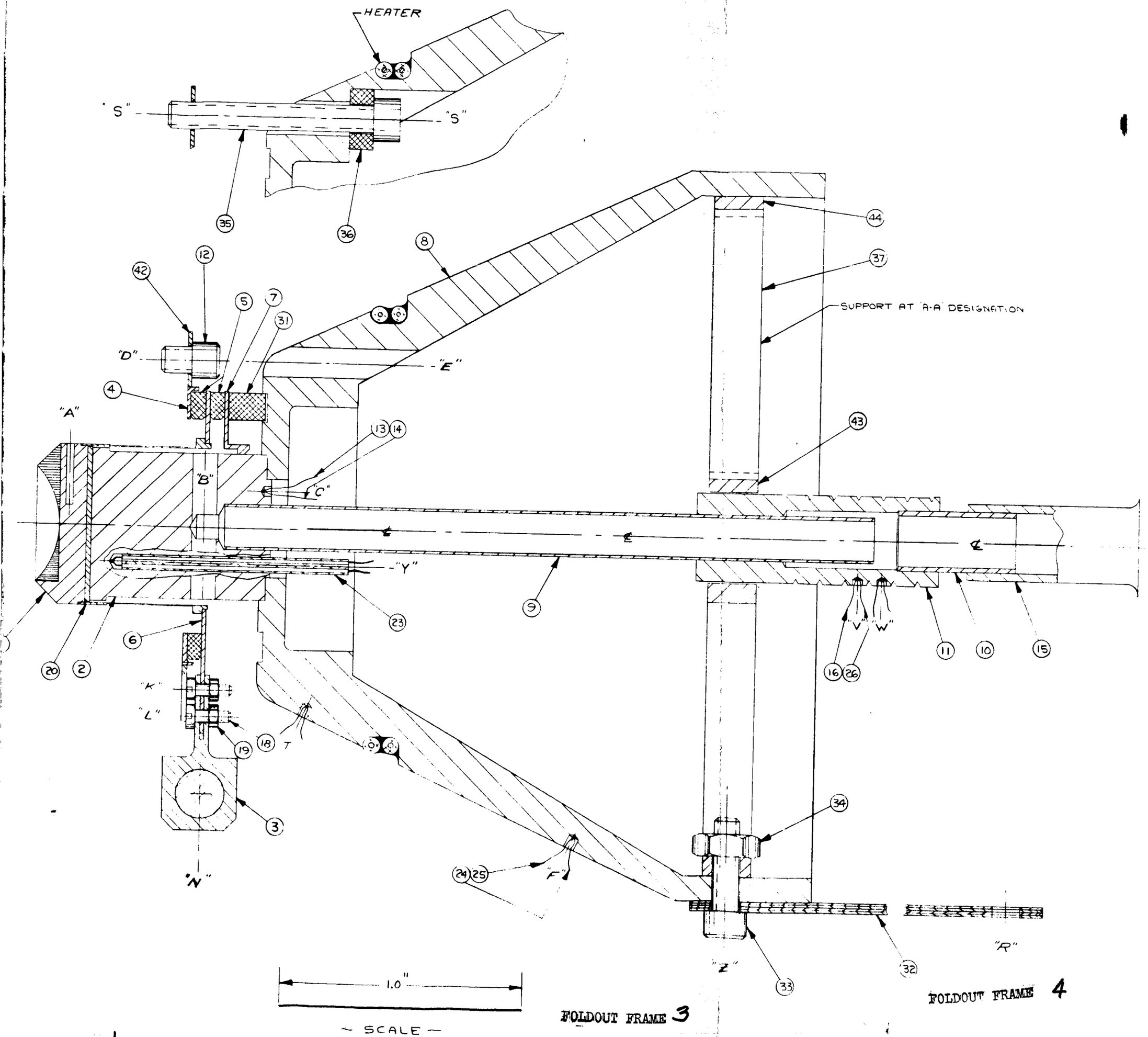
HEATER
"S"
"S"
35
36
8
12
42
5
7
31
"D"
"E"
4
"A"
13
14
"C"
"B"
44
37
SUPPORT AT "A-A" DESIGNATION
43
"Y"
23
9
6
20
2
"K"
"L"
19
18
T
3
"N"
24
25
"F"
"V"
"W"
11
10
15
16
26
34
"Z"
33
32
"R"
1.0"
~ SCALE ~
FOLDOUT FRAME 3
FOLDOUT FRAME 4
90°

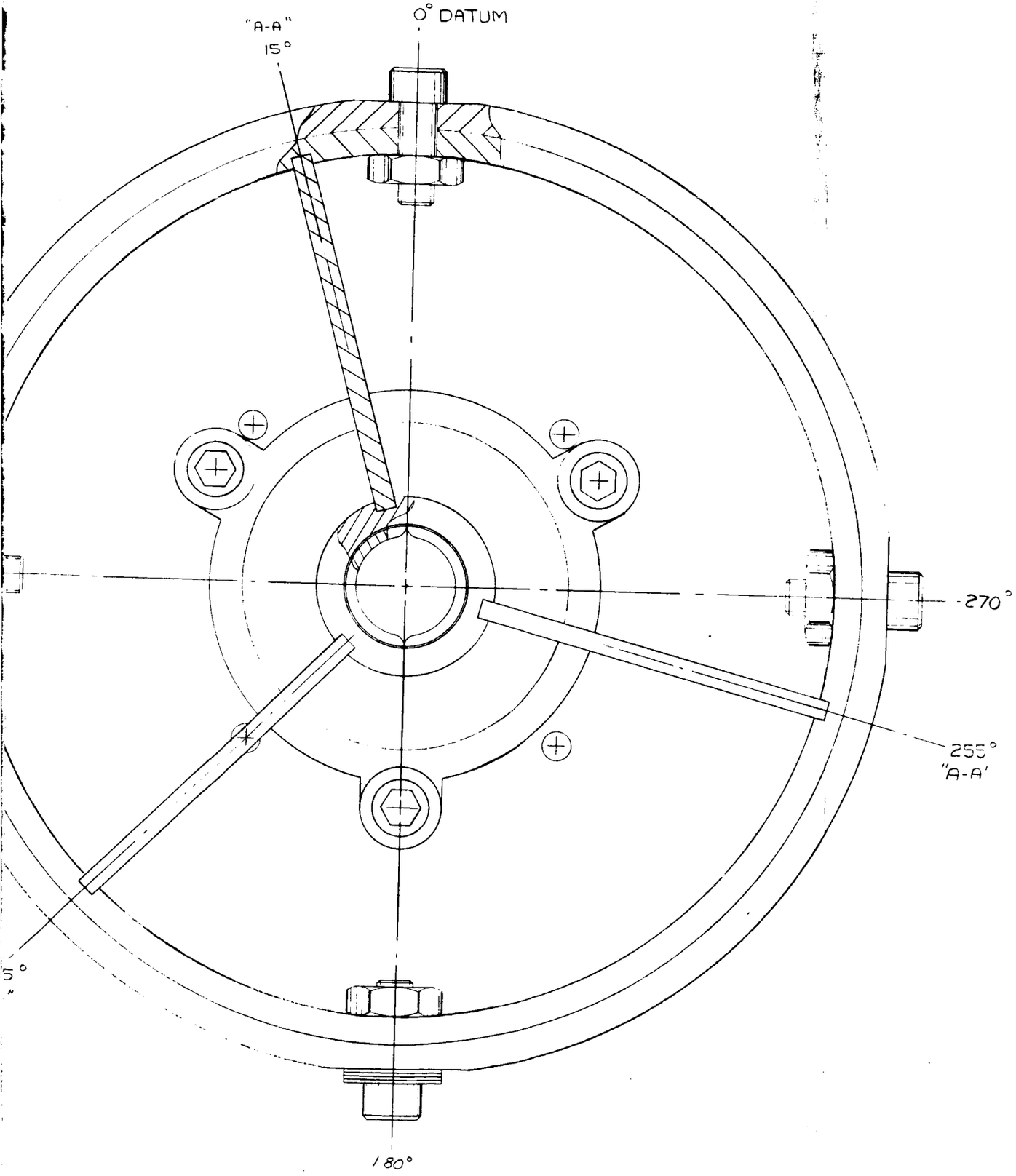

FOLDOUT FRAME 5

44	D		1	S.S.	
43	B		1	S.S.	
42	C		1		
41					
40					
39					
38					
37	B		3	S.S.	
36	A		4	Al_2O_3	
35	ND		4	S.S.	#4-40 x .84 LG S.H.C.S
34	ND		4	S.S.	#4-40 HEX NUT
33	ND		4	S.S.	#4-40 x .38 LG S.H.C.S.
32	B		4	Cu	
31	B		1	Al_2O_3	
30					
29					
28					
27					
26	ND		1	Chromel	
25	ND		1	Alumel	
24	ND		1	Chromel	
23	ND		1	Al_2O_3	
22					
21					
20	C		1	Ta	
19	B		2	Ti	#00-96 x .T
18	B		2	Ti	#00-96 x .125 LG
17	ND		1	Cu	#4-(2-3) C A W RE
16	ND		AS REQ'D	Alumel	
15	C		1	Cu	
14	ND		1	Alumel	
13	ND		1	Chromel	
12	A		4	S.S.	#4-40 x .125 LG S.H.C.S (MOD)
11	C/C		1	Ni	
10	C		1	Ni	
9	C		1	Ta	
8	D		1	Cu	
7	C		1	Nb	
6	C		1	Nb	
5	B		2	Al_2O_3	
4	B		1	Nb	
3	C		1	Nb	
2	C		1	Mo	
1	C		1	Ta	

PART	SIZE	REV	REQ	MAT'L	NOTES

THERMO ELECTRON

DRAWN	CHECKED	ENGINEER

TITLE: VIII-P-2 LAYOUT

SIZE	DRAWING NUMBER	SHEET	REV
H	479-1000	1	E

FIGURE 4.1

FOLDOUT FRAME 6

masking of the outer circumferences of the 3/4"-diameter slugs during deposition, to prevent chemical attack of the tantalum and to prevent deposition of rhenium on the cylindrical surface. Such chemical attack was discussed in Chapter 3.

The first two pieces received were both 1" in diameter, with approximately 15 mils of rhenium deposited. The first (No. 1) was completely machined without difficulty. Upon processing, however, the face showed visual evidence of a second phase. A microprobe analysis was performed, revealing the presence of tantalum in the rhenium emitting surface. The rhenium surface probed is shown in Figure 4.2. It had an area in the center (where the large crystals can be seen) of 2% tantalum, and this was surrounded by a two-phase region. The two-phase region, shown in Figure 4.3, had 0.4% tantalum distributed throughout. The second (No. 2) specimen failed during the initial electrical discharge machining (EDM) operation; that is, the rhenium disc separated from the substrate, revealing a dark interface. These first two pieces did not exhibit the characteristic dendritic growth of rhenium on tantalum, and did not appear clean when received.

Two additional 1"-diameter specimens were received with approximately 30 mils of rhenium deposited. They were both characterized by dendritic growth of rhenium on tantalum, and appeared to be much cleaner than the previous two. However, during the initial EDM machining, the rhenium separated from the substrate on one (No. 3), showing a dark powdery interface. This is shown in Figure 4.4. The other (No. 4) withstood the preliminary EDM process but separated at the interface during grinding.

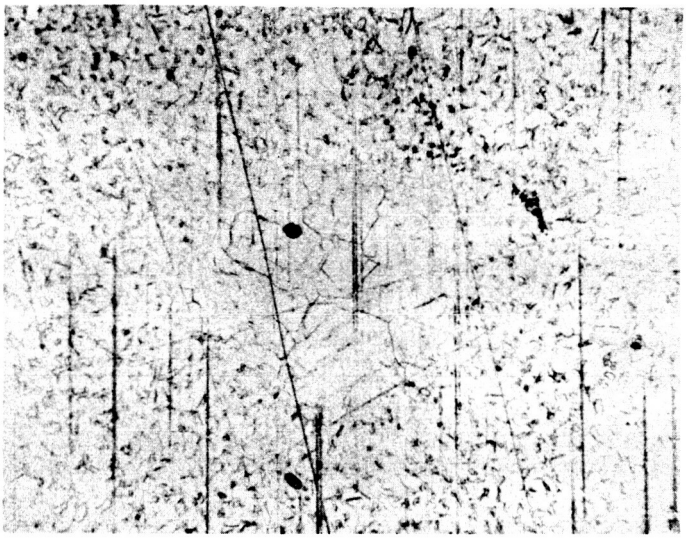

Figure 4.2 No. 1 Pyrolytic Emitter Surface (75X)

Figure 4.3 No. 1 Pyrolytic Emitter Surface (310X)

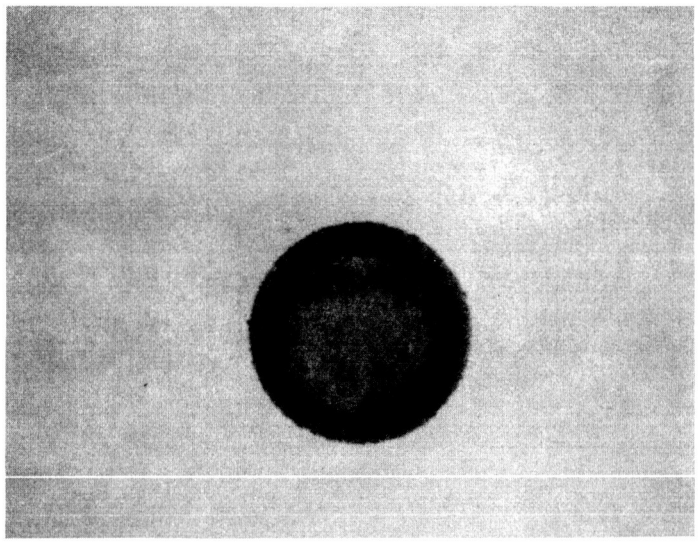

Figure 4.4(a) - No. 3 Pyrolytic Emitter with EDM Cut

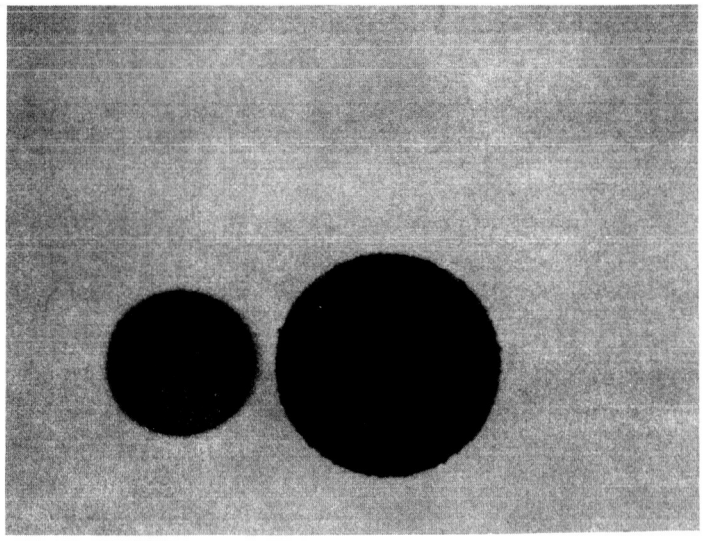

Figure 4.4(b) - No. 3 Pyrolytic Emitter Interface

5449

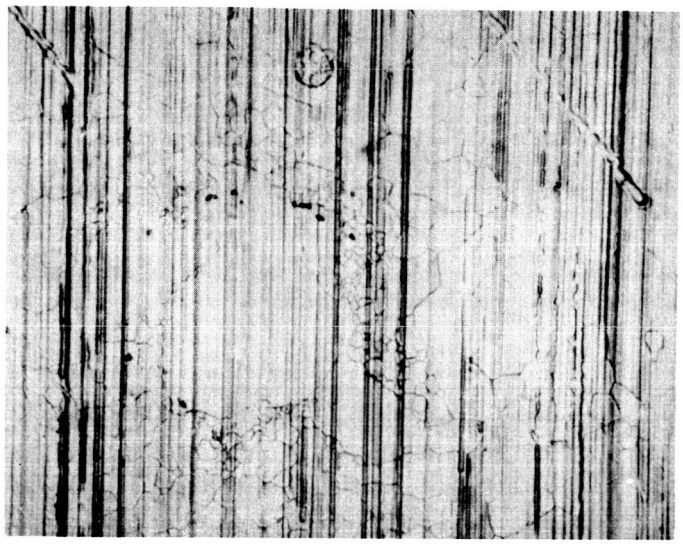

Figure 4.5(a) No. 6 Pyrolytic Emitter Surface (310X)

5450

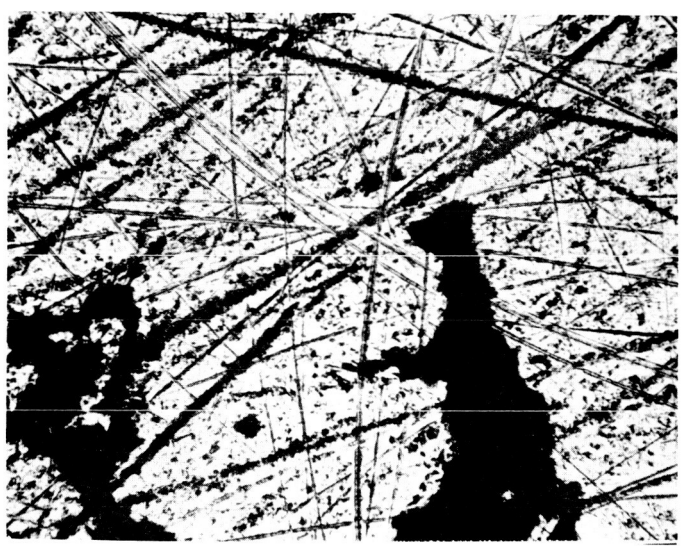

Figure 4.5(b) Pyrolytically Deposited Rhenium Emitter (75X) of poor Quality showing Voids and deep Scratches

compare this emitter's performance with that of the higher-quality emitter in VIII-P-1. In this way, some correlation between visual appearance and eventual performance could be obtained.

Concurrently with the work on the pyrolytically deposited emitters, six rhenium emitters were pressure-bonded to tantalum substrates. To accomplish this, six tantalum cans, each containing rhenium and tantalum slugs, were pressure-bonded. The assembly consisted of placing in a deep tantalum cup first a disc of rhenium, then the tantalum slug, and finally a shallow cup. All parts were chemically cleaned and fired prior to assembly. The lips of the two cups were then welded in vacuum using the electron-beam welder. After the welding, three assemblies were delivered for bonding in an autoclave with a cycle of 3 hours at 2850°F under a pressure of 10,000 psi of helium gas, and three assemblies were hot-pressed in vacuum between graphite dies for 1/2 hour at 2900°F and 8000 psi mechanical pressure. Heating was accomplished in the autoclave furnace process with resistance heaters, and during the hot-pressing by electric induction. To prevent migration of carbon from the graphite dies to the tantalum, thin foils of tantalum were wrapped around the container to act as diffusion barriers. This procedure added to the protection provided by the tantalum cups. Figure 4.6 shows a microstructure with the carbide precipitates in the foil wrapping and in the tantalum cup. Typically, 2 mils of rhenium were removed by grinding from the original 20 mils as a means of ensuring pure rhenium.

Five specimens were returned to Thermo Electron for final machining--three gas-pressure bonded and two hot-pressed. One hot-pressed

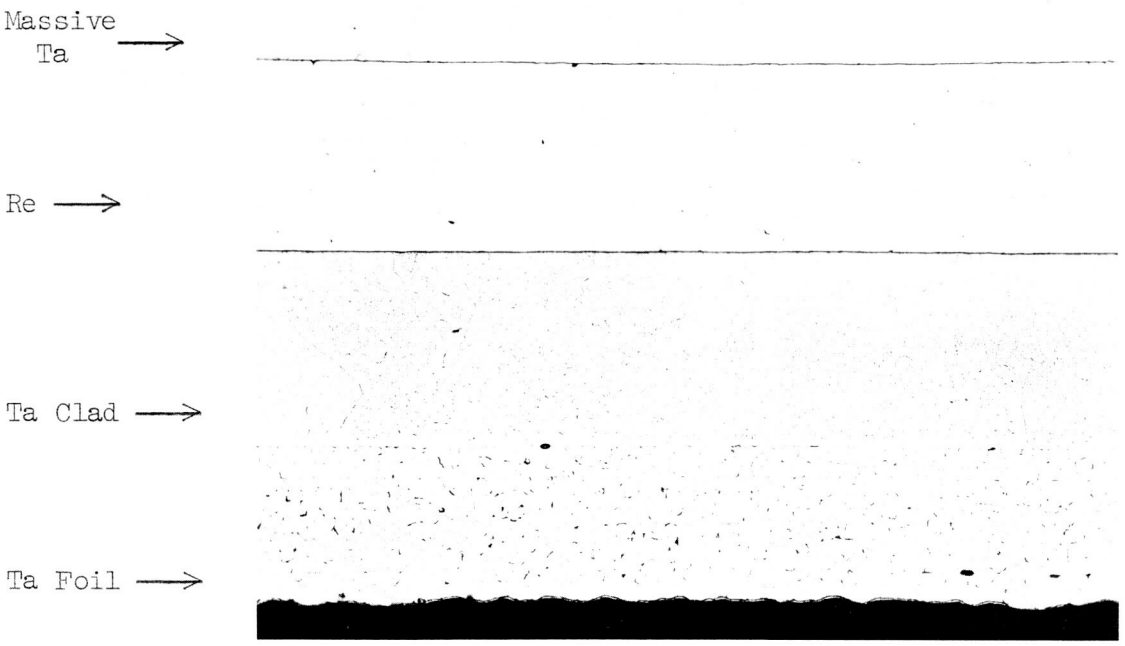

Figure 4.6 Microstructure Showing Carbide Precipitates in the Foil Wrapping and Tantalum Clad

specimen was examined by BMI and destroyed in the process. With the exception of one fabricated with gas pressure, which subsequently separated in grinding, the remainder were all successfully machined into final form.

Figure 4.7 is a photograph of a gas-pressure bonded rhenium surface fired at 2000°C for 20 minutes, which was incorporated into converter VIII-P-2a. The crystal size and distribution are typical for rhenium. Figure 4.8 is an edge view of an electric-discharge machined surface of the same emitter. Beneath the black portion can be seen approximately 18 mils of rhenium, 10 mils of tantalum, and a shiny portion which is also tantalum. This later tantalum region was machined to mate with the tantalum emitter sleeve.

4.3 TESTING

Figure 4.9 shows an overall view of an VIII-P-2 converter. The spider support of the cesium reservoir is shown in Figure 4.10.

Converters VIII-P-2a and VIII-P-2b were both tested under steady-state conditions at 1700°C and 1677°C observed emitter temperatures, with no external cooling of the radiator or reservoir. In addition to static data, work function measurements were performed with all pertinent data being recorded on the graphs.

Figures 4.11, 4.12, 4.13 and 4.14 show the current density versus cesium temperature at various voltages and collector temperatures for VIII-P-2a and VIII-P-2b, respectively, at 1700°C and 1677°C observed. In attempting to raise the collector temperature, it was not possible to keep the cesium at optimum. However, for VIII-P-2b, because the output was considerably lower than VIII-P-2a, it was possible to scan more collector temperatures.

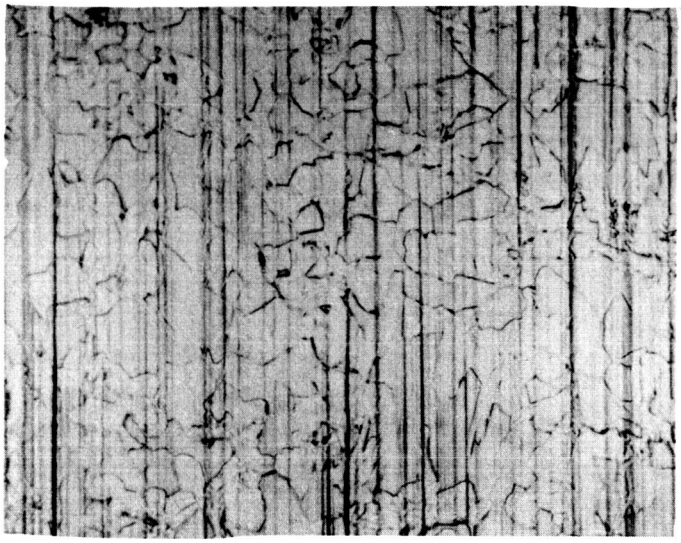

Figure 4.7 VIII-P-2a Emitter Surface (310X)

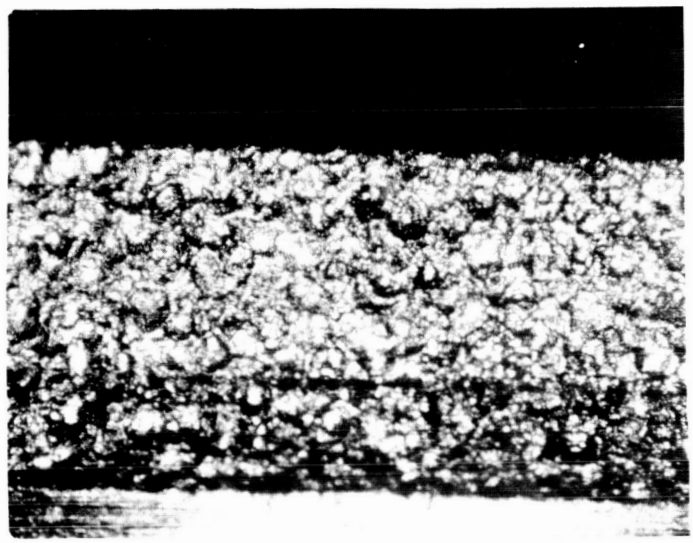

Figure 4.8 Edge View of VIII-P-2a Emitter (75X)

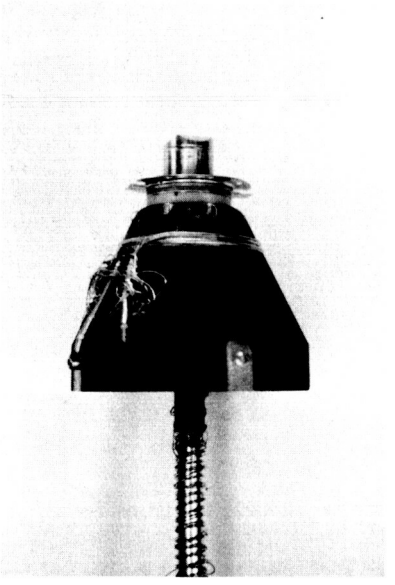

Figure 4.9 Diode VIII-P-2

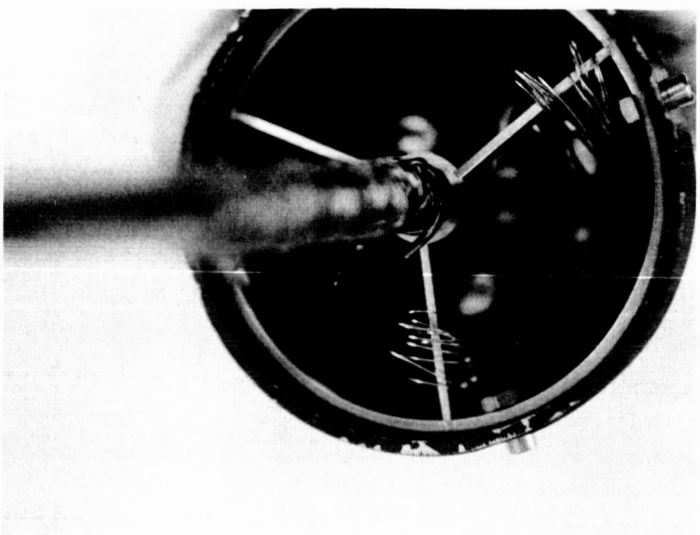

Figure 4.10 Rear View of VIII-P-2 Converter

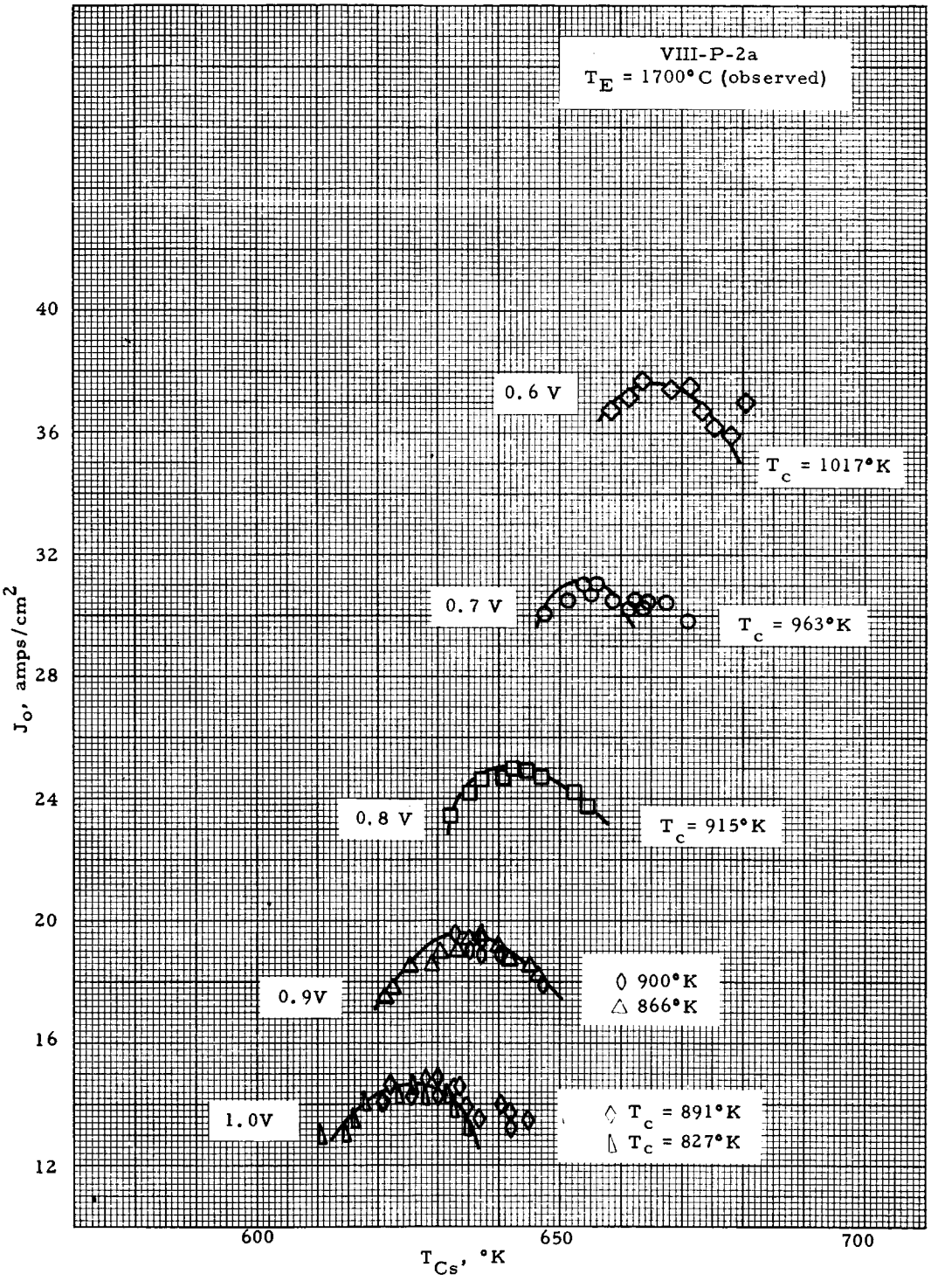

Figure 4.11 Current Density versus Cesium Temperature at various Voltages for Converter VIII-P-2a at T_E = 1700°C (Obs.)

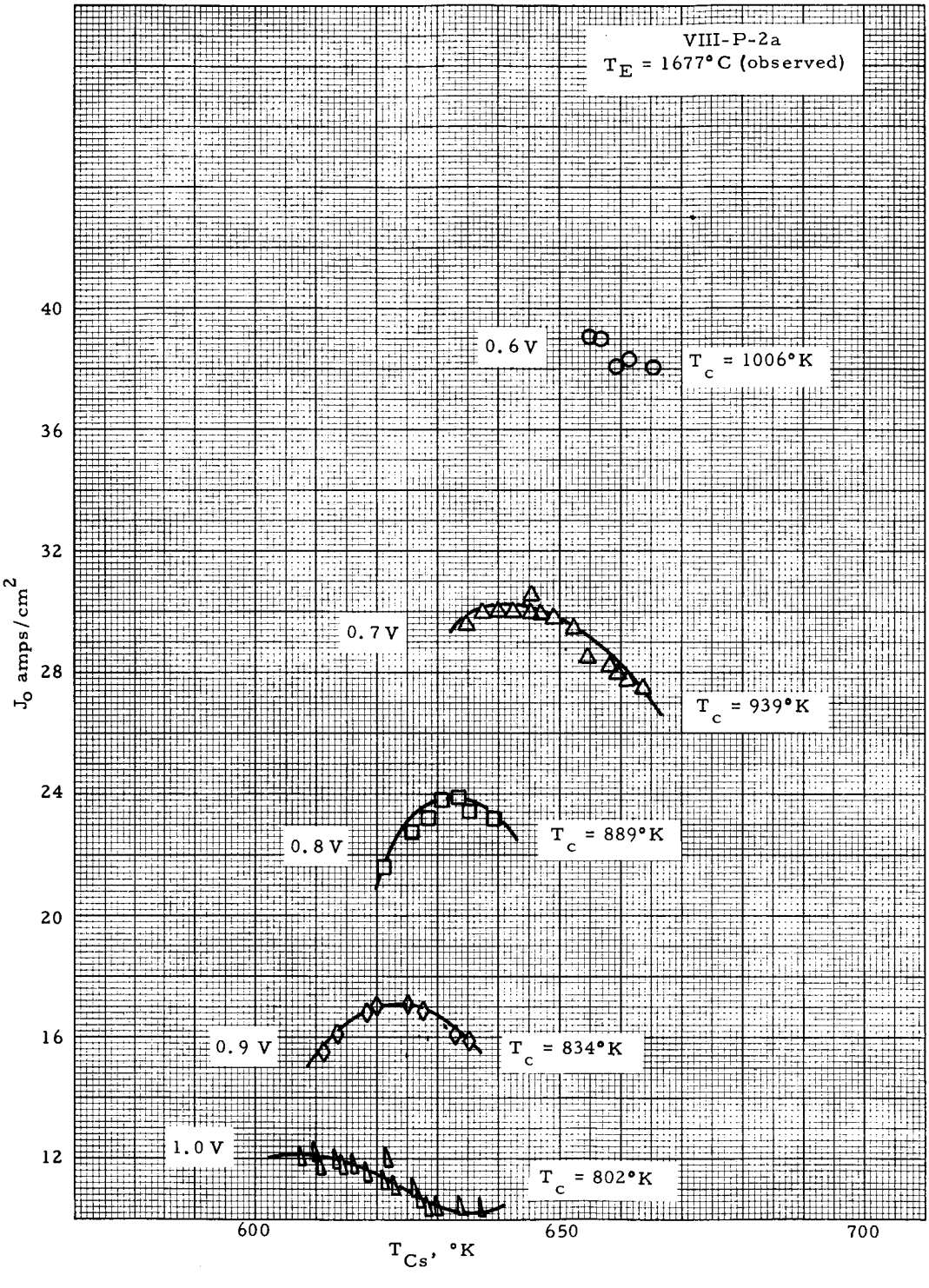

Figure 4.12 Current Density versus Cesium Temperature at various Voltages for Converter VIII-P-2a at T_E = 1677°C (Obs.)

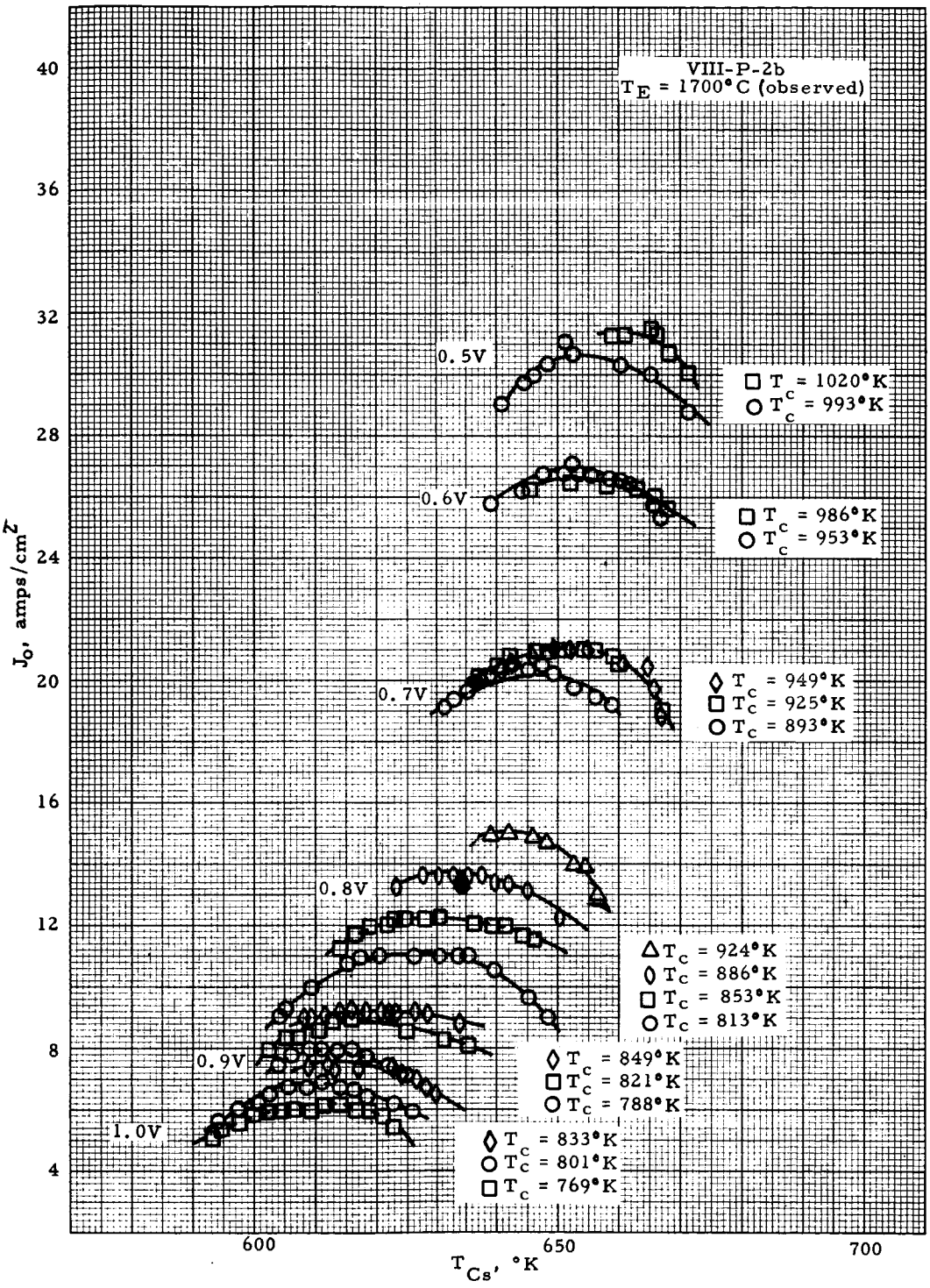

Figure 4.13 Current Density versus Cesium Temperature at various Voltages for Converter VIII-P-2b at T_E = 1700°C (Obs.)

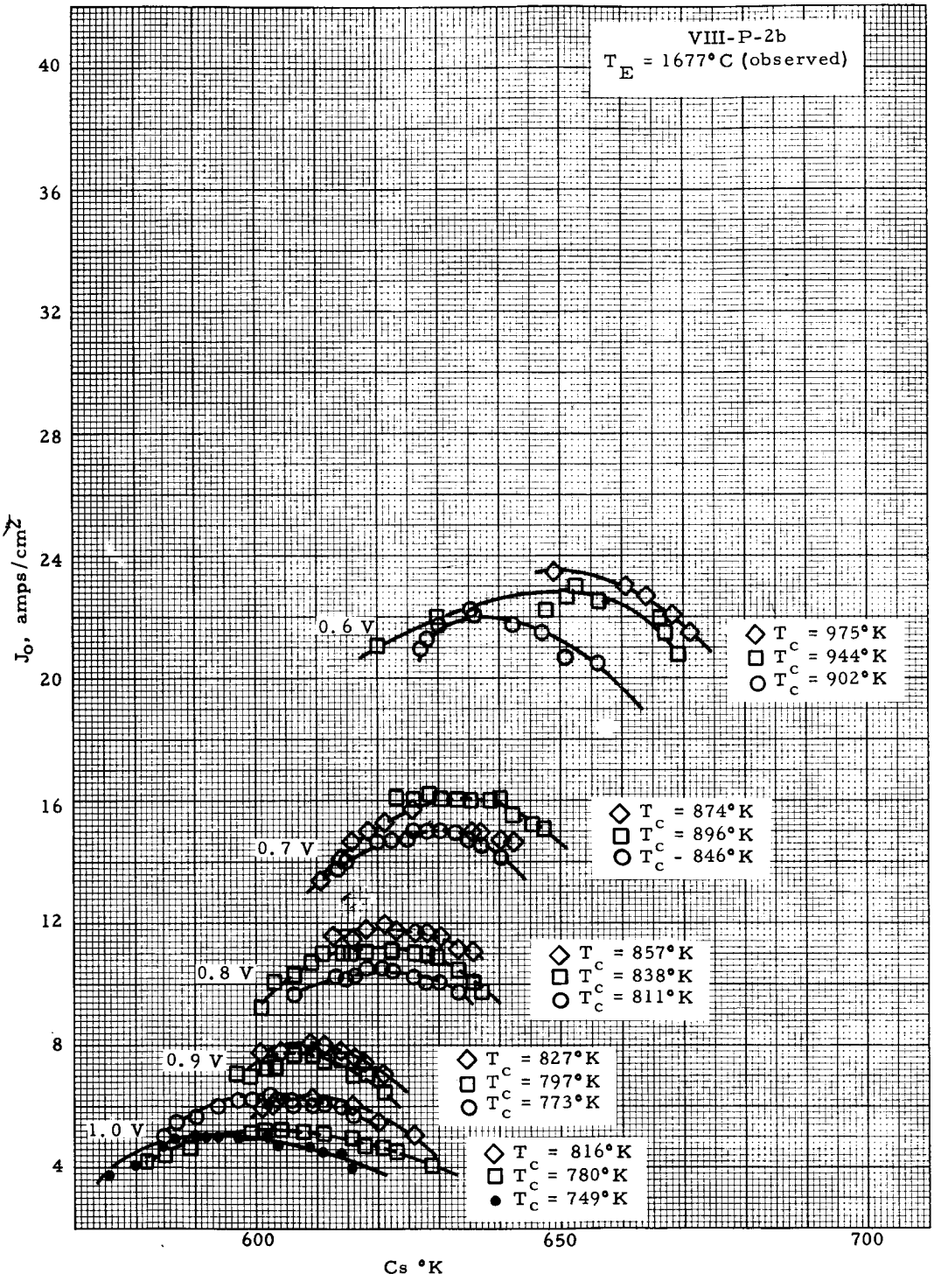

Figure 4.14 Current Density versus Cesium Temperature at various Voltages for Converter VIII-P-2b at T_E = 1677°C (Obs.)

The optimized outputs at each voltage are plotted in Figures 4.15 and 4.16 for 1700°C and 1677°C observed emitter temperatures. From these figures it was apparent that the output of VIII-P-2a was considerably higher than VIII-P-2b.

Tables 4-1 and 4-2 contain collector work function values obtained for VIII-P-2a and VIII-P-2b at various emitter-space and collector-to-cesium-reservoir temperature ratios.

TABLE 4-1

WORK FUNCTION DATA FOR VIII-P-2a

Run	T_E	T_R	T_C	T_C/T_R	ϕ_C
1	1790	470	565	1.20	1.67
2	1850	470	575	1.22	1.71
3	1850	480	603	1.26	1.69
4	1920	482	594	1.23	1.67
5	1850	490	626	1.28	1.69
6	1850	515	647	1.26	1.696

TABLE 4-2

WORK FUNCTION DATA FOR VIII-P-2b

Run	T_C	T_R	T_C	T_C/T_R	ϕ_C
6	1850	524	618	1.18	1.717
7	1490	505	495	0.98	1.982
8	1500	473	561	1.19	1.75
9	1490	478	490	1.03	2.01
10	1640	528	690	1.31	1.695

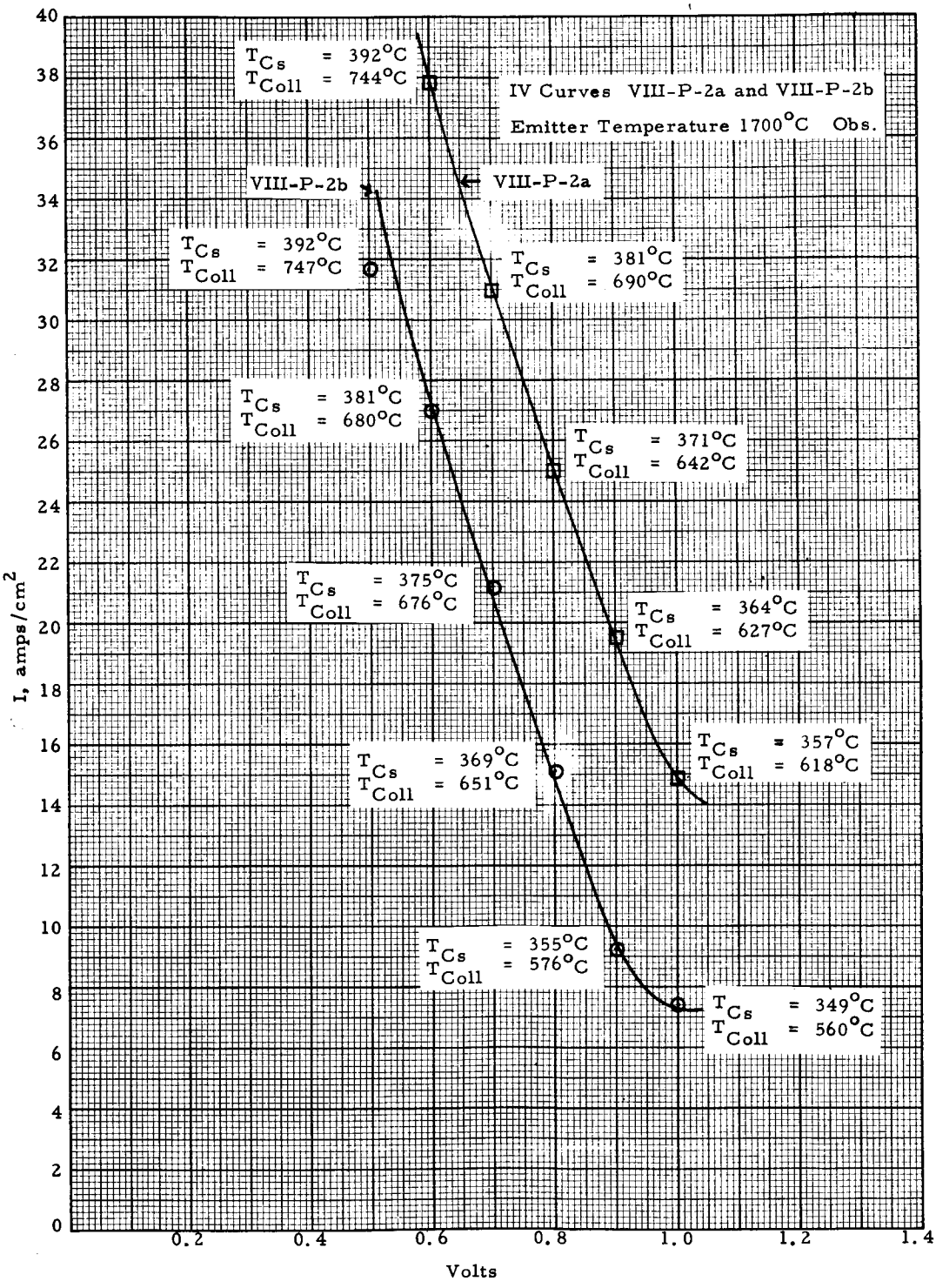

Figure 4.15 IV Curves for VIII-P-2a and VIII-P-2b, Emitter Temperature = 1700°C (Obs.)

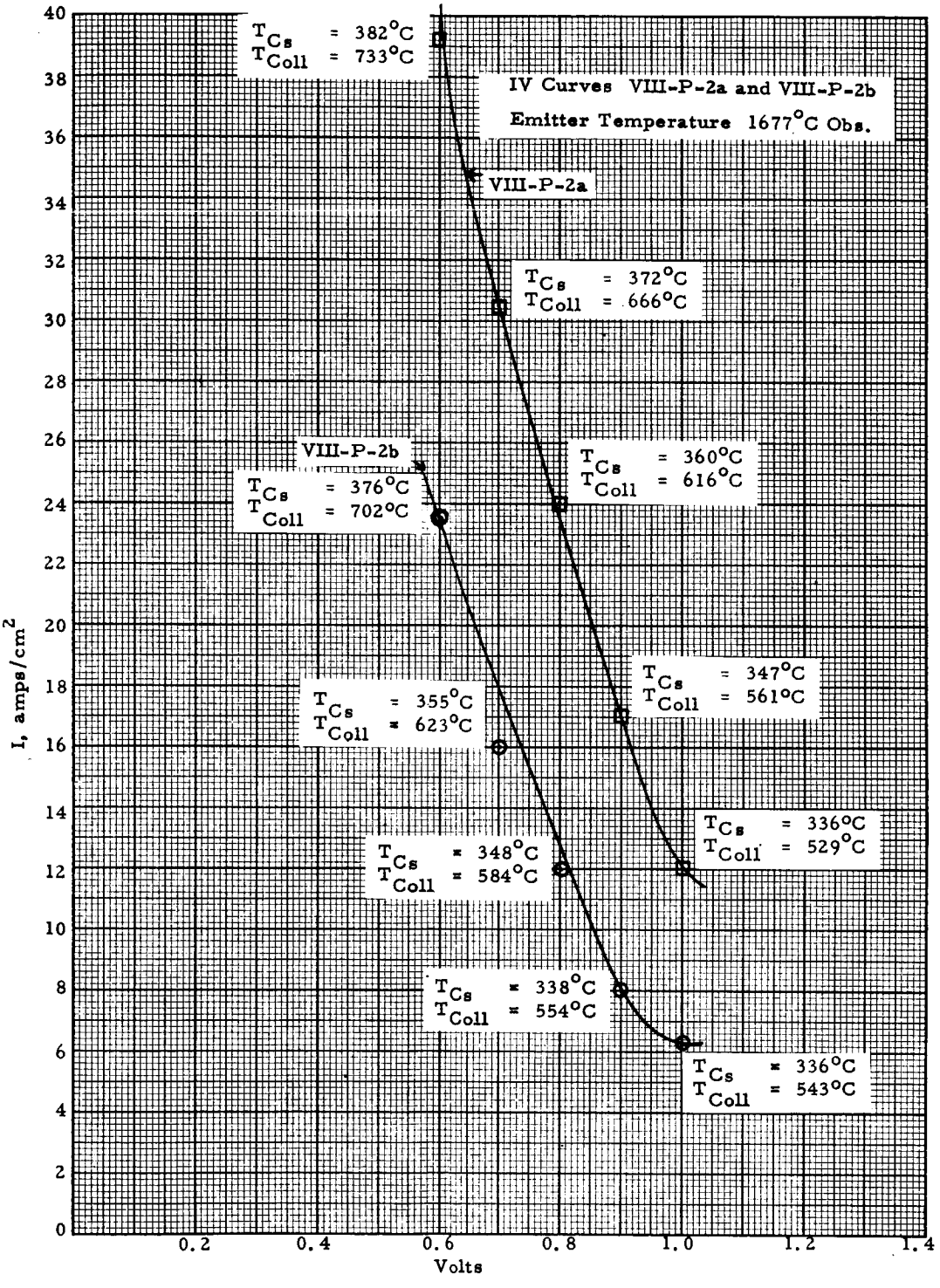

Figure 4.16 IV Curves for VIII-P-2a and VIII-P-2b, Emitter Temperature = 1700°C (Obs.)

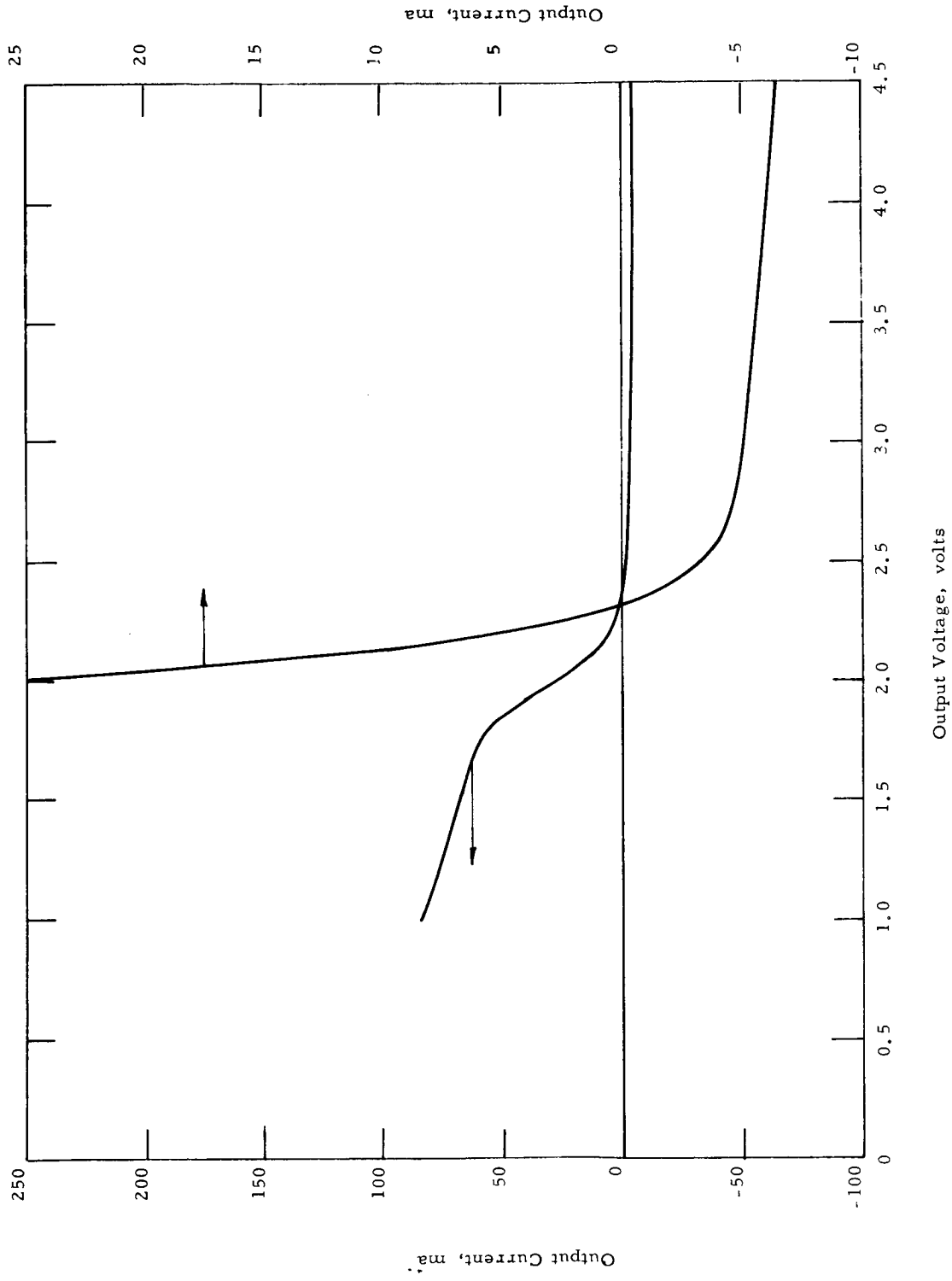

Figure 4.17(a) IV Curve Produced by an X-Y Plotter (Run No. 1)
VIII-P-2a

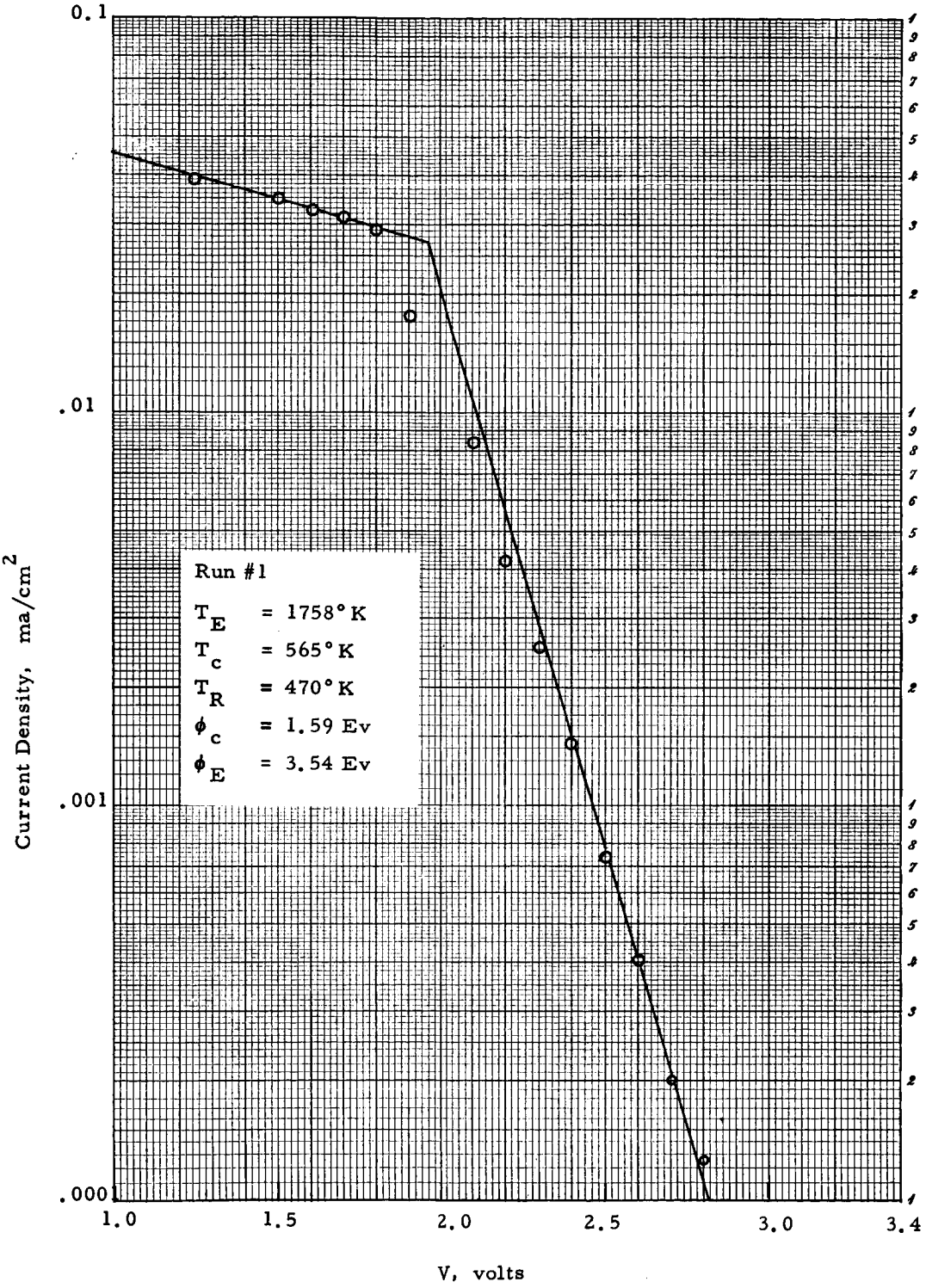

Figure 4.17(b) IV Characteristics (Run No. 1)

VIII-P-2a

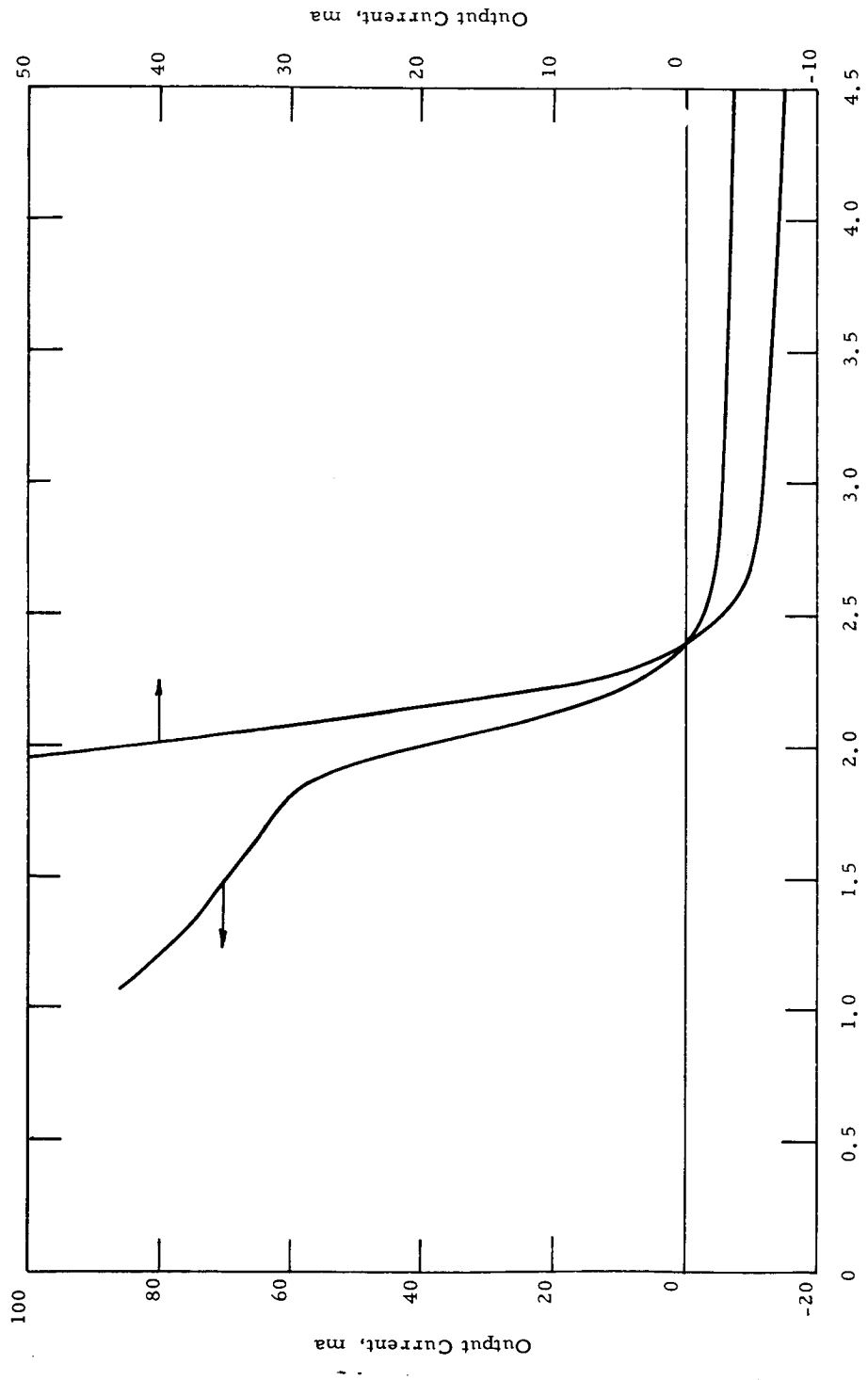

Figure 4.18(a) IV Curve Produced by an X-Y Plotter (Run No. 2)

VIII-P-2a

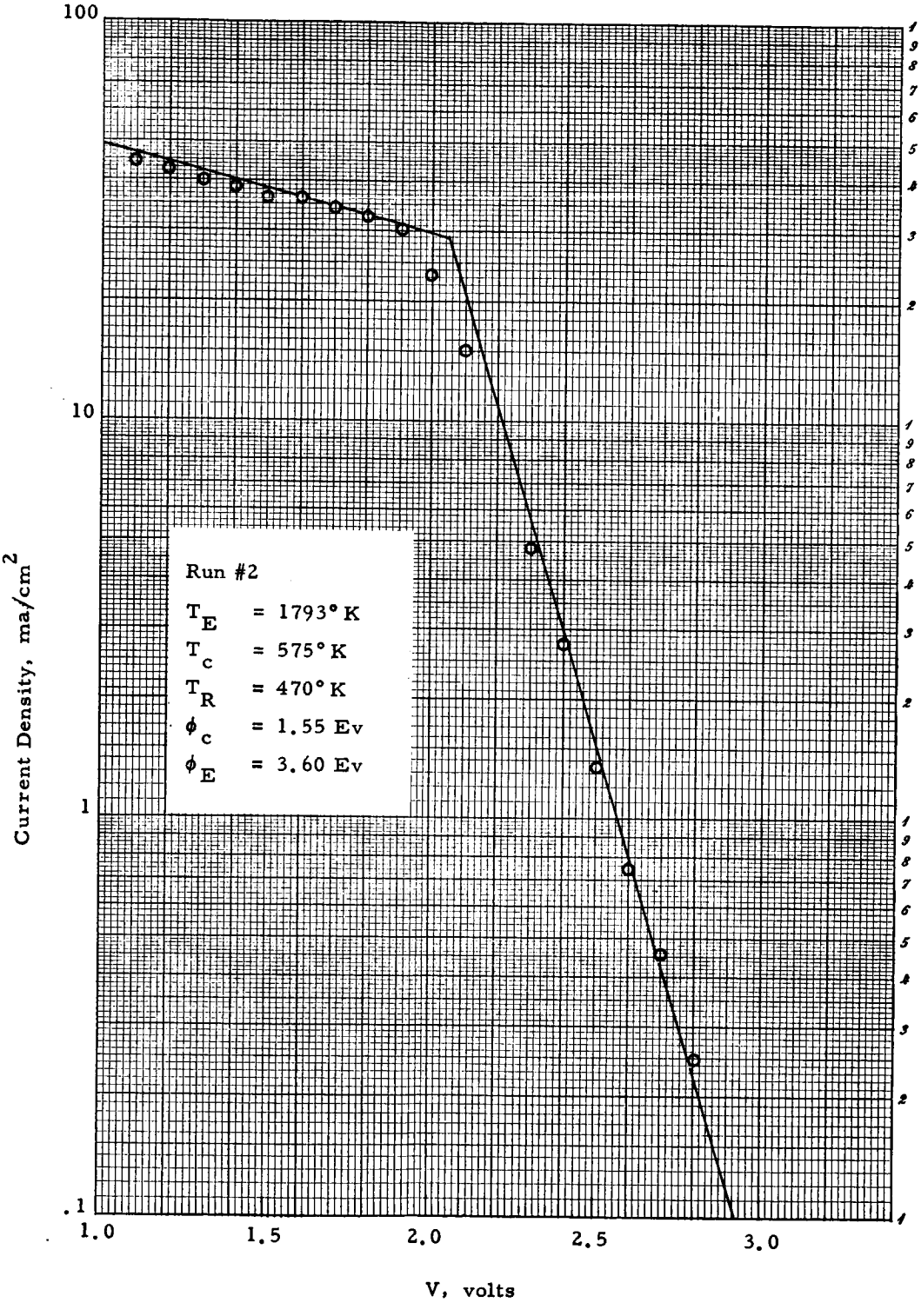

Figure 4.18(b) IV Characteristics (Run No. 2)

VIII-P-2a

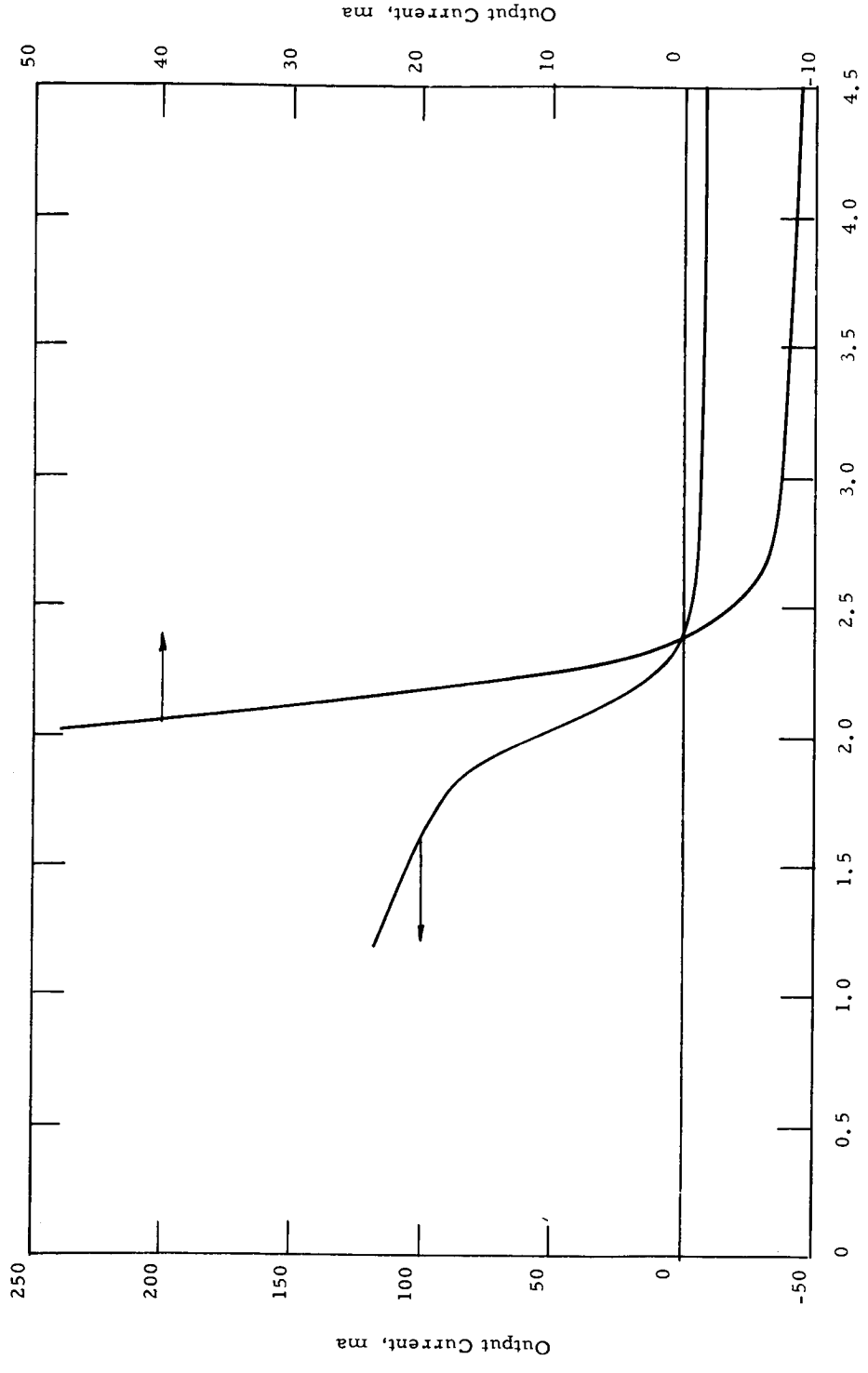

Figure 4.19(a) IV Curve Produced by an X-Y Plotter (Run No. 3)

VIII-P-2a

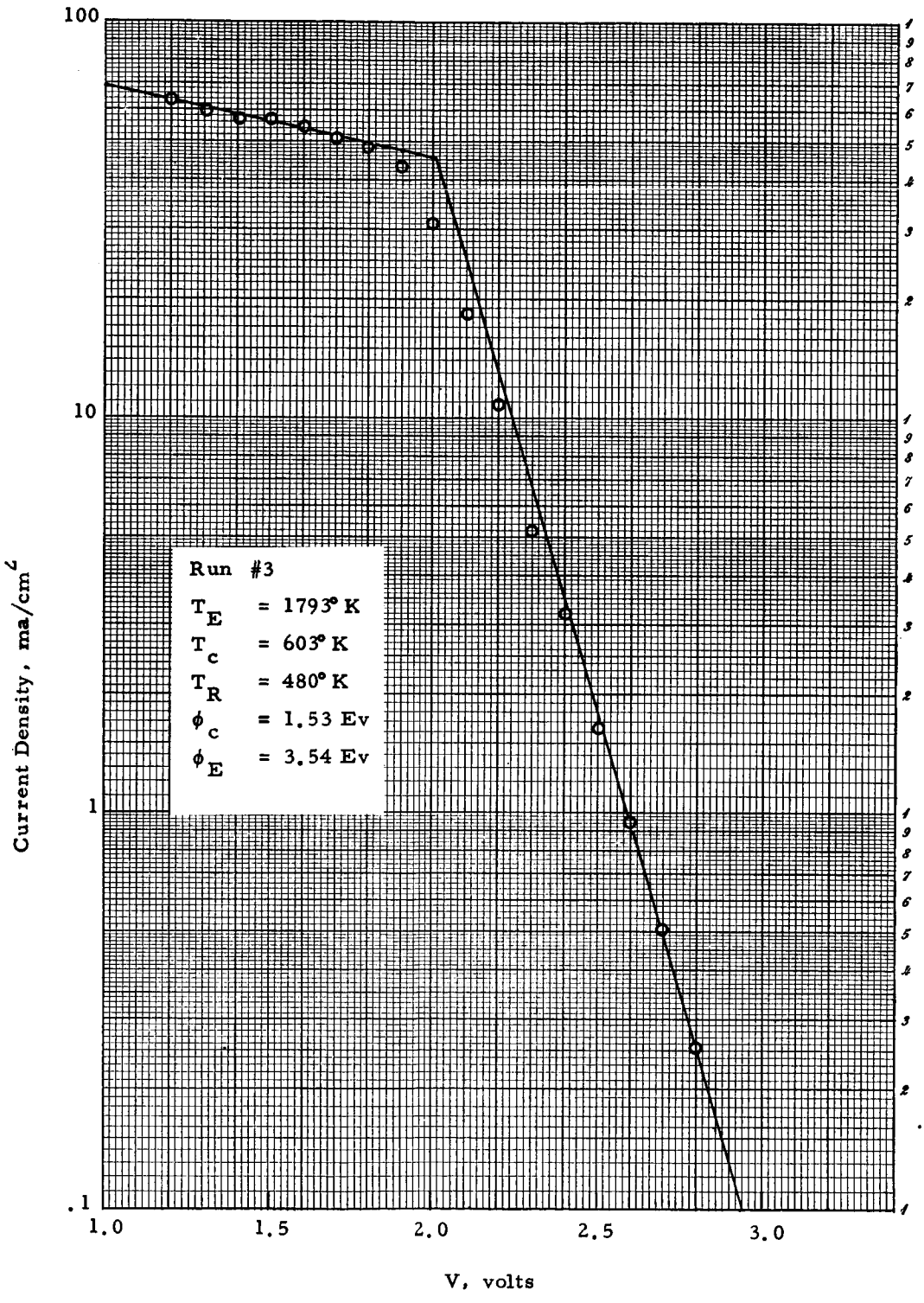

Figure 4.19(b) IV Characteristics (Run No. 3)

VIII-P-2a

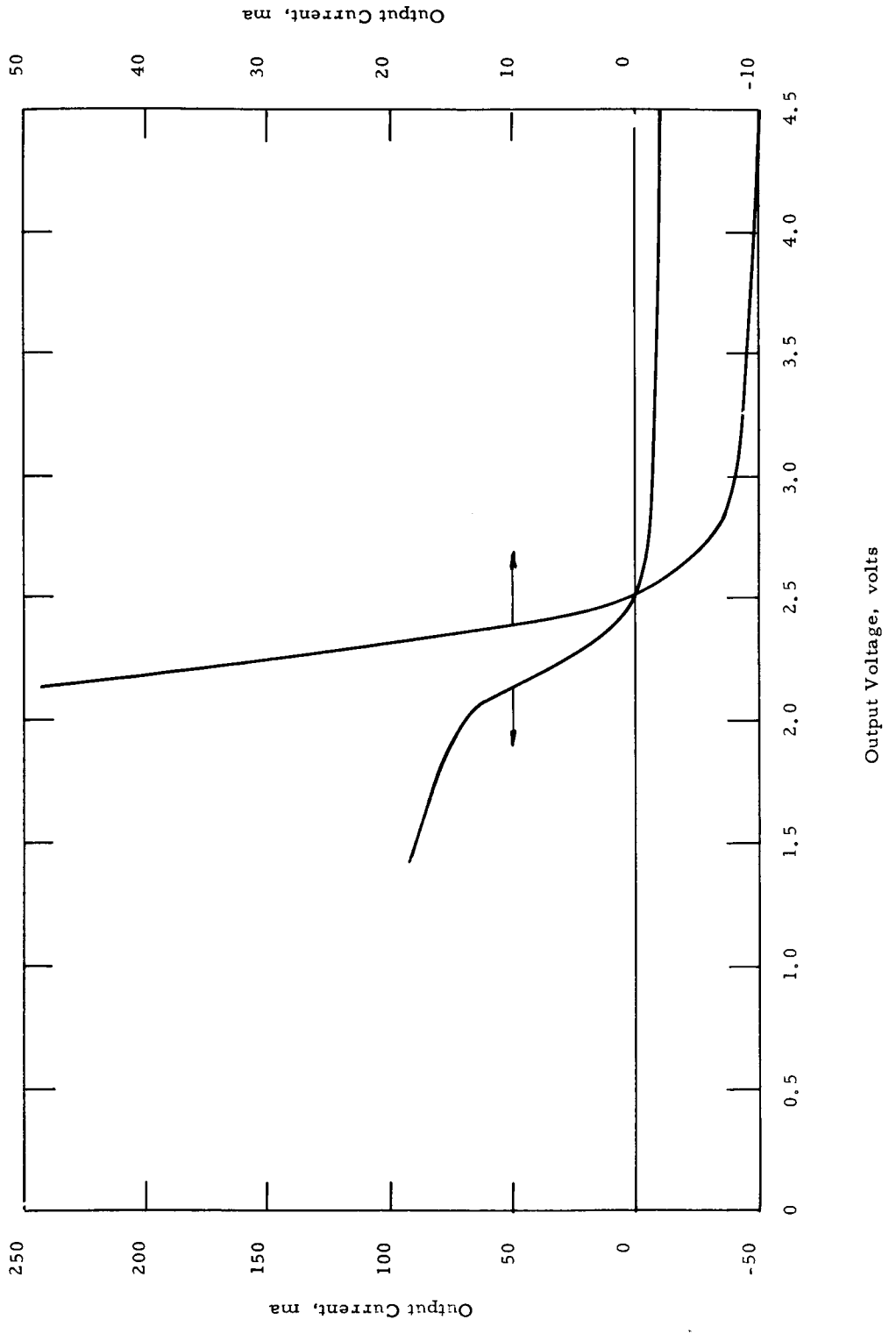

Figure 4.20(a) IV Curve Produced by an X-Y Plotter (Run No. 4)

VIII-P-2a

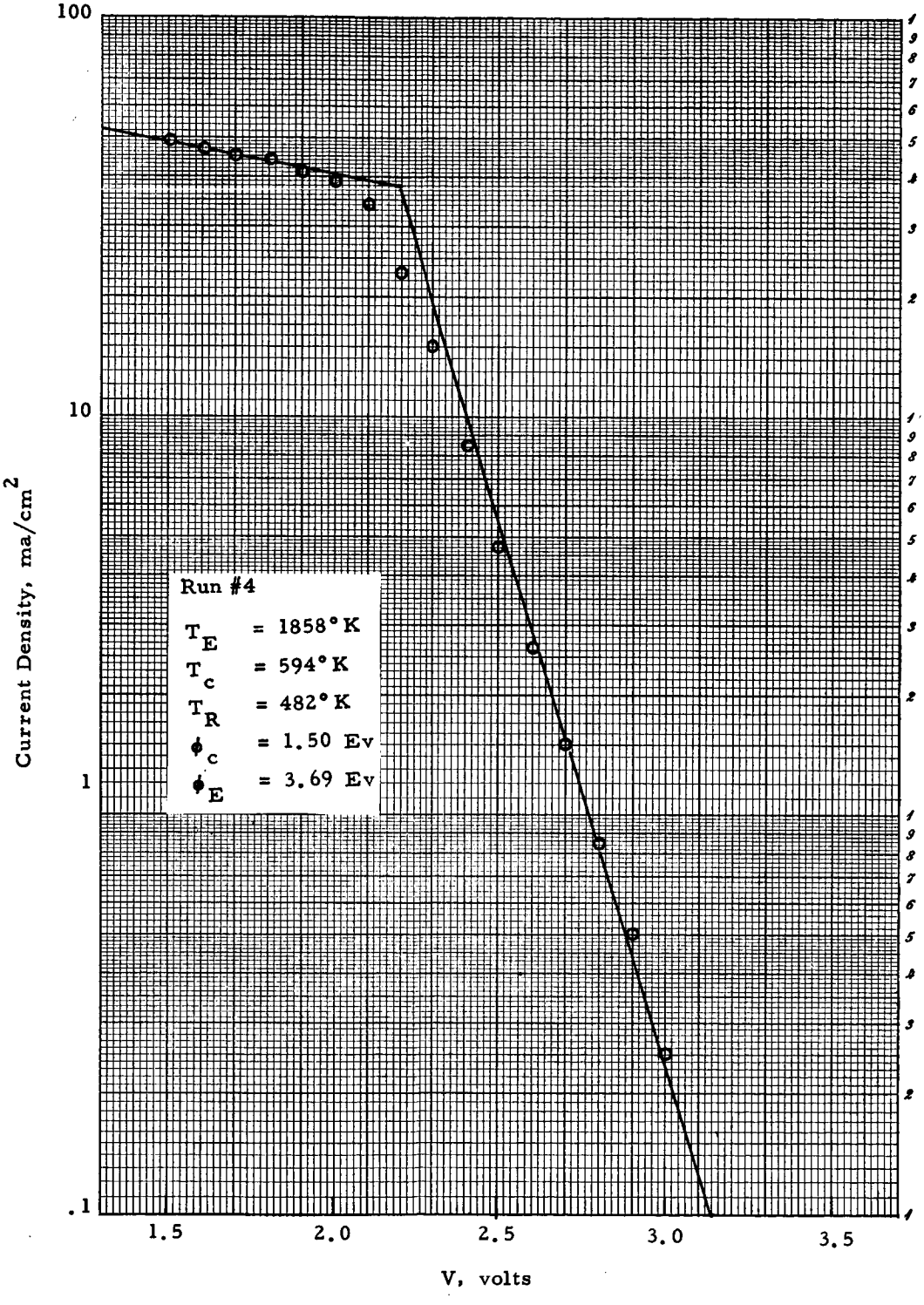

Figure 4.20(b) IV Characteristics (Run No. 4)

VIII-P-2a

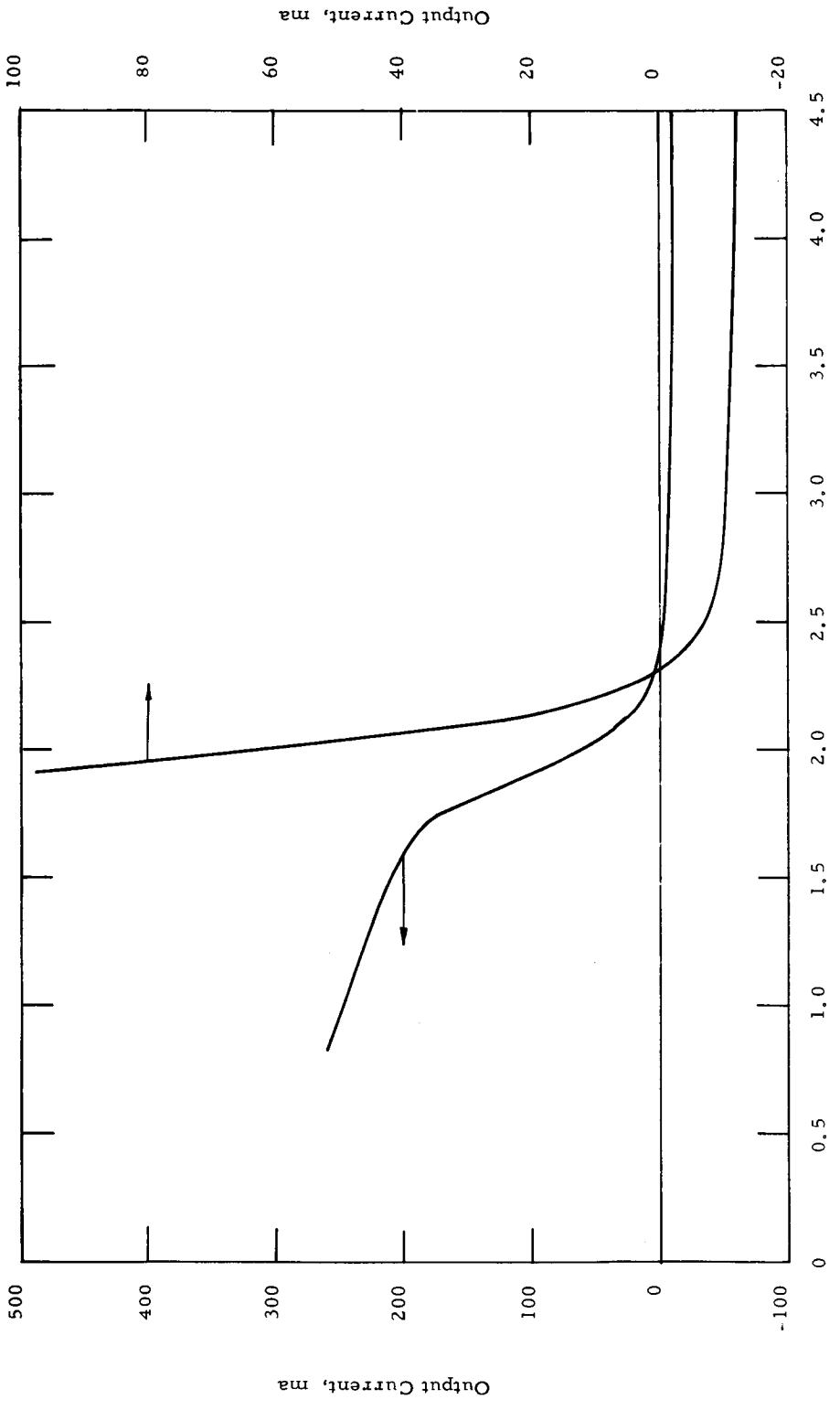

Figure 4.21(a) IV Curve Produced by an X-Y Plotter (Run No. 5)

VIII-P-2a

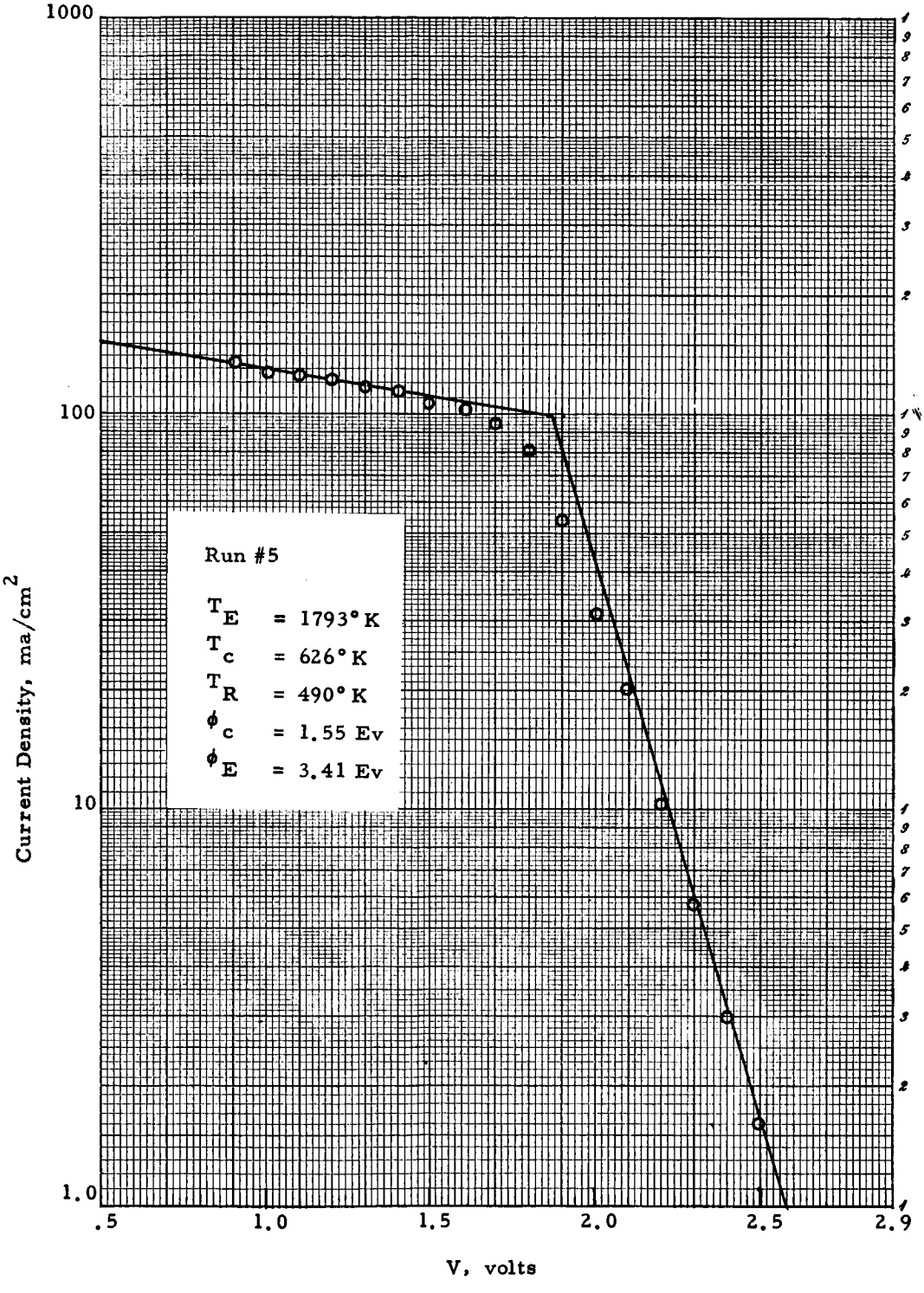

Figure 4.21(b). IV Characteristics (Run No. 5)

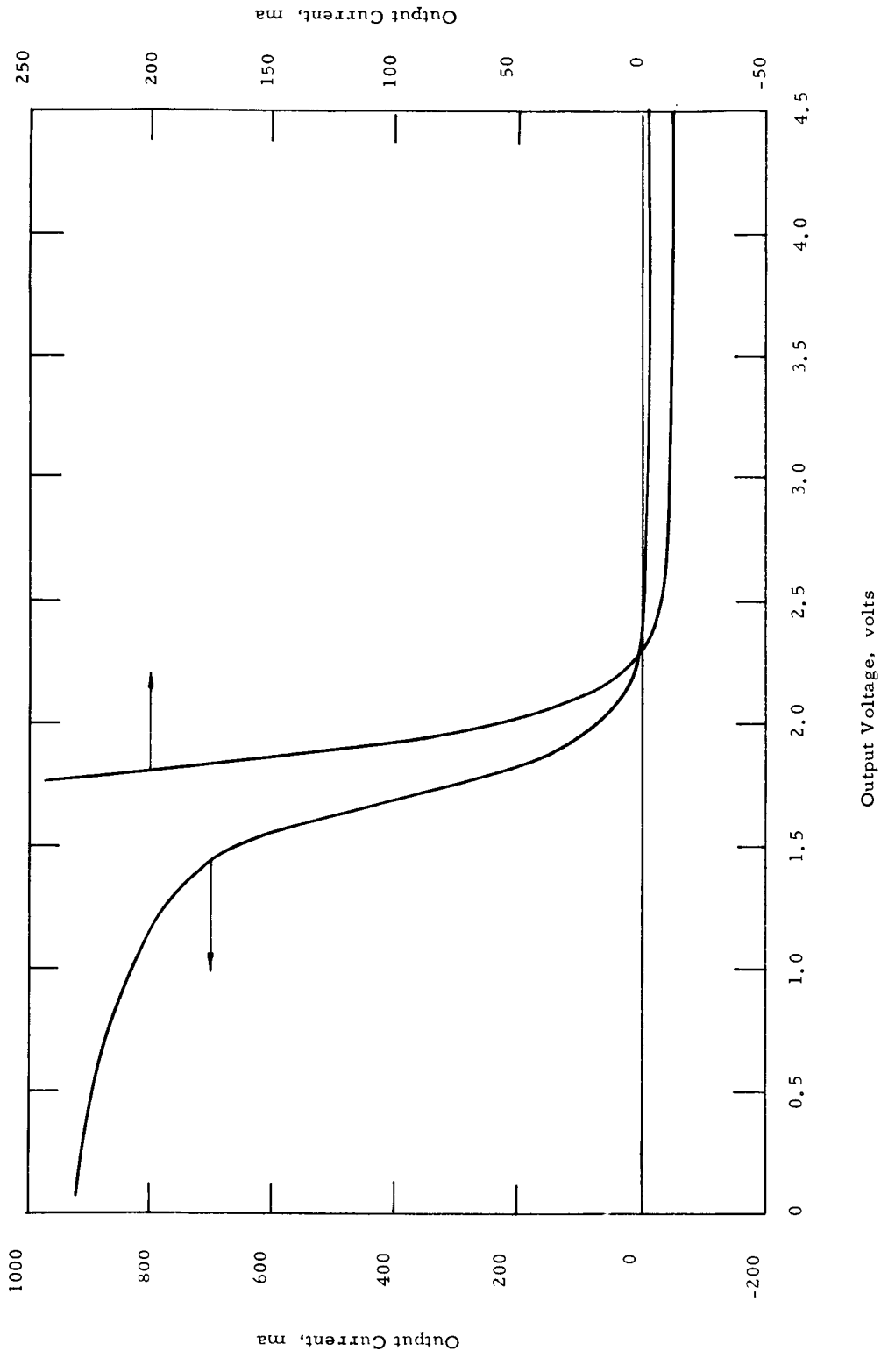

Figure 4.22(a) IV Curve Produced by an X-Y Plotter (Run No. 6)

VIII-P-2a

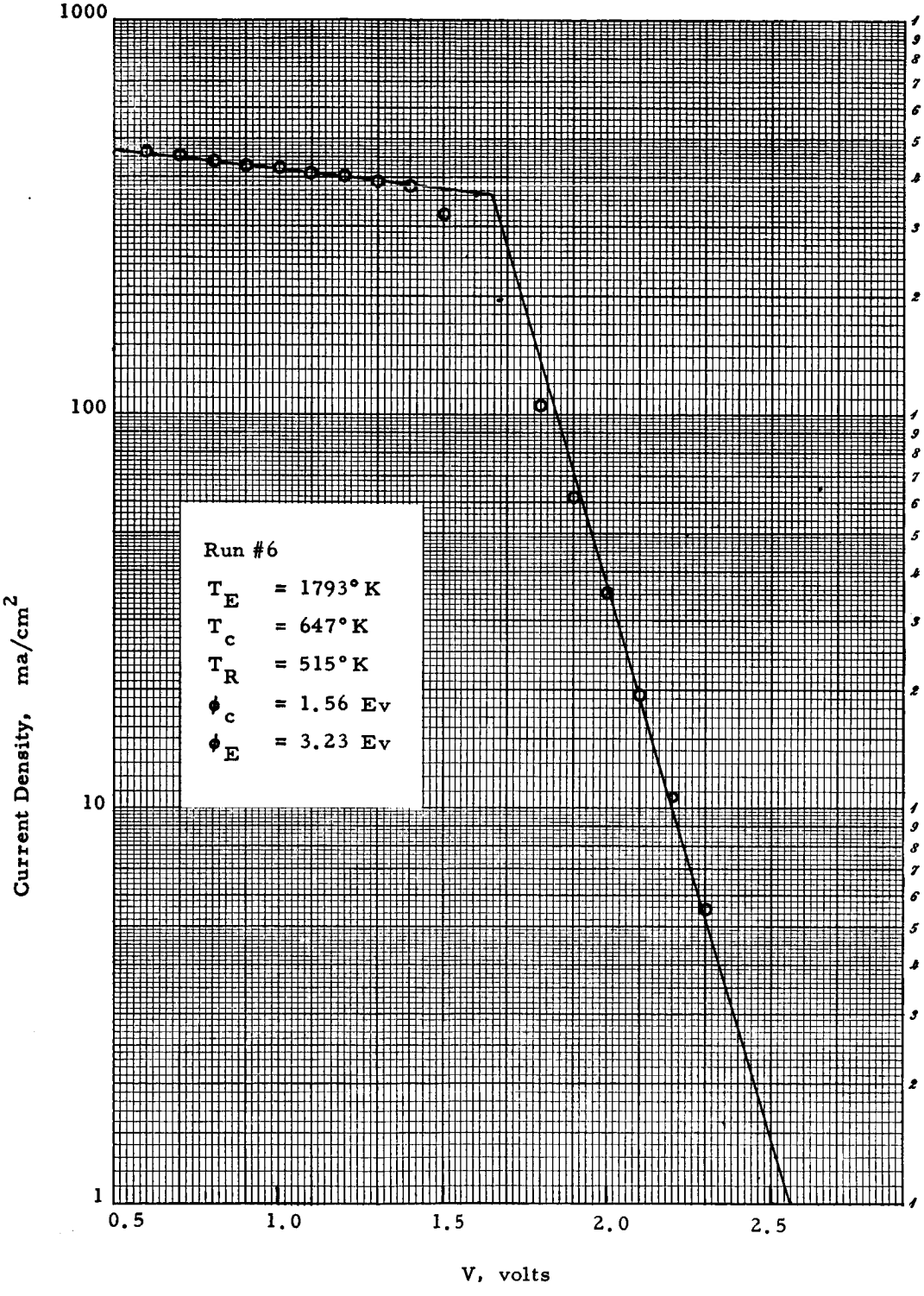

Figure 4.22(b) IV Characteristics (Run No. 6)

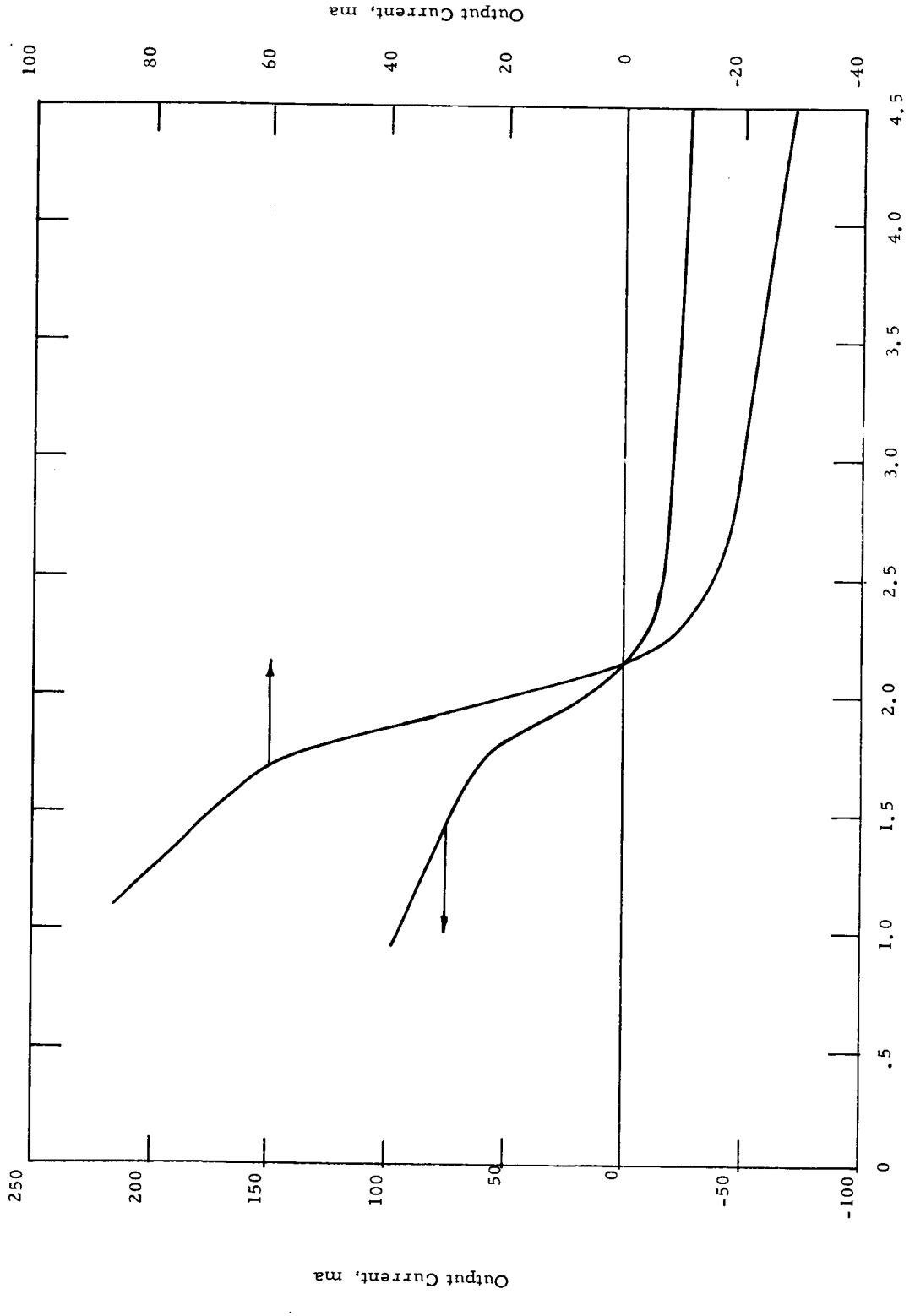

Figure 4.23(a) IV Curve Produced by an X-Y Plotter (Run No. 1)

VIII-P-2b

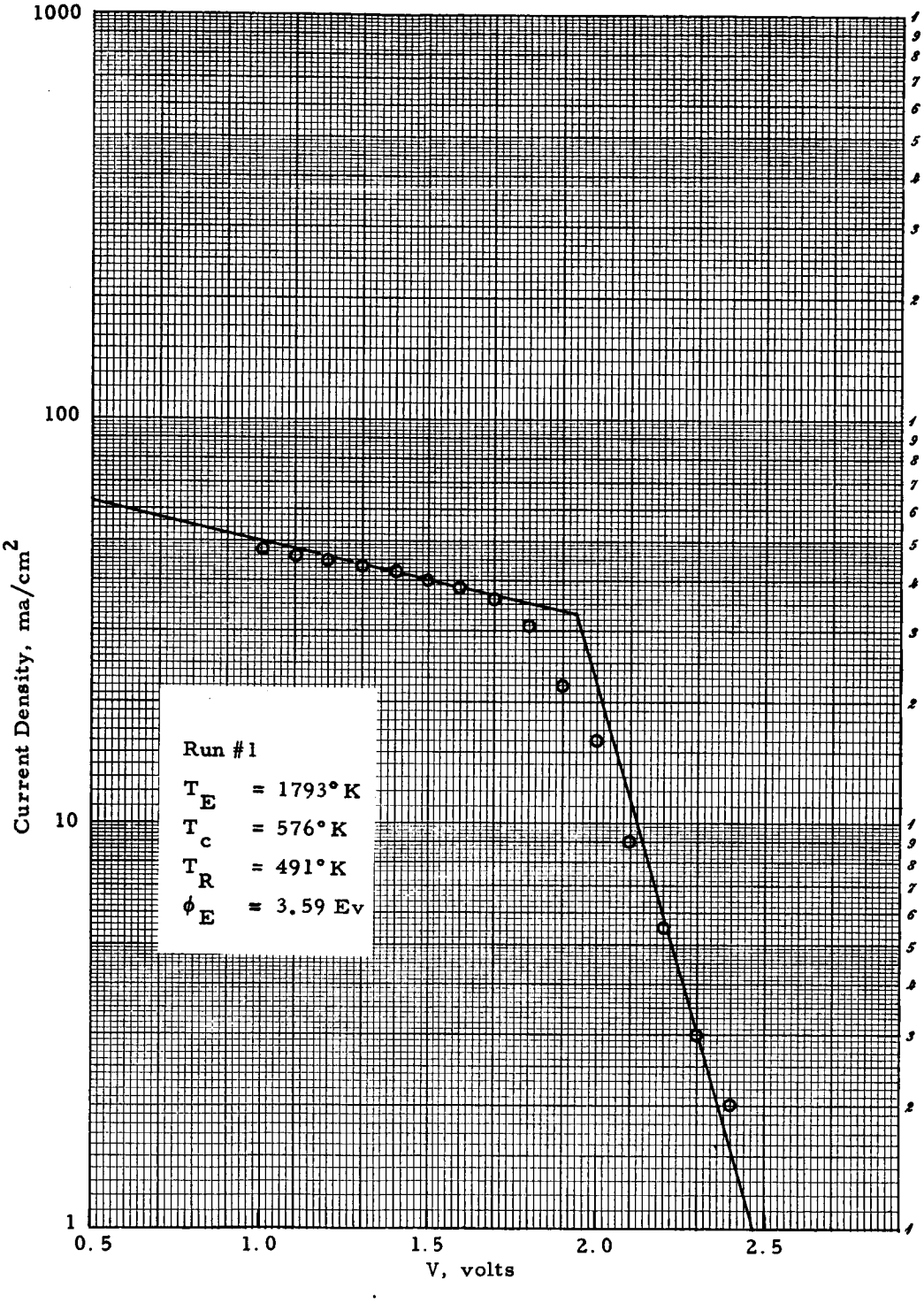

Figure 4.23(b) IV Characteristics (Run No. 1)

VIII-P-2b

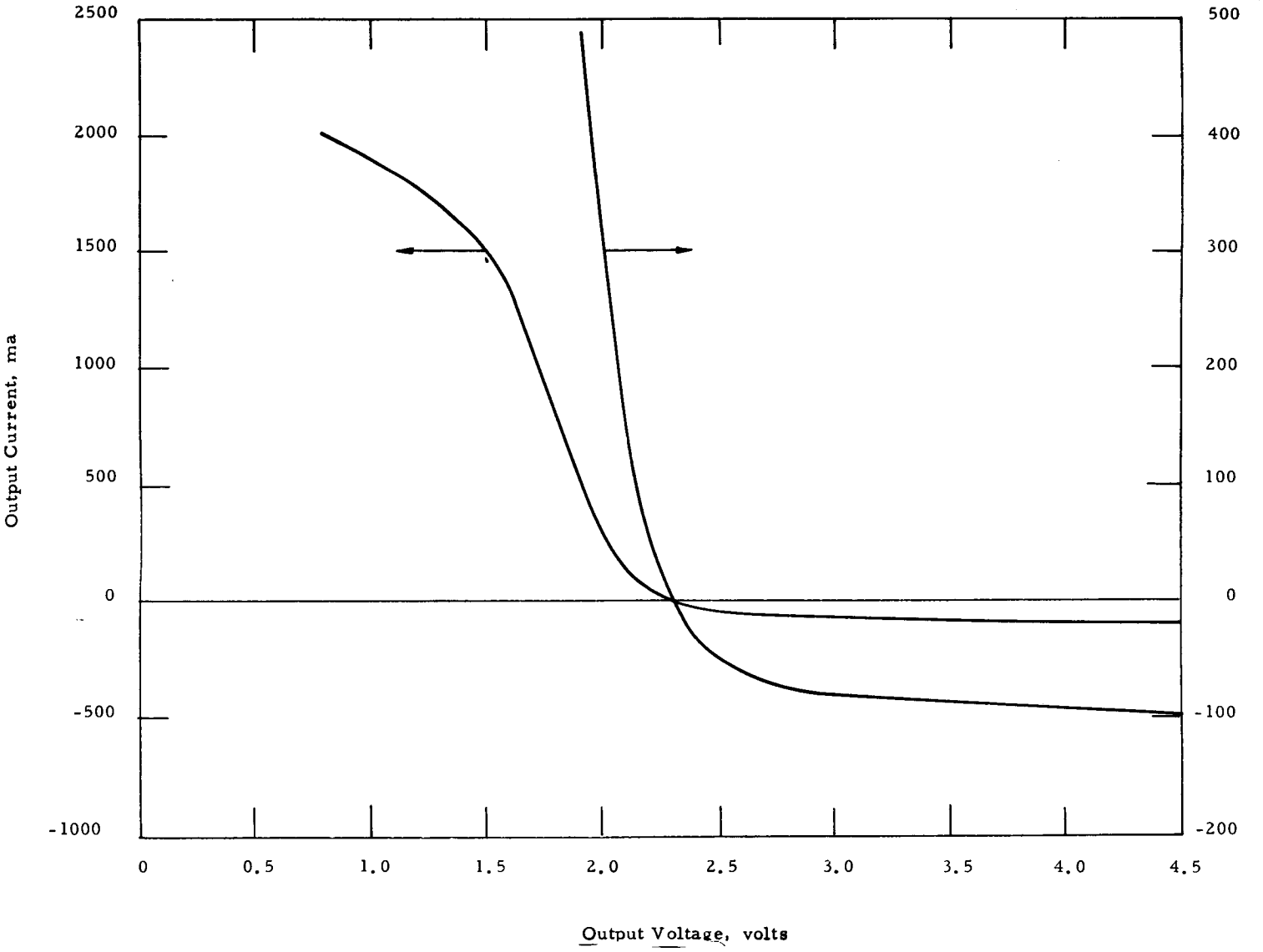

Figure 4.24(a) IV Curve Produced by an X-Y Plotter (Run No. 2)

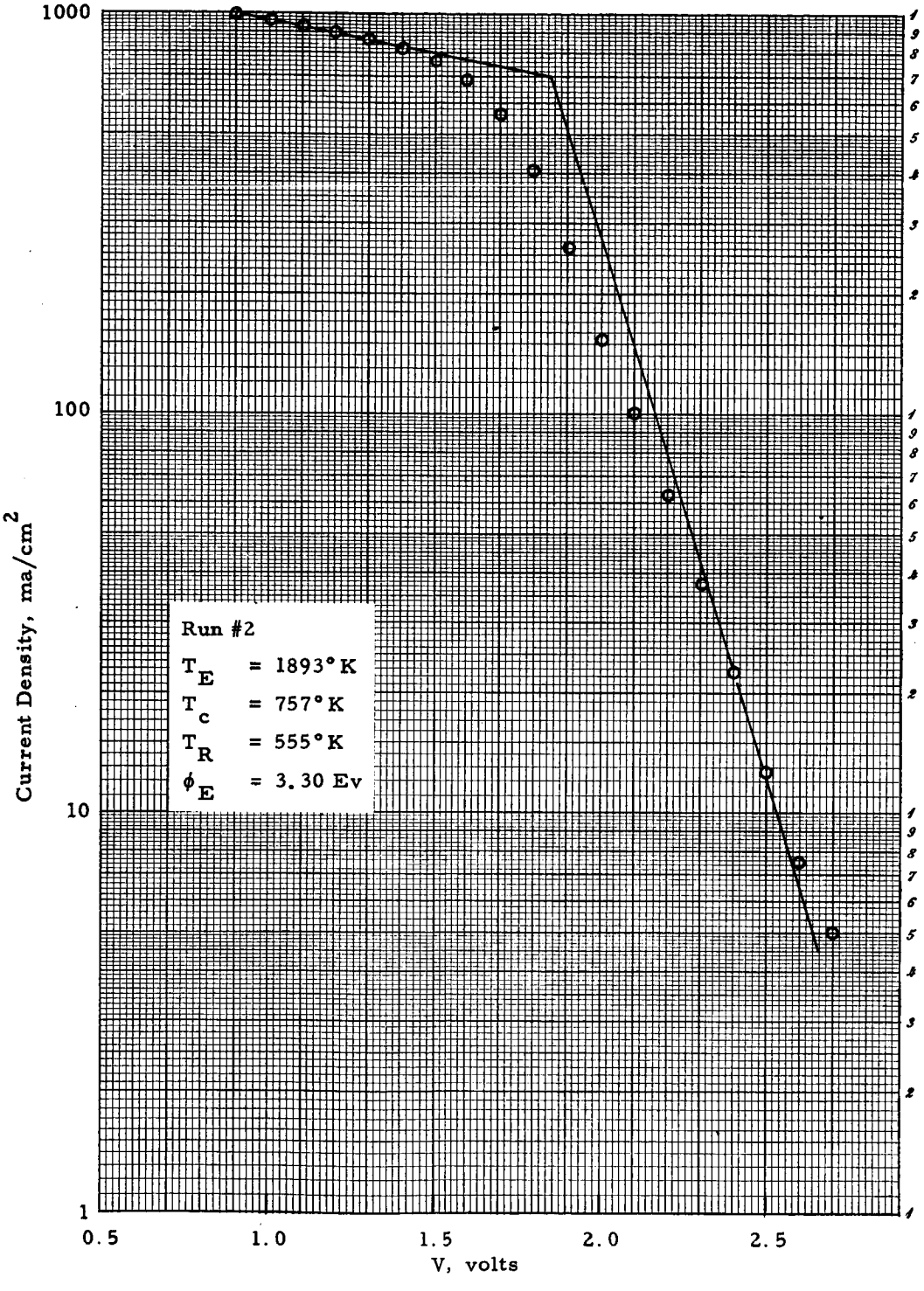

Figure 4.24(b) IV Characteristics (Run No. 2)

VIII-P-2b

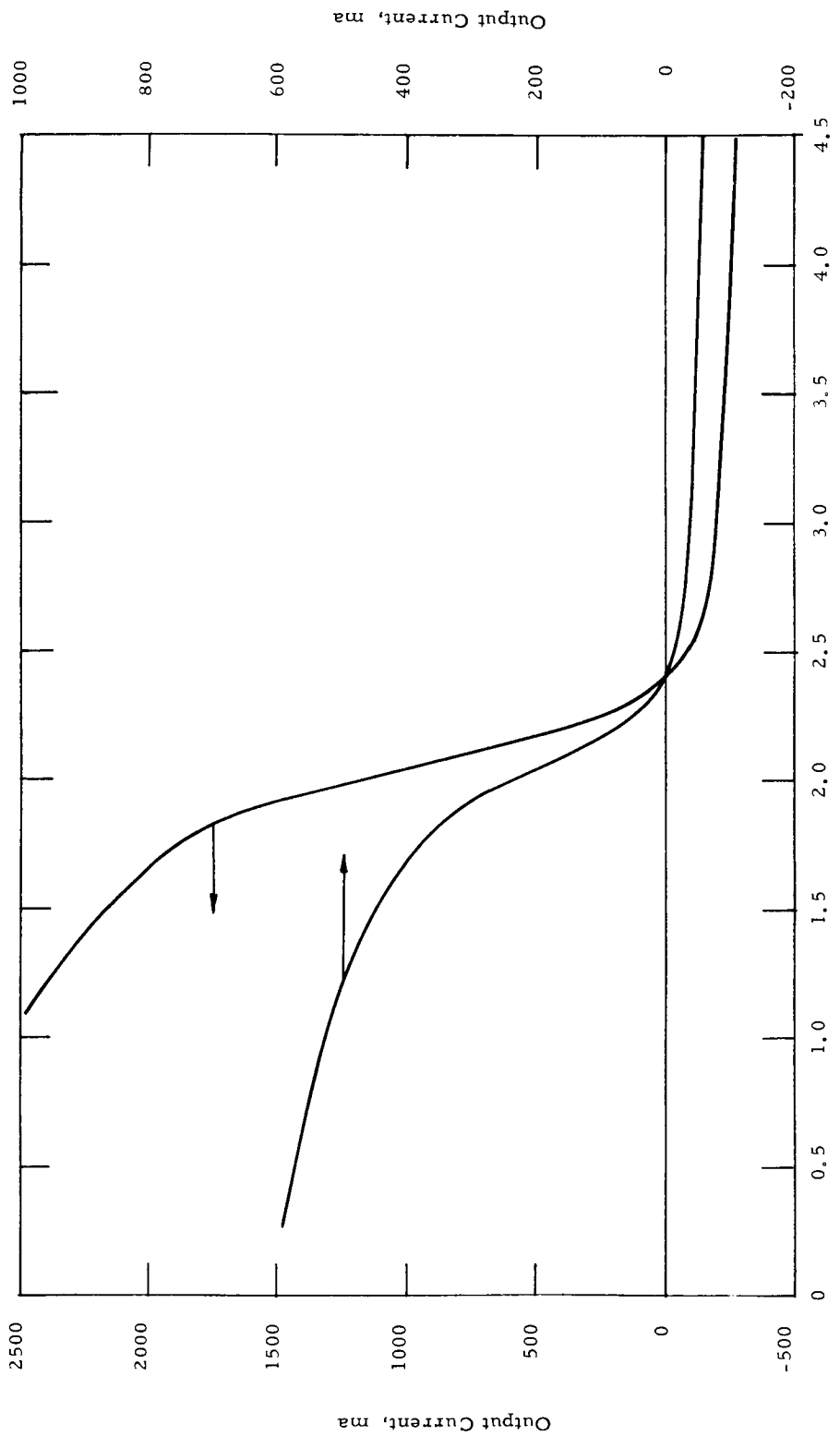

Figure 4.25(a) IV Curve Produced by an X-Y Plotter (Run No. 3)

VIII-P-2b

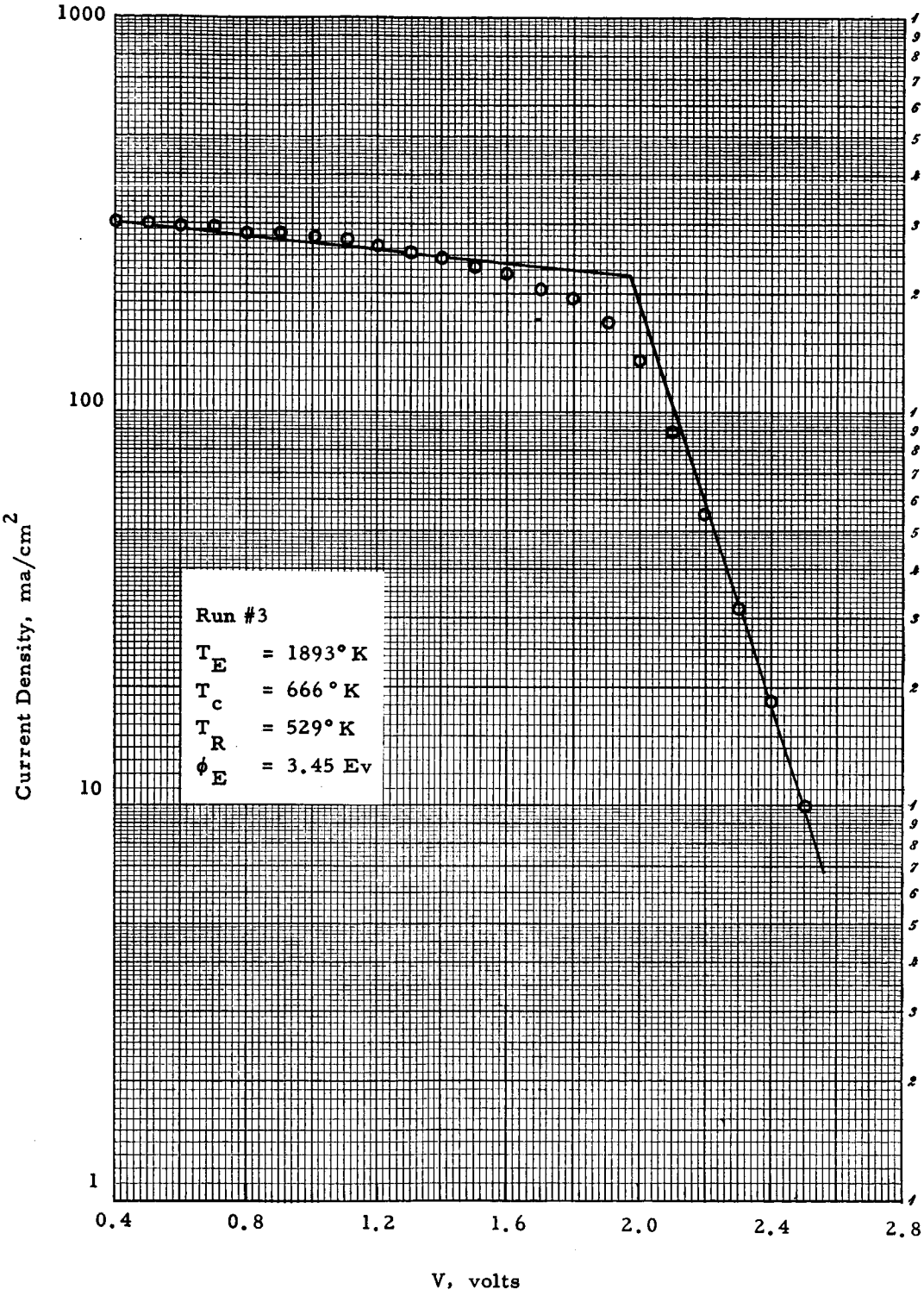

Figure 4.25(b) IV Characteristics (Run No. 3)

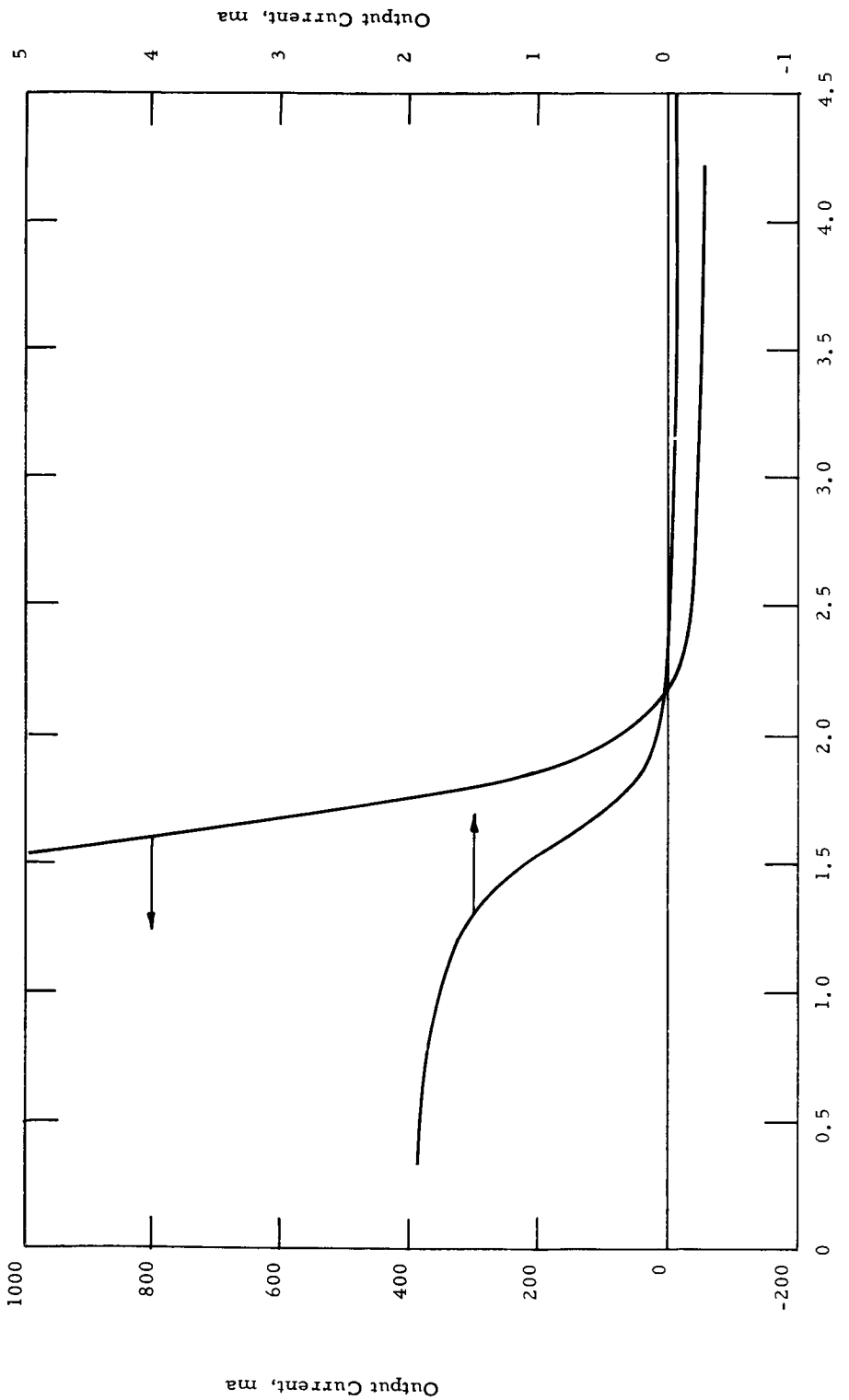

Figure 4.26(a) IV Curve Produced by an X-Y Plotter (Run No. 4)

VIII-P-2b

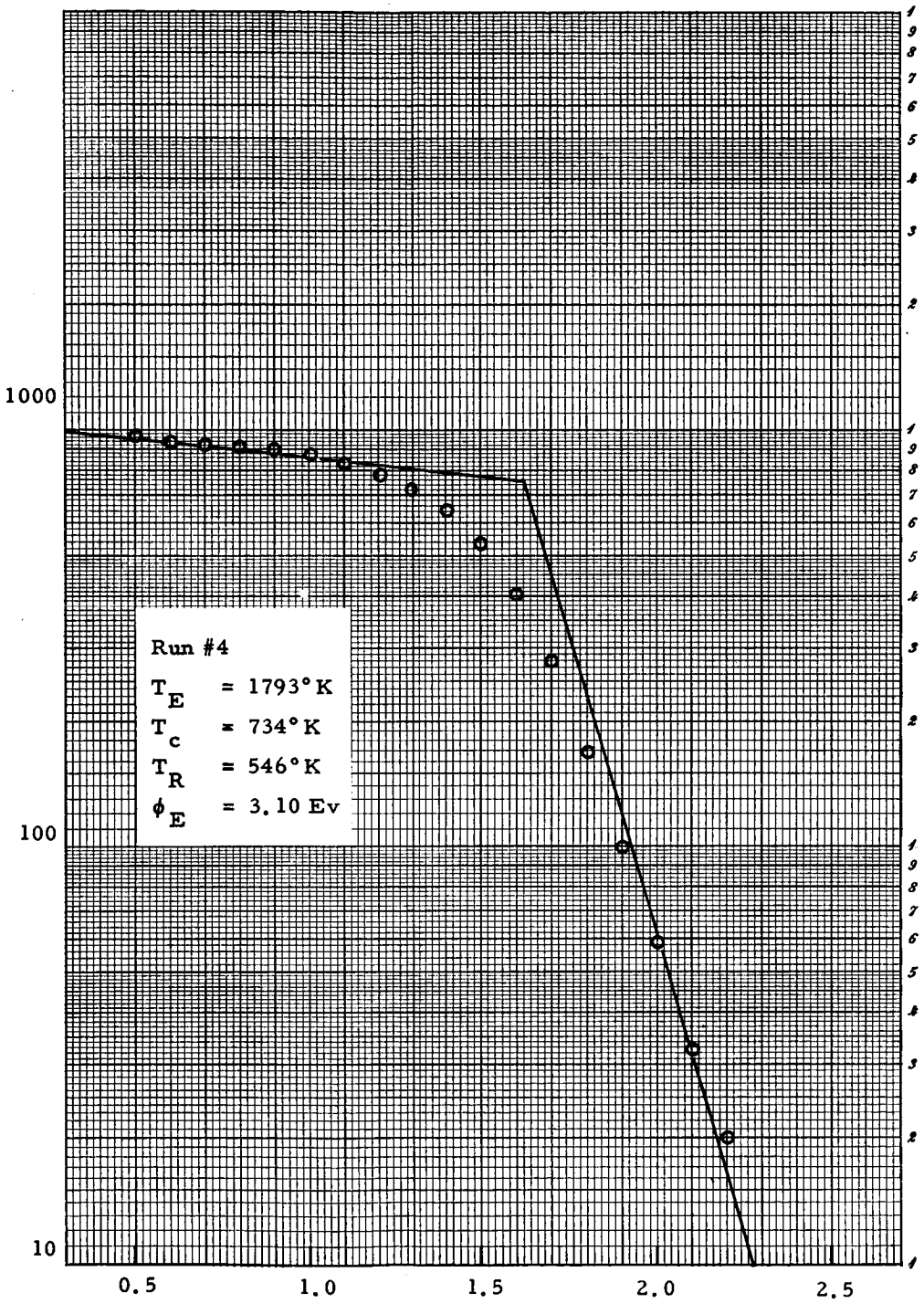

Figure 4.26(b) IV Characteristics (Run No. 4)

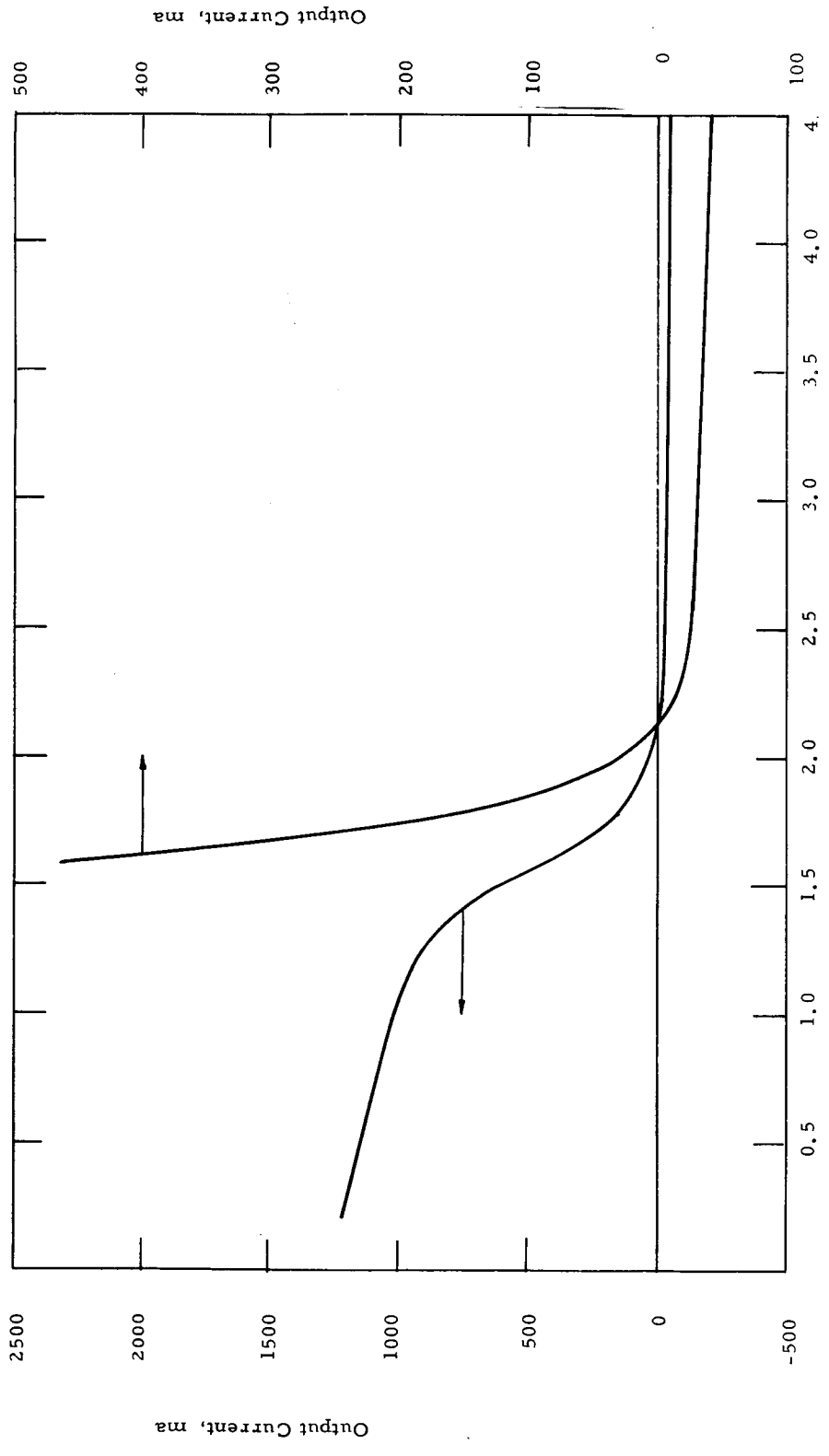

Figure 4.27(a) IV Curve Produced by an X-Y Plotter (Run No. 5)

VIII-P-2b

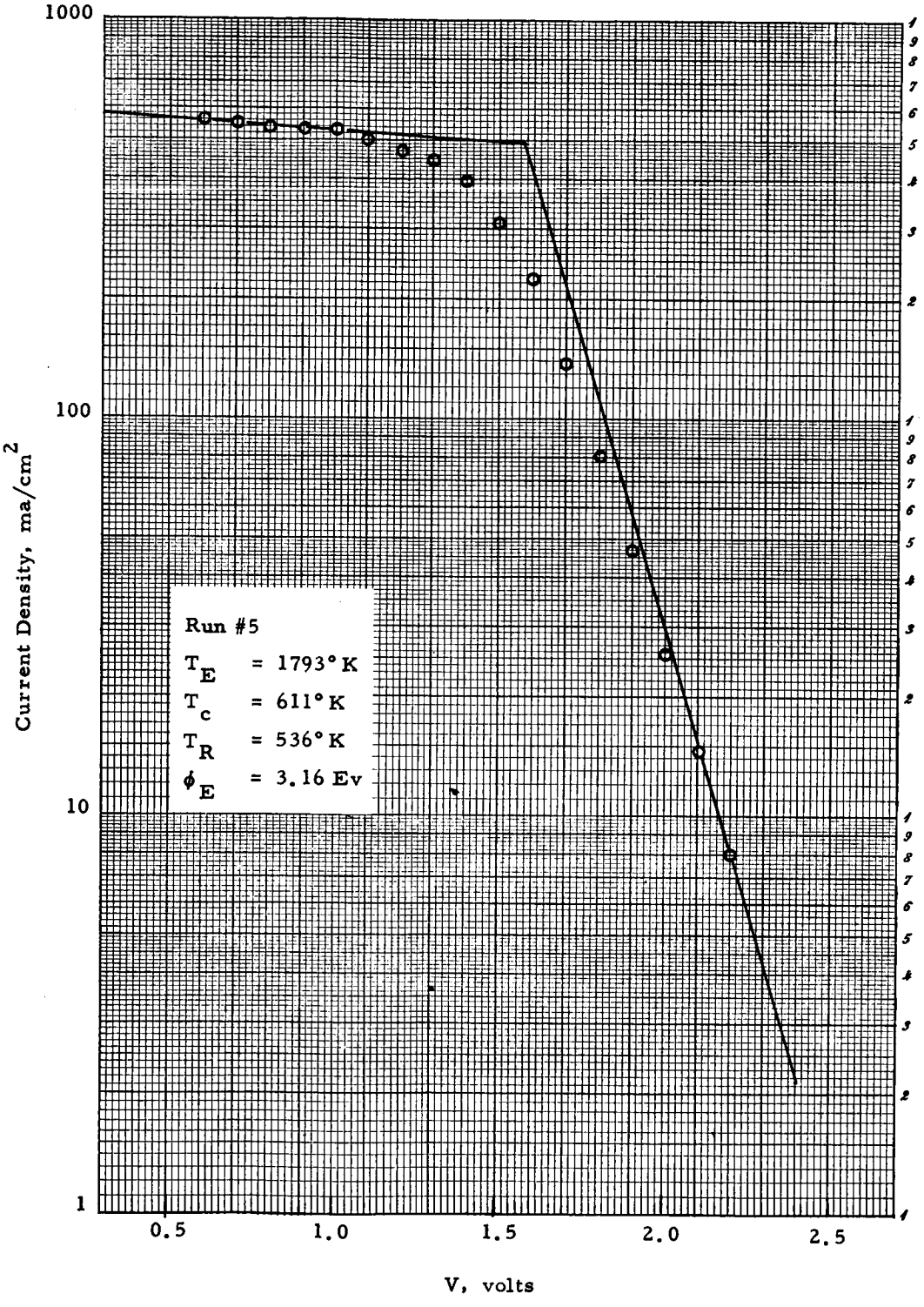

Figure 4-27(b) IV Characteristics (Run No. 5)

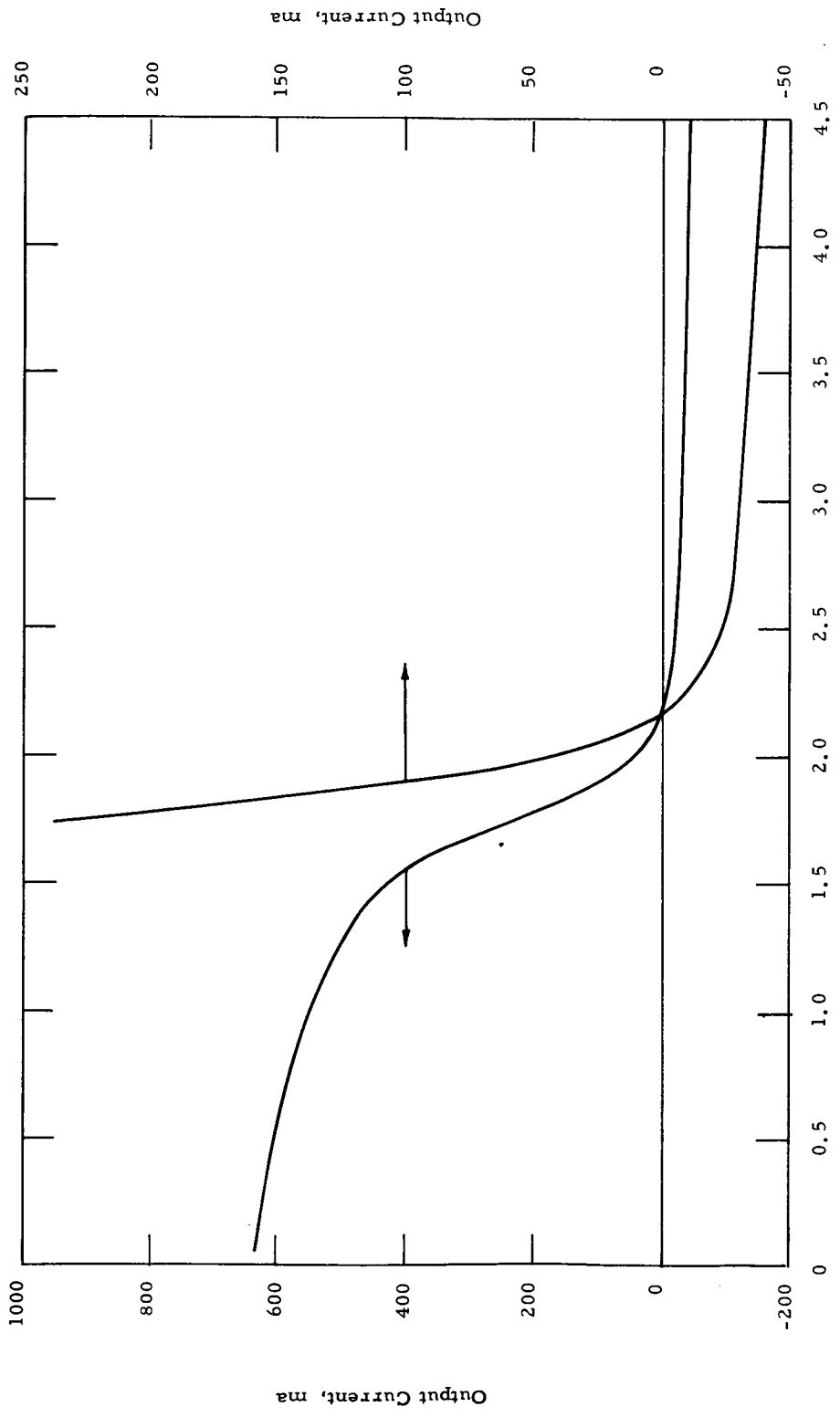

Figure 4.28(a) IV Curve Produced by an X-Y Plotter (Run No. 6)

VIII-P-2b

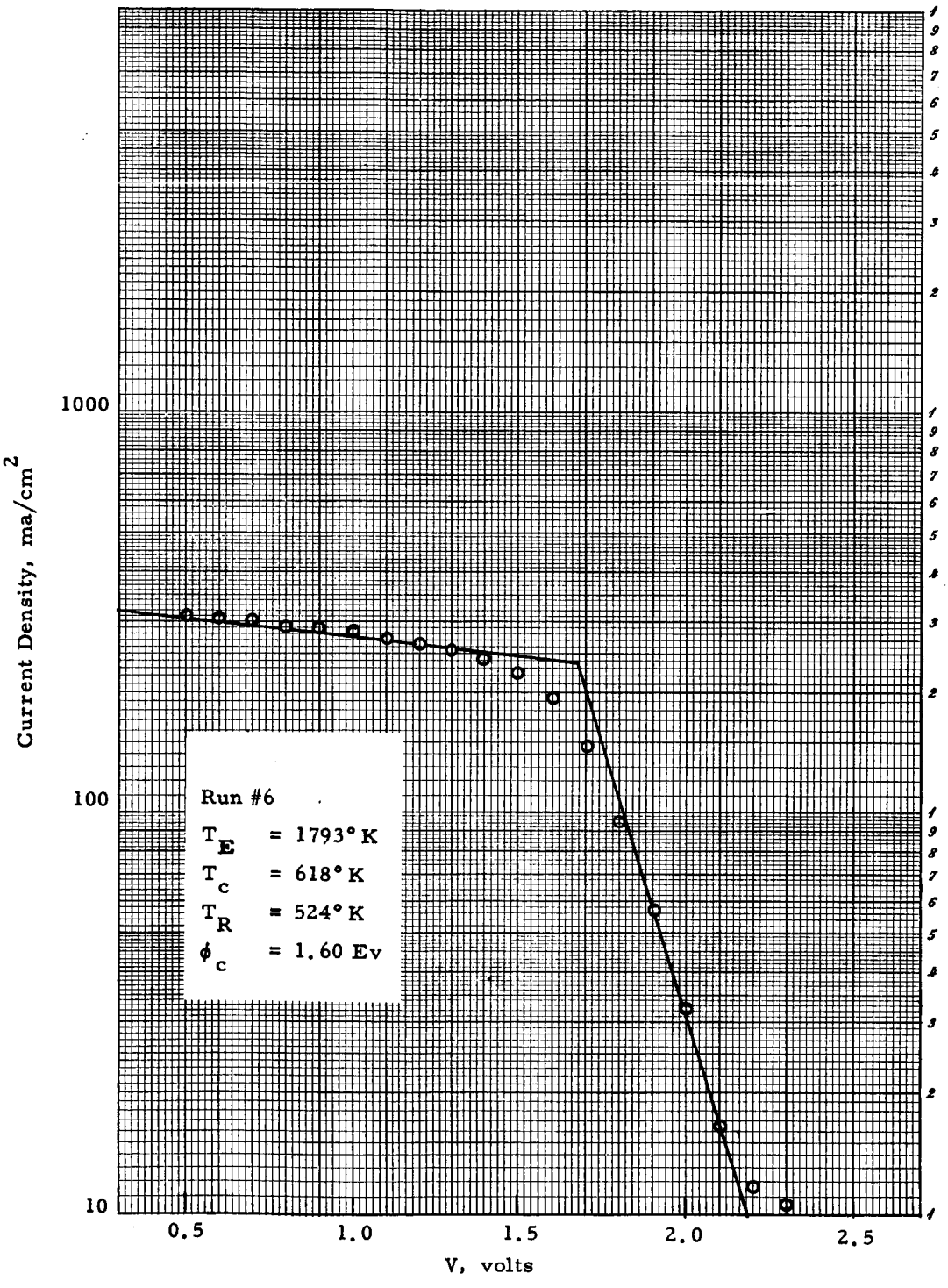

Figure 4.28(b) IV Characteristics (Run No. 6)

VIII-P-2b

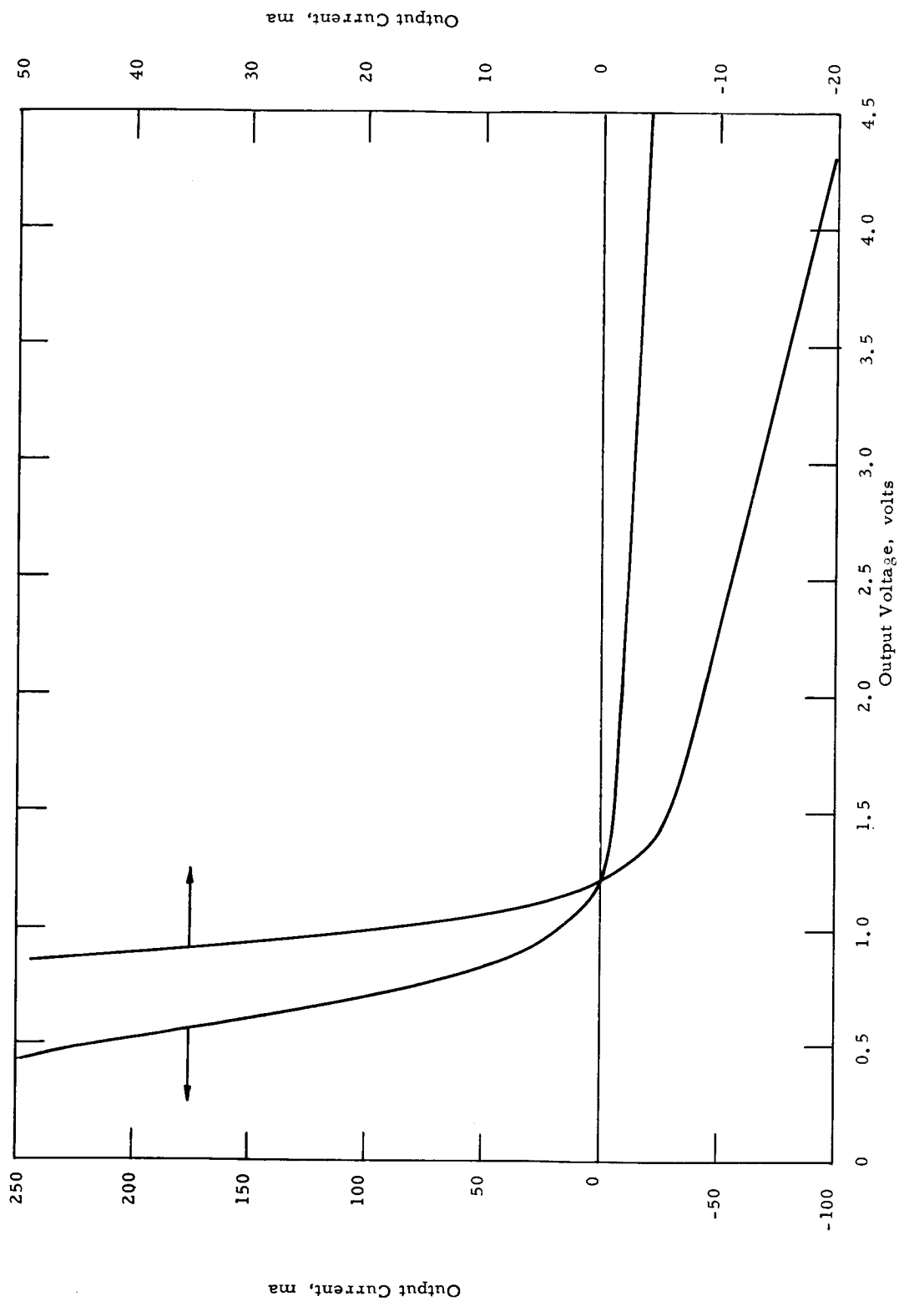

Figure 4.29(a) IV Curve Produced by an X-Y Plotter (Run No. 7)

VIII-P-2b

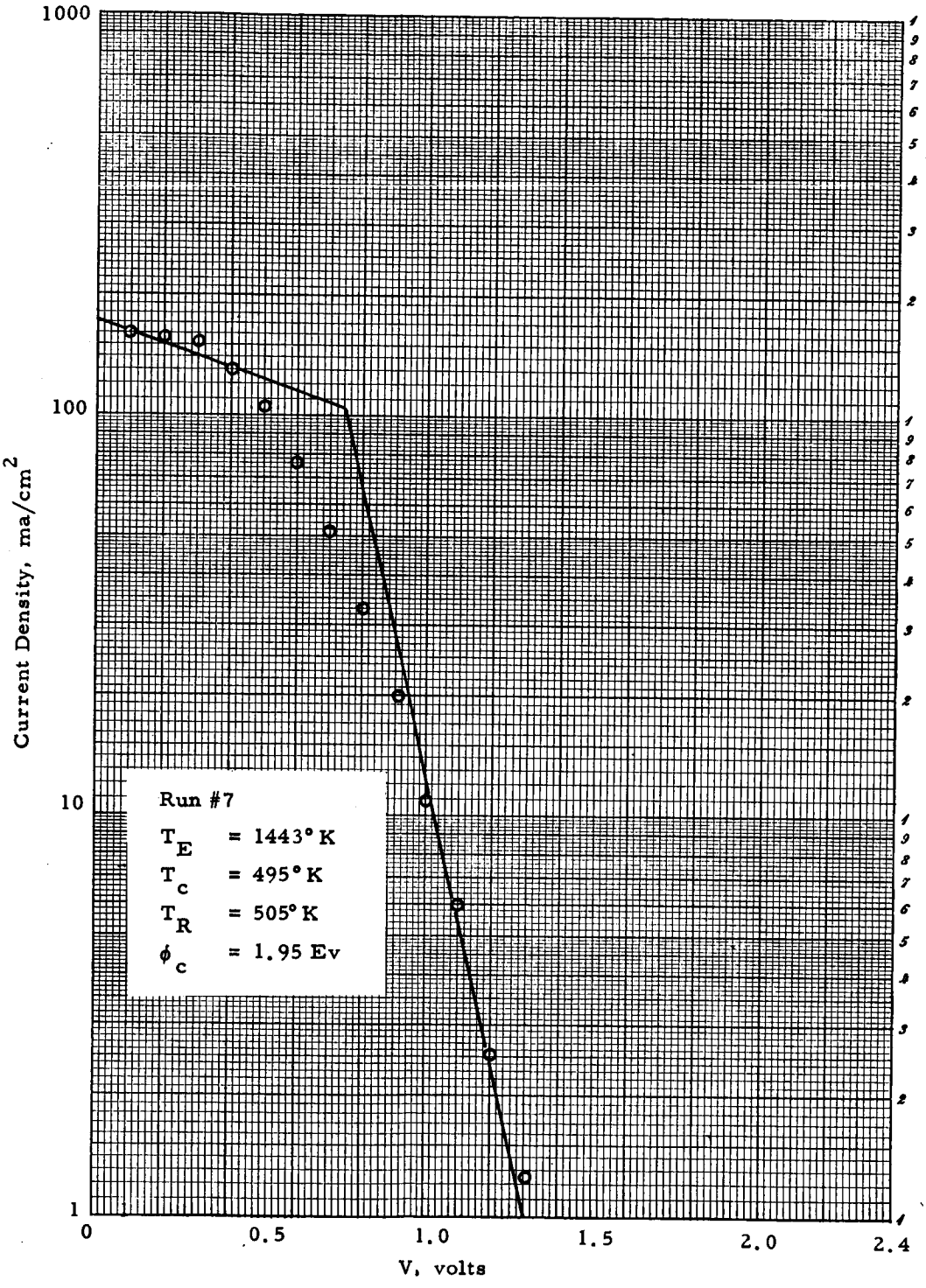

Figure 4.29(b) IV Characteristics (Run No. 7)

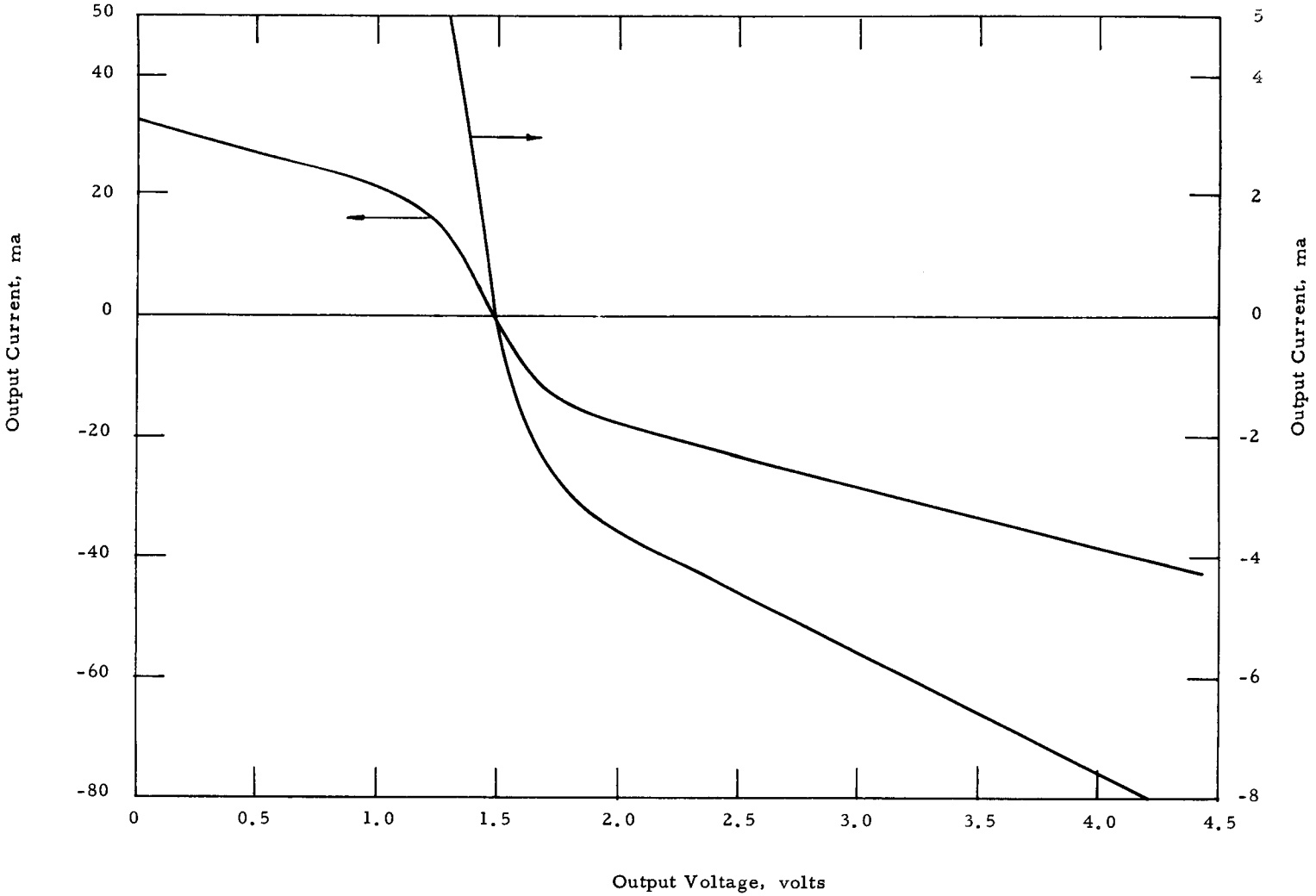

Figure 4.31(a). IV Curve Produced by an X-Y Plotter (Run No. 8)

VIII-P-2b

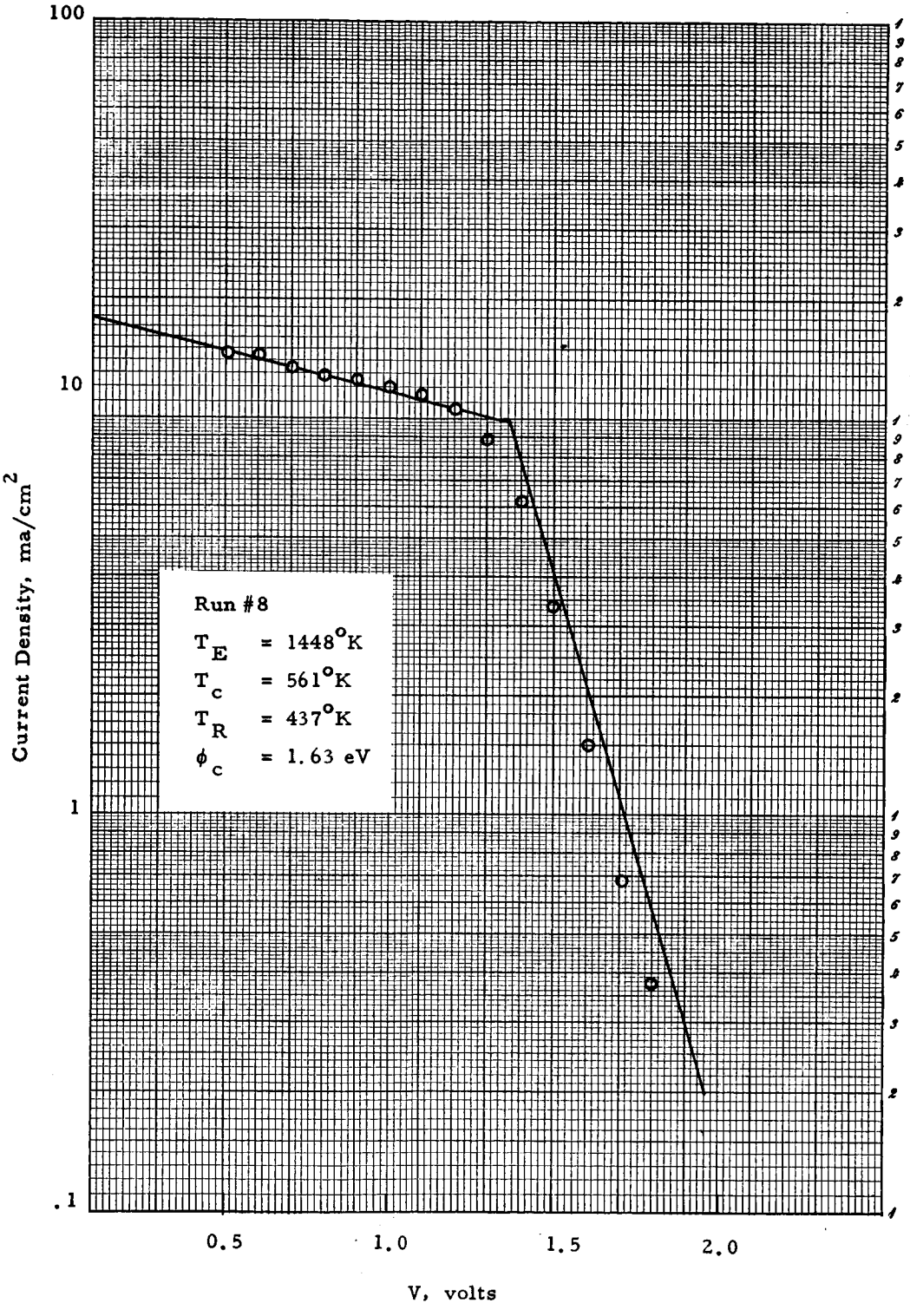

Figure 4.30(b) IV Characteristics (Run No. 8).

VIII-P-2b

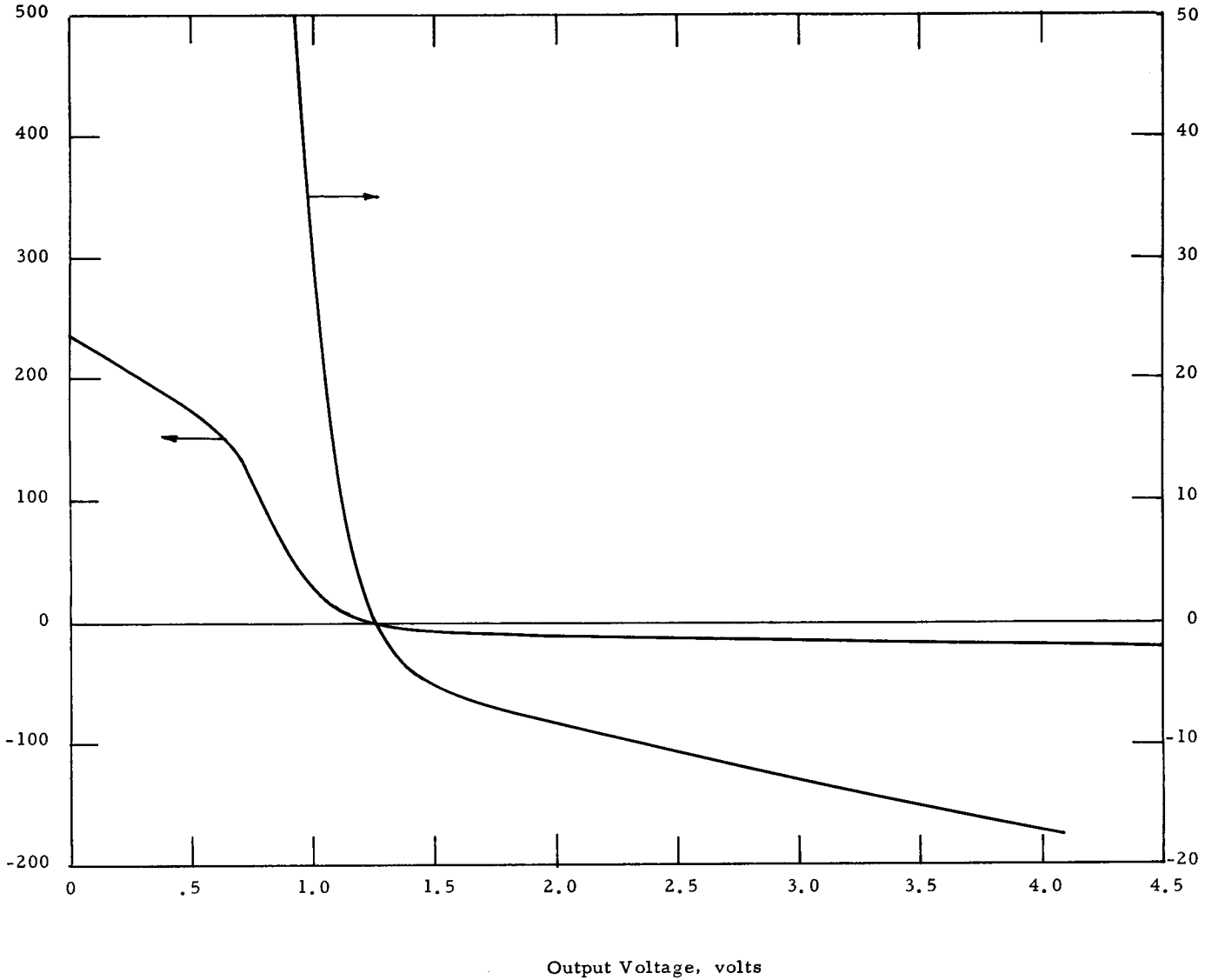

Figure 4.31(a) IV Curve Produced by an X-Y Plotter (Run No. 9)

VIII-P-2b

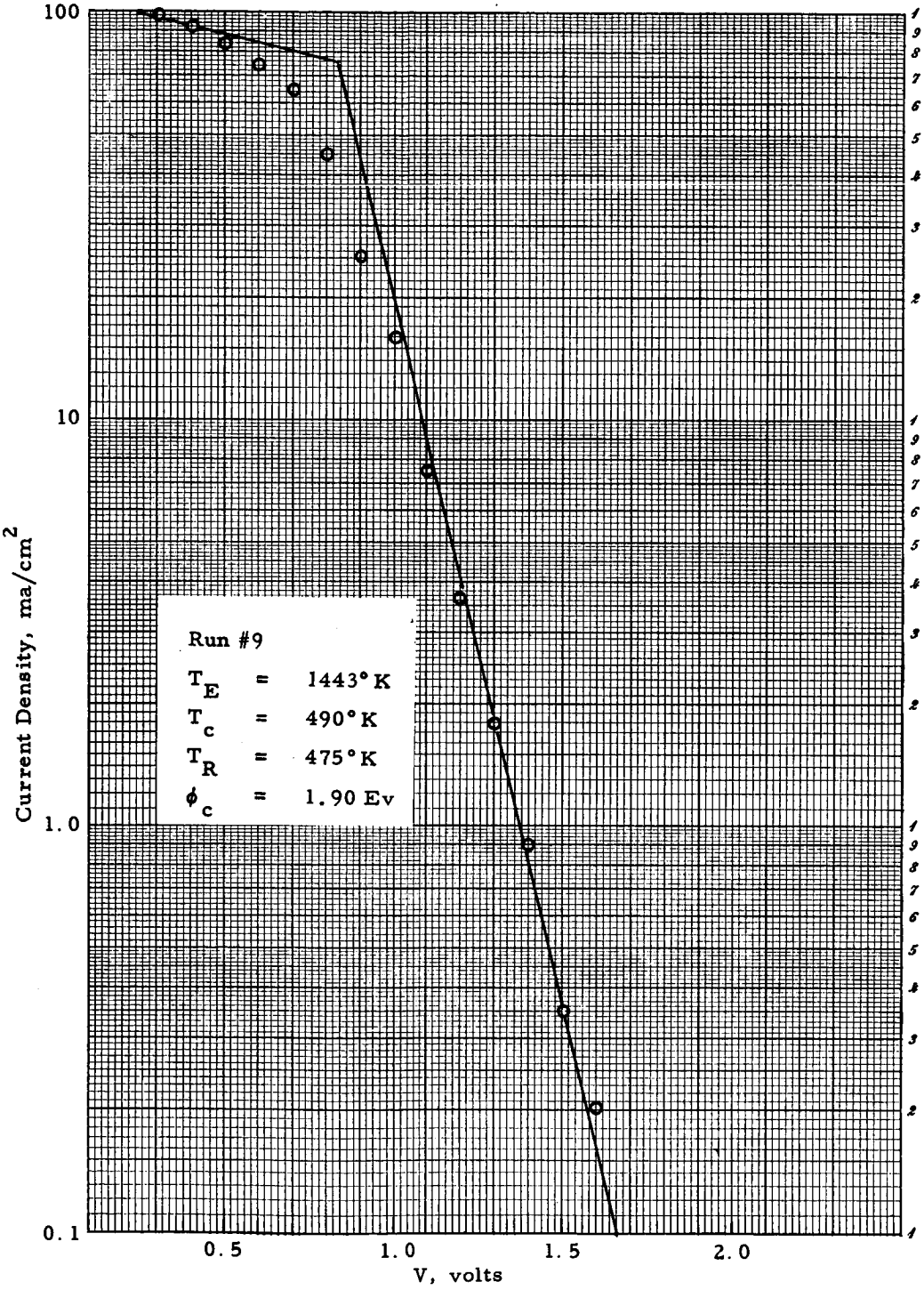

Figure 4.31(b) IV Characteristics (Run No. 9)

VIII-P-2b

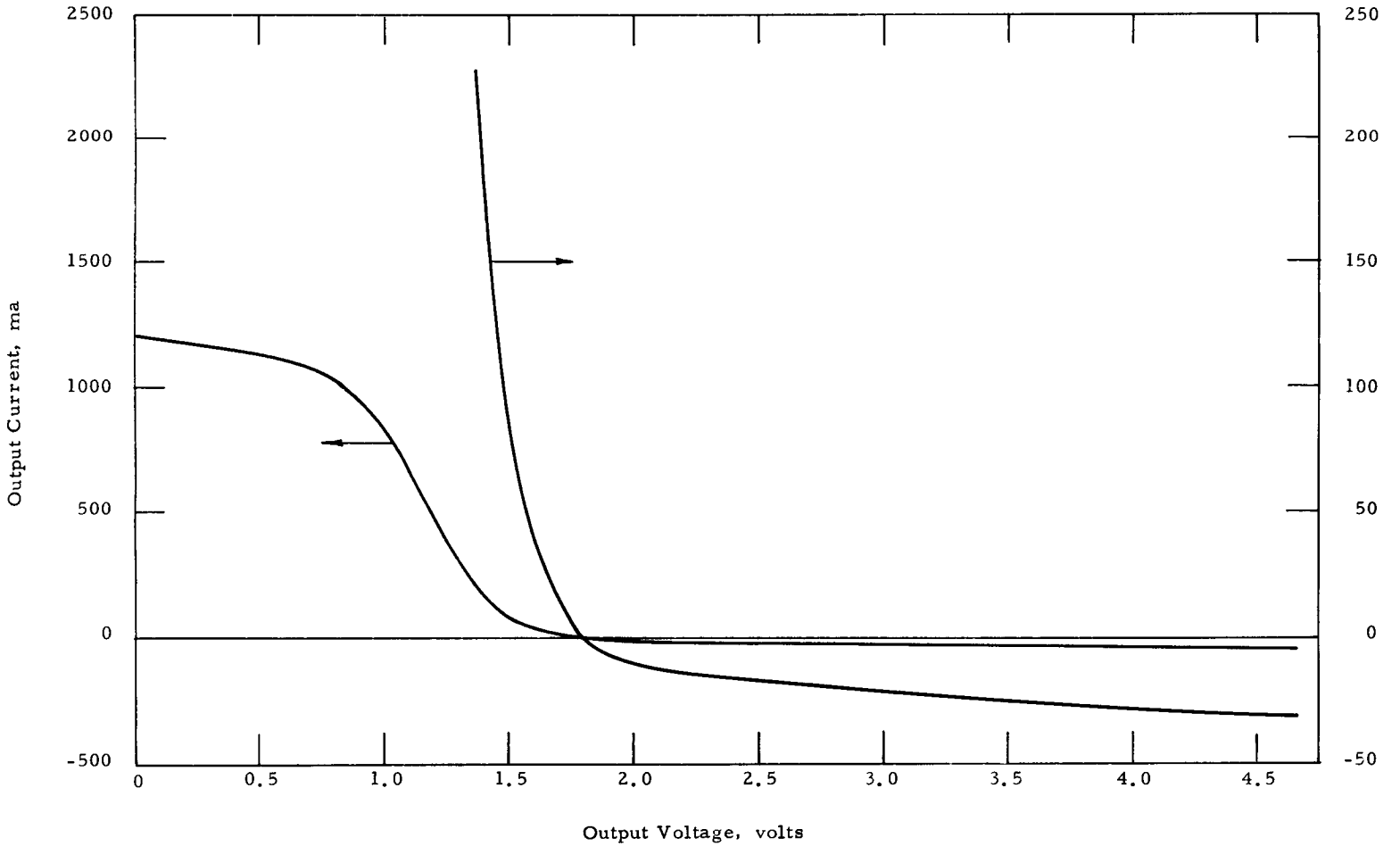

Figure 4.32(a) IV Curve Produced by an X-Y Plotter (Run No. 10)

VIII-P-2b

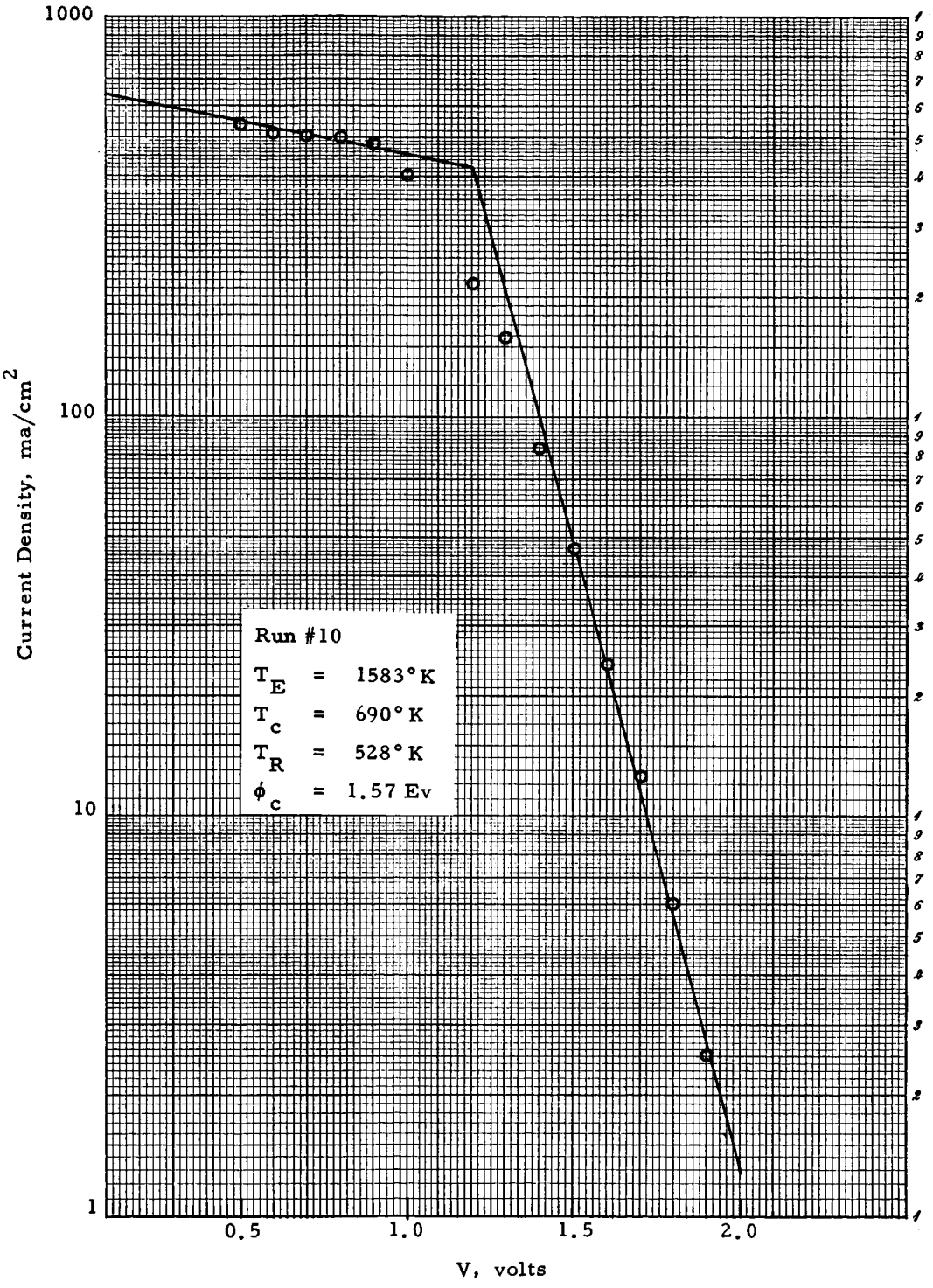

Figure 4.32(b) IV Characterisitcs (Run No. 10)

The X-Y and semi-log plots for runs 1 through 6 and 1 through 10 for VIII-P-2a and VIII-P-2b are shown in Figures 4.17 (a) and (b) through Figures 4.32 (a) and (b).

Figure 4.33 shows the collector work functions of VIII-P-1, VIII-P-2a, and VIII-P-2b plotted versus research data. Figure 4.34 shows the emitter work function of VIII-P-2b plotted on a "Rasor" plot.

The agreement of collector work function among converters and with other data for molybdenum was good. Because these converters were designed for specific equilibrium collector and cesium reservoir temperatures, the T_C/T_R range covered was fairly limited even when external cooling was added.

The data listed for VIII-P-2b in Figure 4.34 falls between the theoretical curves for 4.5 and 5.0 eV bare work function. From the limited data, it appeared that the emitter's bare work function was lower than for typical rhenium, which has a reported value of 4.9 eV.*

*Thermionic Conversion Specialist Conference, Cleveland, Ohio, October 1964. "Test Results of Solar Thermionic Converters Using Rhenium Emitters," S. Merra, Thermo Electron Corporation. Work performed for JPL, sponsored by NASA, under contract No. NAS7-100.

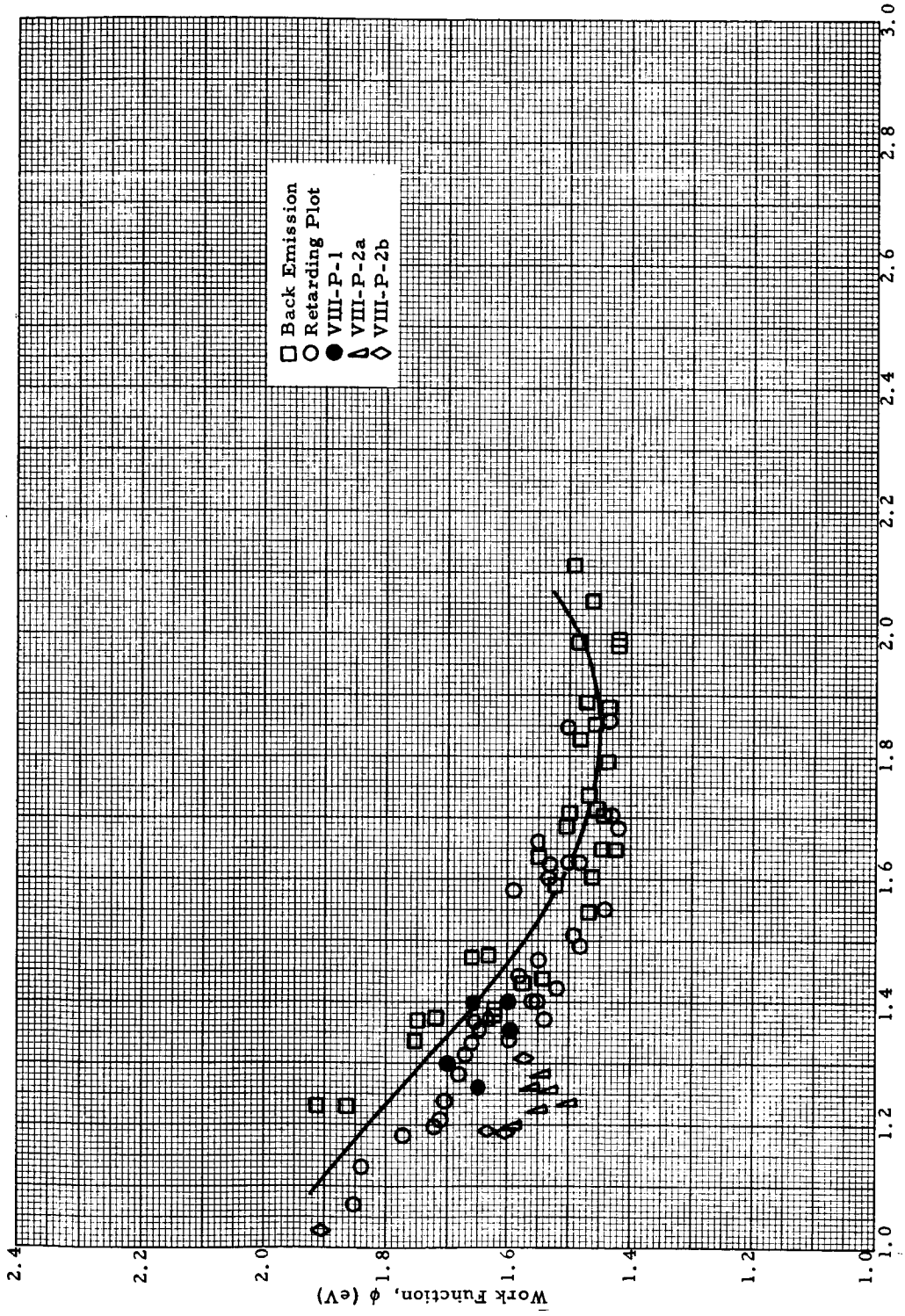

Figure 4.33 Molybdenum Collector Work Function of VIII-P-1, VIII-P-2a and VIII-P-2b versus T_C/T_R

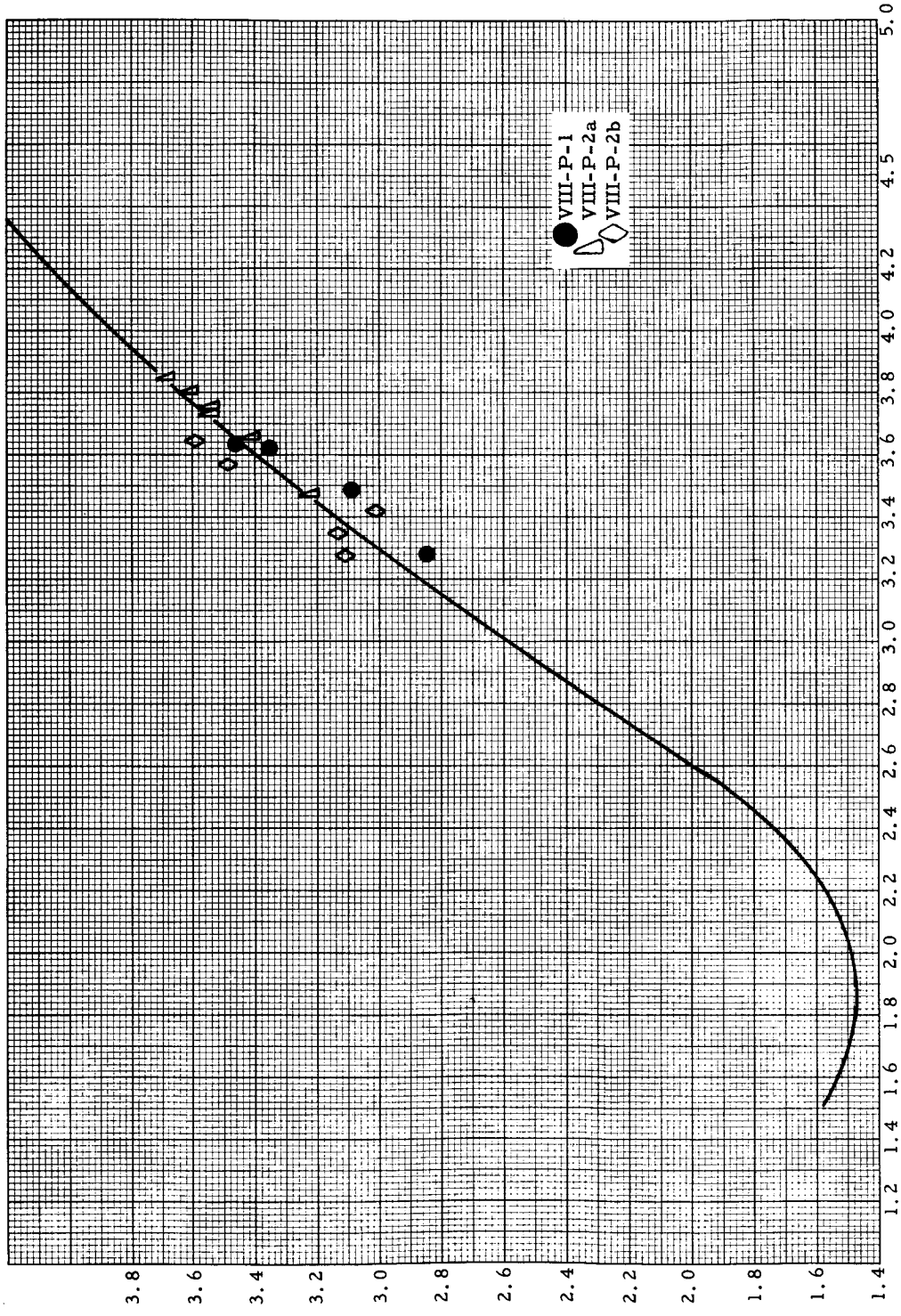

Figure 4.34 Rhenium Emitter Work Function of VIII-P-1, VIII-P-2a and VIII-P-2b versus T_c/T_R

CHAPTER 5

PROTOTYPE VIII-P-3

5.1 DESIGN AND COMPONENT TESTING

5.1.1 Radiator

As described in Chapter 4, prototype diodes VIII-P-2a and VIII-P-2b were constructed with much larger radiators than diode VIII-P-1. Figure 5.1 shows diode VIII-P-1, and Figure 5.2 shows diode VIII-P-2. Dynamic testing of VIII-P-1 established the optimum collector temperature at output voltages between 0.6 and 1 volt. These optima can be seen in Figure 5.3. Diode VIII-P-2 was then designed with ample radiating surface to achieve, without additional heating or cooling, the optimum collector temperature at the 0.7-volt and 29-A/cm^2 condition. The resulting collector temperature achieved by diode VIII-P-2a can be seen in Figure 5.4. For comparison, Figure 5.5 shows the optimum collector temperature of diode VIII-P-2a at several points on its optimized I-V curve. Figure 5.3 shows that the desired collector temperature at 0.7 volt output was 960°K (687°C). Figure 5.4 shows that diode VIII-P-2a reached a thermal balance with its collector at 688°C; consequently the radiator surface area and shape were chosen correctly. Furthermore, Figure 5.5 shows that VIII-P-2a produced maximum power output at a collector temperature of 690°C, which compares very closely with the optimum temperature determined from VIII-P-1, showing that both diodes produced comparable performance and that the method of determining the optima in VIII-P-1, using dynamic testing, was valid and useful.

Because generator calculations, shown later, predicted maximum generator efficiency at a diode voltage of 0.9 volt, the decision was made to optimize at that point and thus reduce the size and weight of the radiator.

To support analytical calculations for the collector-radiator, the following procedure was followed:

1. From VIII-P-2a data and from data obtained by Thermo Electron's Research Department, the heat flow through the collector and into the radiator was calculated over a range of output voltages. The results are shown in Table 5-1.

2. A collector-radiator subassembly of the VIII-P-3 type was constructed and was set up in a bell jar in such a way that heat could be applied to the collector with an electron-bombardment heater. The assembly was instrumented with thermocouples at several points on the collector and radiator.

3. Applying the heat flows calculated in 1, the thermocouple readings were recorded and compared with temperature measurements that had been made on diode VIII-P-2a. If the same temperatures were observed at the same heat flows, the subassembly test was assumed valid.

4. Based on the results in 3 above, another design iteration of the VIII-P-3 radiator was made.

After calculating the heat flows, an instrumented VIII-P-3 type of collector-radiator assembly was constructed. This is shown on the right in Figure 5.6. The radiator had several thermocouples

5648

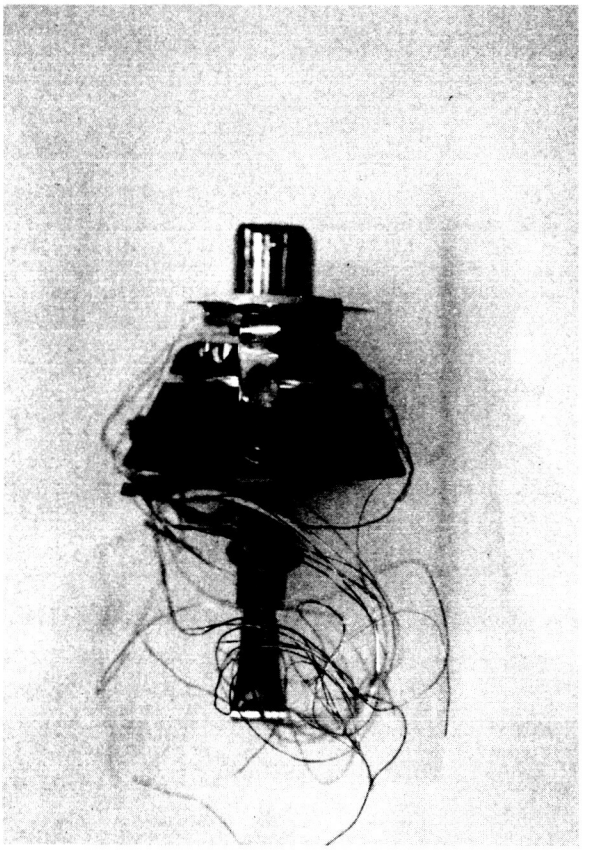

Figure 5.1 Diode VIII-P-1

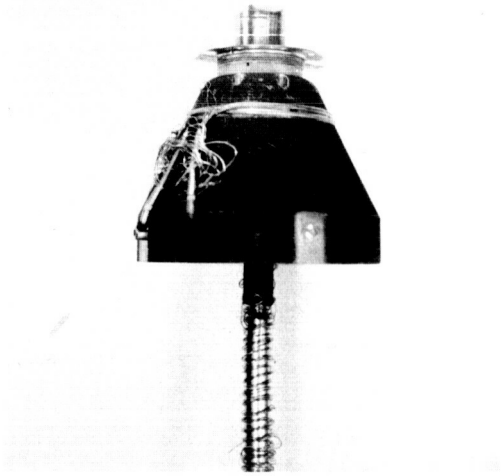

Figure 5.2 Diode VIII-P-2

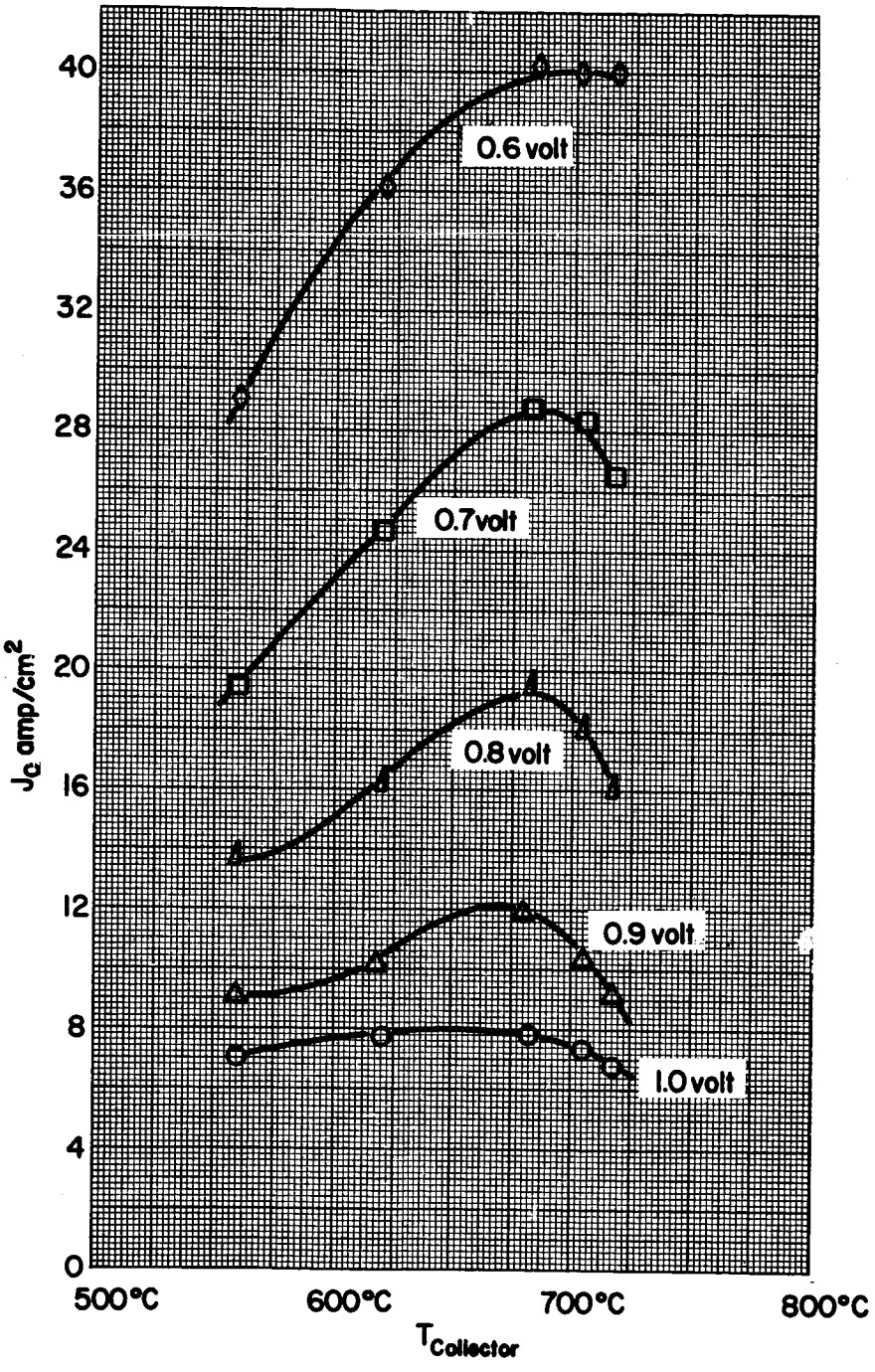

Figure 5.3 Current Density (J_o) versus Collector Temperature at Different Voltages.

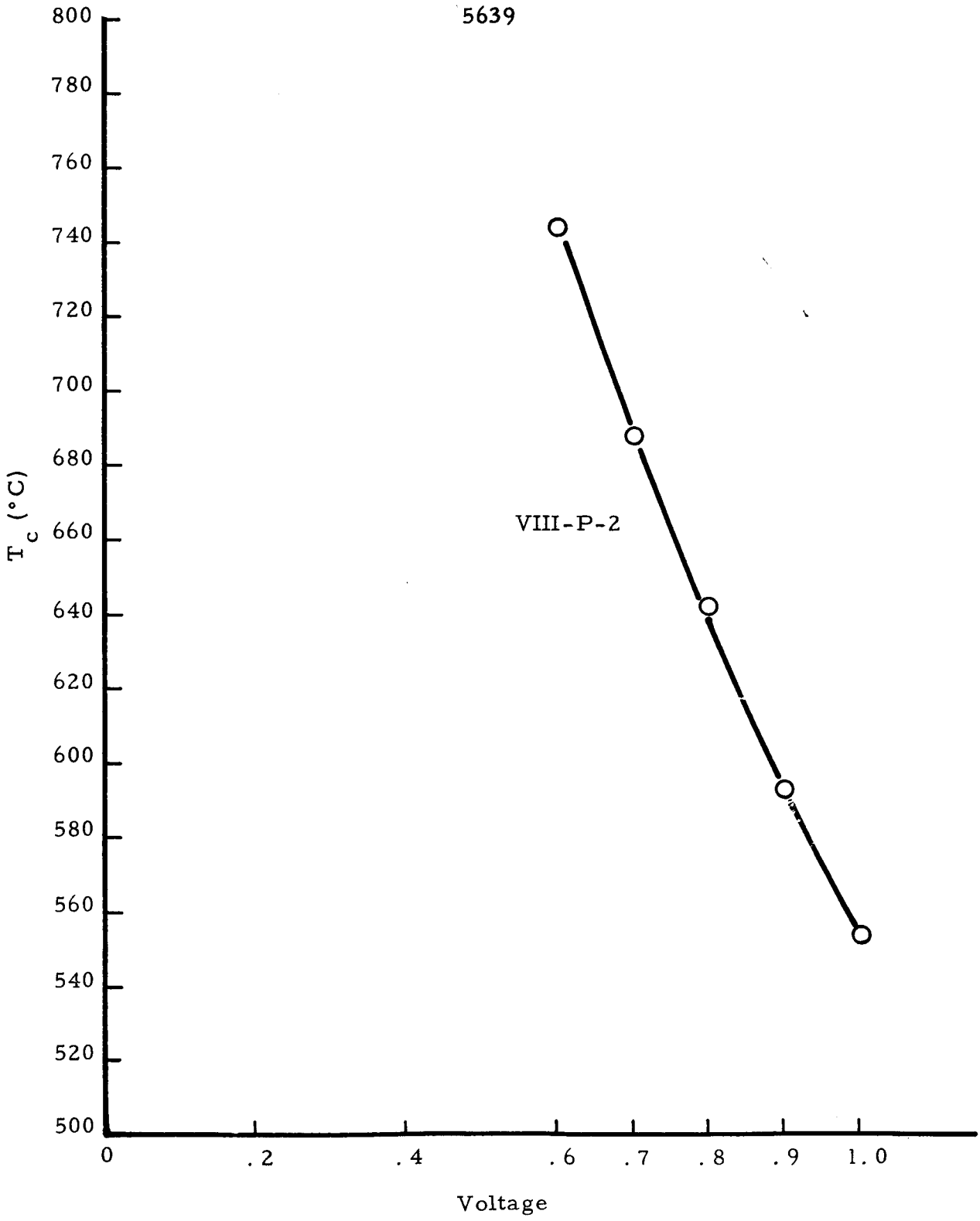

Figure 5. 4 Collector Temperature versus Output Voltage for Diode VIII-P-2a with no additional Heating or Cooling

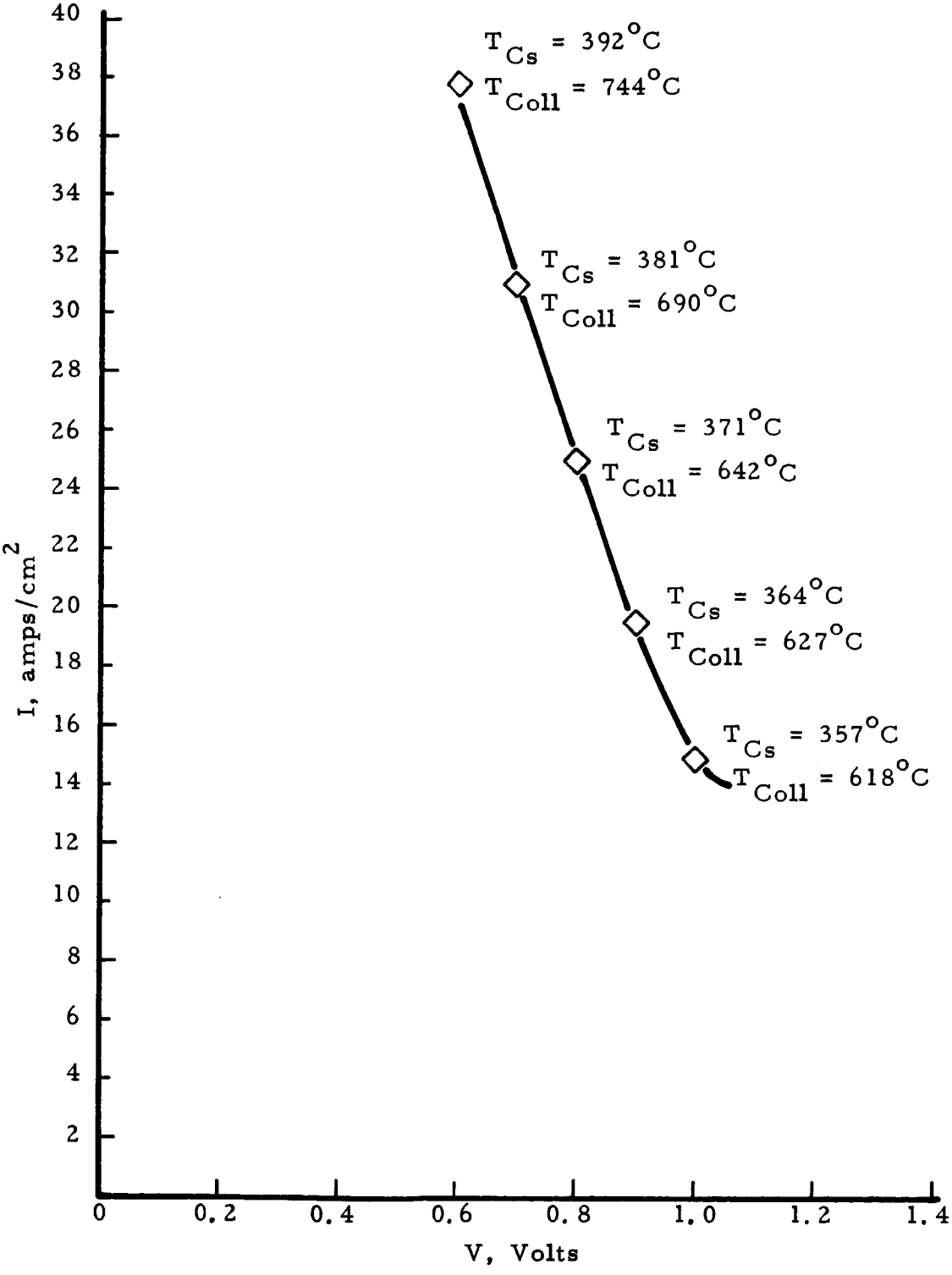

Figure 5.5 IV Curve of VIII-P-2a at an Emitter Temperature of 1700°C (Obs.)

TABLE 5-1

CALCULATION OF HEAT FLOW

THROUGH VIII-P-2a

Output Voltage Volts	Electron Heating eV	Cesium Conduction Watts	Radiation Watts	Total Heat Flow Watts
0.6	167	18.7	26	212
0.7	133	17.7	26	177
0.8	105	17.2	26	148
0.9	79	16.6	26	122
1.0	57	15.5	26	98

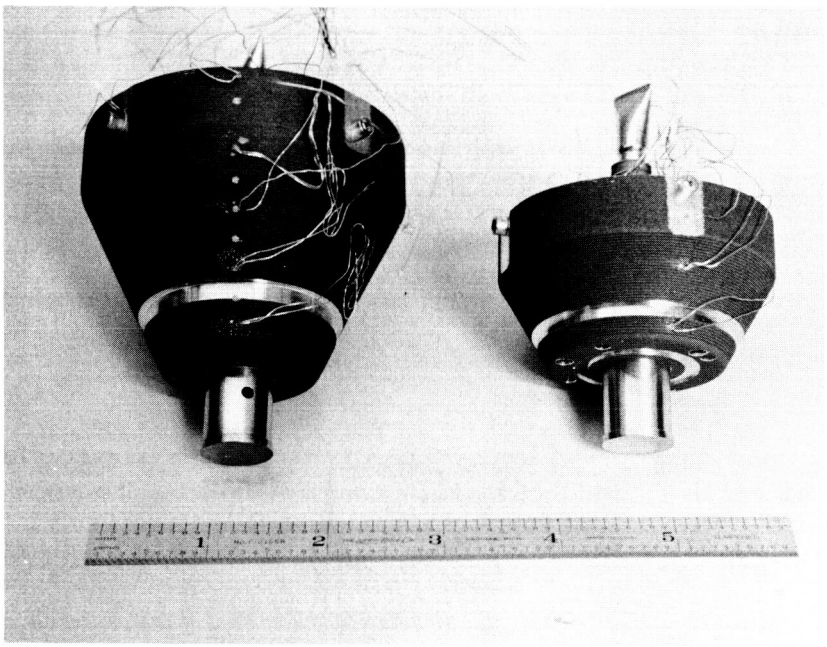

Figure 5.6 Subassemblies of Diodes VIII-P-2 and VIII-P-3

brazed on its outer surface. Similarly, several were also attached on the inner surface. The collector had a thermocouple extending close to its top surface and another at its base. The assembly also included the cesium tube and reservoir as well as the reservoir support.

The first test performed was to apply, by electron-bombardment, a heat input equal to that passing through the collector at a typical operating point of VIII-P-2a. Table 5-2 shows the comparative temperatures at the design point of 0.9 V. This test indicated that the subassembly was a reasonable heat-transfer model for simulating conditions in a converter.

The data taken on this subassembly is summarized in Table 5-3. As can be seen from the table, the various heat inputs corresponding to output voltages between 0.6 and 1 volt were applied, and the resulting temperatures were measured.

In parallel with the work on optimizing the radiator, the cesium reservoir was redesigned so that it would thermally balance below its optimum temperature and allow the optimum to be scanned with the cesium heater. It was found necessary to add a reflective shield between the radiator and the reservoir. This shield was located above the reservoir and was conical in shape. It can be seen in Figure 5.7. As can be seen in the photograph, the shield also blocks radiation from inside the radiator. Consequently, another test was conducted with the same collector radiator subassembly but including the shield. This data is summarized in Table 5-4. The cesium temperature was reduced, with only a very small increase in collector temperature.

TABLE 5-2

Comparison of Temperature Measurements
on VIII-P-3 Collector-Radiator
Subassembly and Converter VIII-P-2a

	VIII-P-3	VIII-P-2a
Output Voltage	0.9	0.9
Heat Input to Collector	122	122
Collector Top	597	593
Collector Bottom	508	501
Radiator - Middle	456	453
Radiator - Bottom	450	433

TABLE 5-3

TEST RESULTS OF THE VIII-P-3

COLLECTOR-RADIATOR SUBASSEMBLY

Output Voltage	0.6	0.7	0.8	0.9	1.0
Heat Input	212	177	151	122	94
Collector Top	797	723	667	597	518
Collector Bottom	647	596	557	508	451
Radiator - Inside Top	589	550	517	477	426
Radiator - Outside Top	568	532	501	464	417
Radiator - Middle	553	519	491	456	411
Radiator - Bottom	546	513	485	450	406
Cesium Reservoir	405	379	360	336	296

5634

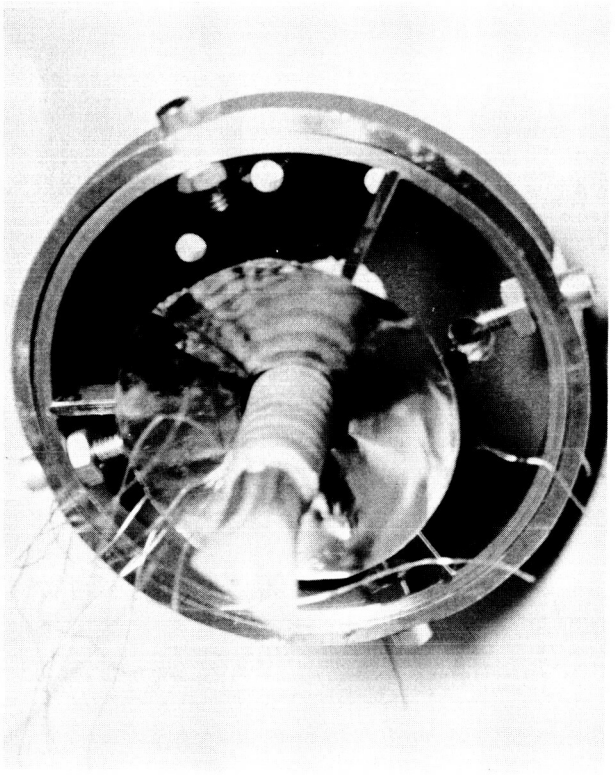

Figure 5.7 Cesium Reservoir Radiation Shield

TABLE 5-4

TEST RESULTS OF THE VIII-P-3

COLLECTOR-RADIATOR SUBASSEMBLY WITH SHIELD

Output Voltage	0.6	0.7	0.8	0.9	1.0
Heat Input	212	177	151	122	94
Collector Top	802	724	667	604	527
Collector Bottom	662	611	571	525	466
Radiator - Inside Top	604	563	531	492	442
Radiator - Outside Top	582	543	513	478	431
Radiator - Middle	568	532	504	470	424
Radiator - Bottom	536	506	480	449	407
Cesium Reservoir	380	359	340	318	289

From the results of optimizing VIII-P-1, a collector temperature of 940°K(667°C) produced maximum current at the 0.9-V output point. Since the collector temperature on the VIII-P-3 subassembly was 604°C, the next collector-radiator subassembly employed a radiator with a shorter skirt. This radiator is shown in Figure 5.8. The three subassemblies are shown in Figure 5.9, with the one referred to in this paragraph at the right. The test data on this subassembly with the smaller skirt is shown in Table 5-5. The collector temperature at the 0.9-V condition is 627°C. Since a typical SET converter heater is capable of raising the collector temperature by 50°C, the desired optimum temperature of 667°C may be scanned with the combination. Consequently this radiator was chosen for diode VIII-P-3. Figure 5.10 shows the final VIII-P-3 collector-radiator subassembly, where PN numbers refer to the numbering in Figure 5.11. Figure 5.11 shows VIII-P-3 in layout form.

5.1.2 Cesium Reservoir

The cesium reservoir and tubulation assembly design of VIII-P-2 was modified to accommodate the shorter radiator and to cause the reservoir to thermally balance at a temperature below the optimum. Thus the cesium heater could be used to optimize the diode. This redesign was accomplished by first calculating the appropriate size and then verifying the results on the VIII-P-3 subassembly described above.

5.2 FABRICATION

From the results of VIII-P-2a and the component tests conducted on various-sized radiators, VIII-P-3 was constructed with the design

shown in Figure 5.12. The emitter, part 1, is welded to the sleeve, part 20, using the electron-beam welder. This assembly is welded to the emitter flange, part 6. Next this assembly is brazed with the seal structure, which is composed of parts 4, 5, and 7, and at the same time the collector, part 2, is brazed to the collector flange, part 7, and the cesium reservoir tubulation assembly, consisting of parts 9, 10, 11 and 15, which have been previously joined. This braze is called the pre-final braze. The last braze joints the seal structure to the mounting flange, part 42, and simultaneously joins the radiator, part 8, to the collector base. During assembly no brazing or welding difficulties were encountered. The weld of the emitter flange, part 6, to the base of the emitter spacer, part 20, was incorporated as in VIII-P-2a. The quality of the weld is readily seen in Figure 5.13.

For outgassing, VIII-P-3 was mounted on a 100-liter/sec Vac-Ion vacuum system. An 8-liter/sec pump was used for internal outgassing of the converter. Figure 5.11 shows the diode mounted on the system. The roughing station for the Vac-Ion is to the left, and the electron-bombardment power supply is to the right. Figure 5.14 shows a close-up of the diode with its exhaust tubulation connected to the 8-liter/sec pump and a shield placed around the emitter. Figure 5.15 shows the diode after being pinched-off from the Vac-Ion pump and prior to cesium distillation, while Figure 5.16 shows a close-up of the emitter after outgassing. From this latter figure it is apparent that a very slight amount of chemical reaction has occurred on the tantalum sleeve even though the sleeve was shielded and the diode was outgassed on a Vac-Ion pump. All vacuum components, such as the base plate, had been leak-checked with a mass spectrometer prior to use.

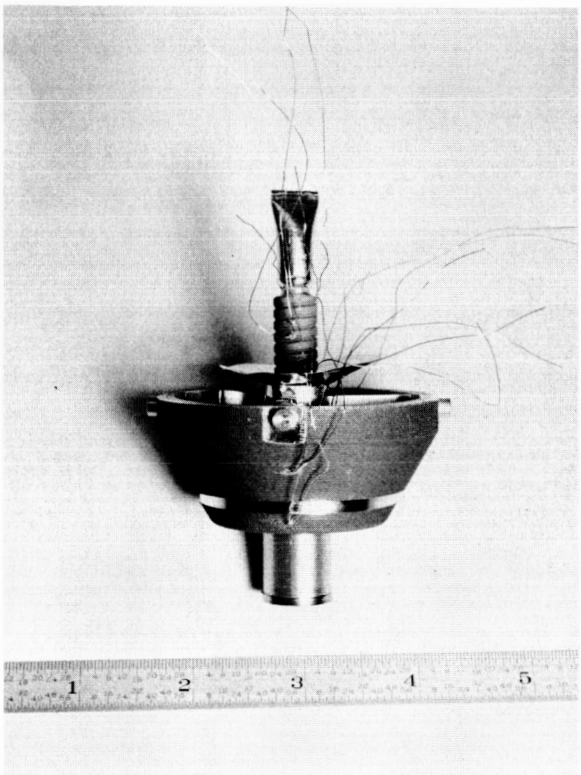

Figure 5.8 VIII-P-3 Collector-Radiator Assembly with reduced Skirt

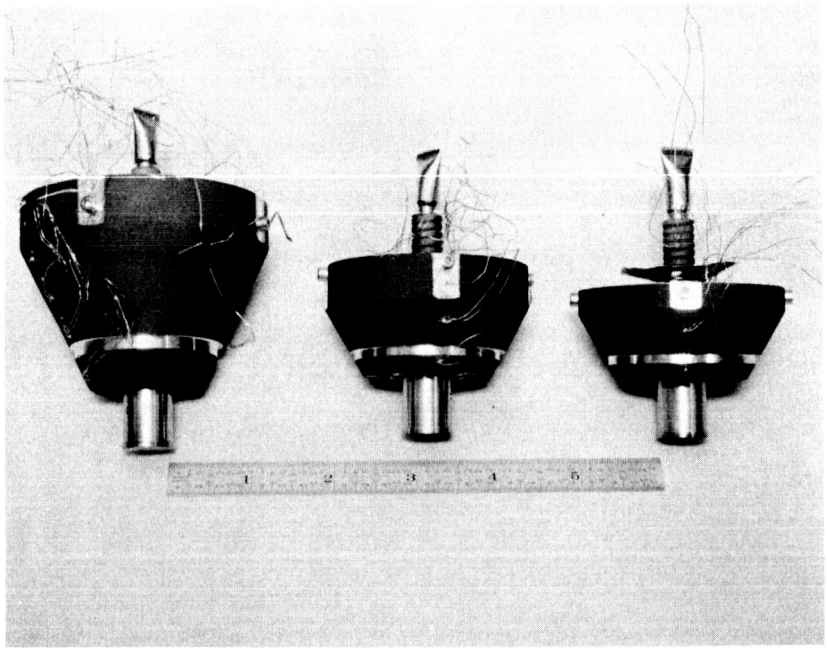

Figure 5.9 VIII-P-2, VIII-P-3 with Original Radiator and VIII-P-3 with Reduced Skirt

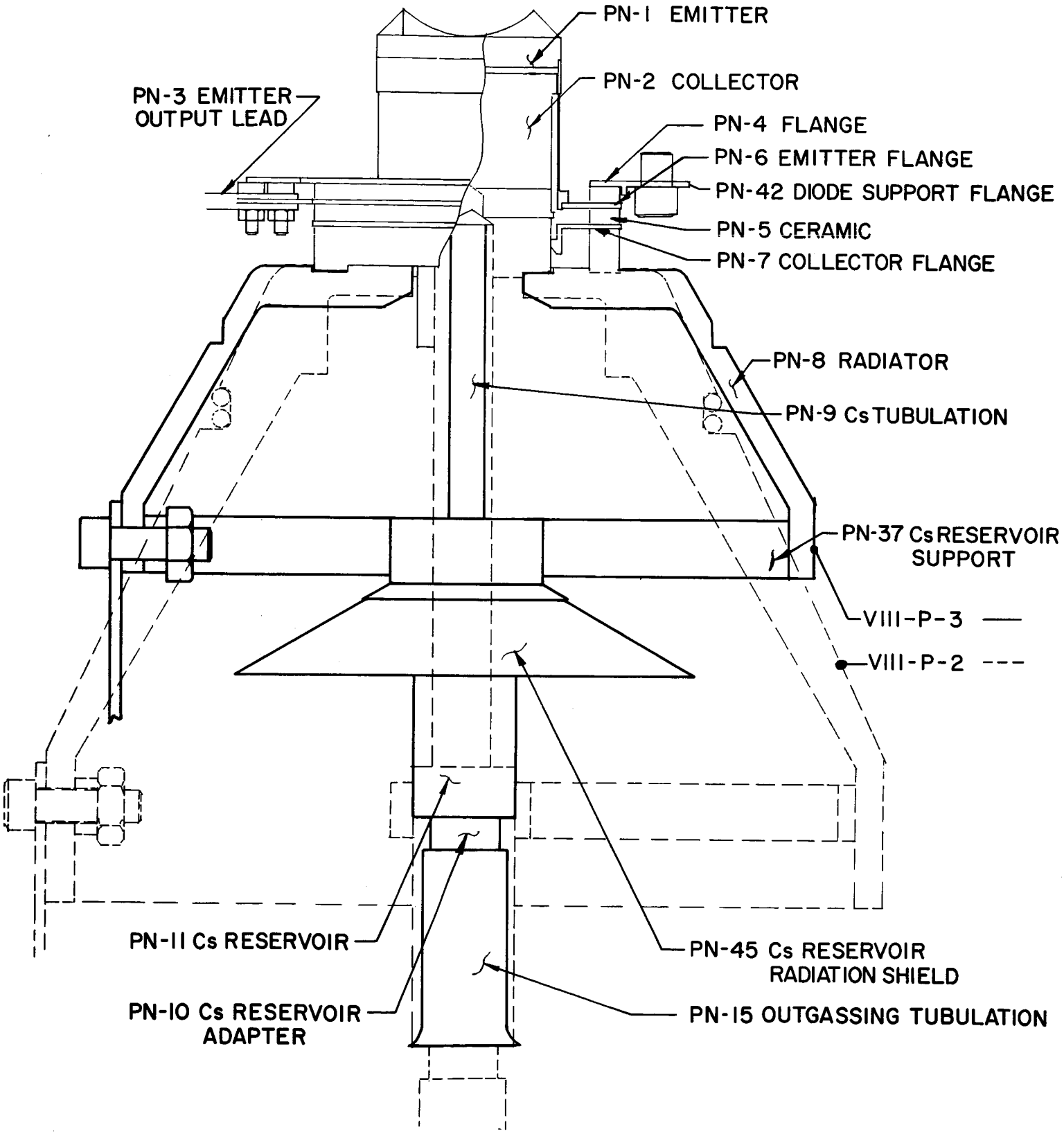

Figure 5.10 Comparison of VIII-P-2 and VIII-P-3 Radiator and Cesium Reservoir

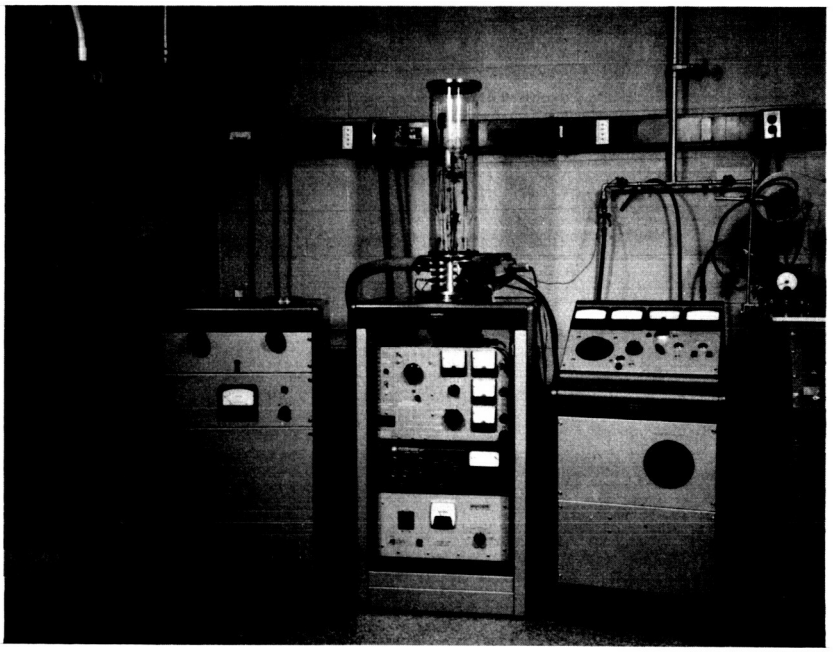

Figure 5.11 View of Vac-ion Pump Setup with Bell Jar

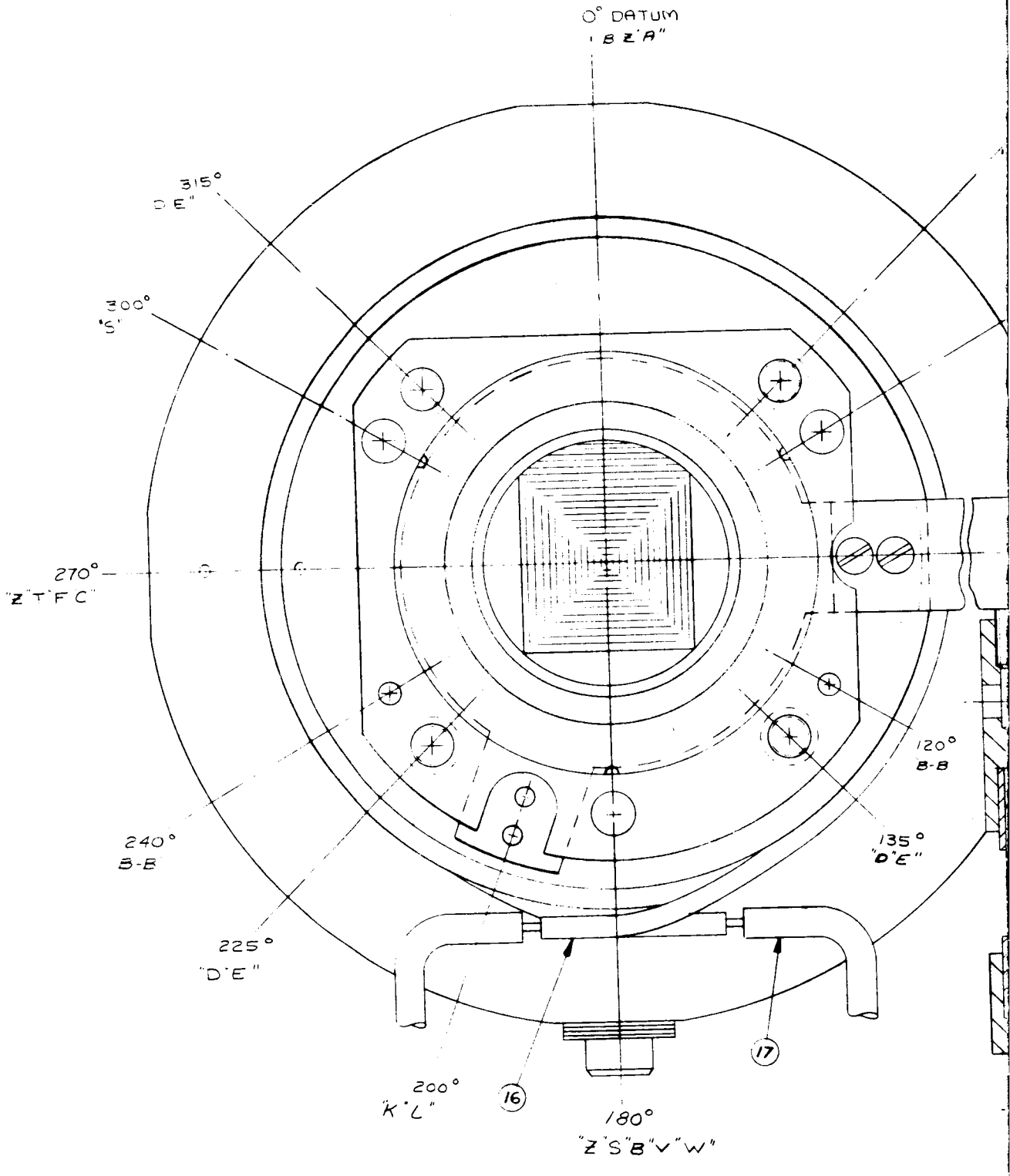

FOLDOUT FRAME 1

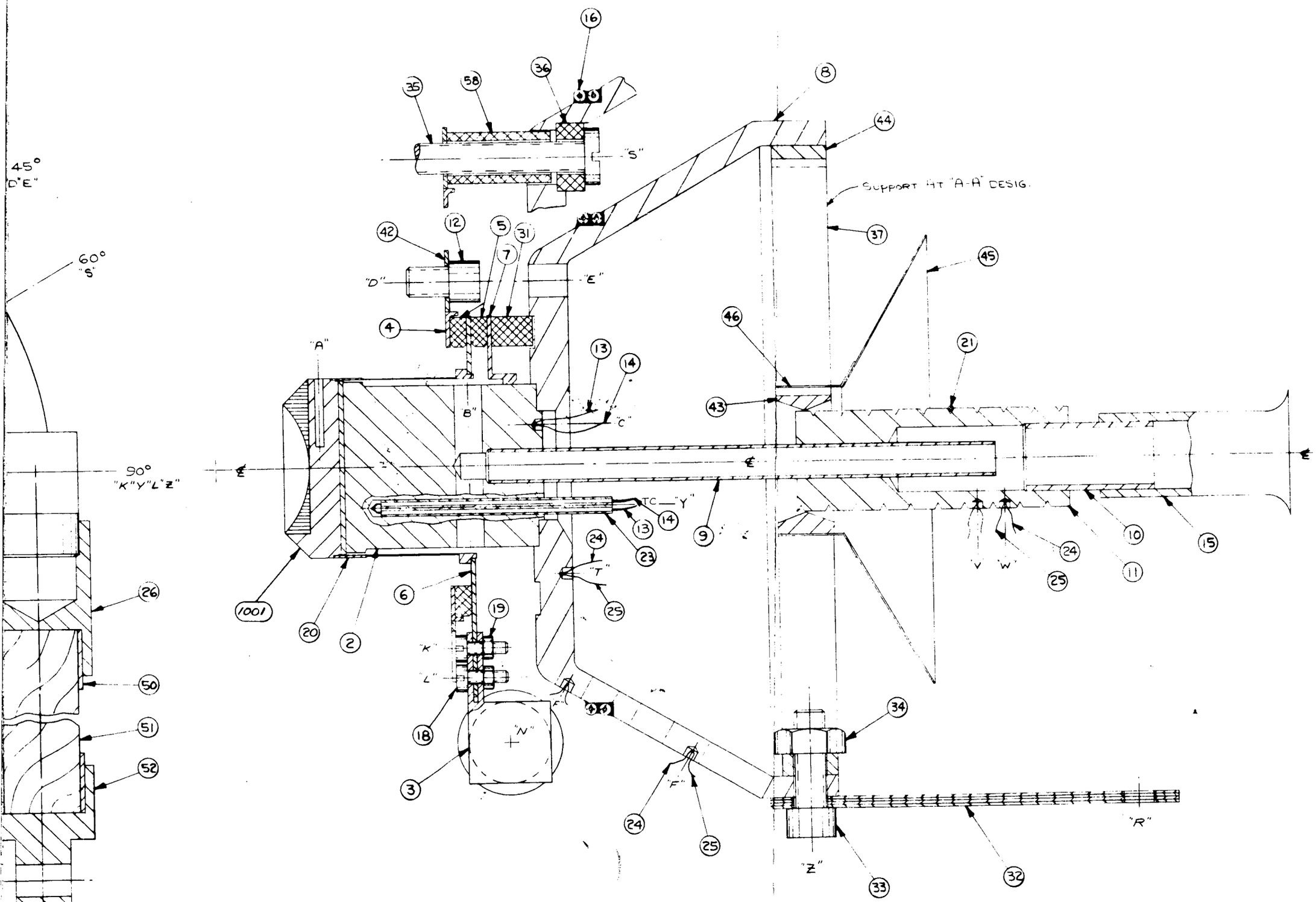

FOLDOUT FRAME 2

FOLDOUT FRAME 3

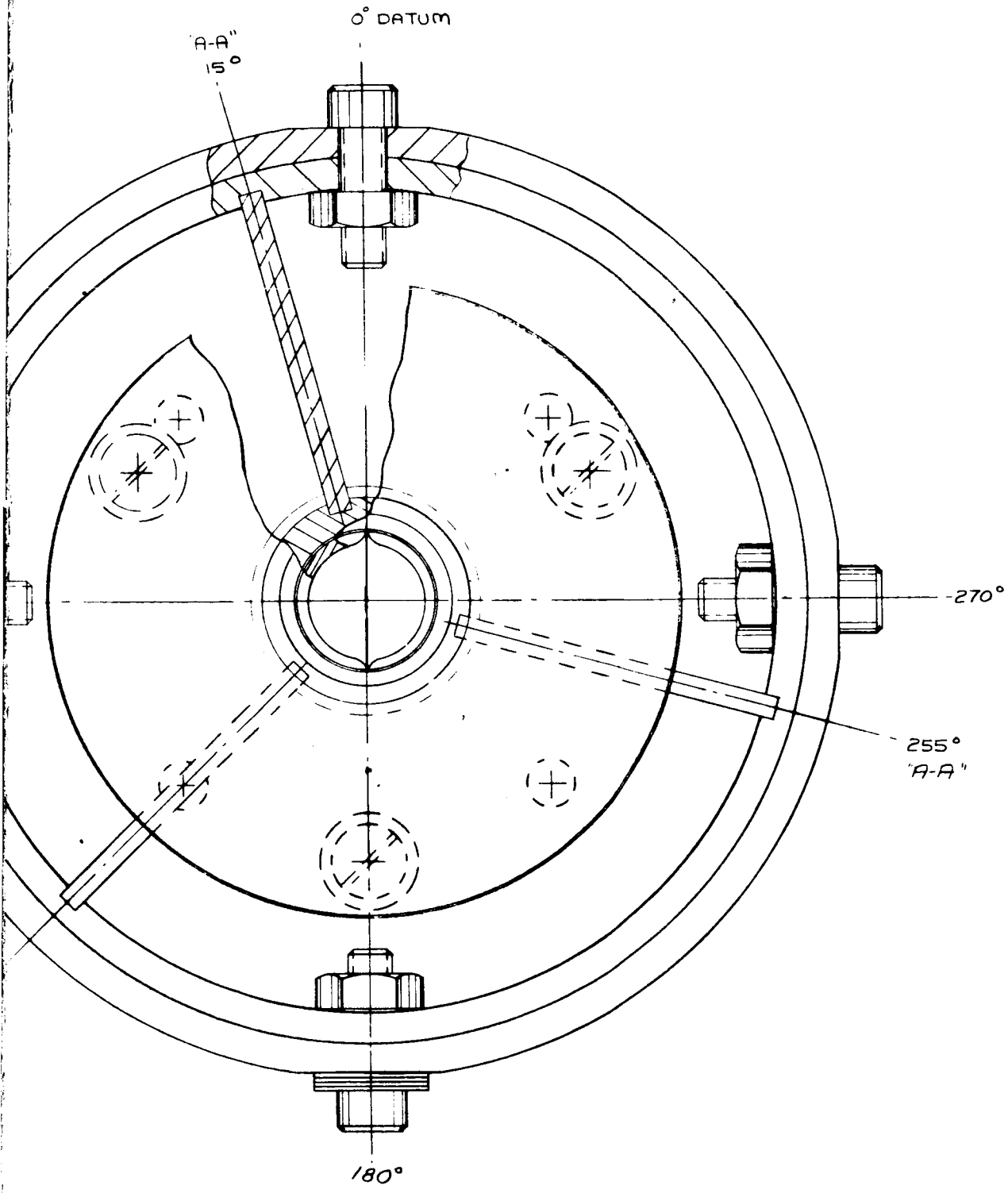

1001	D	A	1	Re EMITTER	PN: 47,48,49 PRESS. BOND.
58	A		3	Al_2O_3	
57					
56					
55					
54					
53					
52	B		1	Cu	
51	B		1	Cu	
50	B		2	Ni	
49	A		1	Ta	
48	A		1	Ta	
47	A		1	Re	
46	C		1	Ni	
45	B		1	Ni	
44	D		1	S.S.	
43	B		1	S.S.	
42	C	D	1	Nb	
41	OBS.				
40	OBS.				
39	OBS.				
38	OBS.				
37	B		3	S.S	
36	A	C	3	Al_2O_3	
35	ND	-	3	S.S	#4-40 x .750 LG. RHCS
34	ND	-	4	S.S.	#4-40 HEX NUT
33	ND	-	4	S.S.	#4-40 X .38 LG S.H.C.S
32	B		4	Cu	
31	B		1	Al_2O_3	
30					
29					
28					
27					
26	B		1	Cu	
25	ND	-	2	Alumel	
24	ND	-	2	Chromel	
23	ND	-	1	Al_2O_3	
22	ND		AS REQ'D	ASTRO CERAM	
21	ND	-	AS REQD		HEATER
20	C		1	Ta	
19	ND	-	2	S.S.	#00-96 HEX NUT
18	ND	-	2	S.S	#00-96 X .125 LG
17	B		4	Cu	
16	ND	-	AS REQ'D		SHEATHED HEATER
15	C		1	Cu	
14	ND	-	1	Alumel	
13	ND	-	1	Chromel	
12	A	A	4	S.S.	#4-40 S.H.C.S. (MODIFIED)
11	S/C		1	Ni	
10	C		1	Ni	
9	C		1	Ni	
8	S/P	D	1	Cu	
7	C		1	Nb	
6	C	B	1	Nb	
5	B		2	Al_2O_3	
4	B		1	Nb	
3	C	A	1	Nb	
2	C		1	Mo	
1	A	A	1	Ta	

PART	SIZE	REV	REQ	MAT'L	NOTES

THERMO ELECTRON

DRAWN	CHECKED	ENGINEER
MN		

TITLE: VIII-P-3 LAYOUT

SIZE	DRAWING NUMBER	SHEET	REV
H	479-1000	1	L

Figure 5.12

FOLDOUT FRAME 4

FOLDOUT FRAME 5

TABLE 5-5

TEST RESULTS OF THE VIII-P-3
COLLECTOR-RADIATOR SUBASSEMBLY
WITH REDUCED SKIRT AND
WITH RESERVOIR SHIELD

Output Voltage	0.6	0.7	0.8	0.9	1.0
Heat Input	212	177	151	122	94
Collector Top	829	758	702	627	551
Collector Bottom	665	616	579	528	475
Radiator - Inside Top	632	589	557	510	460
Radiator - Outside Top	609	569	540	498	451
Radiator - Middle	566	531	505	466	425
Cesium Reservoir	342	321	306	276	261

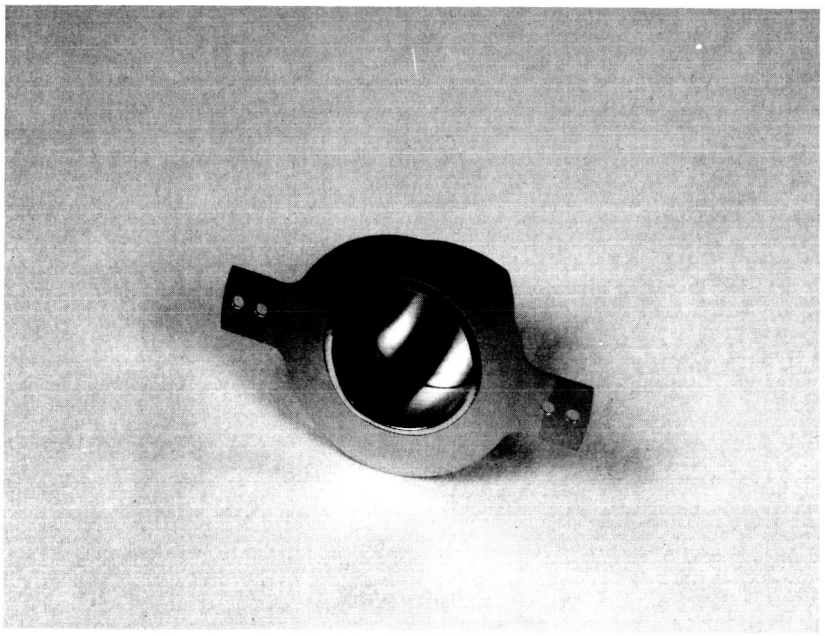

Figure 5.13 Ta-Nb Beam Weld on SET VIII-P-3 Converter

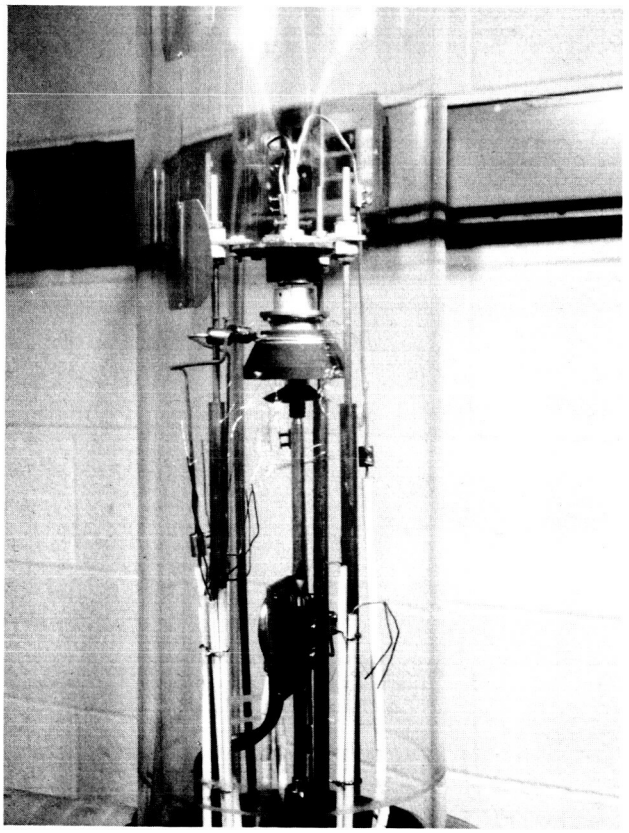

Figure 5.14 Diode Mounted for Outgassing

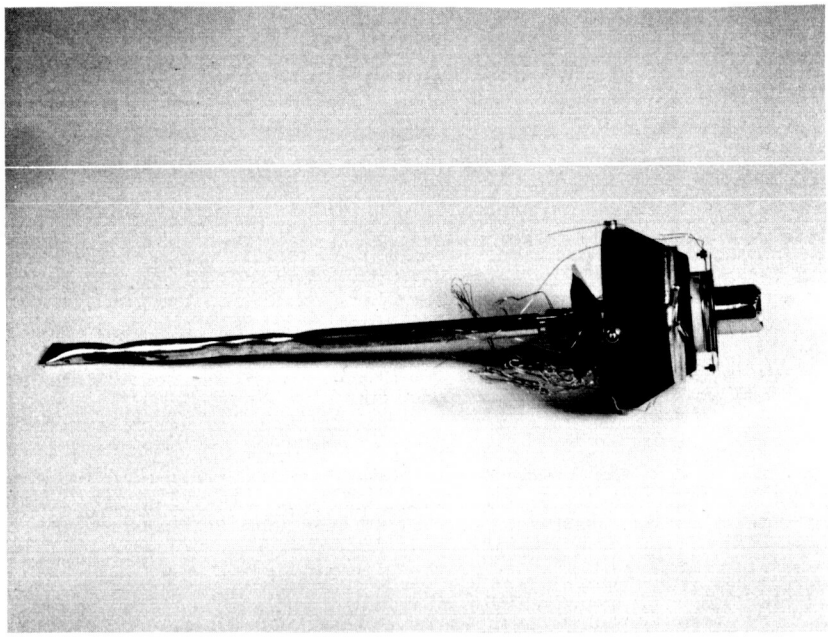

Figure 5.15 Diode Prior to Cesium Distillation

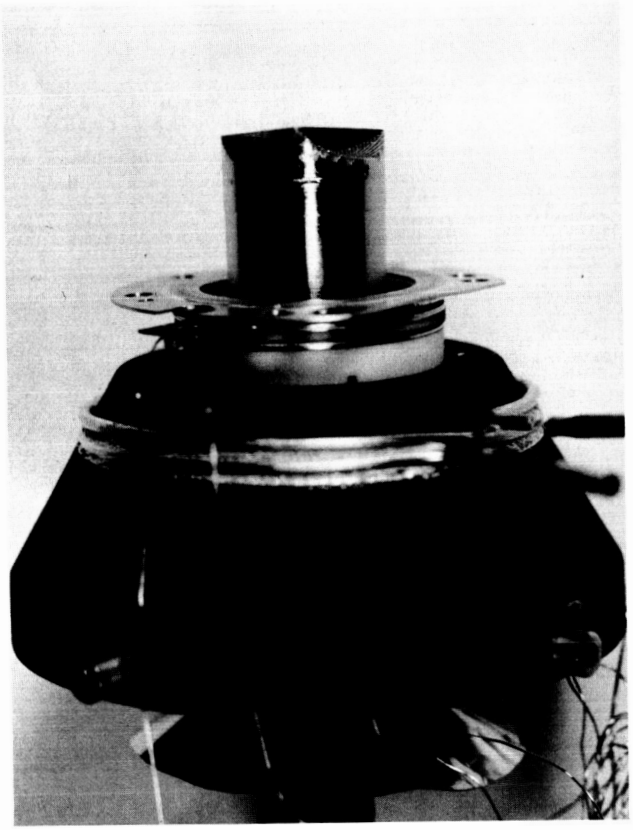

Figure 5.16 Emitter after Outgassing

5.3 TESTING

Converter VIII-P-3 was tested under steady-state conditions at 1700°C and 1677°C observed emitter temperatures. Upon completion of testing, the bell was recalibrated with an NBS standard lamp. The calibration is shown in Figure 5.17 and shows that, for observed temperatures of 1677°C and 1700°C, the hohlraum temperatures would be 1735°C and 1760°C, respectively.

Figures 5.18 and 5.19 show the optimization of current versus cesium temperature of VIII-P-3 at various voltages and at the equilibrium collector temperature. With the design used in VIII-P-3 it was also possible to raise the collector temperature and still optimize the cesium, which was not the case with VIII-P-2a. This was possible because of the radiation shield between the radiator and the reservoir. The resulting steady-state I-V and power curves are plotted in Figures 5.20 and 5.21.

5.4 EMITTER CAVITY-PIECE REFLECTIVITY MEASUREMENTS

Two cavity pieces simulating the emitter were made and tested with the goal of maximizing the surface absorptivity to solar heating. The first (#1) was identical to those incorporated in the earlier Series VI converters and in VIII-P-2a and VIII-P-3, while the second (#2) was made by electro-discharge machining (EDM) rectangular grooves along one axis on the top of the piece. The results, using a reflectometer, indicated that #1 was four times as absorptive as #2 to incoming radiation at any angle.

Solar testing of an earlier generator, JG-2b, which included five diodes, showed that the converter in the rear of the cavity was receiving substantially more heat than the side converters. Therefore it would

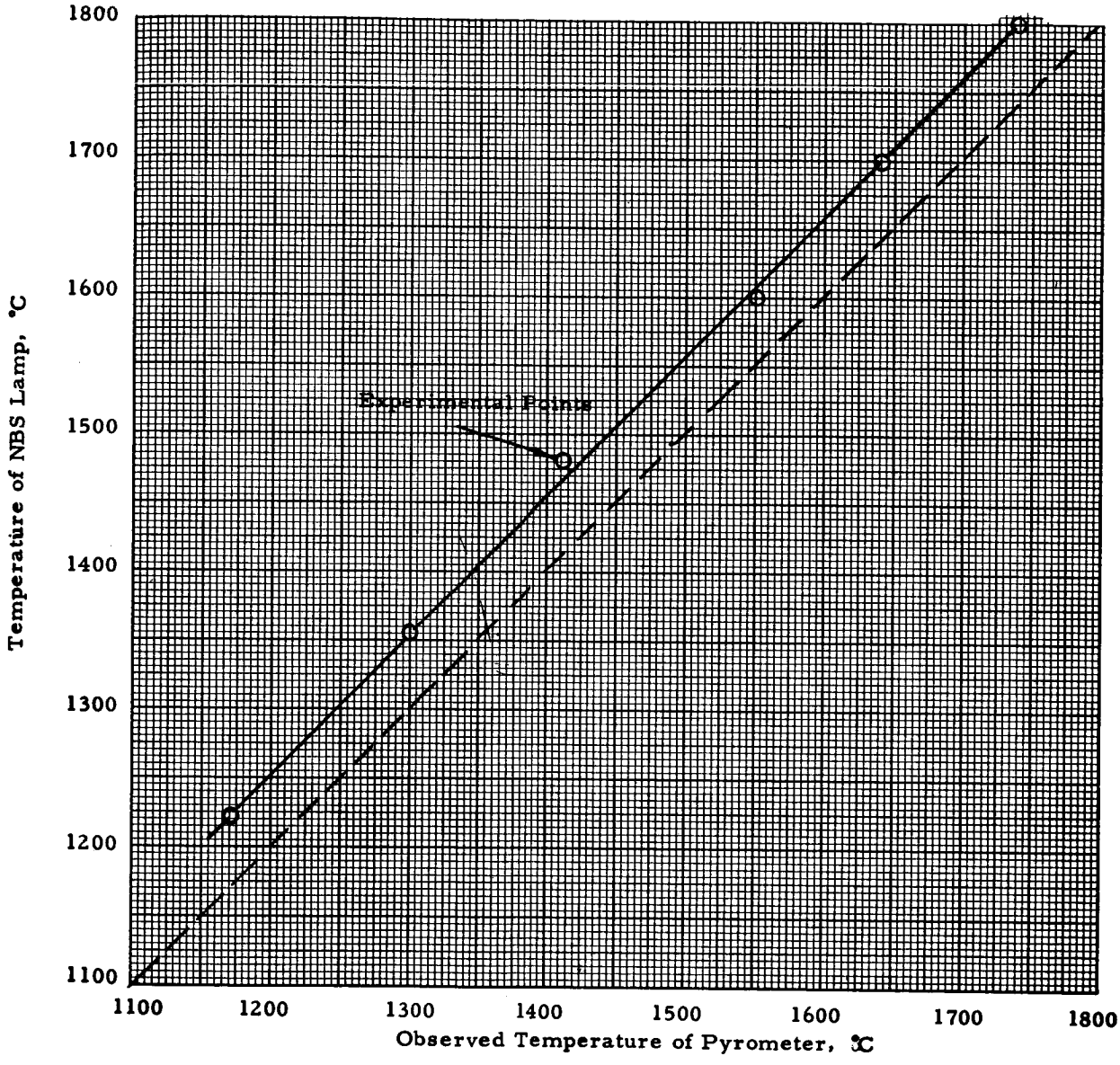

Figure 5.17 **Calibration of Bell Jar used in Testing Converter VIII-P-3**

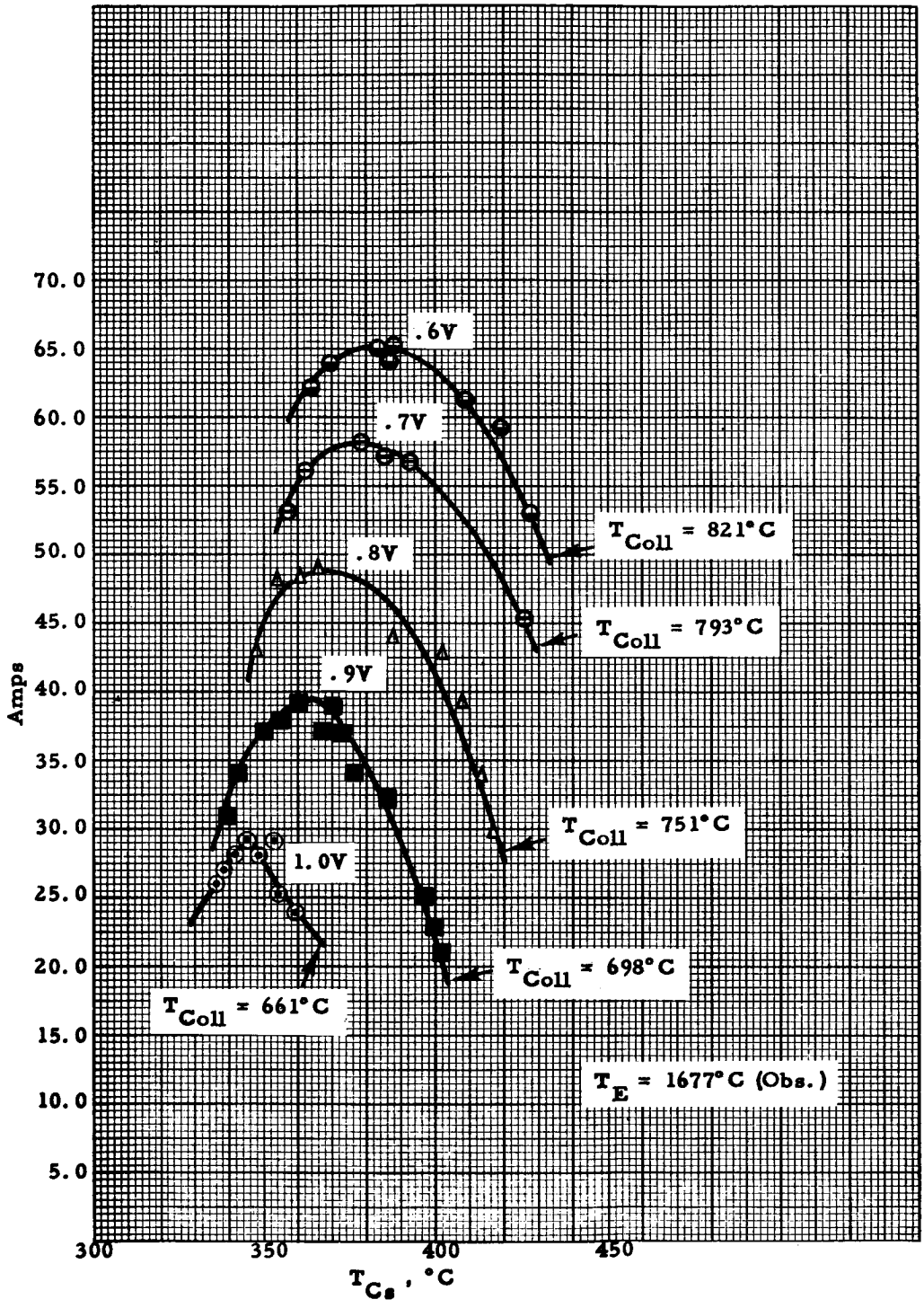

Figure 5.18 Current versus Cesium Temperature at various Voltages for Converter VIII-P-3 at T_E = 1677°C (Obs.)

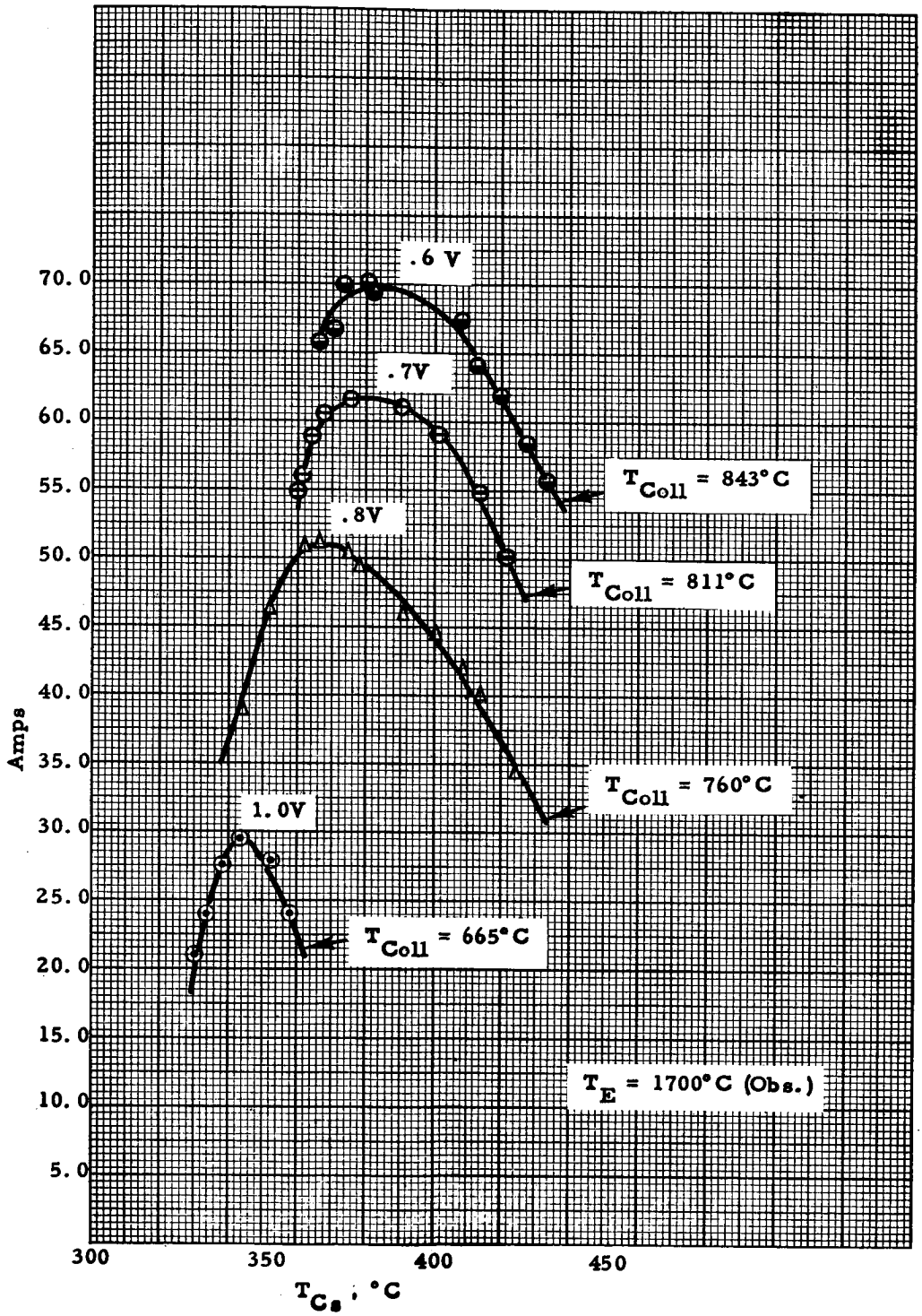

Figure 5.19 Current versus Cesium Temperature at various Voltages for Converter VIII-P-3 at T_E = 1700°C (Obs.)

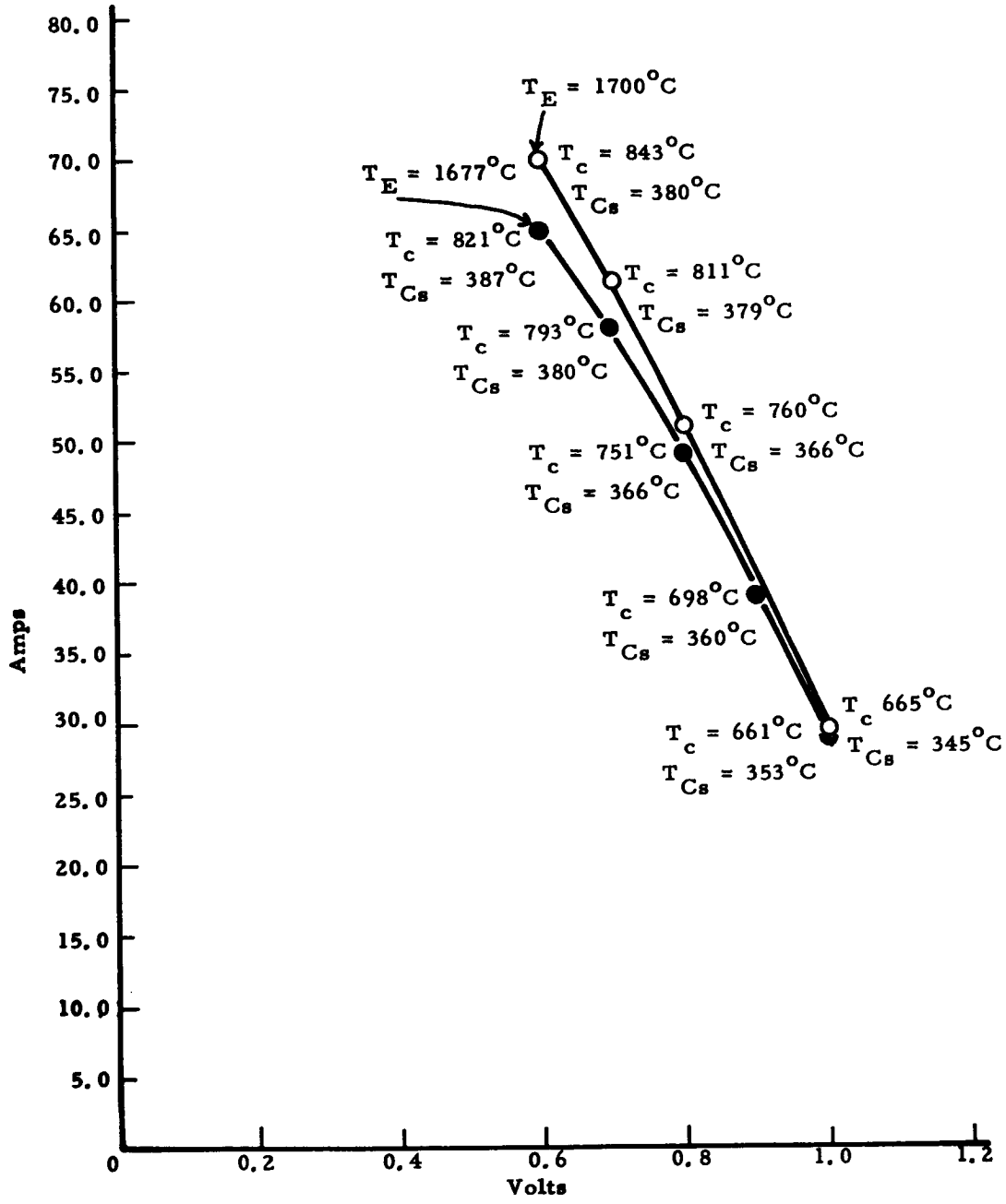

Figure 5.20 **IV Curves for VIII-P-3, Emitter Temperature = 1677°C and 1700°C**

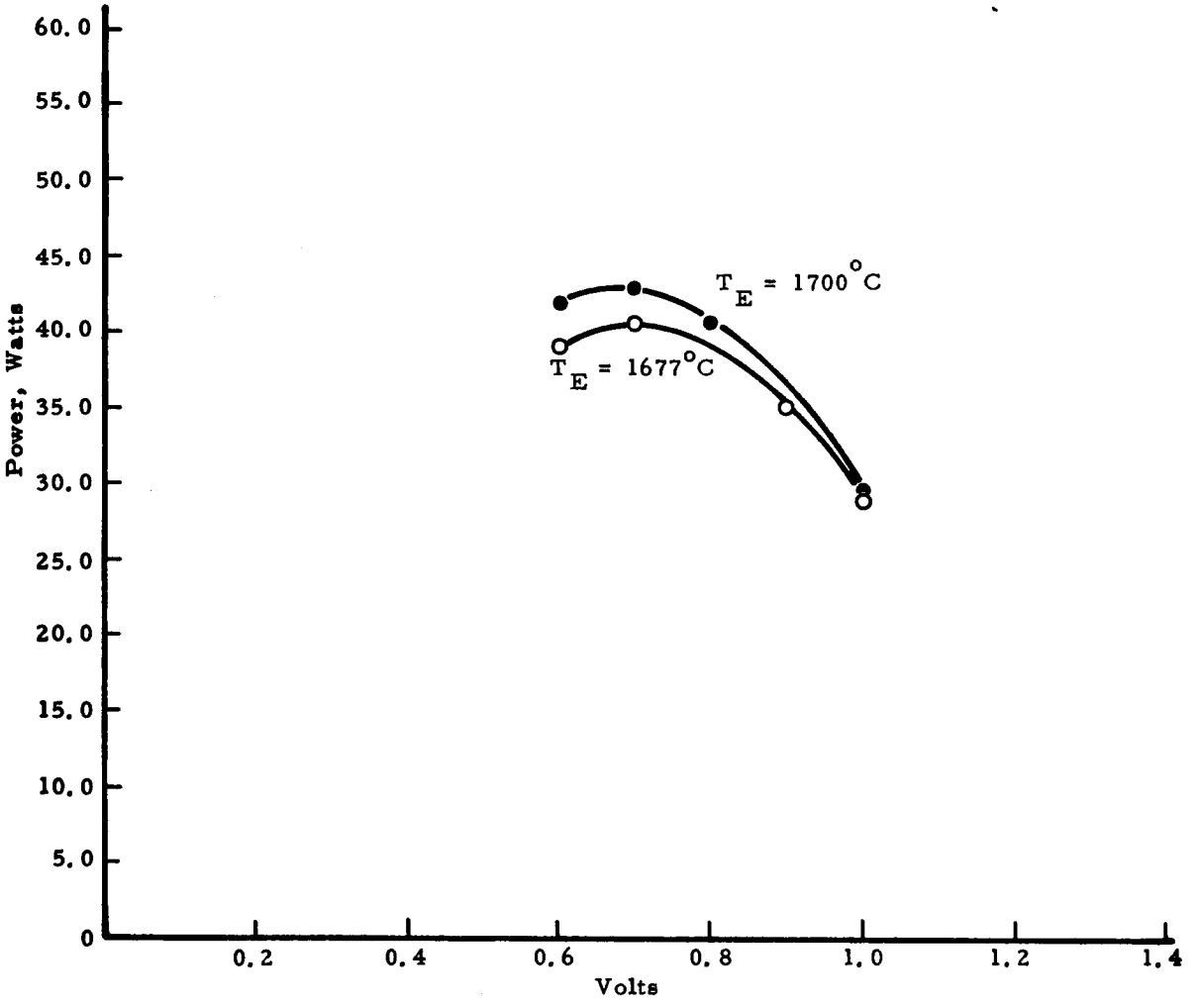

Figure 5.21 **Power versus** Voltage **for VIII-P-3 at** T_E = 1677°C and 1700°C

be desirable to shape an emitter cavity piece to be as absorptive as possible along the side areas of the cavity, and to extend it into the rear of the cavity in order to absorb that available heat, and then to conduct it into the emitters. A third cavity piece (#3) was built toward this goal and is shown in Figure 5.22. Figure 5.23 shows the #1, #2 and #3 emitters from left to right. The cavity formed by #3 is shown in Figure 5.24. The extended portion of this emitter was made shiny to avoid melting and concave to redirect impinging radiation to the side converters to improve heating uniformity.

The #3 piece was fabricated without the use of an EDM operation. Because the grooves (triangular in cross section) are located on a flat surface, it was possible to achieve the desired cross section by using a lathe and a milling machine. This design avoided the need for making specialized EDM tools, which are complicated and expensive, and which wear easily on refractory materials.

Reflectivity measurements were made on the #1, #2 and #3 emitters using a reflectometer, standardizing the detector at a full-scale reading of 100A on shiny flat tantalum. The results are shown in Figure 5.25. Clearly, the #3 piece showed a marked improvement over #2, but it was not so absorptive as #1. An inspection of the #1 emitter revealed that there was sufficient randomness of the grooving to incoming angles of radiation so that only a small percentage of the energy was not trapped.

Next, to simulate the severe heating conditions that would be experienced in solar testing with a 9.5-ft mirror, the #3 piece was supported (by spot-welding) on three 20-mil tungsten pins and positioned in an electron-beam welder. The electron beam was de-focused and positioned to irradiate only the shiny portion of the emitter.

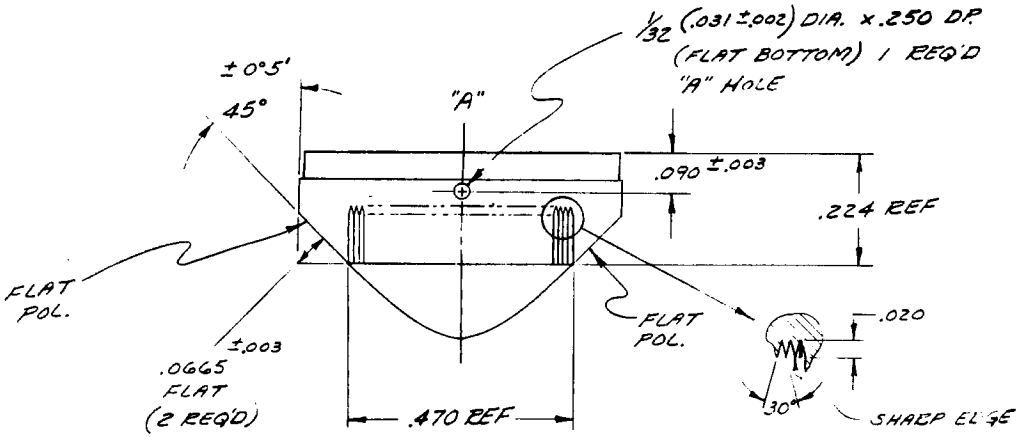

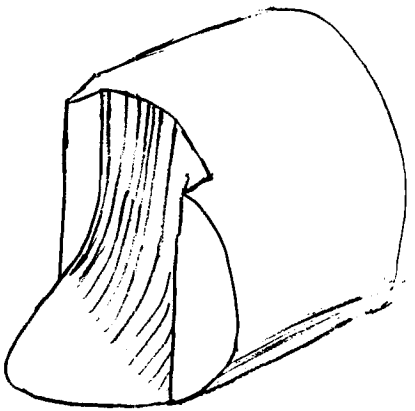

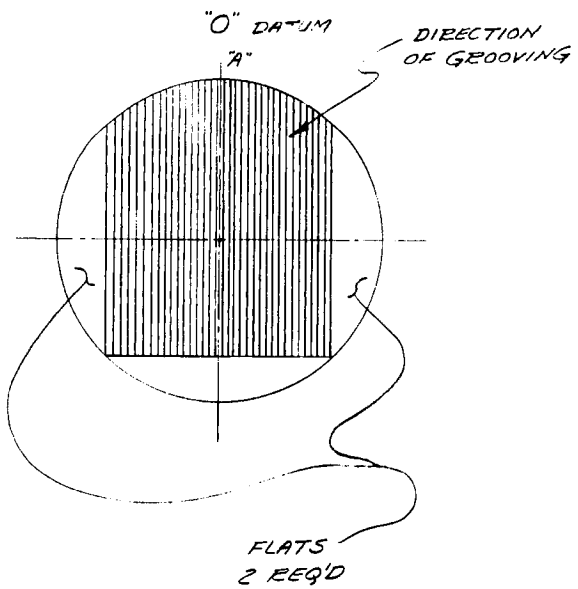

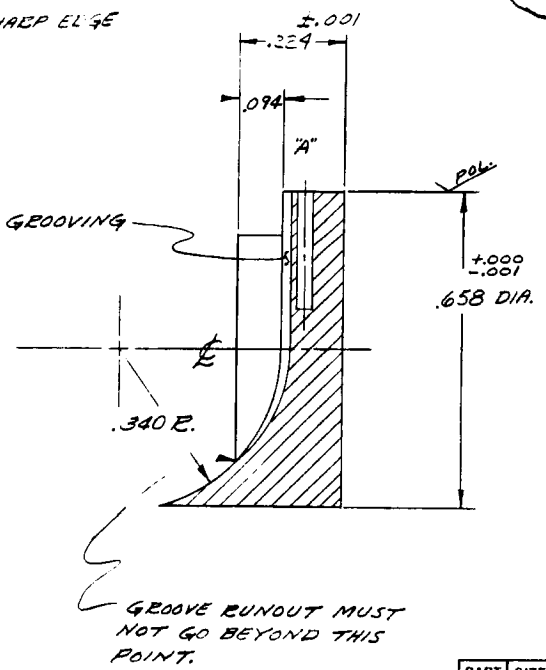

PART	SIZE	LOC	REQ	MAT'L	NOTES
UNLESS OTHERWISE SPECIFIED					THERMO ELECTRON ENGINEERING CORP. WALTHAM 54, MASS.
DEC. .X±1 .XX±.01 .XXX±.005					
SCALE: 5 = 1					
ANGLES ± 0°30'	FINISH 32 MAX				DR RW 9-9-64 ENG
FILLET RAD .010 MAX					CHK [illegible] 9-9-64 APP
THREADS: CLASS 2					TITLE # 3 PROPOSED SERIES VIII EMITTER
ALL DIAS. CONCENTRIC WITHIN .005 TIR					
REMOVE ALL BURRS & SHARP EDGES					
NEXT ASSY	SIM TO				SIZE C NUMBER SK27-1 REV

Figure 5.22 #3 Proposed Series VIII Emitter

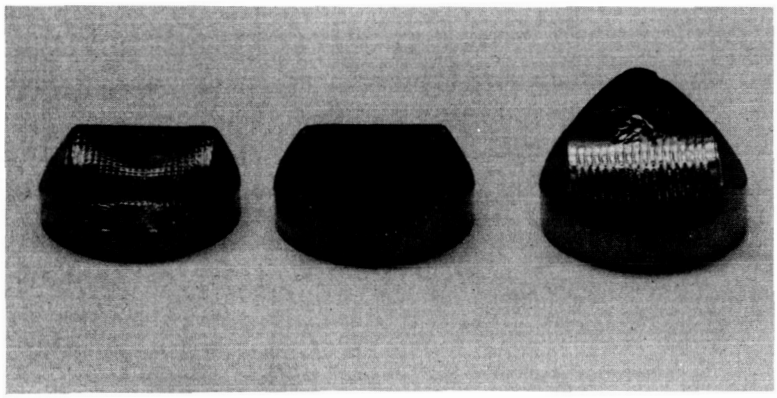

Figure 5.23 #1, #2 and #3 Cavity Emitter Heads

5769

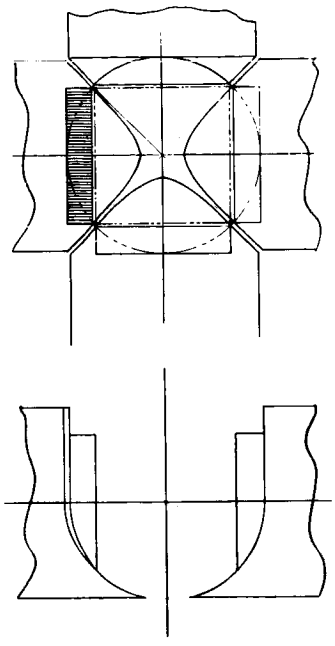

PART	SIZE	LOC	REQ	MAT'L
UNLESS OTHERWISE SPECIFIED				
DEC .X ± .XX ± .XXX ±				
SCALE: 5 X1				
ANGLES ± 0°30'	FINISH √ MAX			
FILLET RAD .010 MAX				
THREADS: CLASS 2				
ALL DIAS. CONCENTRIC WITHIN .005 TIR				
REMOVE ALL BURRS & SHARP EDGES				
NEXT ASSY	USED TO			

NOTES

THERMO ELECTRON
ENGINEERING CORP.
WALTHAM 54, MASS.

DR	R.W.	4-2-69	
CHK			
APP			

TITLE
CAVITY FORMED BY #3 EMITTER

SIZE	NUMBER	REV
D	SK27-1000	

Figure 5.24 **Cavity Formed by #3 Emitter**

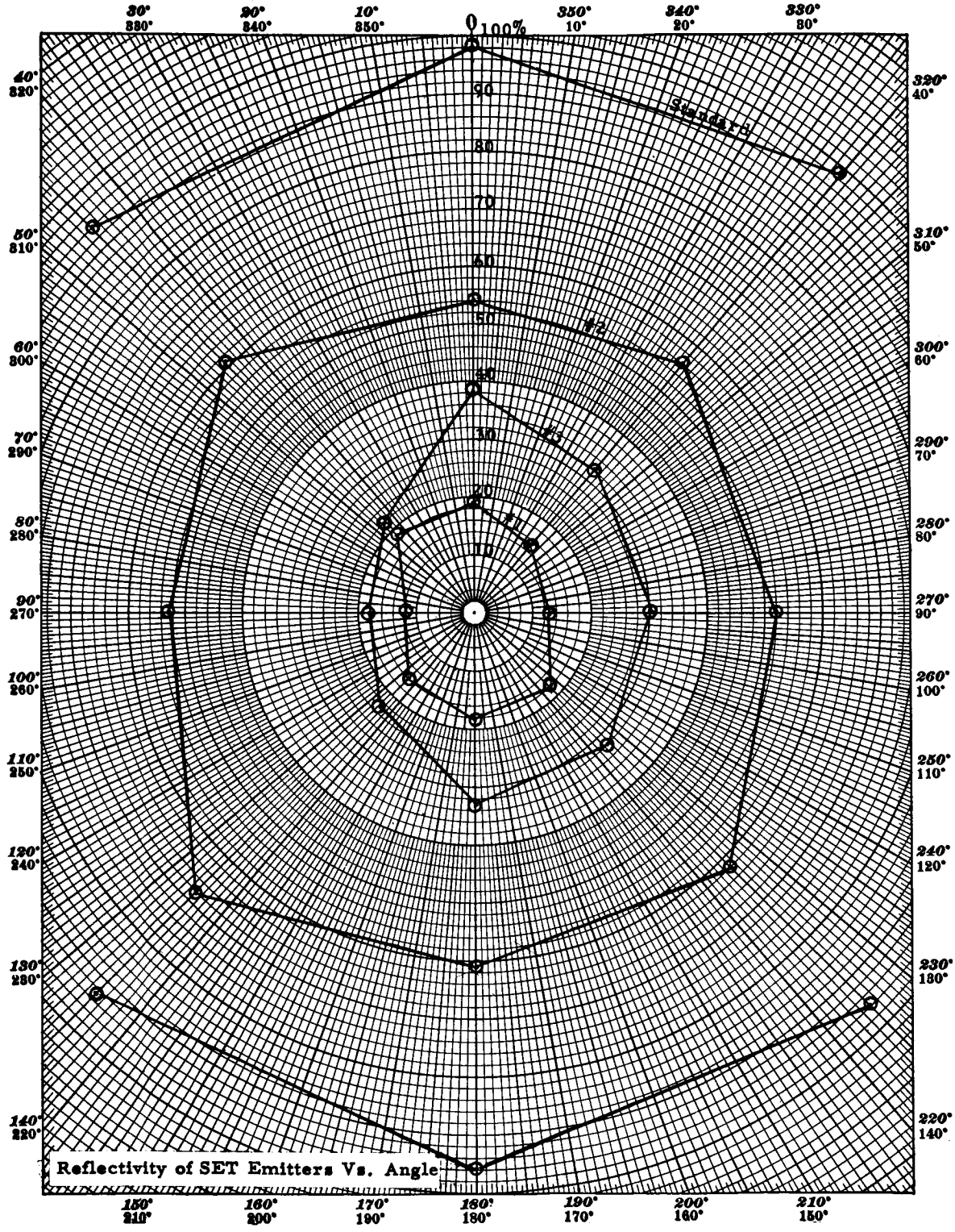

Figure 5.25 Reflectivity of SET Emitters versus Angle

Table 5-6 shows the data recorded under various heat input conditions. For the case of 478 watts input with the pyrometer hole at 1725°C, the temperatures at various points on the surface of the emitter (corrected for emissivity of tantalum) were as follows: 2300°C on the shiny portion, 2010°C on the face opposite the shiny portion, and 1675°C adjacent to the pyrometer hole. This distribution indicates a temperature drop of 2300 - 1675 = 625°C. This value is for 478 watts input with no appreciable heating of the lateral area.

On the basis of the reflectivity measurements and the simulated heating of the emitter, the #1 cavity configuration was considered best for use in subsequent generator converters (VIII-S-1 through VIII-S-6).

TABLE 5-6

TEMPERATURE* DISTRIBUTION IN #3 EMITTER UNDER ELECTRON-BEAM HEATING

Time	Shiny Portion T_1	Pyrometer Hole T_2	Adjacent to Pyrometer Hole T_3	Bottom T_4	Beam Voltage	Beam Current	Power
10:30	1265°C	1145°C	1110°C	1190°C	20 kV	5 mA	100 W
	1510°C	1340°C	1255°C	1330°C	19.6 kV	7.5 mA	147 W
	1645°C	1425°C	1325°C	1440°C	19.5 kV	10 mA	195 W
	1760°C	1500°C	1385°C	1515°C	19.4 kV	12.5 mA	242 W
	1860°C	1565°C	1440°C	1595°C	19.35 kV	15 mA	290 W
	1955°C	1600°C	1475°C	1640°C	19.3 kV	17.5 mA	338 W
	2005°C	1655°C	1520°C	1690°C	19.3 kV	20 mA	386 W
	2060°C	1705°C	1555°C	1755°C	19.2 kV	22.5 mA	432 W
	2065°C	1725°C	1575°C	1800°C	19.1 kV	25 mA	478 W
	(2300°C)**	(1725°C)	(1675°C)	(2010°C)			
10:55	2075°C	1750°C	1590°C	1825°C	19.1 kV	27 mA	516 W

*Values listed are observed temperatures.

**Values in parentheses are corrected for emissivity.

CHAPTER 6

THERMAL ANALYSIS OF GENERATOR JG-3

6.1 INTRODUCTION

A thermal analysis was performed to establish the best way of achieving the following characteristics in the solar thermionic generator, which was the end product of the program:

1. The generator was to employ four converters and to be operated from a 5-foot, 60°-rim-angle solar concentrator. It should deliver a minimum of 75 watts output at between 2.5 and 3.0 volts, with a total constant power input of 1100 watts. This input value was not to include any losses by re-radiation or thermal conductivity, but should be the sum of all energy supplied by an electron-bombardment gun.

2. Radiation shielding was to be included around the emitter spacer of each converter so that thermal shields would be formed to the greatest extent possible between the high-temperature portions of the converter and the generator block structure.

3. Cooling fins were to be attached to the diode support-block structure to increase its heat rejection.

4. The generator's support structure was to be capable of providing a reliable and lightweight means of support for the generator.

5. Positioning of the converters in the cavity for maximum use of the solar energy flux, but with consideration of the thermal expansion to avoid possible short circuits between one converter and another or between parts of a converter and the cavity.

The generator cavity was formed by the cavity pieces of the four thermionic converters and a cavity back-piece that was provided with lateral shielding to minimize heat transmission to the generator block. The rear of the back-piece was left unshielded because the heat transfer calculations discussed subsequently indicated that, with the narrow cone of light produced by the JPL concentrator, excessive amounts of radiation would impinge on this piece, and its temperature could be kept within reasonable limits (below 2000°C) only by allowing it to radiate heat as freely as possible.

The design was based on generating more than 100 electrical watts on ground test, but at the same time keeping the generator design from departing radically from the optimum configuration for space, namely, the use of the generator with a 5-foot-diameter concentrator. The aperture selected for all calculations was 0.68 in. in diameter. Increasing the cavity aperture beyond this size would necessitate shoe pieces on the converters, which in turn would increase the difficulty of shielding the diodes. Furthermore, the thin tantalum sleeve that supports the emitter would then have to support more weight.

6.2 DISTRIBUTION OF HEAT FLUX IN THE CAVITY

In the analysis of the cavity of the solar thermionic generator, the distributed energy flux was divided into two component fluxes in order to simplify the calculations and the interpretation of the flux distribution. One flux component was thermal, where all the elements of flux were those produced by thermal radiation from the cavity walls, and the second was the solar component, where correspondingly all the elements of flux were those produced by the incoming solar flux and its reflections on the cavity surfaces.

6.2.1 Thermal

Figure 6.1 shows schematically the various heat quantities in the generator cavity which correspond to the thermal flux distribution. Arriving at any one cavity surface (including the aperture, where any arriving flux is lost by the cavity) are the heat quantities Q_1, Q_2 and Q_3. For each one of these a certain amount is absorbed, and a certain amount is reflected at the corresponding surfaces. The net amount absorbed by the cavity back-piece was called q_1, and correspondingly the net amount absorbed by the emitters and all cavity walls and clearance spaces was called q_2. The following equilibrium equations were written:

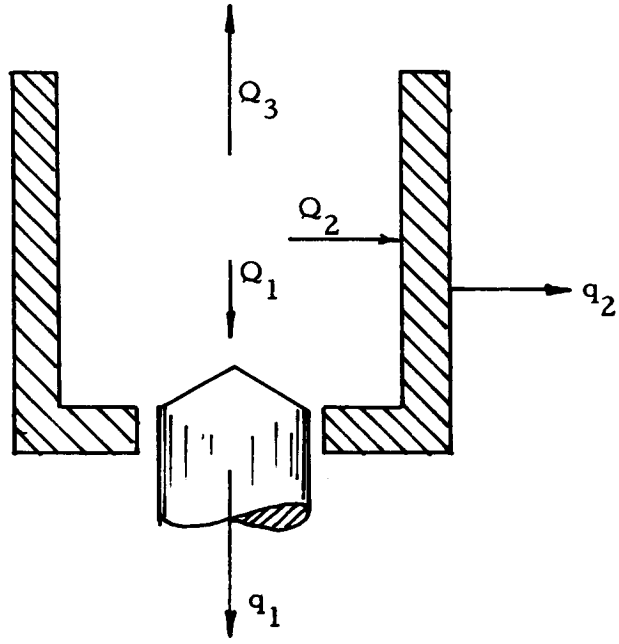

Figure 6.1 Thermal Flux Distribution in Generator Cavity

$$Q_1 - (1 - \epsilon_2) F_{21} Q_2 = \epsilon_2 \sigma T_2^4 F_{21} A_2 \tag{1}$$

$$-Q_1(1 - \epsilon_1) F_{12} + Q_2 [1 - (1-\epsilon_2) F_{22}] = \epsilon_1 \sigma T_1^4 A_1 F_{12} + \epsilon_2 \sigma T_2^4 A_2 F_{22} \tag{2}$$

$$-(1-\epsilon_1)F_{13}Q_1 - (1-\epsilon_2)F_{23}Q_2 + Q_3 = \epsilon_1 \sigma T_1^4 A_1 F_{13} + \epsilon_2 \sigma T_2^4 A_2 F_{23} \tag{3}$$

which simplify to

$$Q_1 = \frac{\eta_1 \epsilon_1 F_{12} H_1 + \epsilon_2 H_2 (\eta_1 F_{22} + \eta_3 F_{21})}{\eta_3 - \eta_1 \eta_2} \qquad q_1 = \epsilon_1 (Q_1 - H_1) \tag{4}$$

$$Q_2 = \frac{\epsilon_1 F_{12} H_1 + \epsilon_2 H_2 (F_{22} + \eta_2 F_{21})}{\eta_3 - \eta_1 \eta_2} \qquad q_2 = \epsilon_2 (Q_2 - H_2) \tag{5}$$

$$Q_3 = \eta_4 Q_1 + \eta_5 Q_2 + \epsilon_1 F_{13} H_1 + \epsilon_2 F_{23} H_2 \tag{6}$$

where the new parameters appearing in these equations are defined by

$$(1-\epsilon_2)F_{21} = \eta_1 \tag{7}$$

$$(1-\epsilon_1)F_{12} = \eta_2 \tag{8}$$

$$1 - (1-\epsilon_2)F_{22} = \eta_3 \tag{9}$$

$$(1-\epsilon_1)F_{13} = \eta_4 \tag{10}$$

$$(1-\epsilon_2)F_{23} = \eta_5 \tag{11}$$

$$\sigma T_2^4 A_2 = H_2 \tag{12}$$

$$\sigma T_1^4 A_1 = H_1 \tag{13}$$

The view factors, F_{ij}, appearing in the equations are derived from the basic formula for two parallel discs of different diameters opposed to each other on the same center line (NACA TN2836, December 1952) and, for the cavity dimensions of generator JG-3, they have the following values:

$$F_{13} = \underline{0.13} \qquad \left(\frac{r_1}{d} = 0.42, \quad \frac{d}{r_3} = 1.68\right)$$

$$F_{12} = 1 - F_{13} = \underline{0.87}$$

$$F_{21} = \frac{A_1}{A_2} F_{12} = \underline{0.115}$$

$$\left.\begin{aligned} F_{23} &= \frac{A_3}{A_2} F_{32} \\ F_{32} &= F_{31} = 1 \\ F_{31} &= \frac{A_1}{A_3} F_{13} \end{aligned}\right\} \qquad F_{23} = \underline{0.242}$$

$$F_{22} = 1 - F_{23} - F_{21} = \underline{0.643}$$

where the cavity areas assumed are

$$A_1 = 1.20 \text{ cm}^2$$

$$A_2 = 9.04 \text{ cm}^2$$

$$A_3 = 2.34 \text{ cm}^2$$

The temperature in the cavity was known except for the temperature of the cavity back piece. Therefore, Equations (4), (5) and (6) could be solved as a function of this unknown temperature. Assuming $\epsilon_1 = \underline{0.25}$, $\epsilon_2 = \underline{0.35}$ (because of grooving), and $T_2 = 2000°K$, the results obtained are given in watts in Table 6-1 for three values of cavity back-piece temperature.

TABLE 6-1

HEAT FLUX QUANTITIES

	$T_1 = 2200°K$	$T_1 = 2400°K$	$T_1 = 2800°K$
Q_1	66.9	68.9	74.8
Q_2	451.3	478.3	557.3
Q_3	152.2	158.7	178.2
q_1	-23.2	-39.0	-86.1
q_2	-129.0	-119.7	-92.2

6.2.2 Solar

Three cases of solar flux distribution were analyzed:

Case I: Corresponded to the operation of the generator in earth space with a 5-ft concentrator of 60° rim angle and assumed a total shadow area of 1 sq ft (generator shadow 0.3 sq ft and supporting arms shadow 0.7 sq ft).

Case II: Corresponded to ground test of the generator with a 9-1/2-ft diameter concentrator of 42° rim angle with a 1-inch thick quartz window at a location where the solar constant is 90 watts/sq ft (vacuum chamber shadow of 2 sq ft and supporting arms shadow of 3 sq ft).

Case III: Corresponded to Case II, except that the concentrator was masked to leave an effective diameter of 7.5 ft.

Of the incoming fluxes, a certain portion strikes the cavity back piece directly and the balance strikes the other internal cavity surfaces. In these calculations it has been assumed that the incoming flux is distributed in correspondence with the solid angles subtended from the focal plane by cavity back piece and by the rim of the concentrator. Figure 6.2 shows these two angles. After taking into account the effects of the shadow areas, the following amounts of the total incoming flux were calculated to strike directly the cavity back piece.

Case I: Flux striking cavity back-piece = 8.7% of total incoming flux.

Case II: Flux striking cavity back-piece = 20.5% of total incoming flux.

Case III: Flux striking cavity back-piece = 31.7% of total incoming flux.

Figure 6.3 shows the distribution diagram for the case of solar flux. A similar group of equations, as were derived for the case of thermal flux distribution, apply to the solar distribution, namely

$$Q_1' = (1-\epsilon_2')Q_2'F_{21} + E_1 \tag{14}$$

$$Q_2' = (1-\epsilon_1')Q_1'F_{12} + E_2 + (1-\epsilon_2')Q_2'F_{22} \tag{15}$$

$$Q_3' = (1-\epsilon_1')Q_1'F_{13} + (1-\epsilon_2')Q_2'F_{23} \tag{16}$$

which can be reduced to

$$Q_1' = \frac{\eta_3 E_1 + \eta_1 E_2}{\eta_3 - \eta_1 \eta_2} \tag{17}$$

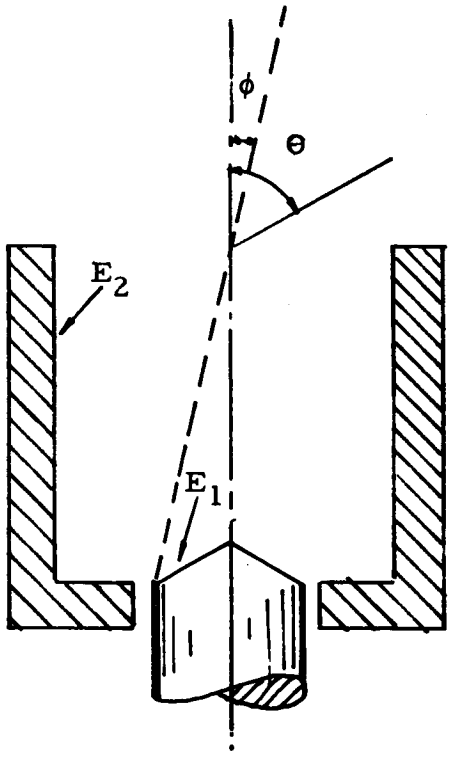

Figure 6.2 Angles of Incoming Solar Flux

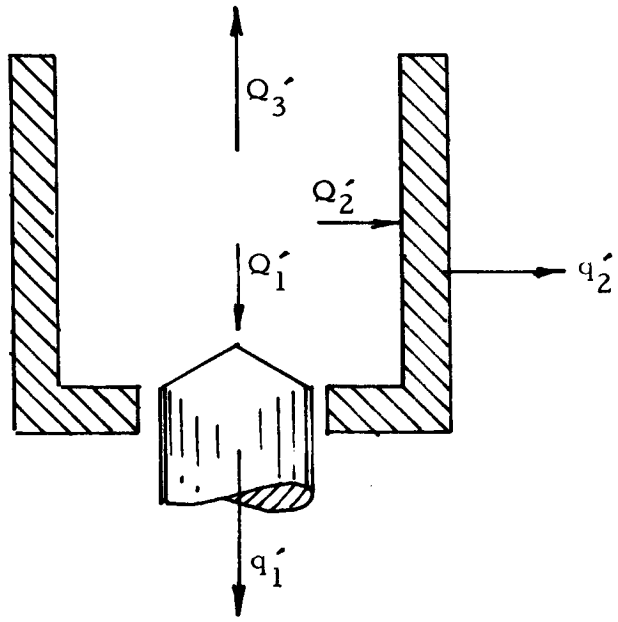

Figure 6.3 Solar Flux Distribution in Generator Cavity

$$Q_2' = \frac{\eta_2 E_1 + E_2}{\eta_3 - \eta_1 \eta_2} \tag{18}$$

$$Q_3' = \eta_4 Q_1' + \eta_5 Q_2' \tag{19}$$

where the new parameters are defined by

$$(1-\epsilon_2')F_{21} = \eta_1 \tag{20}$$

$$(1-\epsilon_1')F_{12} = \eta_2 \tag{21}$$

$$1 - (1-\epsilon_2')F_{22} = \eta_3 \tag{22}$$

$$(1-\epsilon_1')F_{13} = \eta_4 \tag{23}$$

$$(1-\epsilon_2')F_{23} = \eta_5 \tag{24}$$

The view factors are the same as those for the thermal flux distribution, but the values of emissivity are different because of the shorter average wavelength of the solar radiation. Since the effective absorptivity of the grooves on the cavity walls is not accurately known, the calculations were made for two values: 0.60 and 0.80. The absorptivity for the cavity back piece surface was assumed to be 0.45. The results of the calculations are shown in Tables 6-2, 6-3 and 6-4.

TABLE 6-2

Case I

5 ft - 60° 130 w/ft^2

E = 2060 watts

	$\epsilon'_2 = 0.60$	$\epsilon'_2 = 0.80$
Q'_1	305	233
Q'_2	2730	2290
Q'_3	286	127
q'_1	137	105
q'_2	1637	1828

TABLE 6-3

Case II

9.5 ft - 42° 90 w/ft^2

E = 2120 watts

	$\epsilon'_2 = 0.60$	$\epsilon'_2 = 0.80$
Q'_1	555	485
Q'_2	2633	2205
Q'_3	294	141
q'_1	250	218
q'_2	1576	1761

TABLE 6-4

Case III

7.5 ft - 34° 90 watts/ft^2

E = 1580 watts

	$\epsilon_2' = 0.60$	$\epsilon_2' = 0.80$
Q_1'	585	535
Q_2'	1830	1532
Q_3'	219	112
q_1'	263	241
q_2'	1098	1227

The total incoming energy for Cases II and III corresponds to the data obtained in solar tests by JPL at Table Mountain.

6.2.3 Summary

The net flow of energy in the cavity was obtained by direct superposition of the thermal and solar distributions. In order to do this, however, it was necessary to know the equilibrium temperature of the cavity back piece. This was a function of the thermal impedance of this element, which was calculated and which is given in Figure 6.4. It was then possible, by the process of iteration, to find the cavity back-piece temperature for which the net heat absorbed equaled the heat loss. The results of such iterations are presented in Tables 6-5, 6-6 and 6-7.

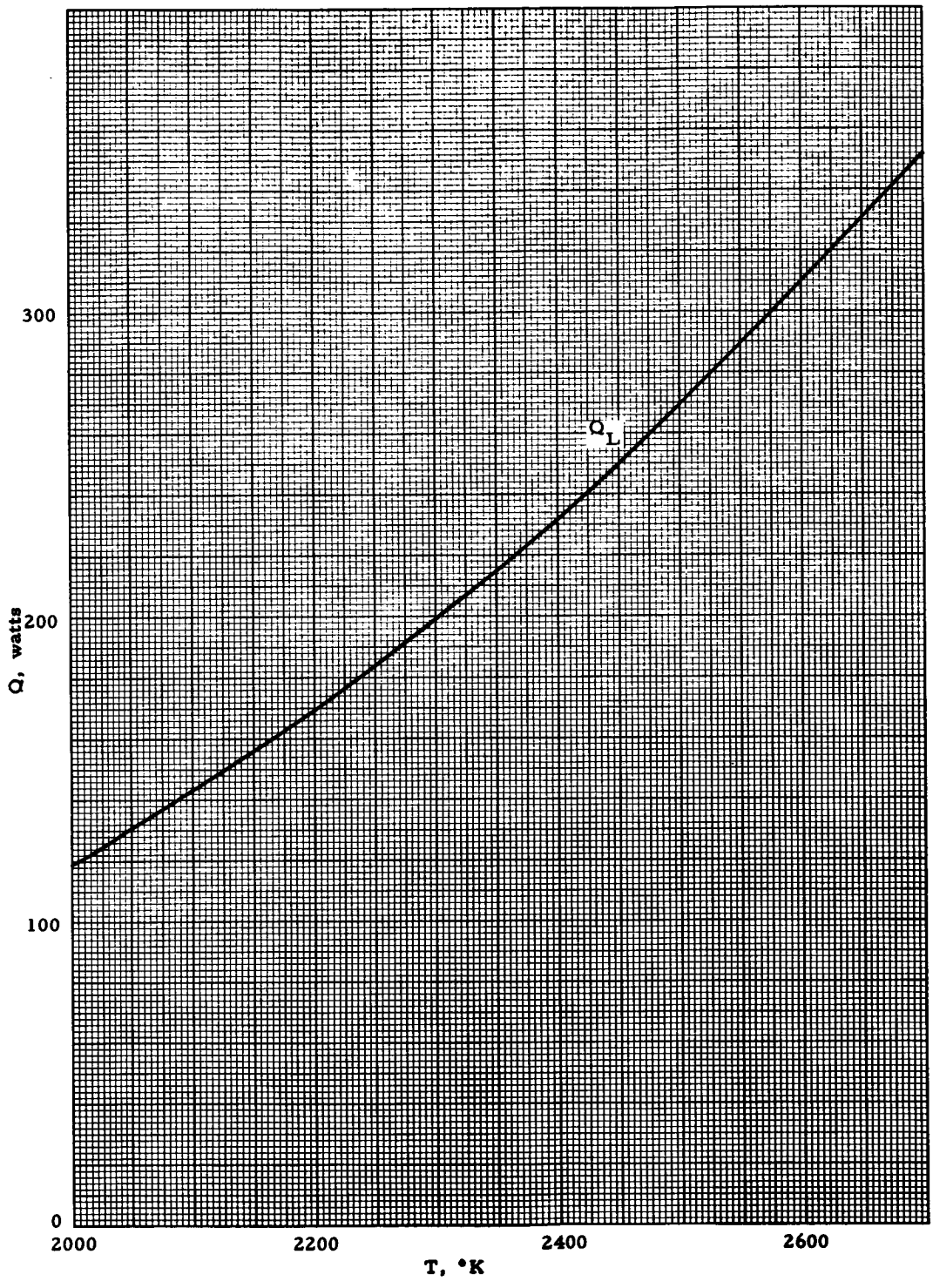

Figure 6.4 **Heat Loss of Cavity Back Piece**

TABLE 6-5

Case I

5 ft - 60° 130 watts/ft^2

E = 2060 watts

	$\epsilon'_2 = 0.60$	$\epsilon'_2 = 0.80$
q_{10}	99	80
q_{20}	1517	1700
Q_{30}	444	280

TABLE 6-6

Case II

9.5 ft - 42° 90 watts/ft^2 quartz window

E = 2120 watts

	$\epsilon'_2 = 0.60$	$\epsilon'_2 = 0.80$
q_{10}	161	143
q_{20}	1485	1664
Q_{30}	474	313

TABLE 6-7

Case III

7.5 ft - 34° 90 watts/ft^2 quartz window

E = 1580 watts

	$\epsilon'_2 = 0.60$	$\epsilon'_2 = 0.80$
q_{10}	226	209
q_{20}	977	1101
Q_{30}	377	270

6.3 HEAT TRANSFER

In Section 6.2 the heat absorbed by the generator cavity was calculated. This section discusses in detail how this absorbed energy is further subdivided in the various elements of the thermionic generator.

6.3.1 Cavity Back Piece

Figures 6.5 and 6.6 show the basic configuration of the cavity back piece and the nomenclature used to identify the various heat losses. The expressions for these various heat losses are as follows:

$$Q_1 = \frac{1}{\frac{1}{0.25} + \frac{1}{0.25} - 1} \sigma A_1 (T^4 - 2000^4) \qquad (1)$$

$$Q_2 = \frac{1}{\frac{1}{0.25} + \frac{1}{0.25} - 1} \sigma (A_2 + \ell_1 \pi D)(T^4 - 900^4) \qquad (2)$$

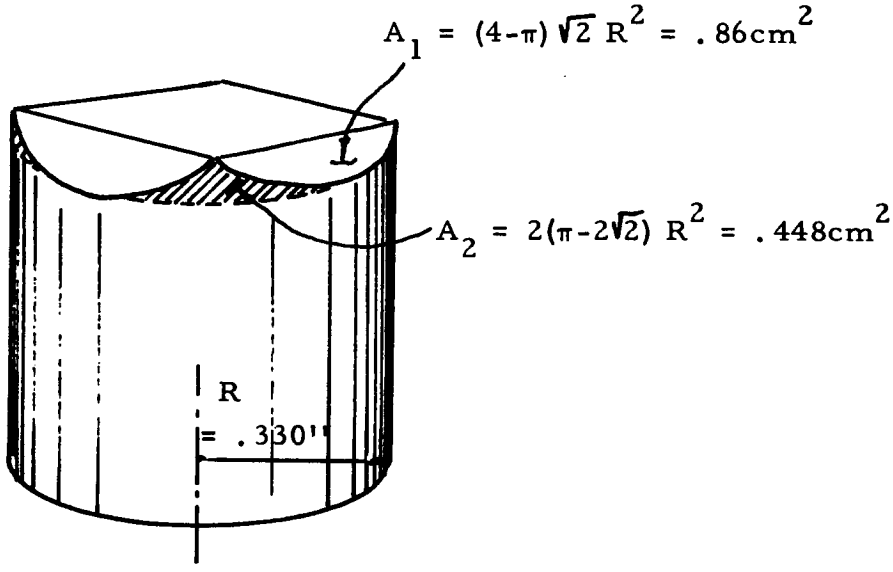

Figure 6.5 Configuration of Back Cavity Piece

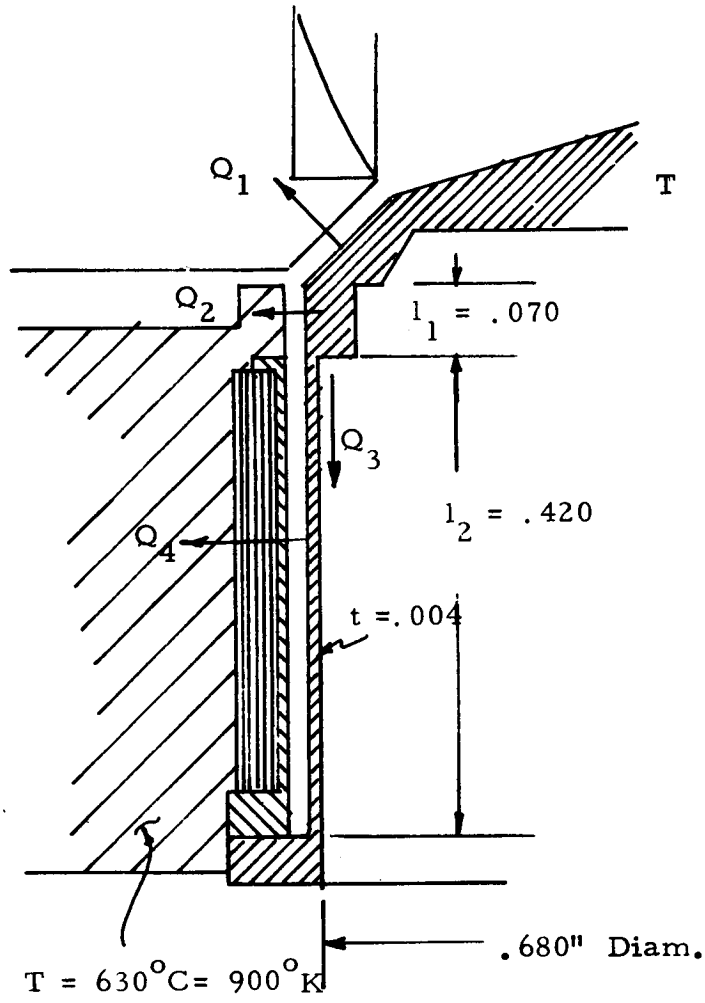

Figure 6.6 Cross Section of Back Cavity Piece and Shielding

$$Q_3 = k\pi Dt \frac{T - 900}{\ell_2} \tag{3}$$

$$Q_4 = \pi D \ell_1 \frac{1}{\frac{1}{0.25} + \frac{1}{0.25} - 1} \sigma (T^4 - 900^4) \tag{4}$$

$$Q_5 = \frac{\pi D^2}{4} \times 0.25 \sigma T^4 \tag{5}$$

where it has been assumed that all emissivities are equal to 0.25, that the generator supporting block operates at 900°K, and that the loss through the shielding, Q_4, is equal to the heat radiated between two concentric cylinders of diameter equal to the shield diameter, of height equal to 0.070, and where the inner and outer cylinder temperatures are 2000°K and 900°K respectively. This last assumption is purely arbitrary; it is the best estimate that can be made of this loss. The numerical values of the dimensions appearing in Equations (1) through (5) are as follows:

$A_1 = 0.86\ cm^2$ $\qquad$ $\ell_1 = 0.175\ cm$

$A_2 = 0.44\ cm^2$ $\qquad$ $\ell_2 = 1.07\ cm$

$D = 1.68\ cm^2$ $\qquad$ $t = 0.01\ cm$

Assuming a conductivity for tantalum at the operating temperature of the wall supporting the cavity back piece of 0.75 watt/cm°C, the heat loss calculated for the cavity back piece is that shown in Figure 6.4 of Section 6.2

6.3.2 Cavity to the Block

Of the amount, q_{20}, calculated in Section 6.2, a certain amount is lost by heat transmission to the generator block, and the remainder is transmitted to

the emitter pieces of the thermionic converters. Figure 6.7 shows the different cavity surfaces, which are as follows:

a. An inner circular lip of the entrance cone of height, h
b. A curved front interstitial space, i_1
c. Four curved triangular elements of area, A
d. Four longitudinal interstitial spaces, i_2
e. Four converter face areas, A_c
f. A rear square interstitial space, i_3
g. The area of the cavity back piece, A_b

The values of these areas are as follows:

$A_b = 1.41 \text{ cm}^2$

$4A_c = 7.58 \text{ cm}^2$

$i_1 + i_2 + i_3 = 0.37 \text{ cm}^2$ (assuming interstices to be 0.010 in wide)

$4A = 0.44 \text{ cm}^2$

inner lip of cone $= 0.66 \text{ cm}^2$

The heat losses occurring at the inner lip of the cone are assumed here to be offset by the additional heat input to the cavity that results from the flux trapping effects of the entrance cone of the generator cavity. The remainder cavity loss areas, namely, $i_1 + i_2 + i_3 + 4A$, then represent 8.3% of the total cavity area. Assuming next that, when the absorptivity of the areas A_c equals 0.80, the heat absorbed by the block is 5% of the available heat in the cavity and that, when the absorptivity of the areas A_c equals 0.60, 6% of the available heat is absorbed by the block, the actual resulting amounts of heat absorbed by the block are as shown in Table 6-8.

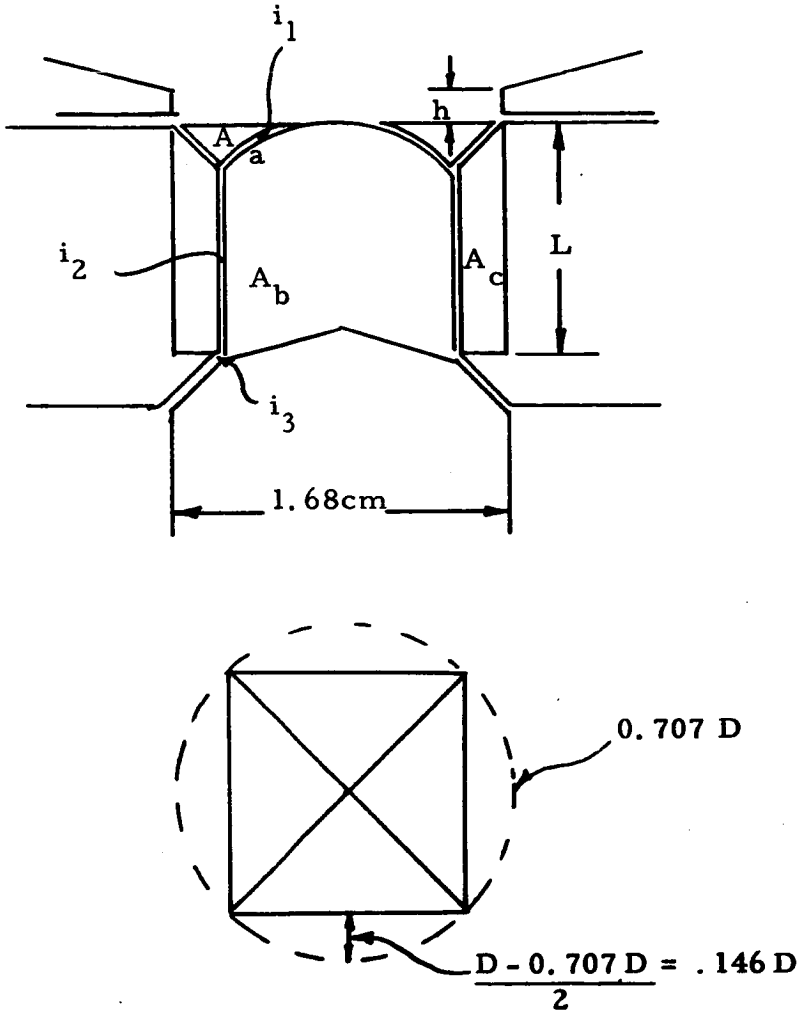

Figure 6.7 Generator Cavity Surfaces

TABLE 6-8

	$\epsilon_2' = 0.60$	$\epsilon_2' = 0.80$
Case I	91	85
Case II	60	56
Case III	89	83

6.3.3 Converter Heat Transfer

Of the heat available in the cavity, a certain amount, q_{10}, is lost to the cavity back piece, and an amount as given in Table 6-4 is lost to the generator block. The remaining heat is then available to power the thermionic converters and must be sufficient to overcome the following losses:

a. Emitter Support Conduction: This loss is assumed to be 150% of the ideal conduction loss in the absence of radiation by the emitter support in order to account for the effects of such radiation heat transfer on the temperature gradient along the length of the emitter support. This assumption is partially justified by the general experience obtained from detailed calculations of heat transfer in such elements of various configurations. Such detailed calculations have not been made here because the problem was greatly complicated by the presence of a large amount of radiation shielding which is subject to an unpredictable amount of longitudinal conduction. Assuming an emitter temperature of 2000°K and a base temperature of 900°K (lower than the expected value in order to give a conservative result), and assuming a spacer wall thickness of 3.5 mils, the conduction loss calculated for four converters is then 196 watts.

b. Interelectrode Radiation: Assuming an emitter emissivity of 0.25, a collector emissivity of 0.35, an emitter temperature of 2000°K and a collector temperature of 900°K, the interelectrode radiation for four converters is 119 watts.

c. Cesium Conduction: Assuming a reservoir temperature of 370°C and an interelectrode spacing of 2 mils, the calculated cesium conduction from the experimental results of S. S. Kitrilakis and M. Meeker is 6.4 watts/cm^2 for an emitter temperature of 2000°K and a collector temperature of 900°K. For four converters, this is then equal to 50 watts.

d. External Radiation by the Emitter Piece to the Generator Block: From the calculations of the heat losses for the cavity back piece, this loss is found to be 17 watts per converter, or 68 watts for all four.

e. Electron Cooling: This loss is given by the equation

$$q_e = 4(\phi_E + 2k T_E) I_o \qquad (6)$$

Assuming a saturation current of 100 amps/cm^2 and an emitter temperature of 2000°K, the value of $\phi_E + 2k T_E$ was 3.01 electron volts. This value is relatively independent of the accuracy with which the saturation current is actually known. Equation (6) can, therefore, be simplified to

$$q_e = 12.04 I_o \qquad (7)$$

The actual value of I_o (the output current of each thermionic converter) was obtained from the data for Converter VIII-P-2a at 1700°C observed emitter temperature. Assuming that the converters in the

generator are connected in series, the electron cooling loss was calculated as a function of generator output voltage. This value, added to that of the other converter losses, then gave the result plotted in Figure 6.8, which shows both the total power produced by the generator and the heat absorbed by the thermionic converters as a function of generator output voltage.

6.3.4 Other Losses

In order to arrive at the complete heat-transfer diagram for generator JG-3, it was necessary to compute some additional heat terms.

a. Connecting Leads: This loss was calculated assuming ideal conduction in the copper output leads. The temperature at the connecting point on the thermionic converter was assumed to be 600°C, and that at the other end of the lead was assumed to be 350°C; the length of the lead was assumed to be 6 inches and its cross section 1/8 x 1/2 inch. For a total of 8 such leads connected to the generator, the heat loss then calculated is 192 watts.

b. Radiation by the Converters to the Block: This loss was assumed to be equal to the sum of the loss terms Q_2 and Q_4 of the cavity back piece shown in Figure 6.6, and for four converters it is equal to 114 watts.

c. Back Piece to the Block: Of the heat loss terms of the cavity back piece shown in Figure 6.6, all but Q_1 are transmitted to the generator block. Using the equations presented earlier in this section, this heat transfer was found to be 86 watts for Case III, with an absorptivity of 0.8, and 92 watts for the same case with an absorptivity of 0.6.

d. Generator Support: This loss was small because of the generator supports were not joined metallurgically into the generator radiator. The loss

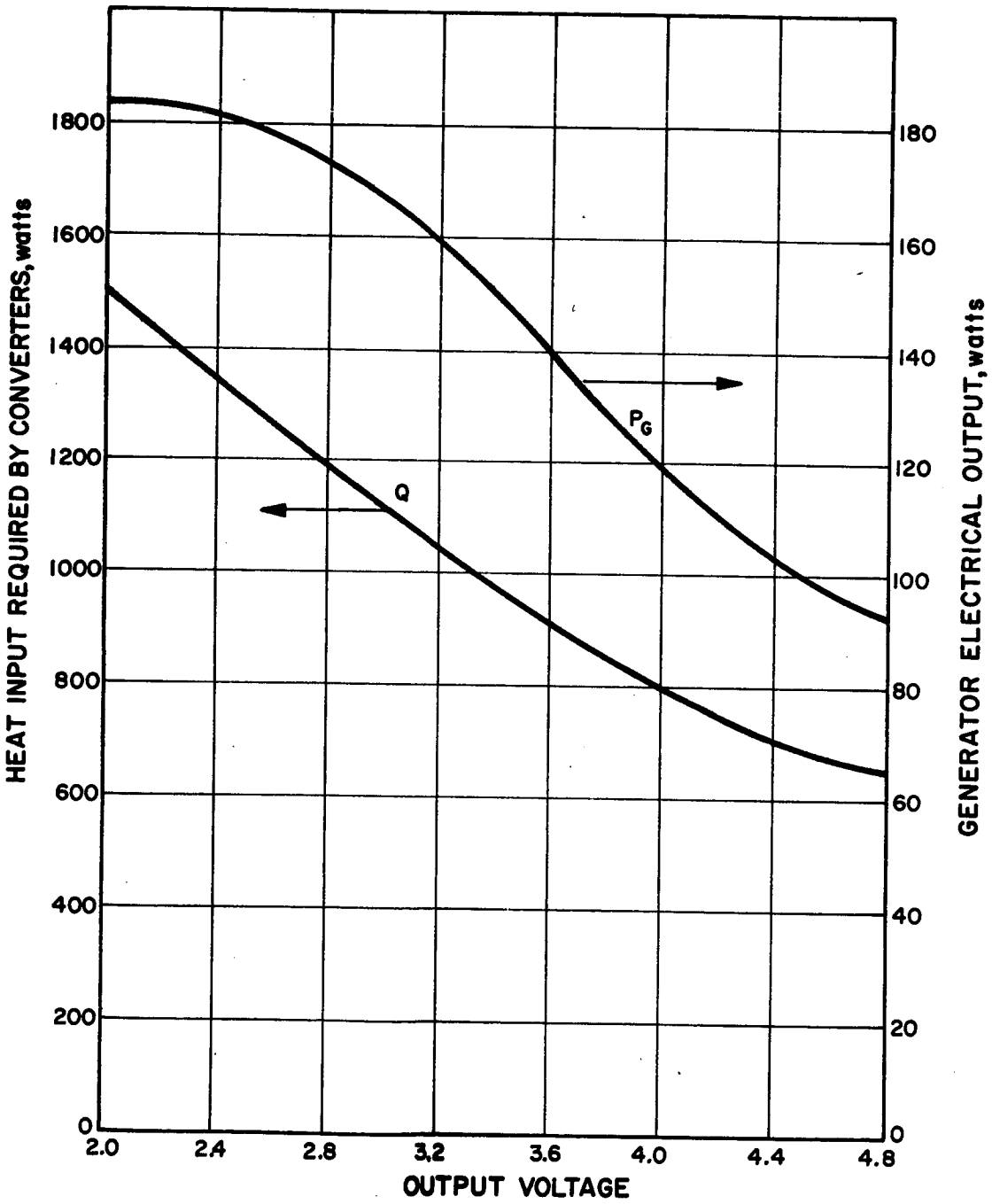

Figure 6.8 **Predicted Generator** Performance

was calculated assuming that the magnitude of the thermal conduction through the parts in mechanical contact will be equal to 10% of that which would occur if these parts were brazed together, and the value arrived at is 30 watts.

6.3.5 Results

Figures 6.9 and 6.10 show in schematic form the flow of all the heat terms calculated above for Case II for cavity wall absorptivity values of 0.6 and 0.8 respectively.

6.4 THERMAL EXPANSION CALCULATIONS AND TESTS

In view of the desire to position the diode cavity pieces as close as possible to minimize radiation losses through the cracks, an analysis was made of the expansion of the various parts as the generator heats up. The expansions of the diode emitter structures and of the radiation shields around it were both considered. When a satisfactory mechanical configuration was established, a heat balance for the generator, calculated earlier, was used to establish the size of the generator block radiator. A simulated generator, incorporating such a radiator, was then thermally tested using electron-bombardment heating. The thermal test confirmed the adequacy of the radiator and also verified various other calculated heat terms.

Figure 6.11 shows the JG-3 generator design. Four Series VIII converters, placed orthorgonally, are held by a molybdenum block so that their emitter cavity pieces form the solar cavity. The converters and the block are designed to accommodate a solar flux cone of 60°. Each converter is attached to the block with four screws passing through the converter's mounting flange. Three additional screws attach each

Concentrator Diameter: 7.5 feet
Cavity Wall Absorptivity: 0.6

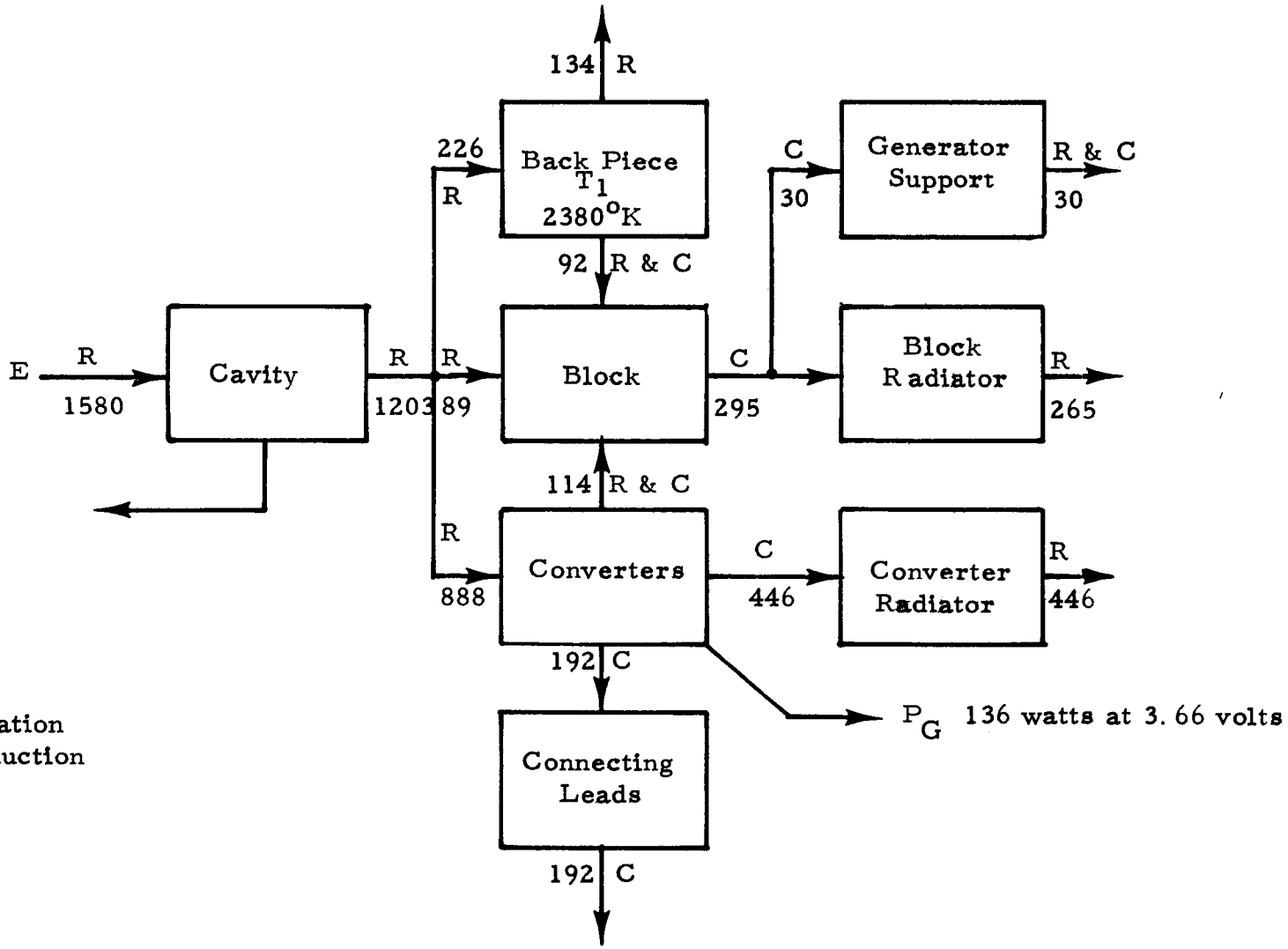

R = Radiation
C = Conduction

Figure 6.9 Generator Heat Transfer Diagram for 0.6 Cavity Absorptivity

Concentrator Diameter: 7.5 feet
Cavity Wall Absorptivity: 0.8

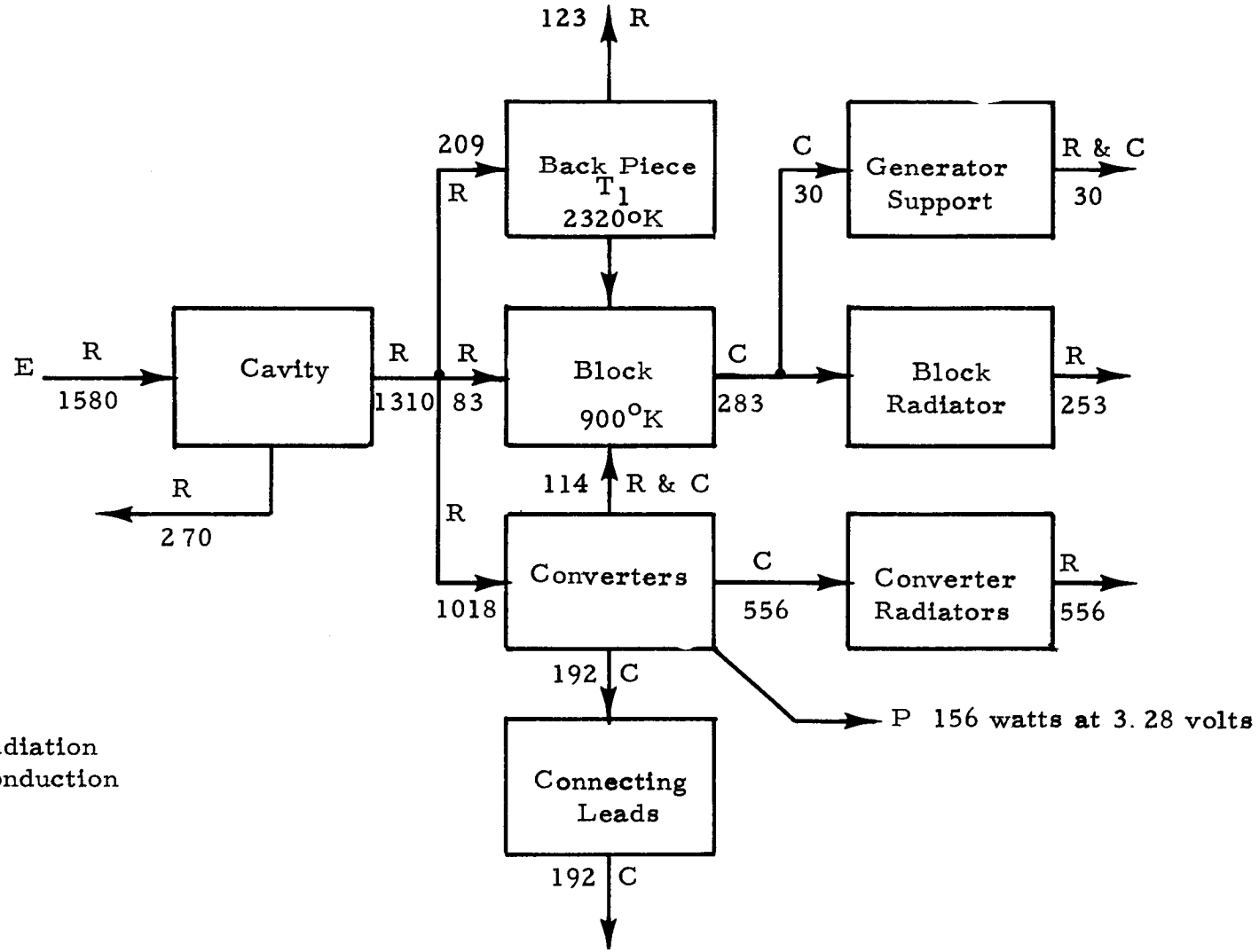

R = Radiation
C = Conduction

Figure 6.10 Generator Heat Transfer Diagram for 0.8 Cavity Absorptivity

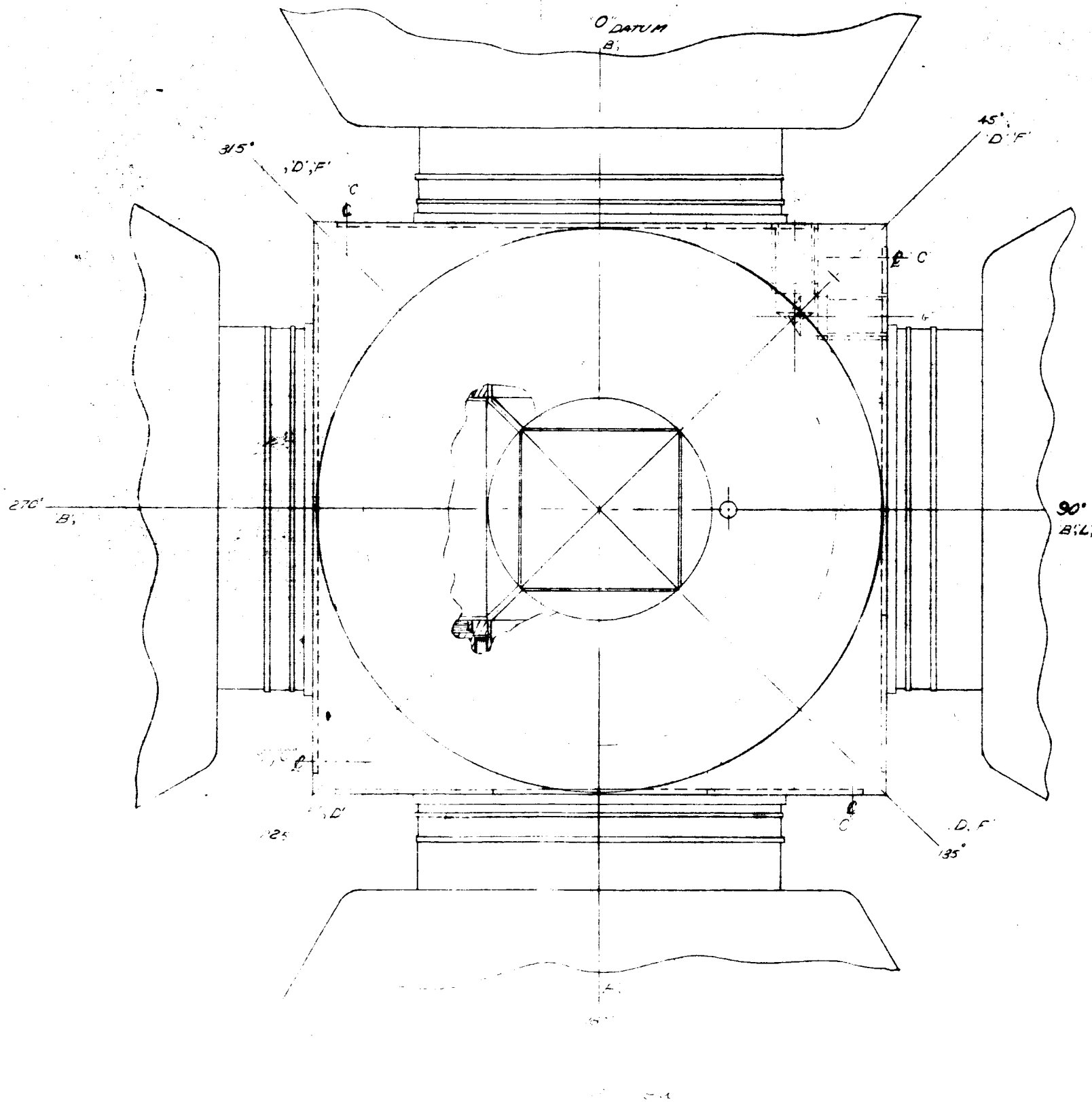

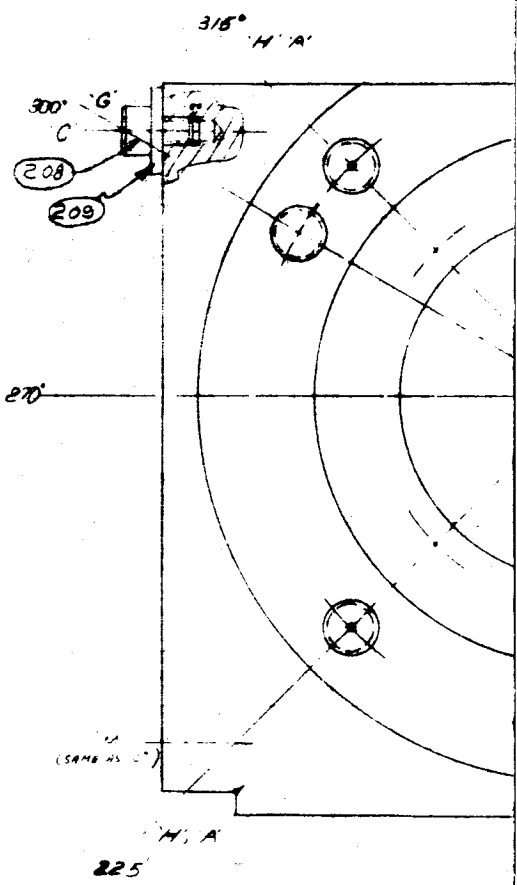

FOLDOUT FRAME 1

FOLDOUT FRAME 2

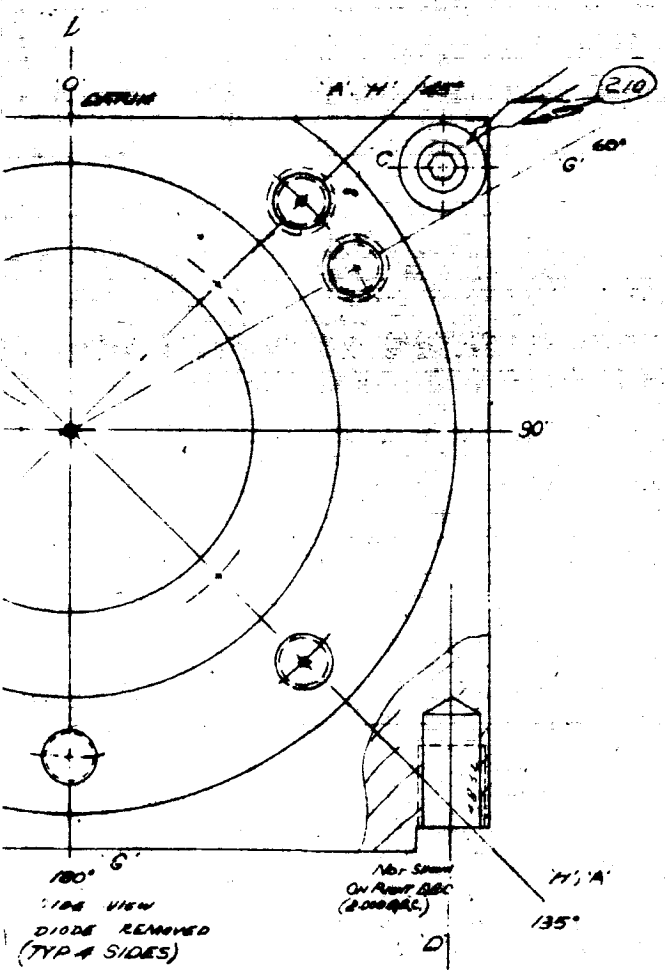

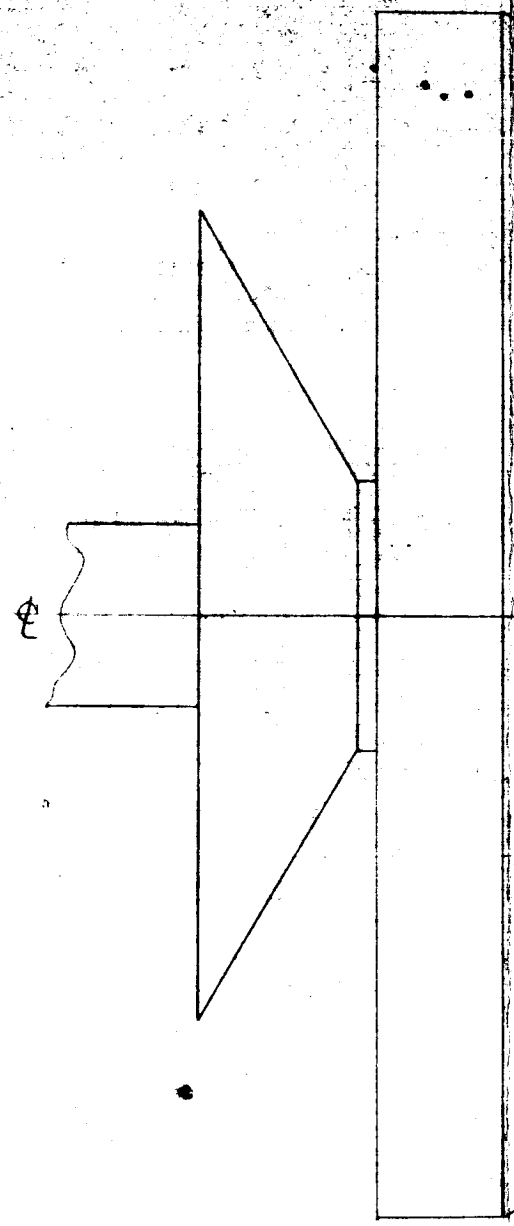

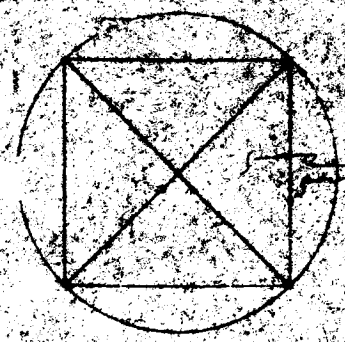

VIEW 'A'-'A'

VIEW 'A'-'A' IS NOT A SECTION THRU DIODES, BUT A VIEW OF P. NO. 1

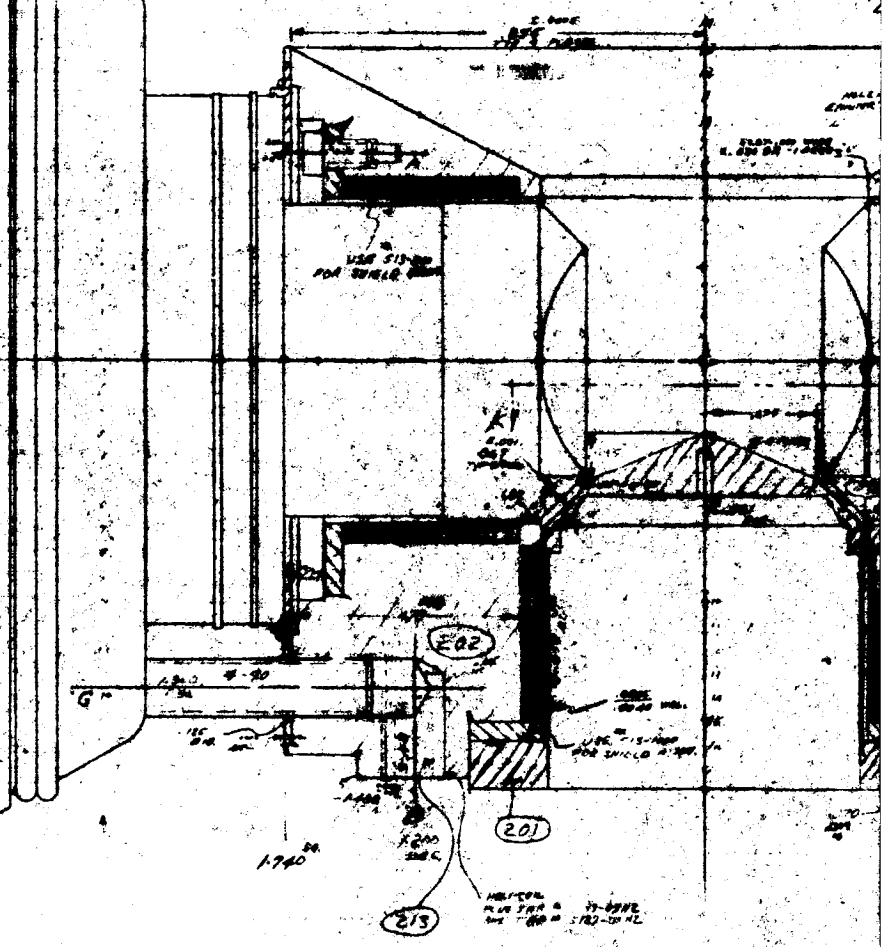

FOLDOUT FRAME 3

FOLDOUT FRAME 4

REV	DESCRIPTION	DATE	BY	APPR
A	SEE OBSOLETE LAYOUT (8-6-69)	8/[illegible]-69	[illegible]	
B	SEE OBS L.O. (8-29-69)	9-29-69	VP	
C	SEE OBS L.O. (10-22-69)	10-22-69	VP	
D	SEE OBS L.O. (11-29-69)	11-29-69	VP	

PLAN

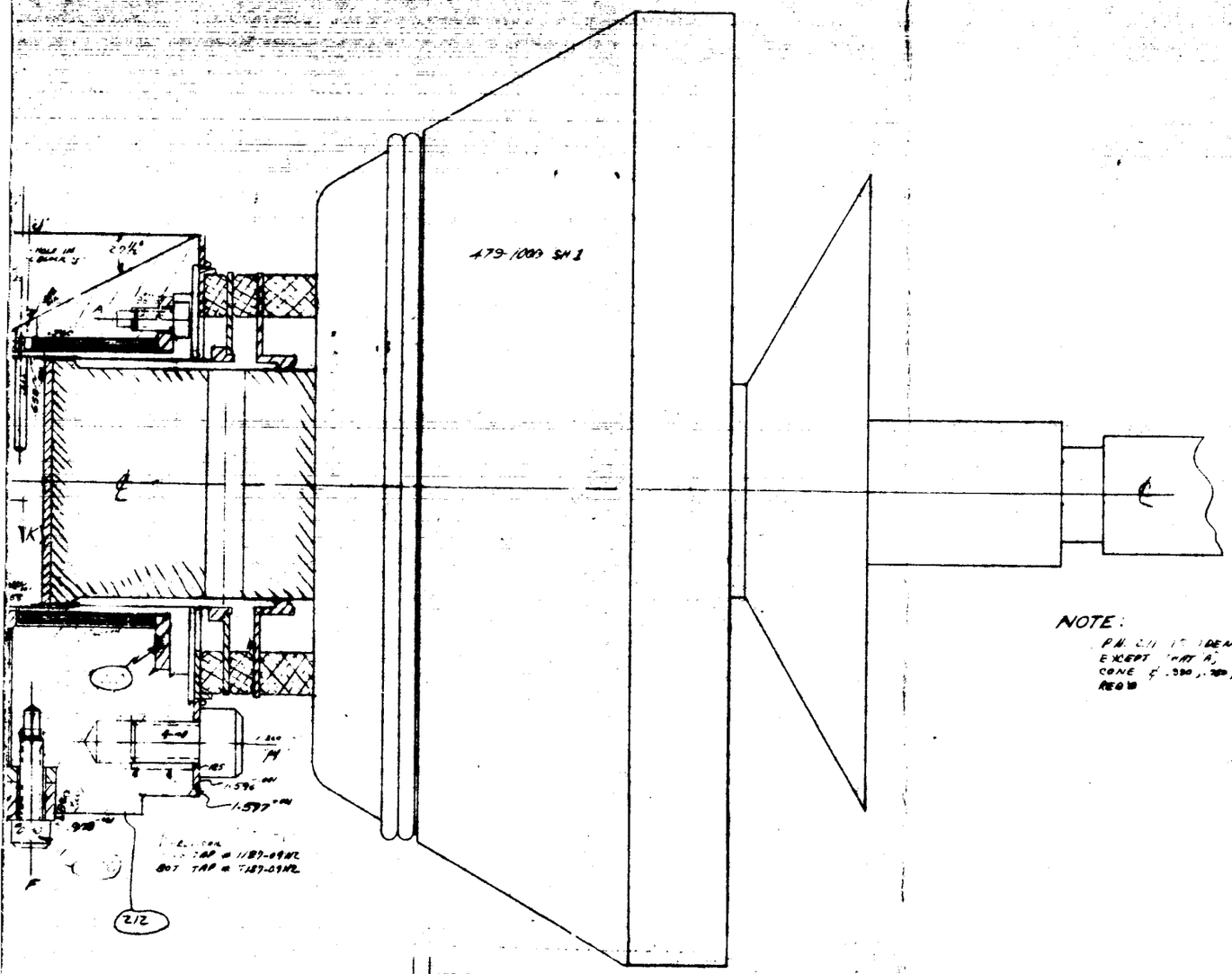

NOTE:
P.N. 211 IS IDENTICAL TO P.N. 202 EXCEPT THAT A, "J" HOLES & CONE ⌀ .590, .700, .1100 DIA. ARE NOT REQ'D

7	SEE FIXTURE LAYOUTS (2000, 2100 ETC.) FOR FIXTURE INFORMATION.
6	UNS = MANSON R.D. = NO DRAWING, PROCURE FROM THIS L.O.
5	DOTTED LINES INDICATE ROUGH OR PRELIMINARY MACHINING.
4	ALL MATING CORNERS & FILLETS ARE .010 X 45° CHFR. AND .010 R. RES.
3	MAX. PERMISSABLE TAP DRILL DEPTH AND MIN. PERMISSABLE FULL THREAD DEPTHS ARE SHOWN.
2	SECTION LOCATIONS DEFINED BY LETT. R LOCATION AT END VIEW.
1	NOTES 2 THRU 7 APPLY UNLESS OTHERWISE SPECIFIED.

NOTES

DESIGN FINALIZED	DATE	INT.	DATE	INT.	DATE	INT.	DATE	INT.

	A	B	C	D	E	F	G	H	J	K	L	M	N	P	R	S	T	U	V	W	Y	Z
1												✓										
2																						
3																						
4																						

FOLDOUT FRAME 5

LAYOUT OF GENERATOR JG-3
FIGURE 6.11

FOLDOUT FRAME 6

PART	SIZE	REQ	NOTES
			LAYOUT & SUB-ASSEM
1010		1	MOD. OF 513-1000 (½" SLOT ADDED).
213	NO	9	SS	#3585-032H-0168 HELI-COIL
212	NO	28	SS	#3585-094H-0168 HELI-COIL
211	M	B	1	Mc	ALT FOR NO 202 SEE NOTE
210	NO	3		CHROMEL - ALUMEL THERMOCOUPLE
209	NO	5	SS	SST.	#0 FLANG WASHER
208	NO	5	SS	SST.	#0-80 x .094 H. SOC. S
207	—	—	—	—	
206	NO	4	SS	SST.	#-80 X 254 H.S.C.S
205	—	—	—	—	
204	—	—	—	—	
203	—	—	—	—	
202	H	B	1	Mc	
201	C	B	1	Mc	

PART	SIZE	REV	REQ	MAT'L

UNLESS OTHERWISE SPECIFIED
DEC .X± .1 .XX± .01 .XXX ± .005
SCALE FULL
ANGLES ± 0°30' FINISH √ MAX
FILLET RAD .010 MAX
THREADS CLASS 2
ALL DIAS CONCENTRIC WITHIN .005 TIR
REMOVE ALL BURRS & SHARP EDGES

NEXT ASSY | SIM TO

NOTES

THERMO ELECTRON
ENGINEERING CORP
WALTHAM 54, MASS

DR | ENG
CHK | APP

TITLE
GENERATOR JG 3

SIZE 17 | NUMBER 479000 | REV D

FOLDOUT FRAME

converter's radiator to the block. These latter screws are designed to expand sufficiently to relieve their restraint when the generator is heated. The rear of the block, shown at the bottom in Figure 6.11, is fitted with a cavity piece shaped to reflect the incoming solar flux toward the four emitters. To minimize heat transfer from the back cavity piece to the support block, a thin-walled support is used to hold the cavity piece, and several layers of radiation shielding are provided around the thin wall. Radiation from the converters to the block is also minimized with similar radiation shields. A radiator is attached to the rear of the support block to maintain the block temperature within safe limits. The generator support structure and the radiator can be seen in Figure 6.12, in which the block can be seen attached to a support ring (PN603) with four rods (PN605). In this case the support ring is shown attached to a mounting plate for environmental testing.

The relative thermal expansions of the cavity components were calculated and are shown in the next several sections.

6.4.1 Calculation of Clearances

6.4.1.1 Clearances Between Cylindrical Wall of Emitter, Shield and Block

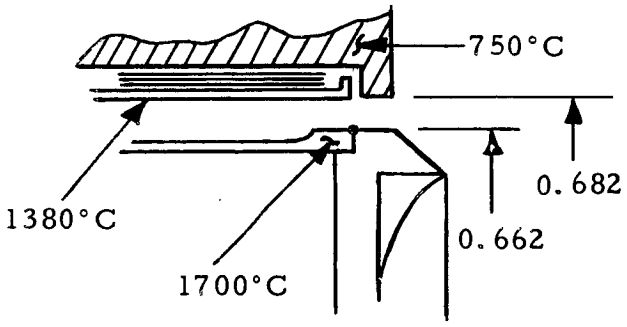

Clearance at room temperature:

$$\frac{0.682 - 0.662}{2} = 0.010 \text{ in.}$$

Clearance* changes at temperature:

$$\text{Emitter expansion} = \frac{0.662}{2} \times 0.125 = 0.00415 \text{ in.}$$

$$\text{Shield expansion} = \frac{0.682}{2} \times 0.010 = 0.00341 \text{ in.}$$

$$\text{Block expansion} = \frac{0.682}{2} \times 0.004 = 0.00138 \text{ in.}$$

Clearance at operating temperature, emitter to shield:

$$\left[\left(\frac{0.682}{2} + 0.00341\right) - \left(\frac{0.662}{2} + 0.00415\right)\right] = 0.00926 \text{ in.}$$

Clearance at operating temperature, emitter to block:

$$\left(\frac{0.682}{2} + 0.00138\right) - \left(\frac{0.662}{2} + 0.00415\right) = 0.00723 \text{ in.}$$

*Thermal expansion data published in Handbook of Thermophysical Properties of Materials.

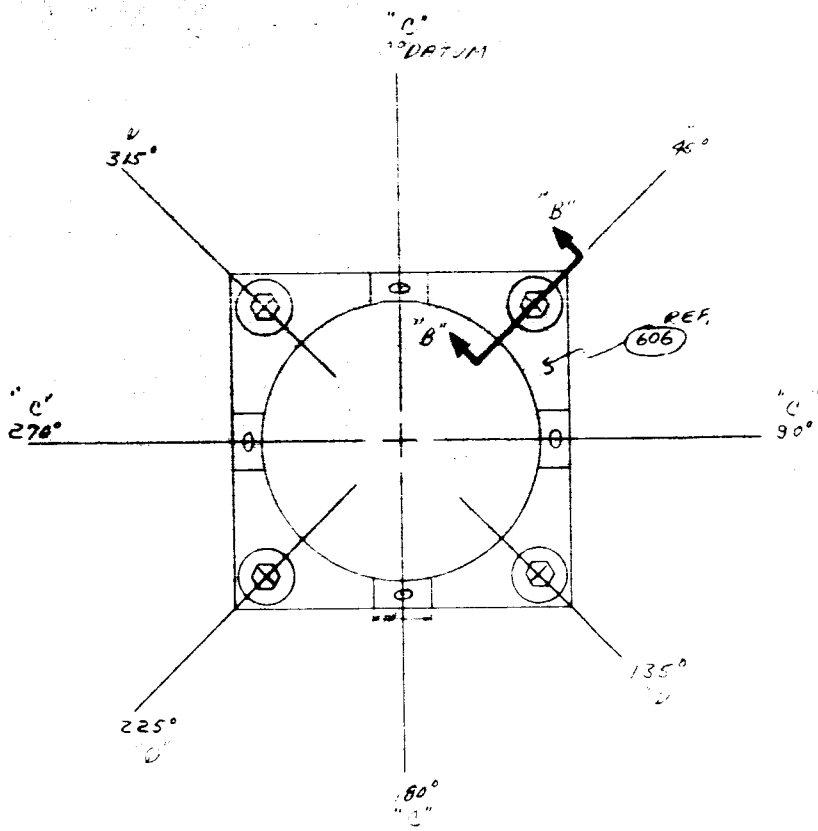

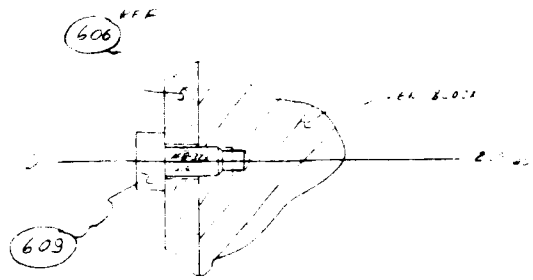

"B-B"

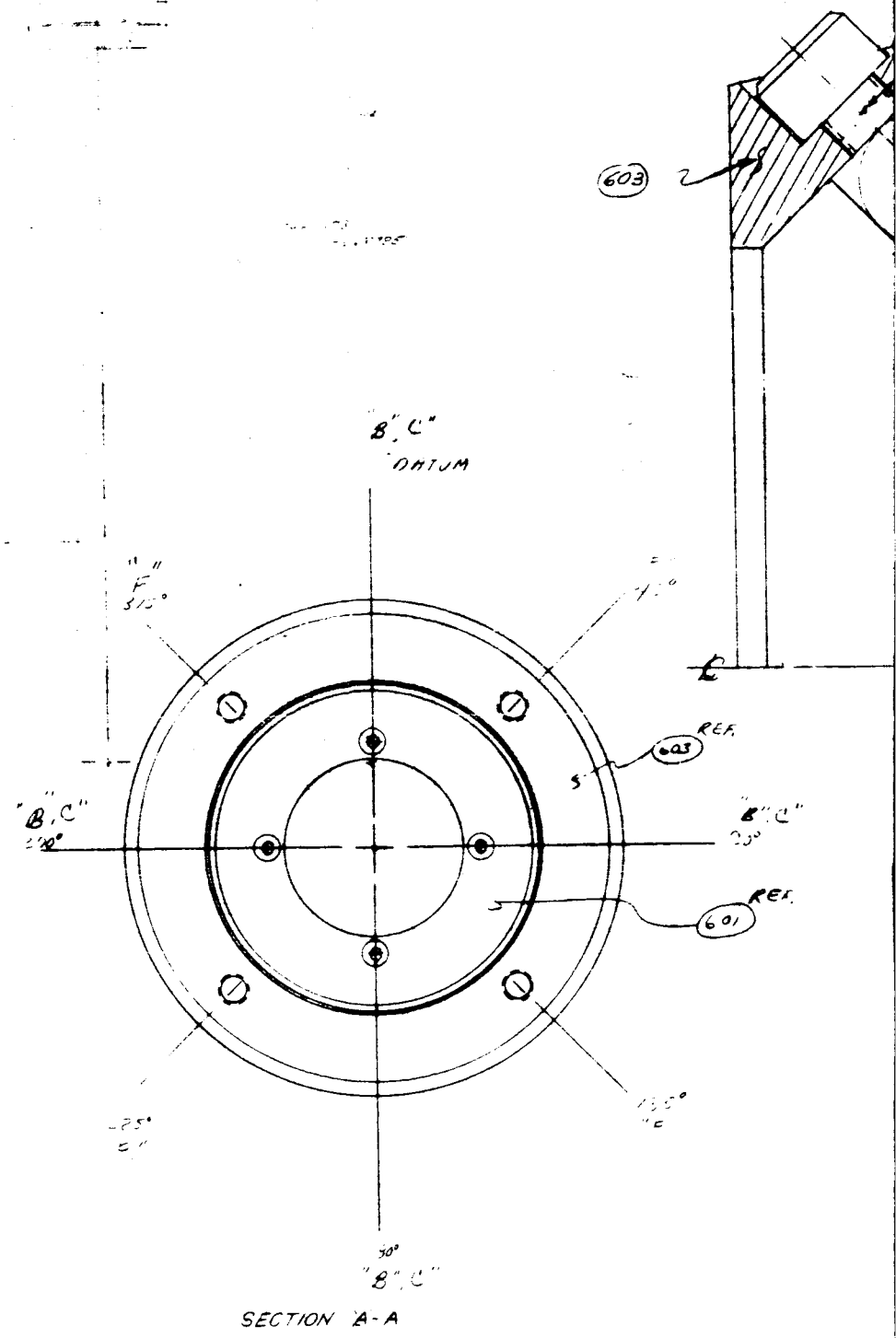

SECTION A-A

FOLDOUT FRAME 1

FOLDOUT FRAME 2

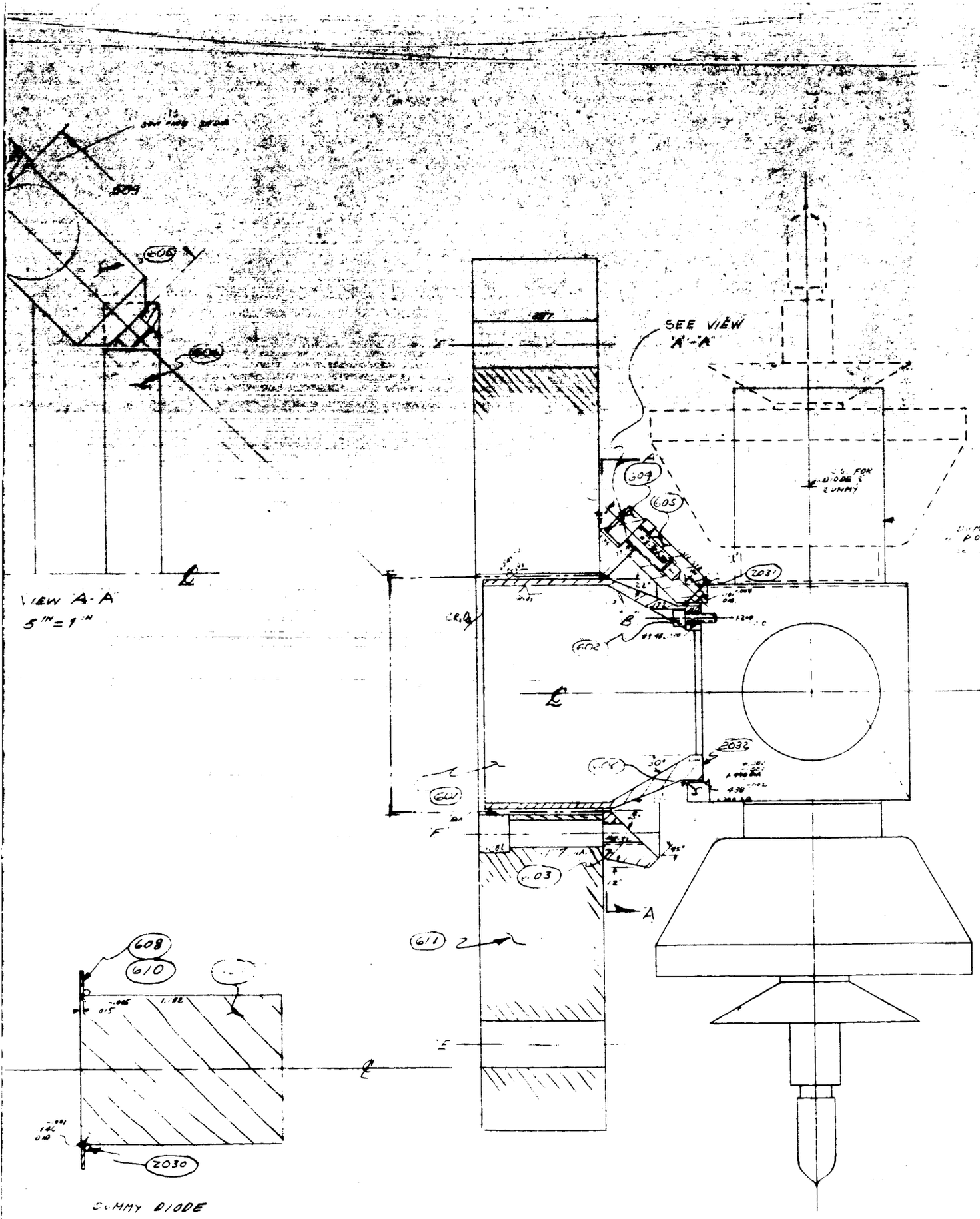

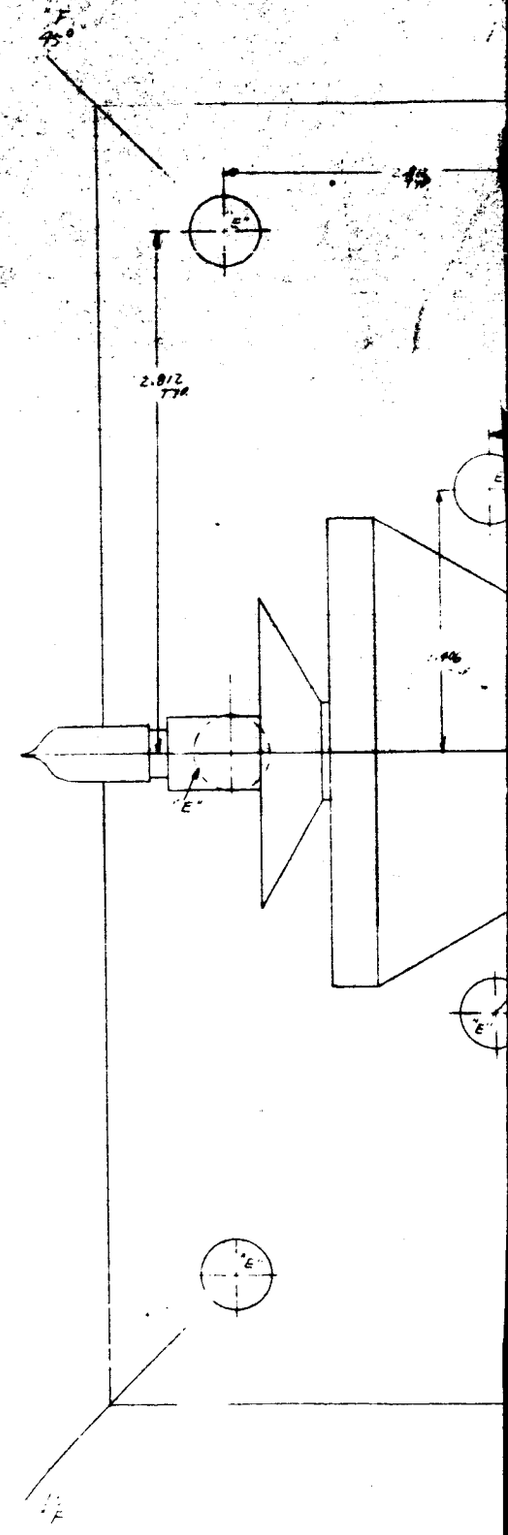

FOLDOUT FRAME 3

FOLDOUT FRAME 4

REV	DESCRIPTION	DATE	BY	APPR
J	PER 09 MAS-755	4-29-69	VA	

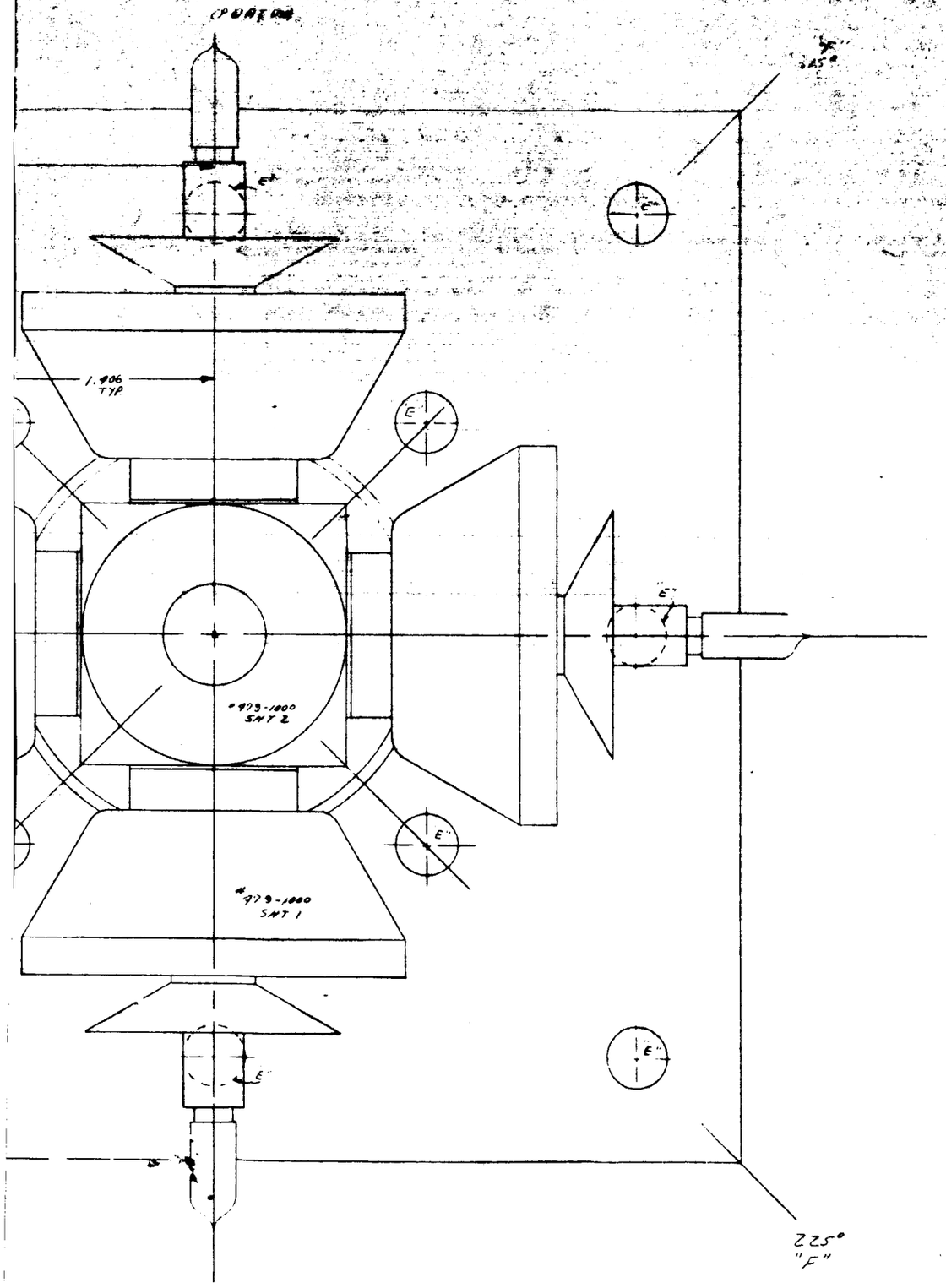

LAYOUT OF GENERATOR SUPPORT STRUCTURE

FIGURE 6.12

PART	SIZE	REQ	LOC	MAT'L	NOTES
		BRAZES			
2030	NO	9	—		.030 DIA. WIRE
2031	NO	9	—		.030 DIA. WIRE
2032	A	1	—		
611	C		1	Al	
610	SEE 979-12		16	SS	#4-40 x .625 LG. SH.CS.(MOD.)
609	NO		-	SS	#8-32 x - LG. H.S.C.S.
608	SEE 979-12		9	Nb	
607	B		9	CU	
606	B		1	SS	
605	A		9	SS	
604	NO		9	SS	#8-32 x .375 H.S.C.S.
603	C		1	SS	
602	NO		9	SS	#3-48 x .250 LG. H.S.C.S.
601	B		1	CU	

PART	SIZE	REV	REQ	MAT'L	NOTES

7 SEE FIXTURE LAYOUTS (3090, 3190 ETC.) FOR FIXTURE INFORMATION.
6 UNK = UNKNOWN N.D = NO DRAWING, PROCURE FROM THIS L.O.
5 DOTTED LINES INDICATE ROUGH OR PRELIMINARY MACHINING.
4 ALL MATING CORNERS & FILLETS ARE .015 X 45° CHFR. AND .010 R. RES.
3 MAX. PERMISSABLE TAP DRILL DEPTH AND MIN PERMISSABLE FULL THREAD DEPTHS ARE SHOWN.
2 SECTION LOCATIONS DEFINED BY LETTER LOCATION AT END VIEW.
1 NOTES 2 THRU 7 APPLY UNLESS OTHERWISE SPECIFIED.

NOTES

DESIGN FINALIZED	DATE	INIT.	DATE	INIT.	DATE	INIT.	DATE	INIT.

	A	B	C	D	E	F	G	H	J	K	L	M	N	P	R	S	T	U	V	W	Y	Z
1																						
2																						
V																						
11																						
1																						
0																						

UNLESS OTHERWISE SPECIFIED
DEC .X ± 1 .XX ± 01 XXX ± 005
SCALE —
ANGLES ± 0°30' FINISH √ MAX
FILLET RAD .010 MAX
THREADS CLASS 2
ALL DIAS CONCENTRIC WITHIN .005 TIR
REMOVE ALL BURRS & SHARP EDGES

NEXT ASSY | SIM TO

THERMO ELECTRON
ENGINEERING CORP
WALTHAM 54, MASS

DR | CHK | ENG | APP

TITLE

SHT 6

SIZE H | NUMBER 479-1000 | REV A

FOLDOUT FRAME 5

FOLDOUT FRAME 6

6.4.1.2 Clearance Between End of Shield and Generator Block

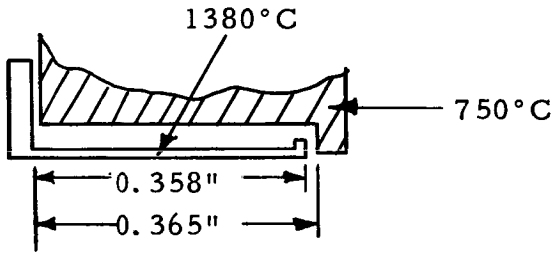

Clearance at toom temperature:

$$0.365 - 0.358 = 0.007 \text{ in.}$$

Shield Expansion = $0.358 \times 0.010 = 0.00358$ in.

Block Expansion = $0.365 \times 0.004 = 0.00146$ in.

Clearance at operating temperature:

$$(0.365 + 0.0146) - (0.358 + 0.00358) = 0.00488 \text{ in.}$$

6.4.1.3 Clearance Between Beveled Emitter Faces of Adjacent Diodes

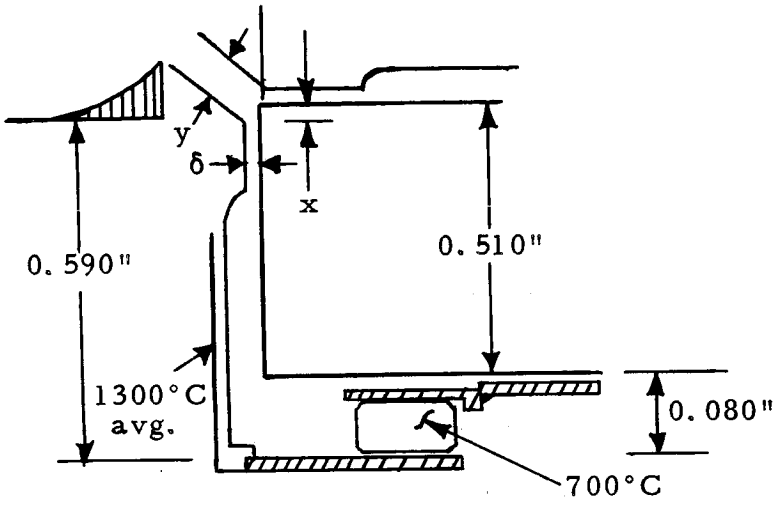

From the geometry described above:

$$y = (\delta + x)\sqrt{2}$$

At room temperature:

$x = 0$

$\delta = 0.010$ in.

$y = 0.010\sqrt{2} = 0.01414$ in.

At operating temperature:

$\delta = 0.00723$ in.

Molybdenum Block Expansion = 0.510" x 0.004 = 0.002 in.

Niobium-Ceramic Expansion = 0.080" x 0.0054 = 0.00043 in.

Spacer Expansion = 0.590" x 0.0094 = 0.00564 in.

$x = 0.002 + 0.00043 - 0.00564 = -0.00321$ in.

$y = (\delta + x)\sqrt{2} = (0.00723 - 0.00321)\sqrt{2} = 0.00569$ in.

6.4.1.4 Clearance Between Beveled Emitter Faces and Back Cavity Piece

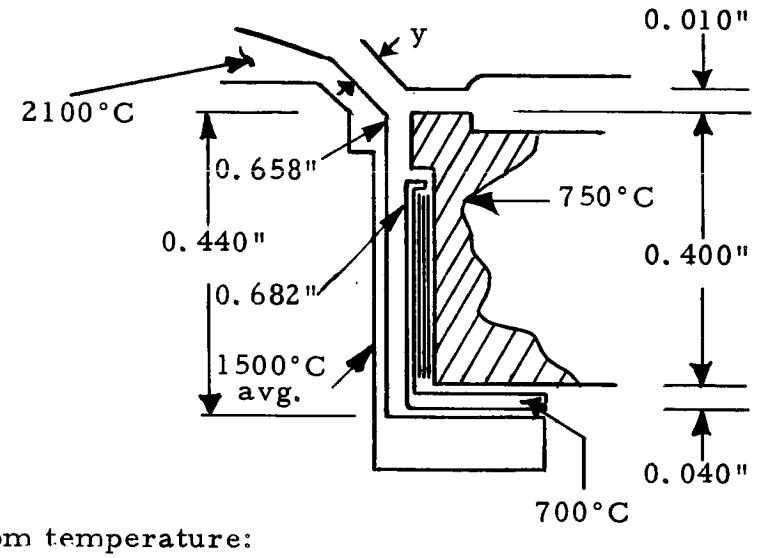

At room temperature:

$$x = 0$$

$$\delta = \frac{0.682 - 0.658}{2} = 0.012"$$

$$y = (\delta + x)\sqrt{2}$$

$$y = (0.012)\sqrt{2} = 0.001698"$$

At operating temperature:

Molybdenum Block Expansion = 0.400" x 0.004 = 0.0016 in.

Tantalum Sleeve Expansion = 0.440" x 0.011 = 0.00485 in.

Tantalum Shield Flange Expansion = 0.080" x 0.0047 = 0.000373 in.

$$x = 0.0016 + 0.000373 - 0.00485 = -0.00288 \text{ in.}$$

Top of Back Cavity Piece Expansion = 0.658 x 0.016 = 0.0105 in.

Block Expansion = 0.682 x 0.004 = 0.00276 in.

$$\delta = \frac{-(0.658 + 0.0105) + (0.682 + 0.00276)}{2} = 0.00813 \text{ in.}$$

$$y = (\delta + x)\sqrt{2} = (0.00813 - 0.00288)\sqrt{2} = 0.00744 \text{ in.}$$

6.5 RADIATION SHIELDING

To minimize losses from the hot emitter sleeves to the support block, experiments were conducted with various radiation shielding configurations. The very small space available for shielding, together with the necessity for preventing electrical contact between the emitters and the block, necessitated a tightly enclosed and well supported shield assembly. A shield support was fabricated and is shown in Figure 6.13. Heat transfer tests were performed using this shield support and various numbers of concentric thin shields.

Lateral conduction from the support to the block and from the thin shields to the support was found to be of sufficient magnitude to negate the reduction in radiation heat transfer. Consequently, the support was changed to the configuration shown in Figure 6.14, where the cross-sectional area for lateral conduction has been substantially reduced. The thin radiation shields were similarly treated, as shown in Figure 6.15. Experiments were conducted with several shield thicknesses and turns, and the combination of 3 turns of 1-mil tantalum foil was found best. By the use of cutouts in the shield assembly, trapped gases are also more readily released during pump-down from atmospheric pressure.

The shielding measurements were made by raising a heat receiver, encircled with the shields, to a temperature of 2000°K with electron bombardment and measuring the power required to reach that temperature with different shielding configurations. The heat receiver was of the same size and shape as the emitter of the converter.

5767

Figure 6.13 The Original Generator Shield Support

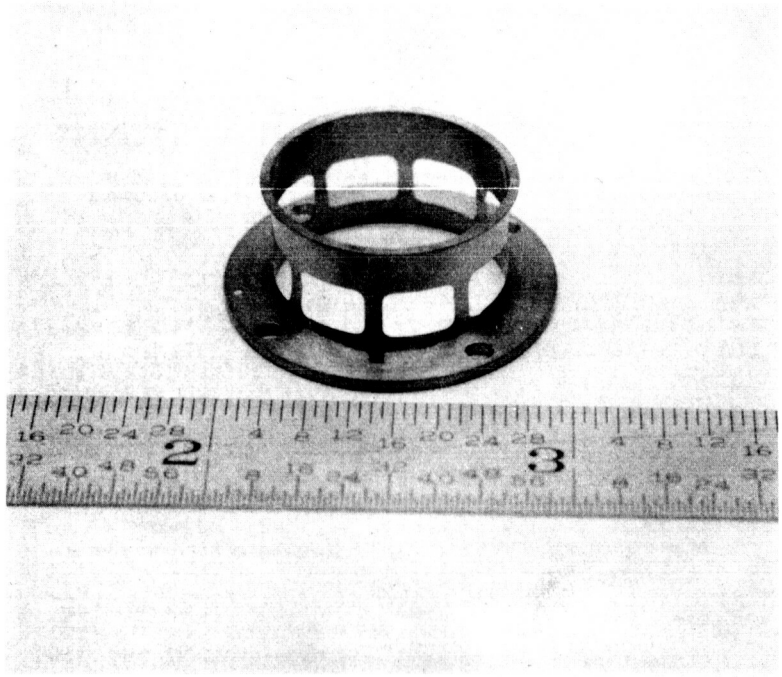

Figure 6.14 Generator Shield Support

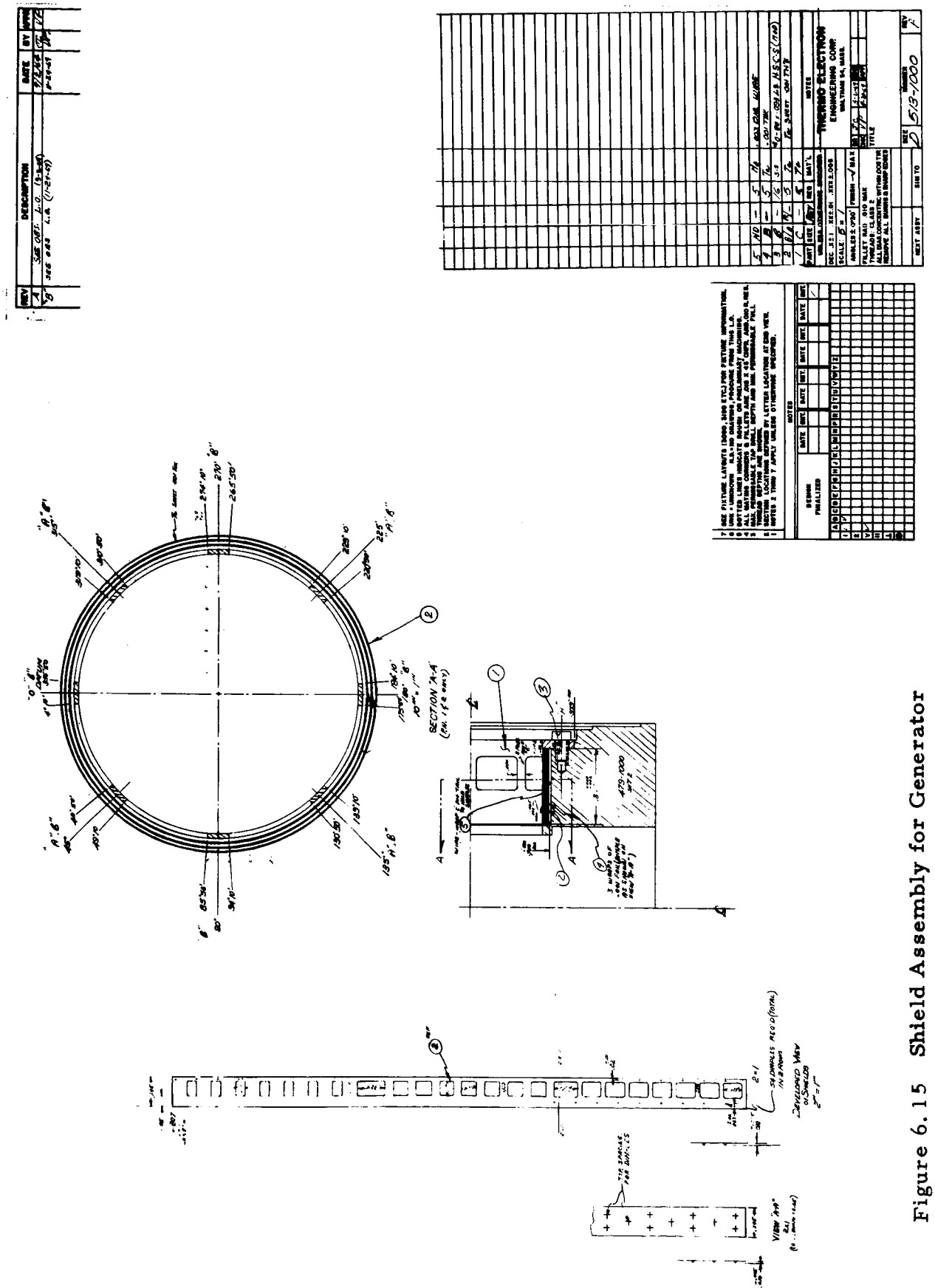

Figure 6.15 Shield Assembly for Generator

6.6 SUPPORT BLOCK COOLING

6.6.1 Design

As shown earlier in the thermal analysis, a maximum of 265 watts had to be rejected from the block. Assuming an average radiator temperature of 900°K and an emissivity of 0.8, the required area is 88.3 cm^2. The radiator shown in Figure 6-16 was designed to have about that area and to fit within the constraints imposed by the generator support structure.

6.7 THERMAL TESTING

After the first group of environmental tests, which are described in the next chapter, the generator assembly with simulated diodes was mounted on a test stand and heated with the same electron-bombardment gun that was later used for generator testing. The gun was used to heat the molybdenum block to operating temperatures. The test setup is shown in Figure 6.17.

Each dummy diode was instrumented with a thermocouple on the mounting flange. The generator radiator had a thermocouple on the top polished section, and also on the lower Rockide section. The temperature of the stainless steel support ring was also measured.

The filament power input and bombardment power input were summed to give the total heat input to the system. Using the measured temperatures with assumed values of emissivity, the various heat loss terms were calculated, namely: radiation from the dummy diodes, radiation from the molybdenum block, radiation from the stainless steel ring, and conduction from the electron-bombardment gun. The total heat input minus the total losses was taken as the heat being dissipated

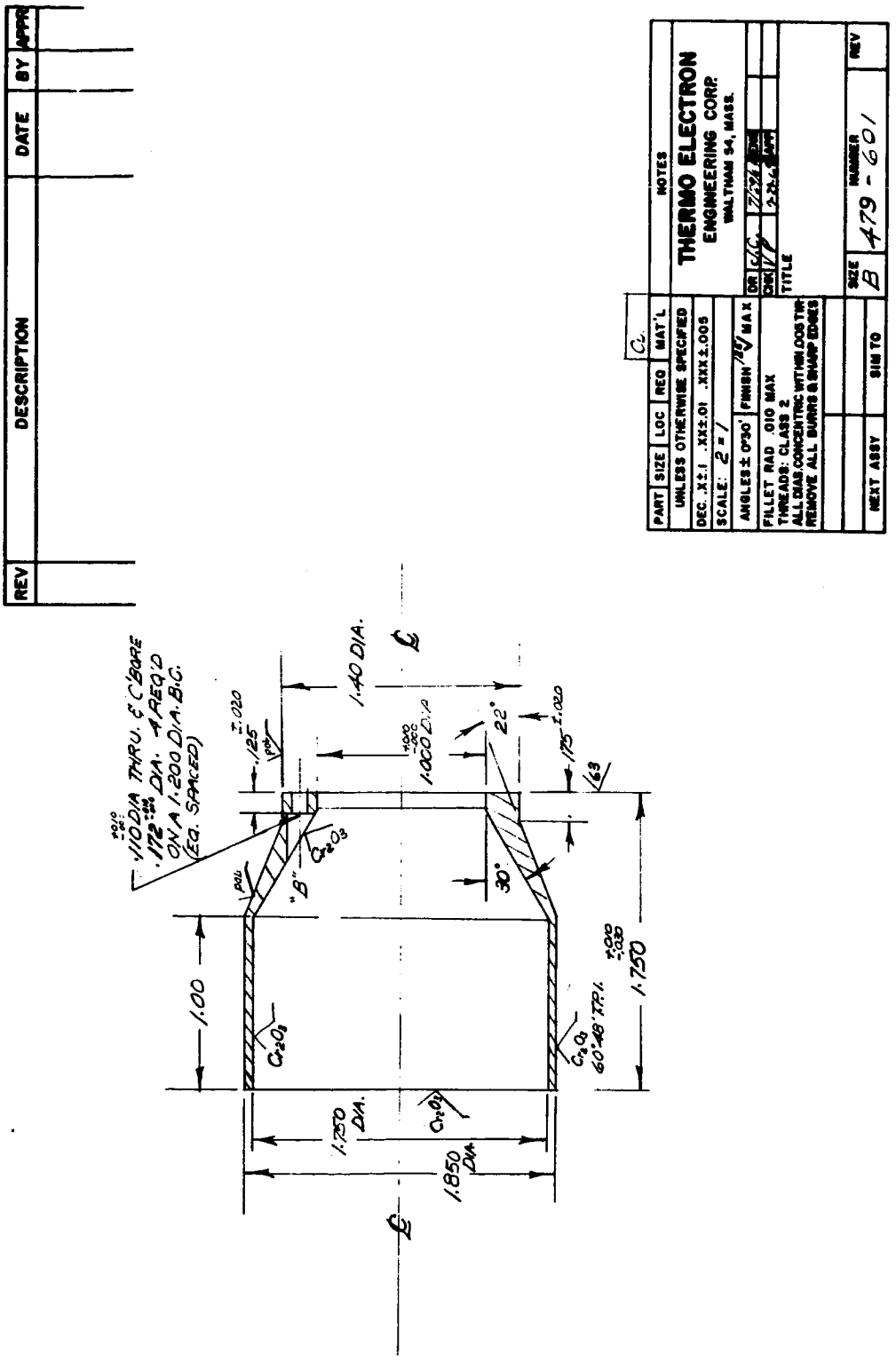

Figure 6.16 Generator Block Radiator

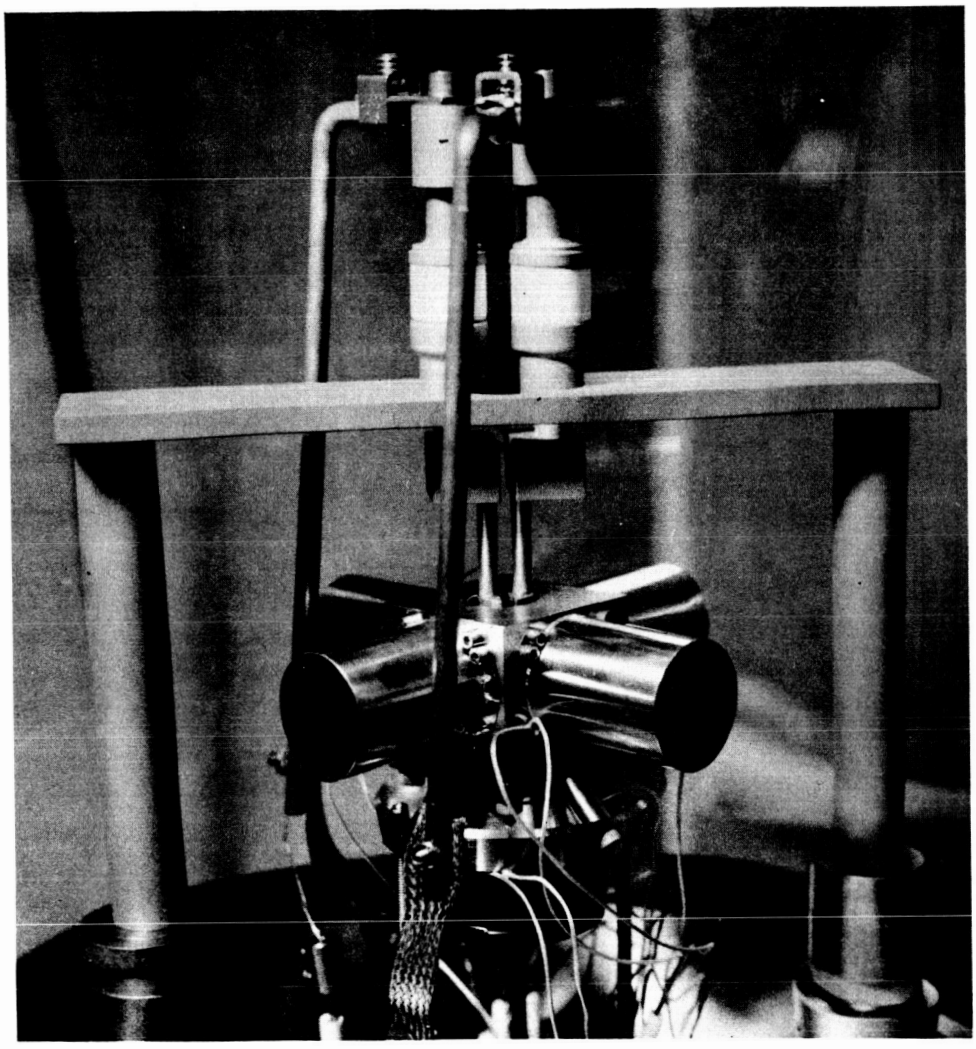

Figure 6.17 **Simulated Generator Structure Mounted for Thermal Testing**

by the generator block radiator. The data taken is included in Table 6-9, which lists filament power input, bombardment power input, radiator temperature top and bottom, dummy diode temperatures, and stainless steel ring temperature.

The following emissivities were assumed for the calculations:

ϵ = 0.2 for copper
= 0.16 for clean stainless steel
= 0.10 for clean molybdenum

The surface areas were calculated as follows (referring to Figure 6.12):

Surface area of dummy diodes $= 4[(1.19)^2(0.785) + \pi(1.19)(1.585)](2.54\frac{cm}{in.})^2$

$= 181.5\ cm^2$

Net surface area of block $= \{(1.75)^2 + 4[(1.75)^2 - 1.11]\}(2.54\frac{cm}{in.})^2$

$= 70.1\ cm^2$

Lateral area of s.s. ring $= \{\pi(0.45)(2.3) + \frac{\pi}{4}[(2.3)^2 - (1.9)^2]\}(2.54\frac{cm}{in.})^2$

$= 29.5\ cm^2$

The calculated heat conduction from the stainless steel rods of the electron gun is:

$$q = -k\frac{\pi d^2}{4}\frac{\Delta T}{\ell}$$

$\Delta T = -192°C$ (measured with thermocouples)

$d = 0.4$ in.

$\ell = 3.0$ in.

$k = 0.226$ W/cm °C (at 490°C)

Substituting (for two rods):

$$q = 2(0.226)\frac{\pi(0.4)^2}{4} \times \frac{192}{3} \times 2.54\,\frac{cm}{in.} = 9.25 \text{ watts}$$

For the block temperature equal to the dummy diode temperature, the heat terms are listed in Table 6-10.

From the table, the heat being radiated by the stainless steel ring and the heat being conducted by the electron gun are small in comparison with the total heat loss. For the block at 721°C (994°K) the radiator was calculated to dissipate 290 watts, while at lower block temperatures the heat rejection was greater. From these results, the block cooling radiator was judged satisfactory.

TABLE 6-9

TEMPERATURE MEASUREMENTS ON SIMULATED GENERATOR

Filament Power		Bombardment Power		Temperature Measurements (°C)						
V	A	V	mA	Simulated Diode #1	Simulated Diode #2	Simulated Diode #3	Simulated Diode #4	Top of Block Rad.	Bottom of Block Rad.	S. S. Ring
5.0	42.5	1000	210	533	513	540	538	520	483	337
5.2	43.2	1000	280	670	653	668	665	643	580	450
5.3	43.5	1000	310	727	693	717	620	722	718	497

TABLE 6-10

HEAT LOSS TERMS FOR SIMULATED GENERATOR STRUCTURE

Temp. of Block °C	Rad. Heat Flux from Block and Diodes W/cm^2	Rad. from Diodes Watts	Rad. from Block Watts	Temp. of S. S. Ring °C	Rad. Heat Flux from S. S. Ring W/cm^2	Rad. from S. S. Ring Watts	Conduction from Electron Gun Watts	Total Heat Loss Watts	Heat Input Watts	Rad. from Block Radiator Watts
525	2.3	83.5	13.22	337	.78	3.69	9.25	109.66	422	312
664	4.4	160	25.3	450	1.55	7.32	9.25	201.87	505	303
721	5.5	200	31.7	497	2.0	9.44	9.25	250.39	540	290

CHAPTER 7

DESIGN OF JG-3 FOR SHOCK, ACCELERATION AND VIBRATION

7.1 PRELIMINARY DESIGN

One phase of the program was to design a four-converter generator, JG-3. The design was to be such as to allow the generator to withstand the shock, vibration and acceleration tests specified in JPL Specification No. GMP-34203-TAT, " Environmental Test Specification, SET S/C Flight Equipment T/A Requirements, Power Subsystems Solar Energy Thermionic Converter," dated 1 November 1963, Sections 4.8.4.1, 4.8.4.2, 4.8.4.3, and 4.8.4.4.

The above specifications, summarized briefly, call for radial acceleration forces of 14 g's, impact shocks of 200 g's and a time duration of 1.5 milliseconds, and random vibration and combined sinusoidal and random vibration at overall levels up to ± 15 g rms.

In the preliminary design, tubing was selected as the means of joining the top of the diode support block to the generator support ring. Because the available area at the top of the block was small, an adapter was planned between the tubing and the point of attachment. Attempts at positioning such a tube between converters and at the same time keeping the length of tubing short proved impractical. Moreover, since a water-cooled shield would be used on the front of the generator during solar testing, use of a frontal ring presented a further complication.

To overcome these difficulties, the design shown in Figure 7.1 (drawing 479-1000 sh 6) was selected. The basic support structure

consisted of two rings, 479-603 and -606, and the interconnecting rods, 479-605. The rods were brazed into ring 606, but the ring was mechanically fastened to the molybdenum. The shock and vibration were transmitted from the rear ring through the rods to the molybdenum block; consequently, a braze between the stainless steel ring and the molybdenum block, whose thermal expansion is dissimilar, was avoided.

The generator block radiator, 479-601, was brazed to the molybdenum block to achieve good heat transfer at the interface. The radiator was located inside the vibration plate 479-611. Once the radiator was brazed in position, the rear ring 603 was removable but the top ring 606 was not. The diodes were simulated with right circular cylinders. The dummy diode 479-607, which was a copper cylinder, was brazed to an identical support flange as used on the diode 479-42. The center of gravity of the diode VIII-P-3 was determined by suspending it on a wire and varying the attachment point until there was no rotation. The center of gravity of the cylinder was made to coincide with that of the diode.

Figure 7.2 shows the simulated generator completely assembled and ready for testing, while Figure 7.3 shows an exploded view of all the parts.

7.2 ENVIRONMENTAL TESTING OF THE GENERATOR STRUCTURE WITH SIMULATED DIODES

The assembly shown in Figure 7.2 was then tested in accordance with the JPL Spec. GMP-34203-TAT, dated 1 November 1963, sections 4.8.4.1, 4.8.4.2, and 4.8.4.4, in two orthogonal directions. The structure was subjected to: (1) a radial acceleration force of 14 g's; (2) ten impact shocks, each impact shock having a peak magnitude

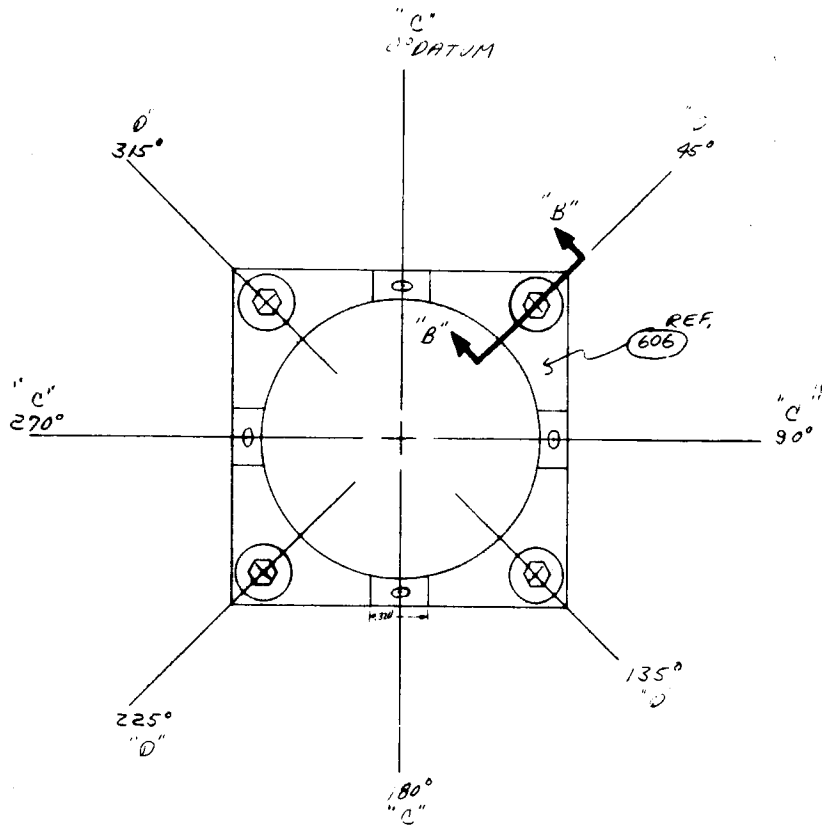

VIEW "A-A"

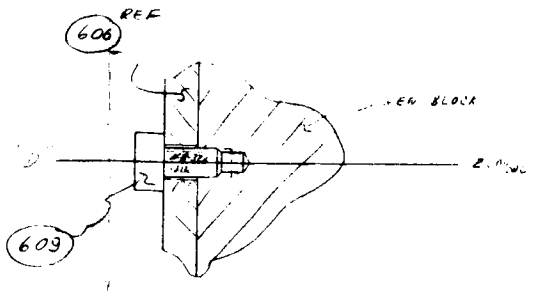

VIEW "B-B"

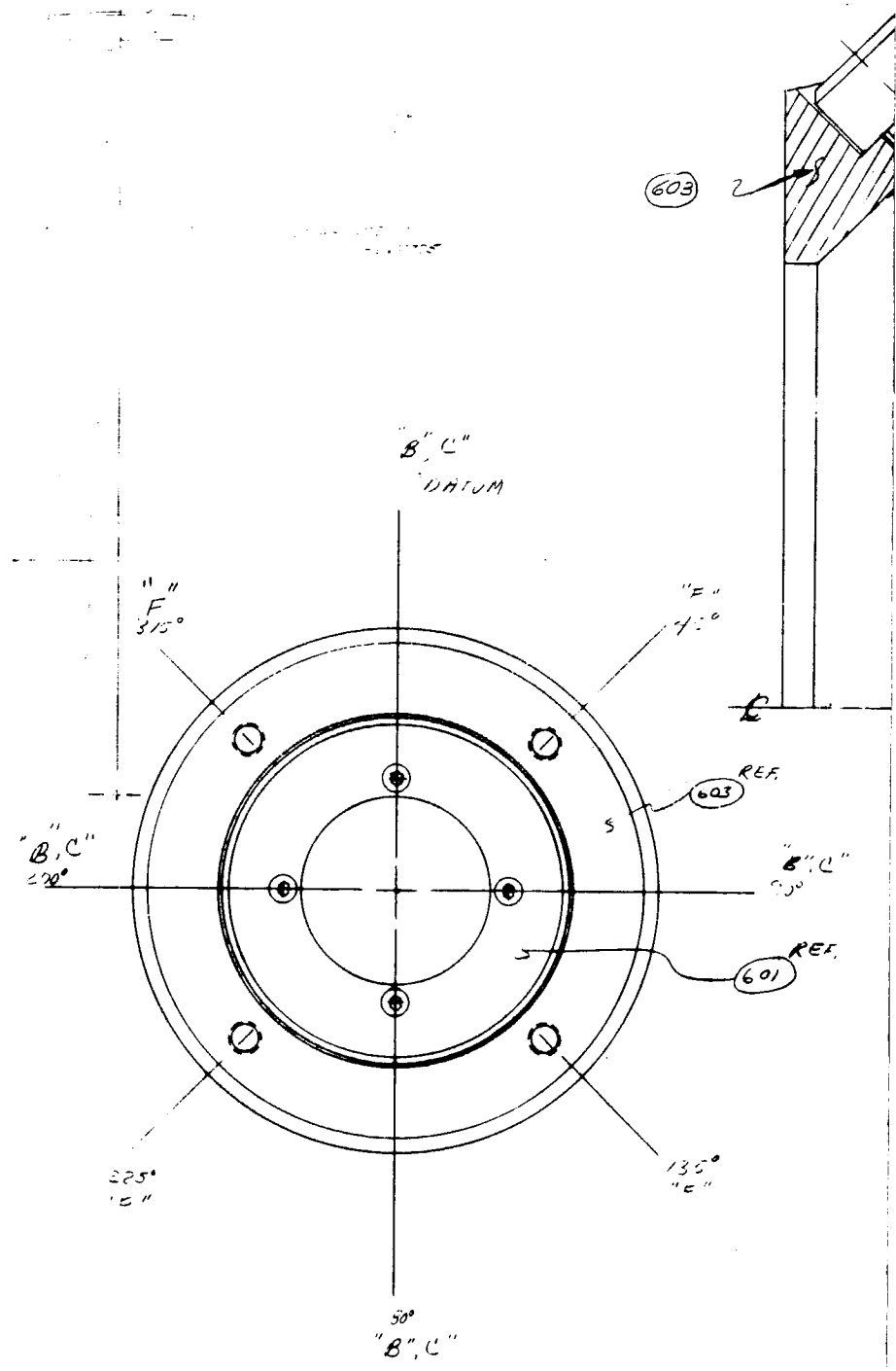

SECTION "A-A"

FOLDOUT FRAME 1

FOLDOUT FRAME 2

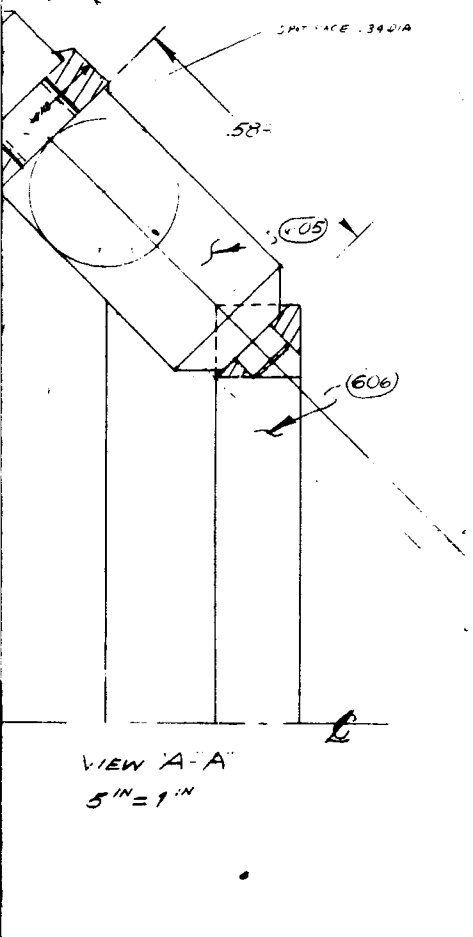

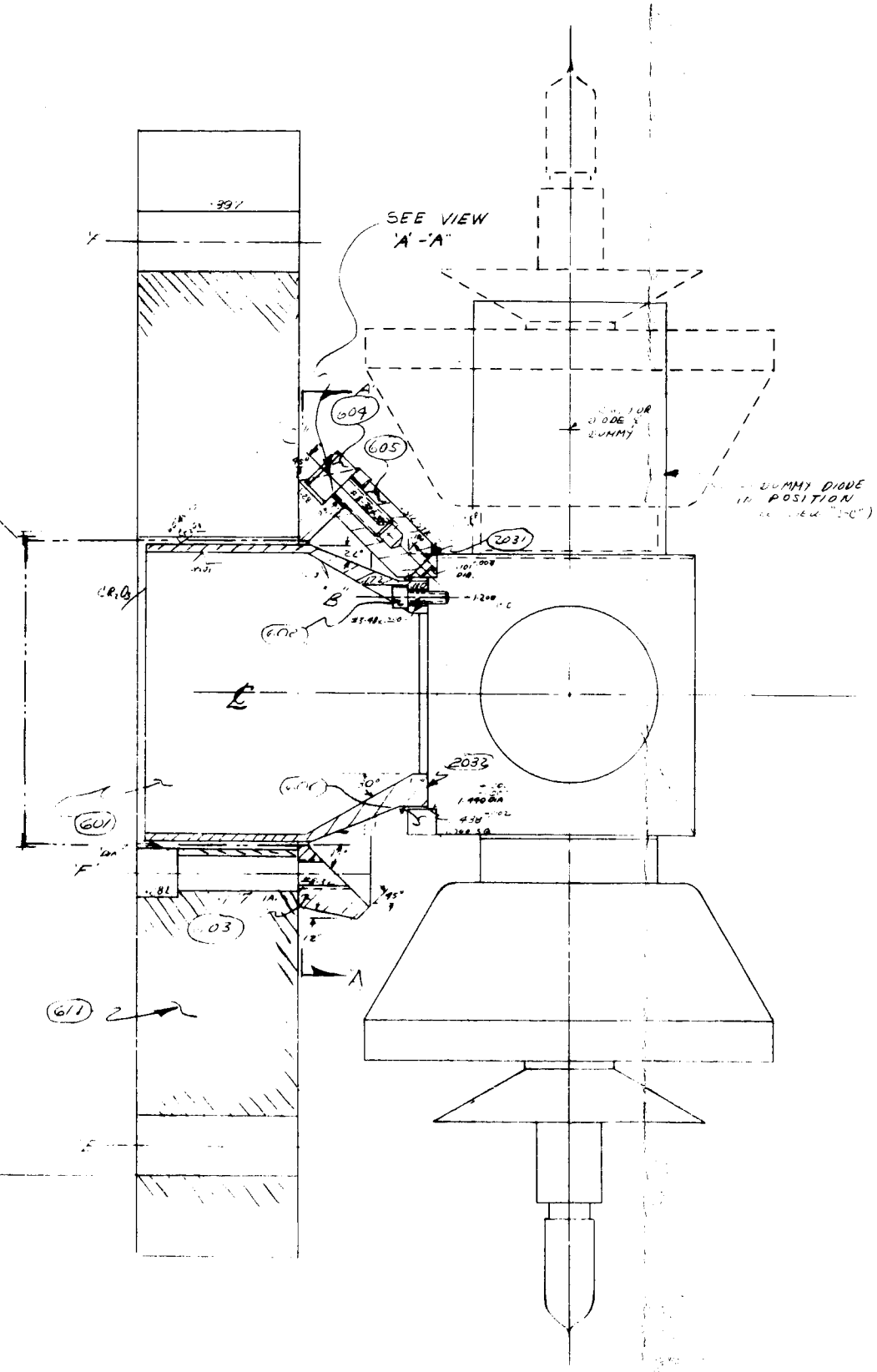

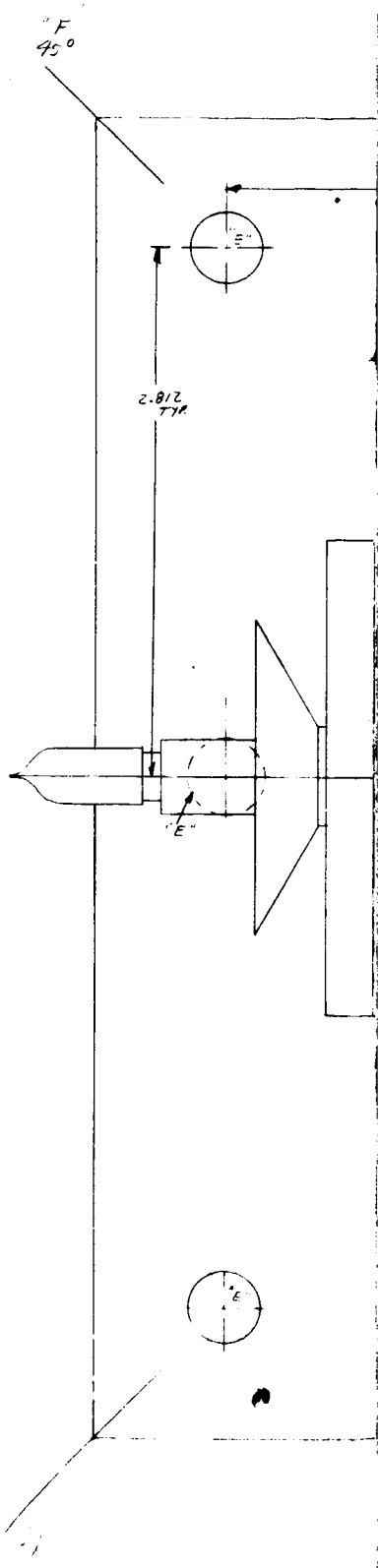

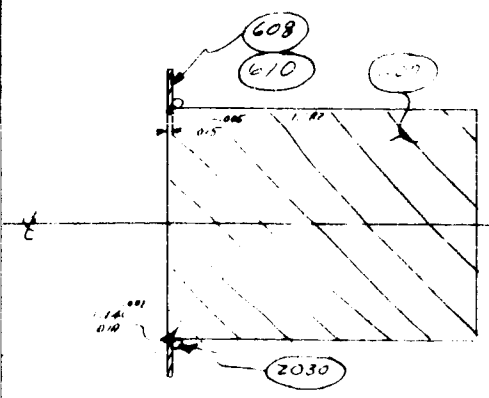

DUMMY DIODE
VIEW 'C-C'

FOLDOUT FRAME 3

FOLDOUT FRAME 4

REV	DESCRIPTION	DATE	BY	APPR
1	P.N. AS WAS ...	10-22-69	...	

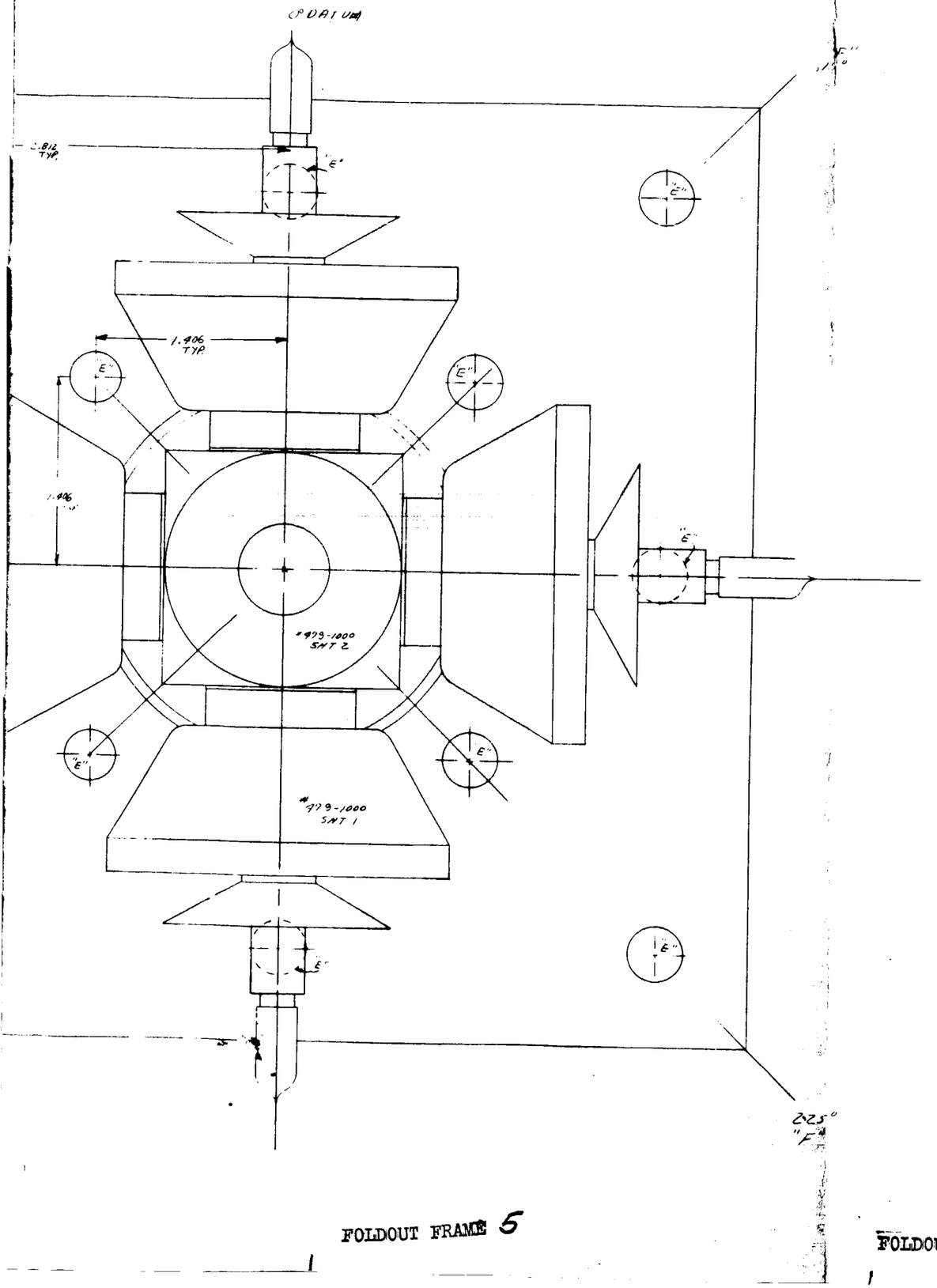

FOLDOUT FRAME 5

FOLDOUT FRAME 6

LAYOUT OF GENERATOR SUPPORT STRUCTURE

FIGURE 7.1

PAGE 7-3

7	SEE FIXTURE LAYOUTS (3090, 3190 ETC.) FOR FIXTURE INFORMATION.				
6	UNK = UNKNOWN N.D. = NO DRAWING, PROCURE FROM THIS L.O.				
5	DOTTED LINES INDICATE ROUGH OR PRELIMINARY MACHINING.				
4	ALL MATING CORNERS & FILLETS ARE .015 X 45° CHFR. AND .010 R. RES.				
3	MAX. PERMISSABLE TAP DRILL DEPTH AND MIN. PERMISSABLE FULL THREAD DEPTHS ARE SHOWN.				
2	SECTION LOCATIONS DEFINED BY LETTER LOCATION AT END VIEW.				
1	NOTES 2 THRU 7 APPLY UNLESS OTHERWISE SPECIFIED.				
NOTES					
DESIGN FINALIZED		DATE	INIT.	DATE	INIT.

PART	SIZE	REV	REQ	MAT'L	NOTES
					BRAZES
2030	WD	9	—		.030 DIA. WIRE
2031	WD	9	—		.030 DIA. WIRE
2032	A	1	—		
611	C		1	Al	
610	USE 979-12		16	SS	#4-40 x .125 LG. SH. CS. (MOD.)
609	WD			SS	#8-32 x .... LG. H.S.C.S.
608	USE 979-12		9	Nb	
607	B		9	CU	
606	B		1	SS	
605	A		9	SS	
604	WD		9	SS	#8-32 x .375 H.S.C.S.
603	C		1	SS	
602	WD		9	SS	#3-48 x .250 LG. H.S.C.S.
601	B		1	CU	

UNLESS OTHERWISE SPECIFIED
DEC .X ± 1 XX ± .01 XXX ± .005
SCALE 1/1
ANGLES ± 0°30' FINISH √MAX
FILLET RAD .010 MAX
THREADS CLASS 2
ALL DIAS CONCENTRIC WITHIN .005 TIR
REMOVE ALL BURRS & SHARP EDGES
NEXT ASSY SIM TO

THERMO ELECTRON
ENGINEERING CORP.
WALTHAM 54, MASS.
DR 2-26-69 ENG
CHK APP
TITLE
SHT 6
SIZE H NUMBER 979-1000 REV F

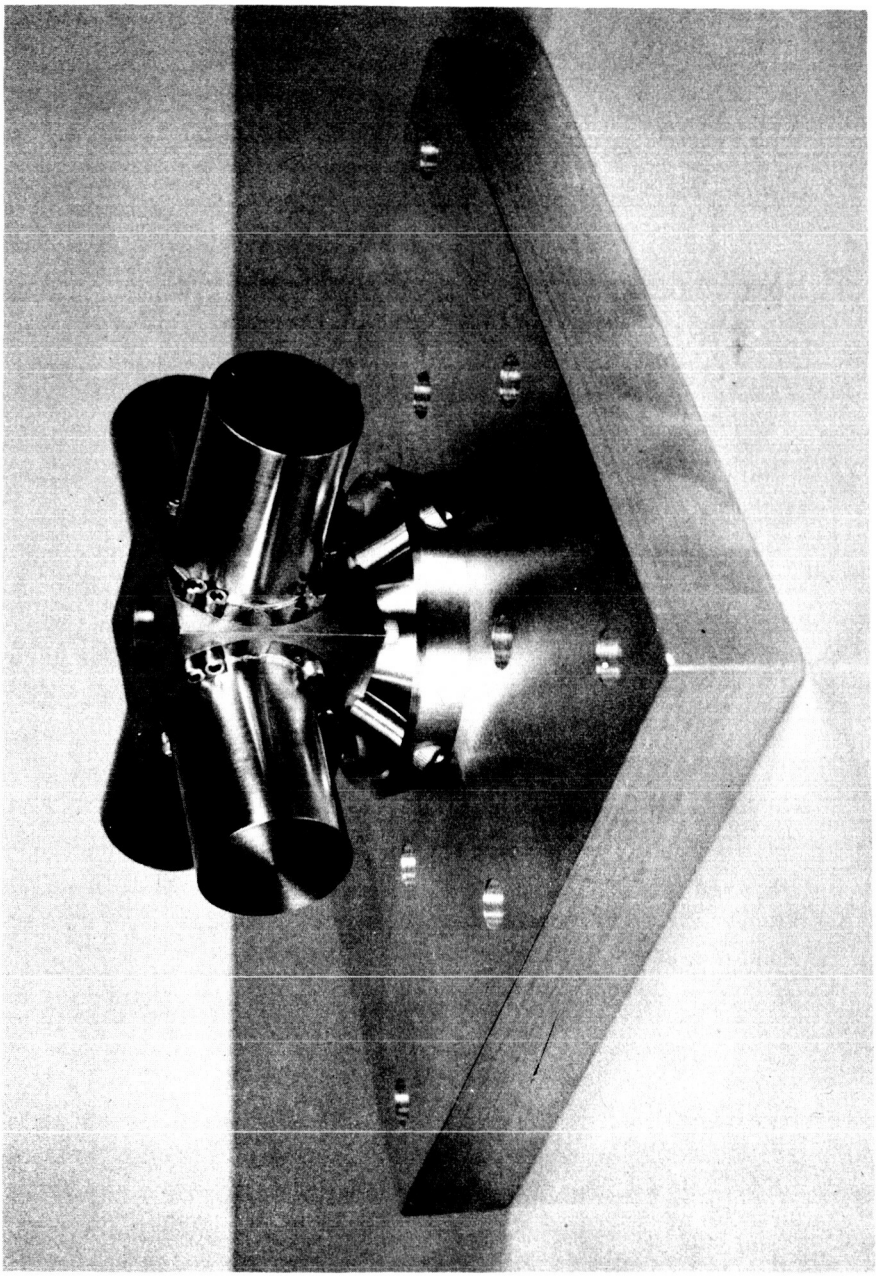

Figure 7.2 Simulated Generator Structure Mounted on the Test Fixture

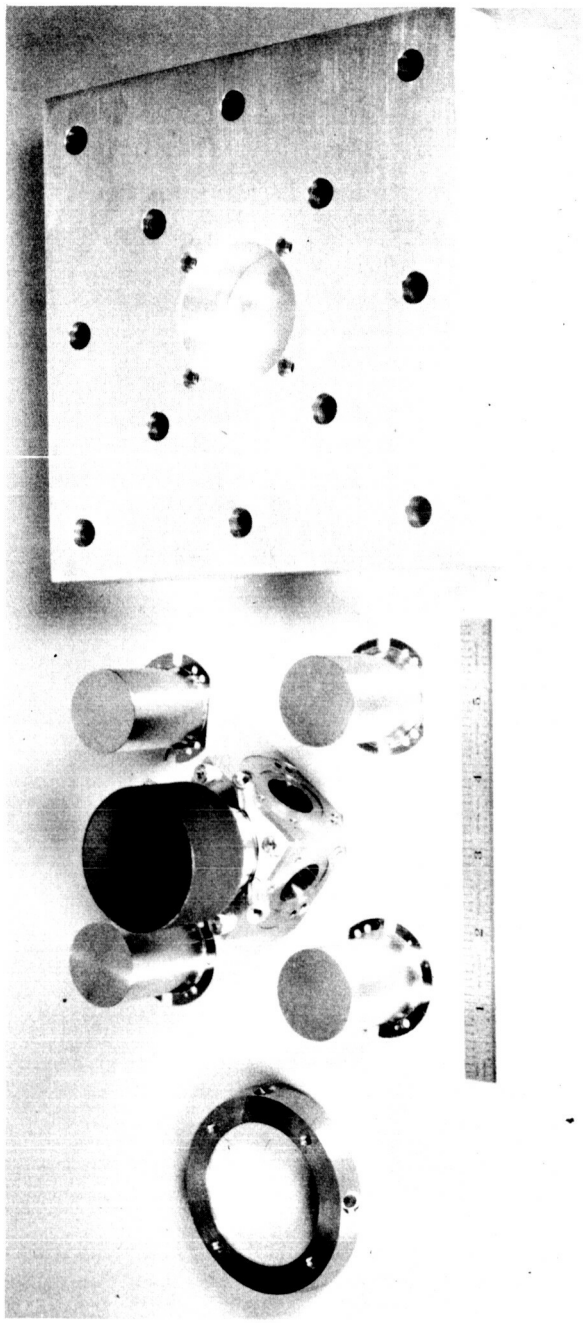

Figure 7.3 Exploded View of Simulated Generator Structure

of 200 g's and a time duration of 1.5 milliseconds; (3) random vibration and combined sinusoidal and random vibration at overall levels up to ± 15 g rms. Upon completion of each environmental exposure, the structure was visually examined for evidence of mechanical damage, and none was observed. Figures 7.4 through 7.9 show the structure mounted in both the x and y directions for acceleration, shock and vibration. The x-axis was perpendicular to the mounting surface of the unit; the y-axis was parallel to the normal mounting surface.

7.3 REDESIGN OF STRUCTURE

After the thermal test of the generator, which is described in the next chapter, the dummy diodes were removed. Approximately 30% of the stainless steel 4-40 screws which held the dummy diodes in position snapped off. The broken screws were removed by dipping the block with screws in acid.

To overcome this problem, component tests were made on a piece of molybdenum similar to that used for the generator block. Regular 4-40 threads were tapped into these samples, as were threads which would accept a stainless steel 4-40 Heli-Coil insert. Stainless steel 4-40 screws were placed in each of four holes (two regular and two with inserts) and cycled to 900°C. When the screws were removed, one without the Heli-Coil insert froze in position, while the others came out easily.

The tapped holes on the molybdenum block were then re-worked to accept 4-40 Heli-Coil inserts. A non-locking type of insert was selected, because in previous shake tests on diodes and structures loosening of the screws was not a problem, and the non-locking insert was easier to install.

The dummy diodes, back cavity piece, and shield support with radiation shield wraps were mounted in the blocks, and the structure was then assembled for further testing.

7.4 ENVIRONMENTAL TESTING OF REDESIGNED STRUCTURE

The generator structure was again subjected to: (1) a radial acceleration force of 14 g's; (2) ten impact shocks, each impact shock having a peak magnitude of 200 g's for a duration of 1.5 milliseconds; (3) random vibration and combined sinusoidal and random vibration at overall levels up to ± 15 g rms. Upon completion of each environmental exposure, the structure was visually examined for evidence of mechanical damage. No damage was observed as a result of the acceleration test. During the shock test the mounting flange on one dummy diode began separating from the block. Then one axis of vibration was performed (x-axis), and two dummy diodes separated and several more screws loosened.

Prior to the random vibration the generator structure was probed for resonant frequencies between 20 and 2000 Hz at a sinusoidal excitation level of ± 5 g's. No resonances were found in the x-axis of applied vibration.

Figure 7.10 shows the shield assembly and back cavity piece after testing. Neither unit experienced any damage. Figure 7.11 shows a close-up of one face where the dummy diode ripped away from the flange, and one of four ring screws vibrated out. One of the cap screws which hold the square ring to the block had also loosened. A top view of the structure is shown in Figure 7.12.

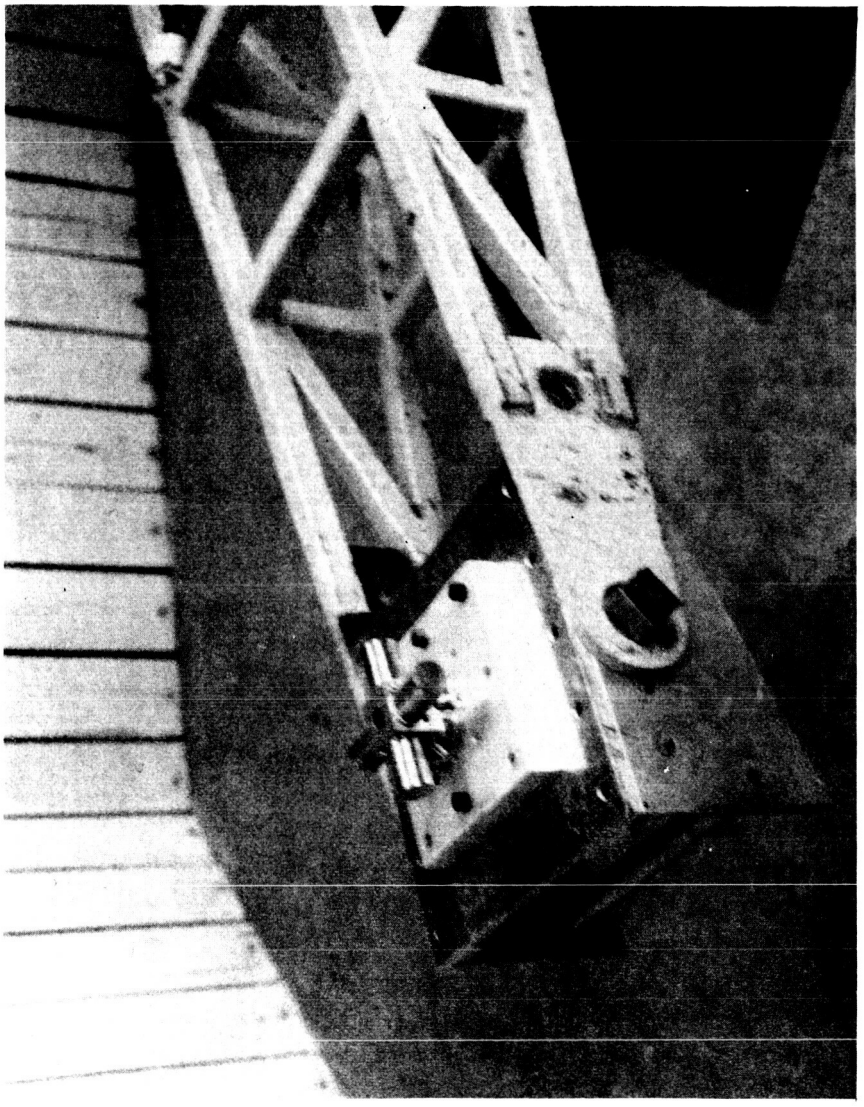

Figure 7.4 Simulated Generator Structure Mounted for X-Axis Acceleration

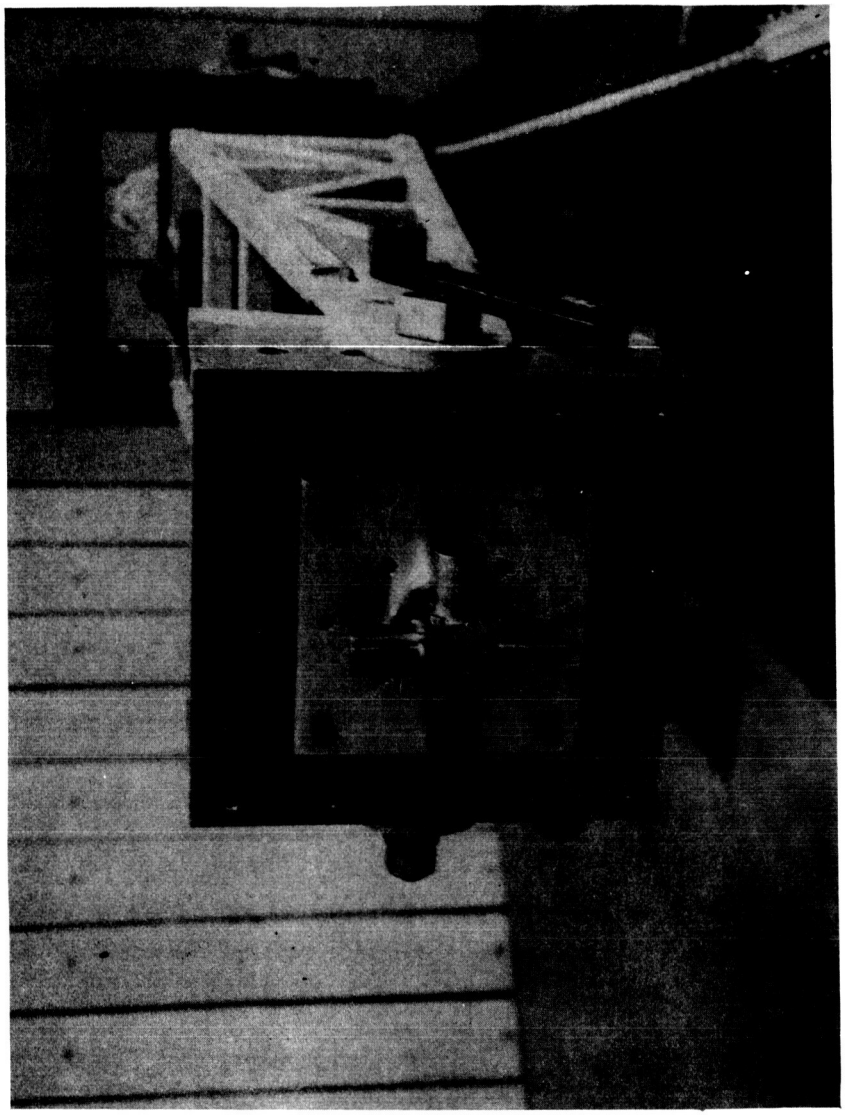

Figure 7.5 Simulated Generator Structure Mounted for Y-Axis Acceleration

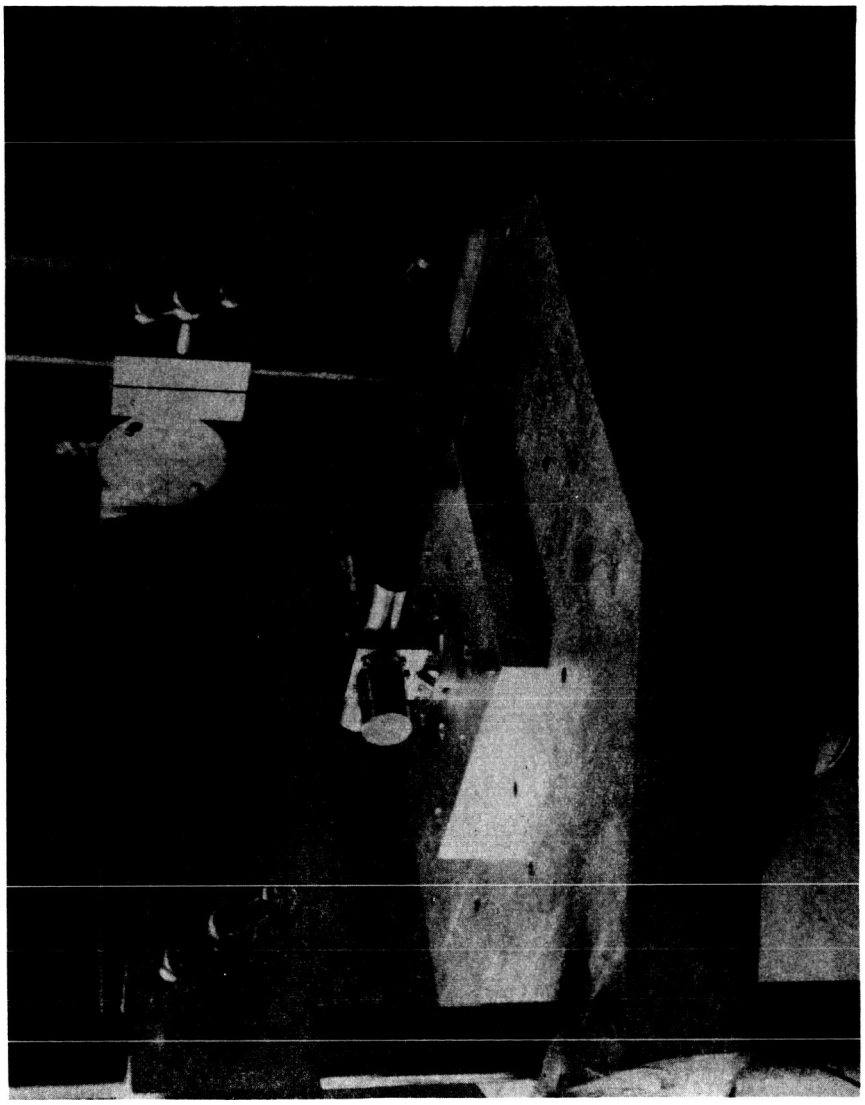

Figure 7.6 Simulated Generator Structure Mounted for X-Axis Shock Test

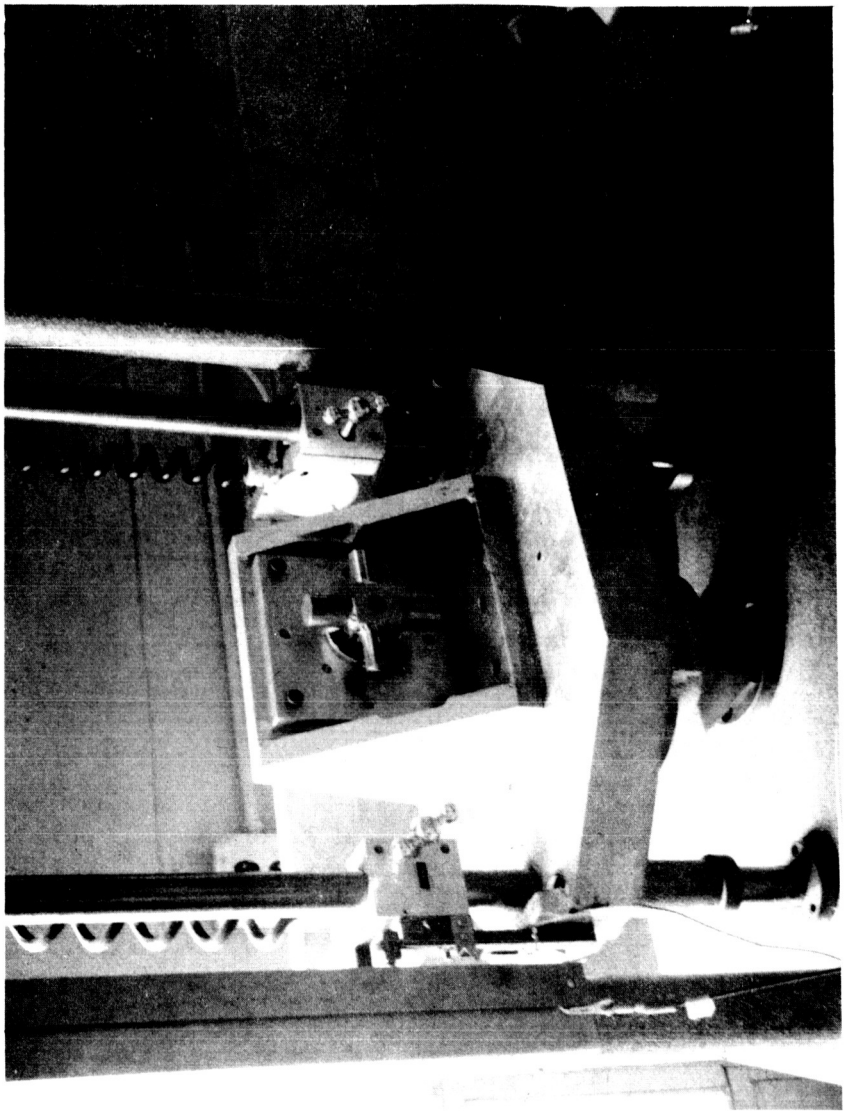

Figure 7.7 Simulated Generator Structure Mounted for Y-Axis Shock Test

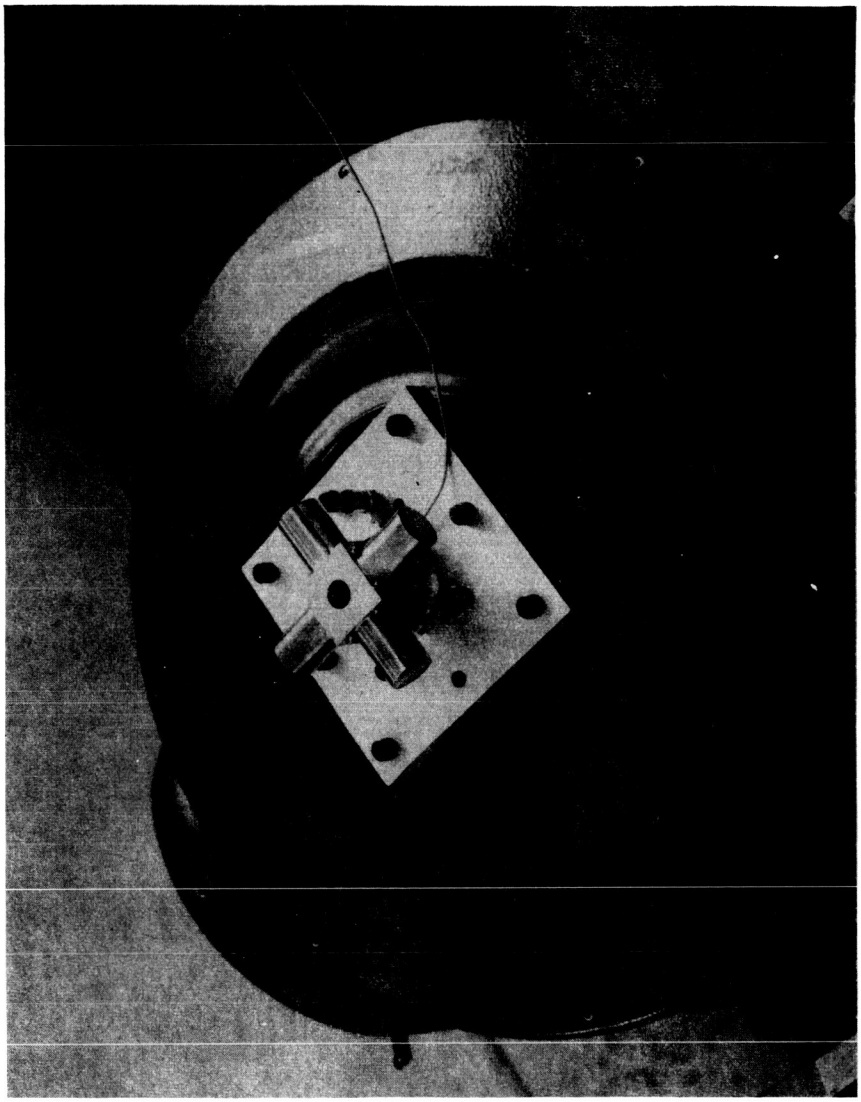

Figure 7.8 Simulated Generator Structure Mounted for X-Axis Vibration

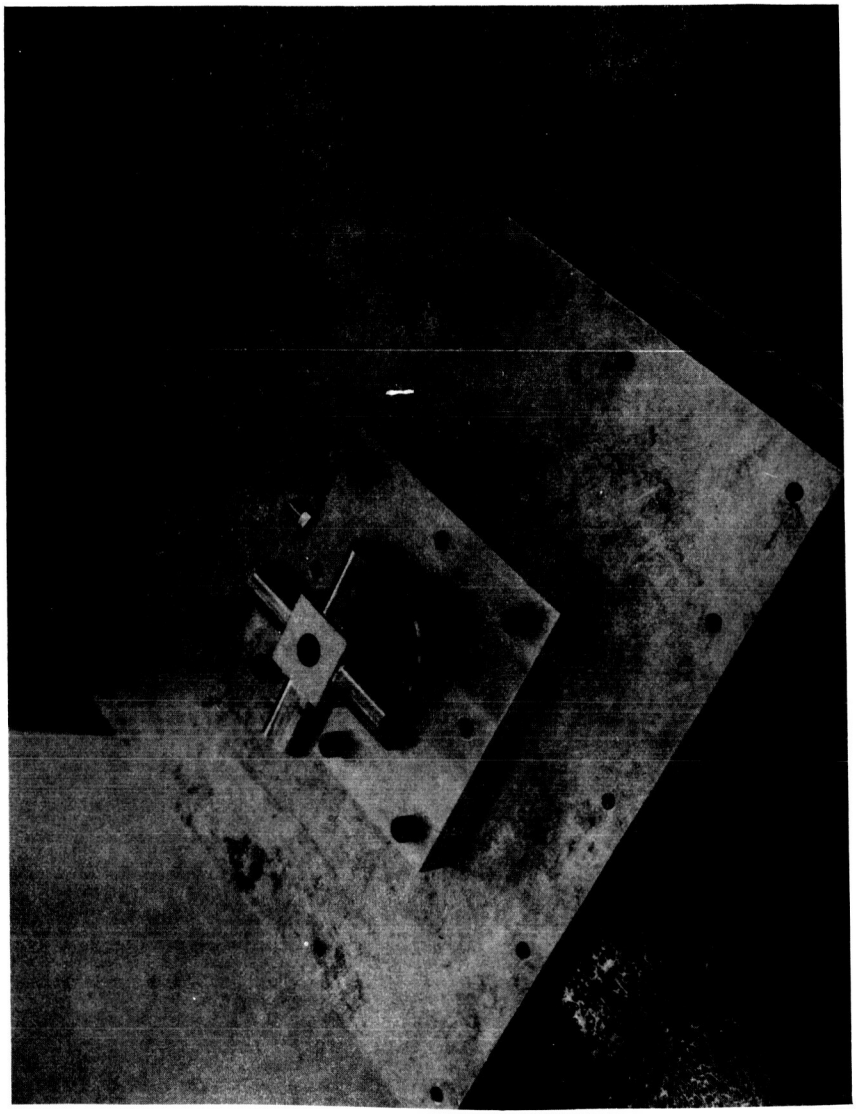

Figure 7.9 Simulated Generator Structure Mounted for Y-Axis Vibration

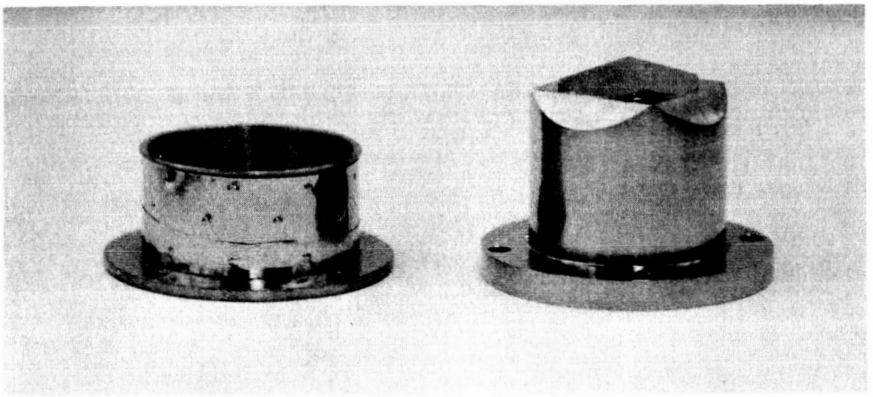

Figure 7.10 Back Cavity Piece and Shield Assembly after Environmental Testing

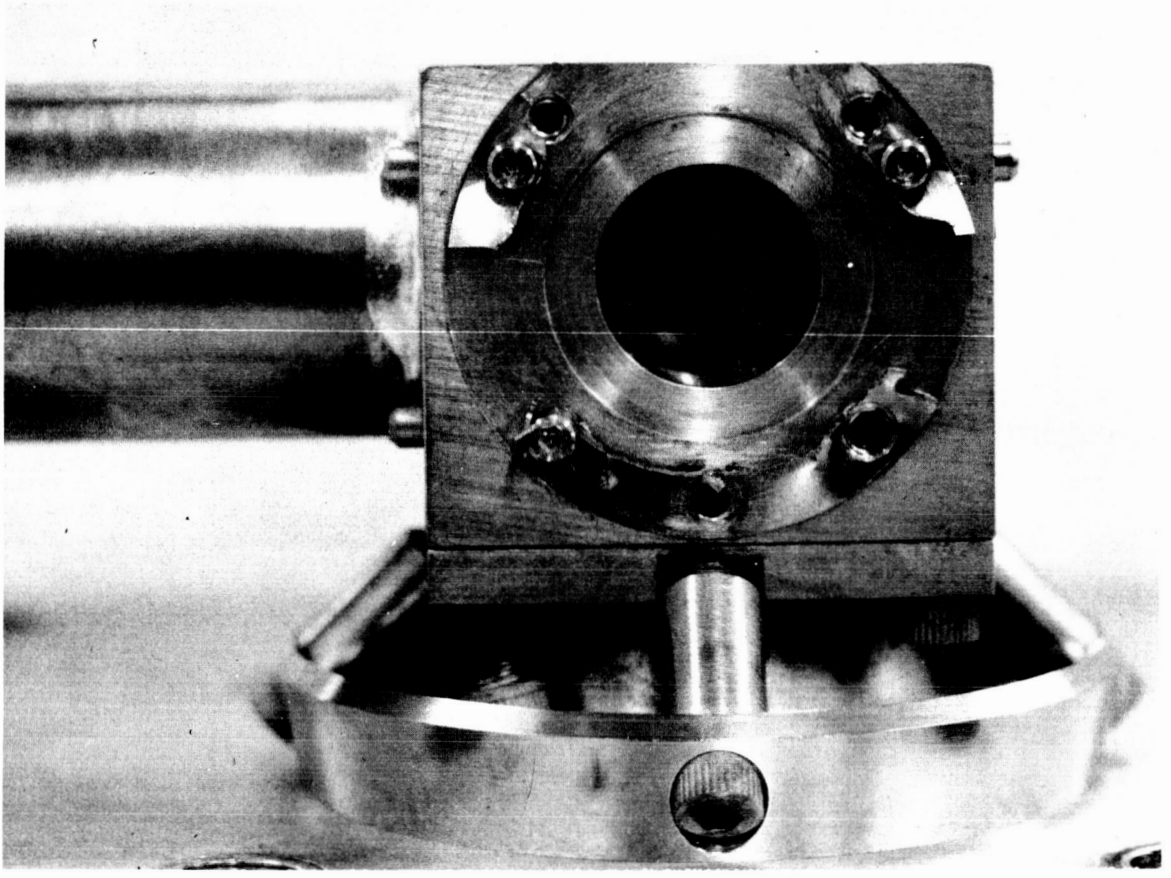

Figure 7.11 Side View of Simulated Generator Structure

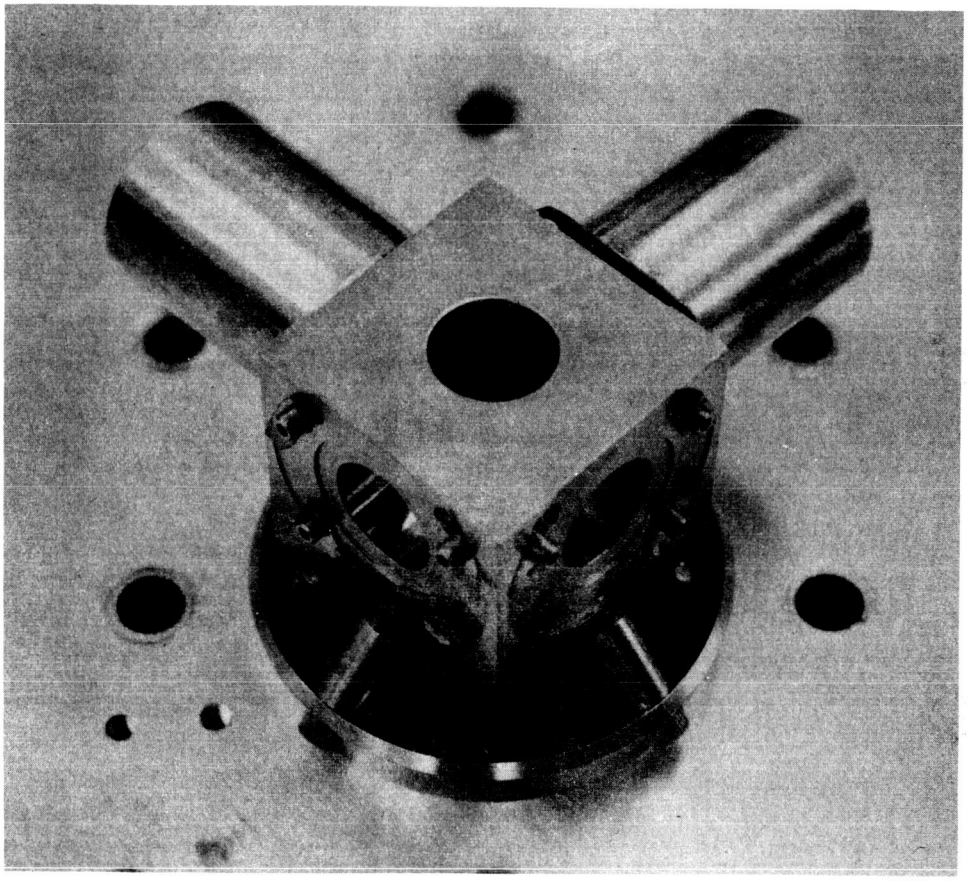

Figure 7.12 Top View of Simulated Generator Structure

Because the simulated diode was not supported in the vicinity of the center of gravity, it was not surprising to find it torn away from the flange. In the actual diode, three 4-40 screws pass from the radiator to the generator block. The purpose of these screws was to restrain oscillations of the center of gravity about the points of support at the niobium flange during launch. During vibration testing of a Series VIII converter, no damage was observed in either the x or y axis of vibration, although no shock tests were performed on this structure. However, the diode tested (VIII-P-2 type) weighed almost twice as much as the final prototype from which the generator converters were designed.

Since the simulated structure with dummy diodes did not suffer damage during the first ten shocks, and since the actual diode was protected from transmitting the entire shock force to the support flange, the later design was considered adequate to meet the prescribed environmental conditions.

7.5 FINAL MODIFICATION

As a result of the two series of environmental tests, locking-type Heli-Coil inserts were used to prevent freezing of the 4-40 screws in the block and to hold the screws during vibration, acceleration, and shock testing.

Because no resonant frequencies were detected in the 20- to 2000-Hz frequency range and because the structure did not suffer damage throughout the tests, no changes were incorporated in the support structure design. The design is shown in Figure 7.1, drawing 479-1000 sh 6 Rev A.

The total weight of the generator structure, generator radiator, generator block, and dummy diodes was measured to be 3.98 lbs. The weight breakdown was as follows:

Generator Structure	0.35 lb
Generator Radiator	0.22 lb
Generator Block	1.13 lb
Dummy Diodes	2.28 lb
Total Weight	3.98 lb

CHAPTER 8

GENERATOR TEST EQUIPMENT

8.1 ELECTRON-BOMBARDMENT GUN

Two electron-bombardment guns were designed during this program. The first consisted of one tantalum ribbon filament heating all four converters. The support structure was designed to minimize bombardment of the back cavity piece. This gun is shown in Figure 8.1. Two hollow columns, part 3, were used to support two heavy tantalum support pieces (part 4). These latter supports were attached to the ends of the tantalum ribbon filament. The tantalum supports, being heavy, were intended to run cool and minimize bombardment of the adjacent back cavity piece. The length and cross-sectional area of the leads and supports were chosen so as to be capable of safely carrying a current of 100 amperes while simultaneously minimizing heat conduction away from the filament.

As mentioned in Chapter 6, this gun was used to conduct the thermal tests of the generator. Because dummy diodes were used, the cavity was never raised to the 2000°K level required by the emitters. During thermal tests the heat input was limited to that required to achieve the desired support block temperature.

When the gun was used to test the complete generator, an extreme sensitivity to gun position in the cavity was noticed. Shortly thereafter, during an attempt to position the filament so as to achieve even heating of the four emitters, the bombardment current rose suddenly to a level well in excess of the design condition. The generator, on subsequent examination, was found to have been severely overheated and damaged.

Analysis of the instability suggested that the emission current from the tantalum filament rose because of a rise in the filament temperature. The filament temperature in turn was affected positively by the rising emitter temperature, in that re-radiation from the emitter (or emitters) to the filament increased. The feedback therefore can be seen to be positive and unstable. Furthermore, if the temperature of one emitter rose above that of the others, the adjacent segment of filament would rise in temperature. Thus, even if the total emission current was externally controlled, the overall system tended toward an uneven heating of the emitters.

As a consequence of the above results, a second gun was designed and constructed, and it is shown in Figure 8.2. In this case four filaments were provided, one for each emitter. Each emitter temperature could then be adjusted individually by adjusting the appropriate filament current. After repair of the generator, this gun was used for the generator tests. Servo control of the total emission current was found important in achieving smooth and stable temperature adjustment, and after its addition testing was conducted with relative ease.

8.2 LOAD AND TEMPERATURE MEASUREMENT

A generator load and temperature measurement setup was designed and constructed during the program. It is shown in Figure 8.3. It consisted of the appropriate ammeters, voltmeters, load resistors and switches to allow measurement of each diode' s output and the total generator output. The wiring was arranged to allow for operation of the generator diodes in series or in parallel. A thermocouple selector switch and ice junction were also included.

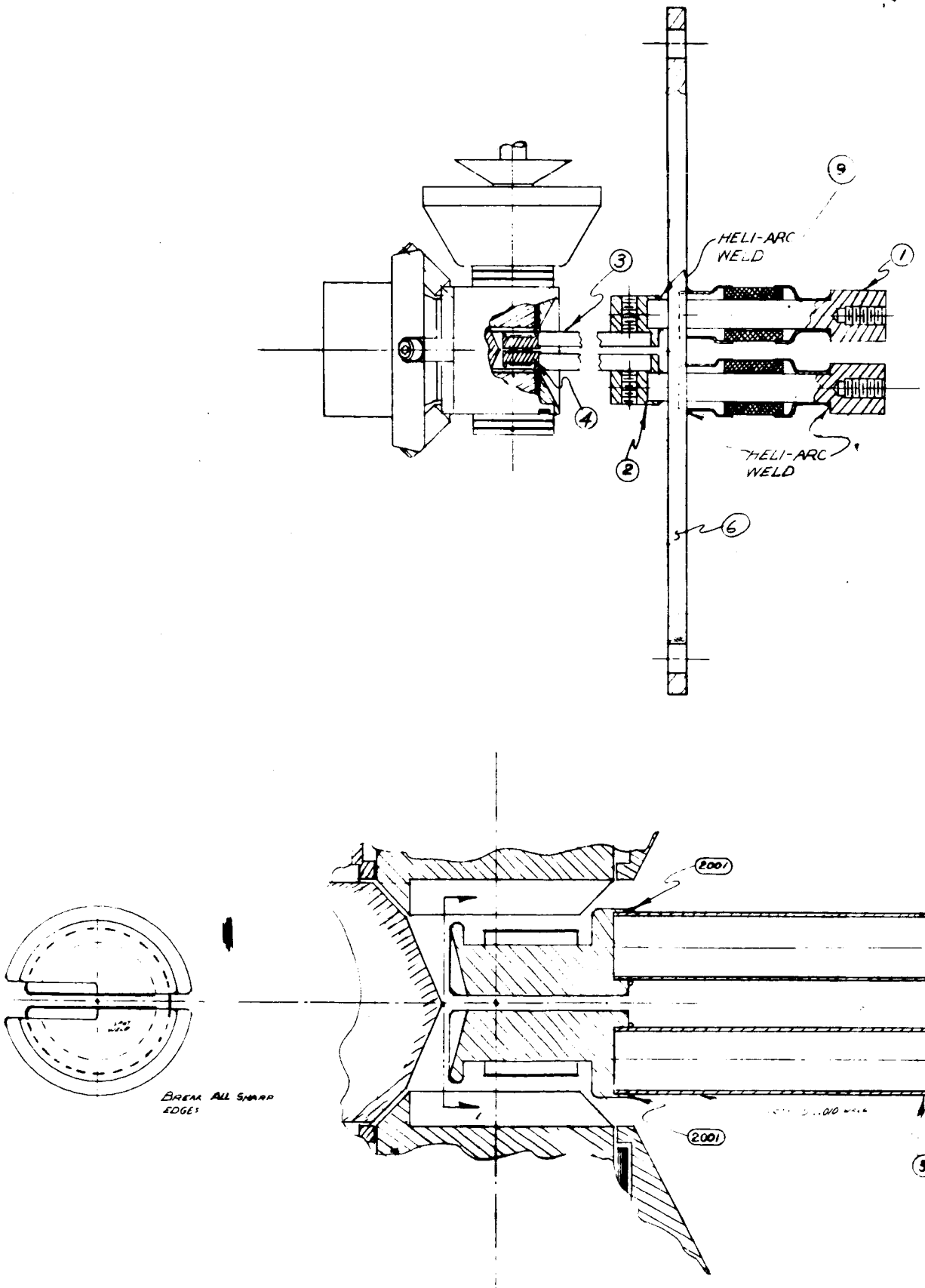

FOLDOUT FRAME 1

VIEW OF HEATER 5=1

REV	DESCRIPTION	DATE	BY	APPR
A	SEE OBS- LAYOUT (8-6-69)	9/10/64	U.C.	
B	SEE OBS I.D. (10-21-69)	10-21-69	VP	

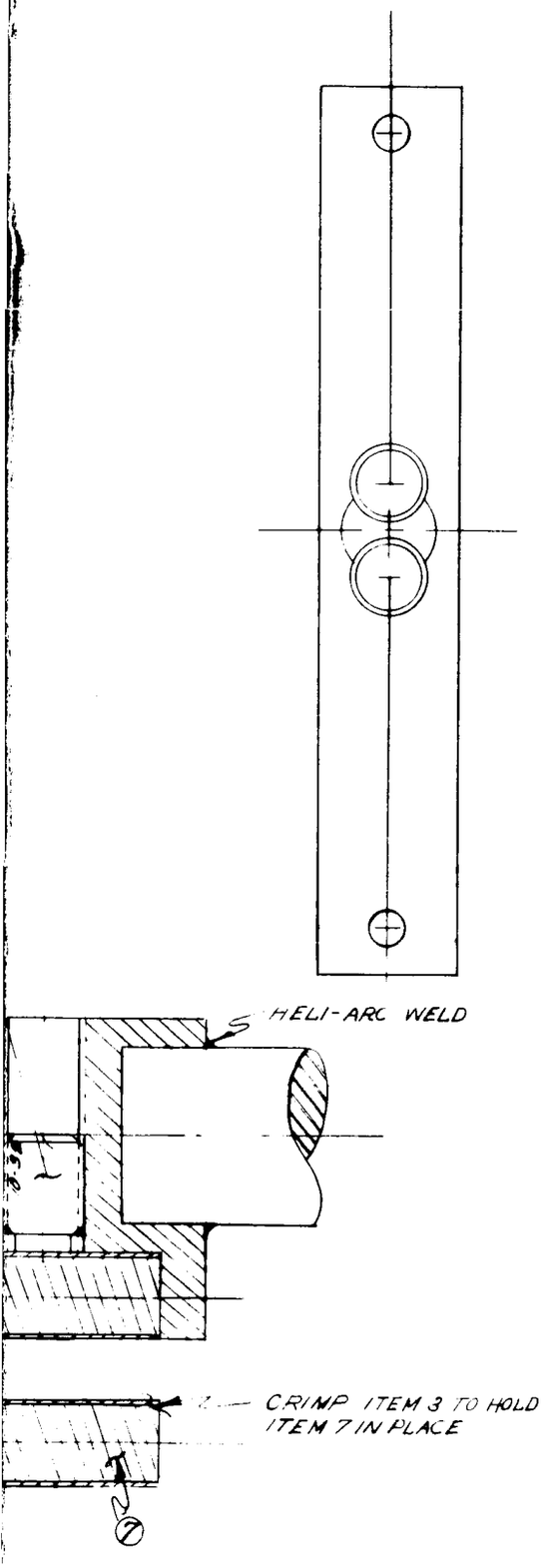

PART	SIZE	REQ	LOC	MAT'L	NOTES
				BRAZES	
2001		2			
9	N.D		2		CERAMASEAL NO. 3058 0105-4
8	N.D		2	S.S	SOCKET SET SC HALF DOG POINT 1/4
7	A		2	Ta	
6	B	B	1	SS	
5					
4	B		1		
3	A		2	Ta	
2	B		2	SS	
1	B		2	SS	

PART	SIZE	REQ	MAT'L	NOTES

UNLESS OTHERWISE SPECIFIED
DEC .X ± 1 .XX ± 01 .XXX ± 005
SCALE 1 = 1
ANGLES ± 0°30' FINISH √MAX
FILLET RAD .010 MAX
THREADS CLASS 2
ALL DIAS CONCENTRIC WITHIN .005 TIR
REMOVE ALL BURRS & SHARP EDGES

NEXT ASSY | SIM TO

THERMO ELECTRON
ENGINEERING CORP.
WALTHAM 54 MASS

DR | ENG
CHK | APP

TITLE

SIZE D | NUMBER 500-1000 | REV

ELECTRON-BOMBARDMENT POWER SUPPLY

FIGURE 8.1

FOLDOUT FRAME 2

PRECEDING PAGE BLANK NOT FILMED.

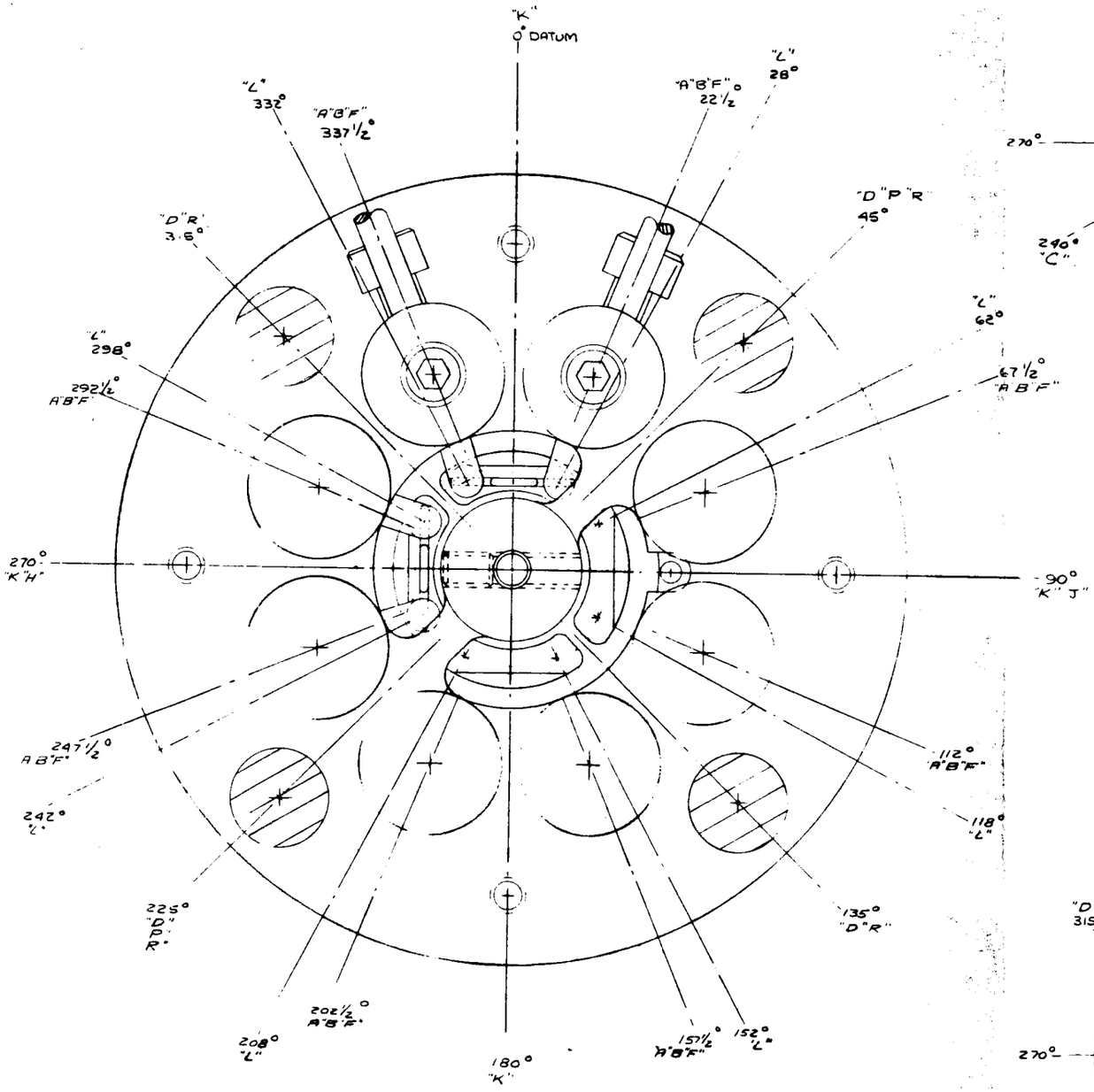

VIEW "C-C"

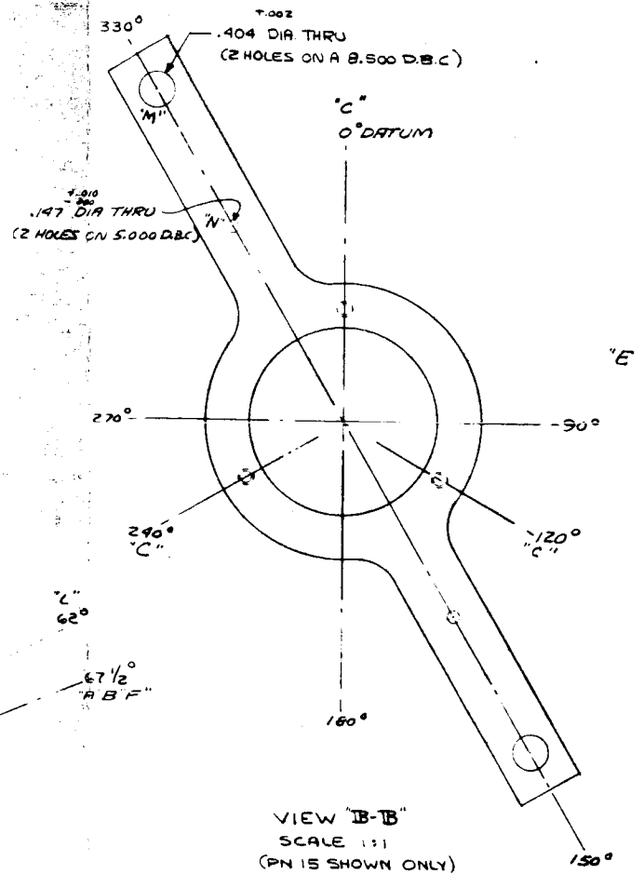

VIEW "B-B"
SCALE 1:1
(PN 15 SHOWN ONLY)

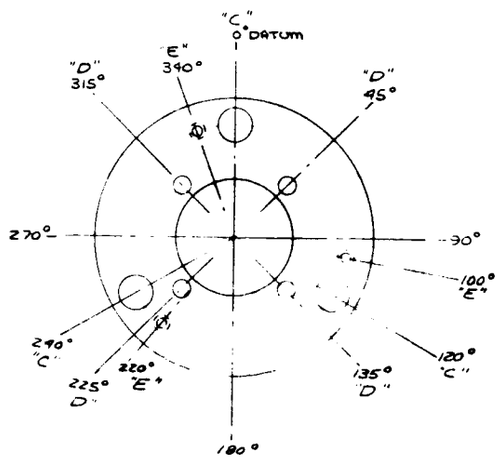

VIEW "A-A"
SCALE 1:1
(PN 17 SHOWN ONLY)

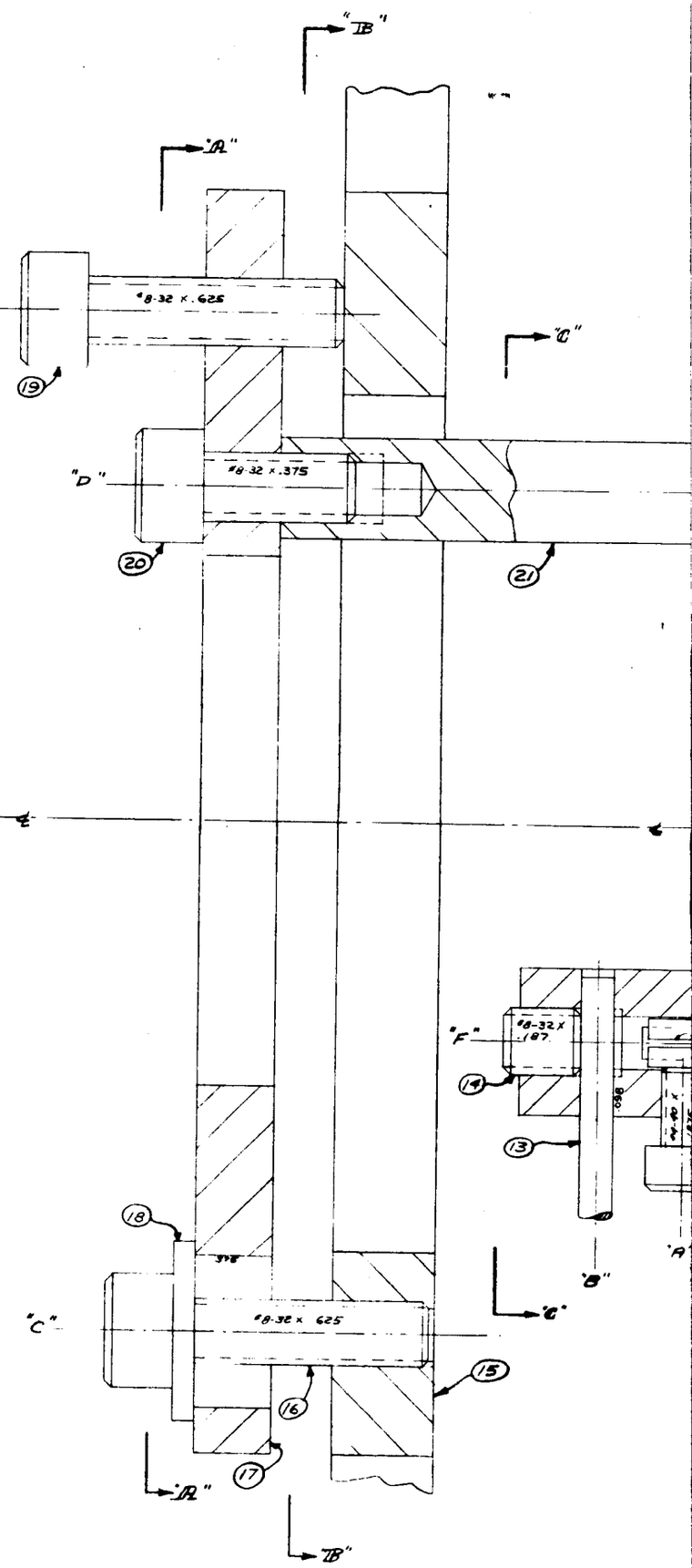

FOLDOUT FRAME 1

FOLDOUT FRAME 2

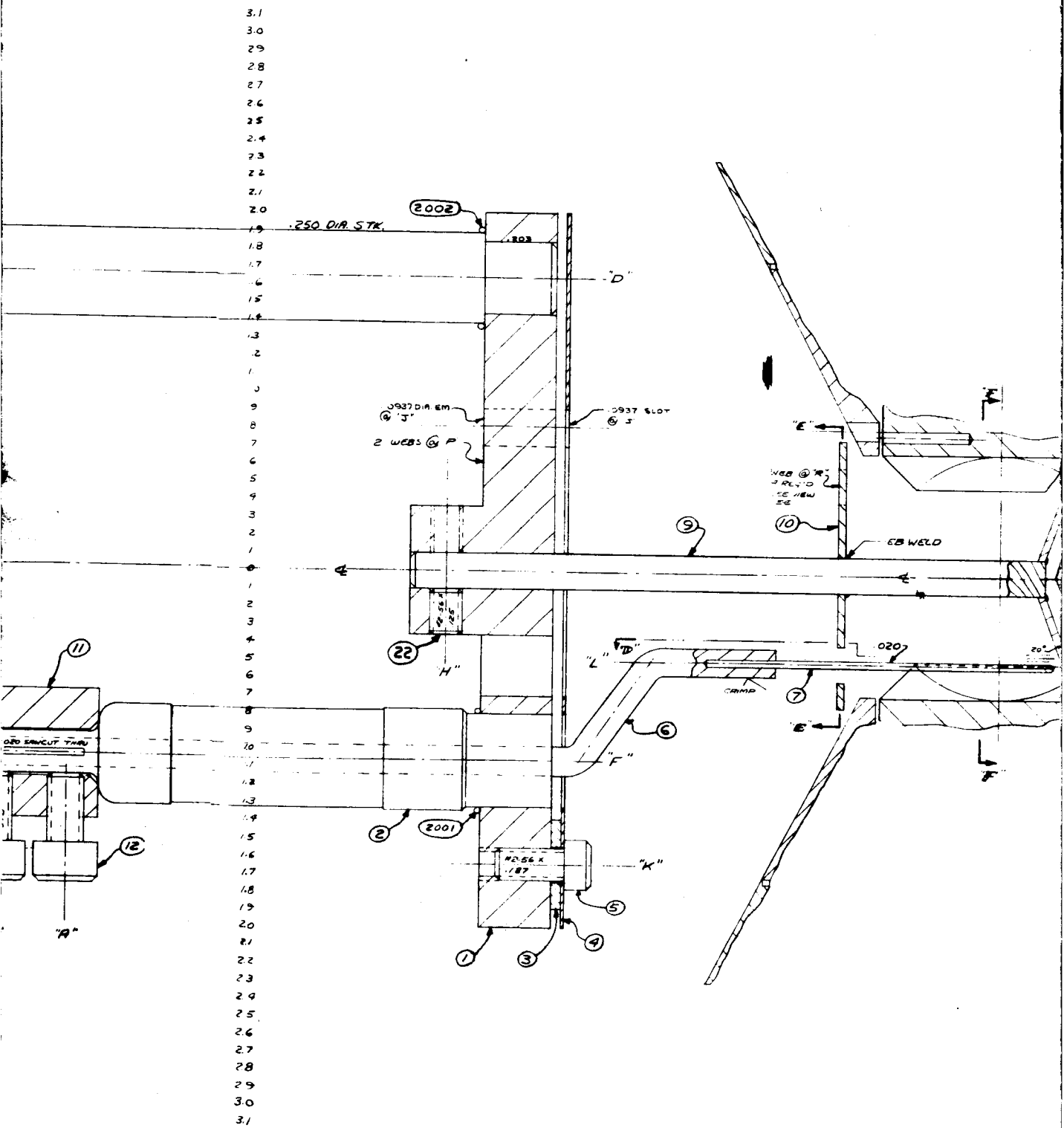

FOLDOUT FRAME 3

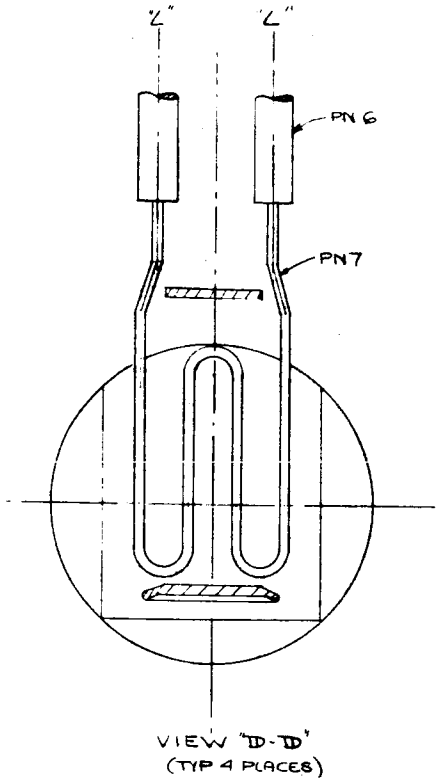

VIEW "D-D"
(TYP 4 PLACES)

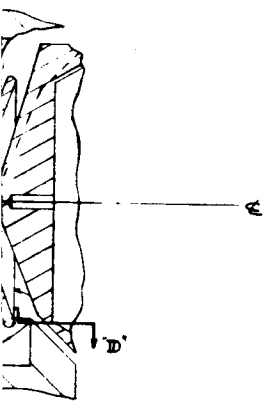

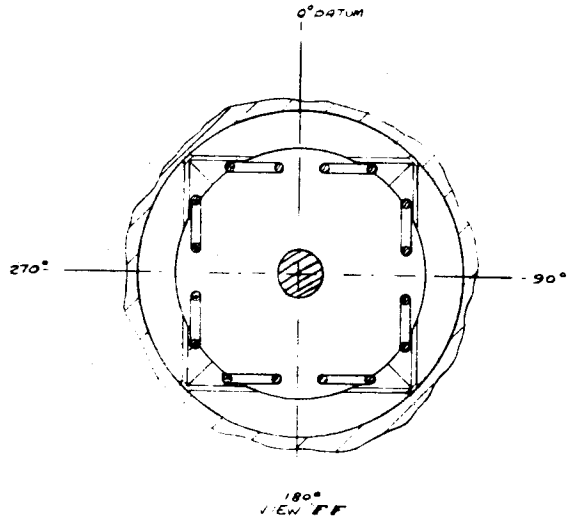

VIEW FF

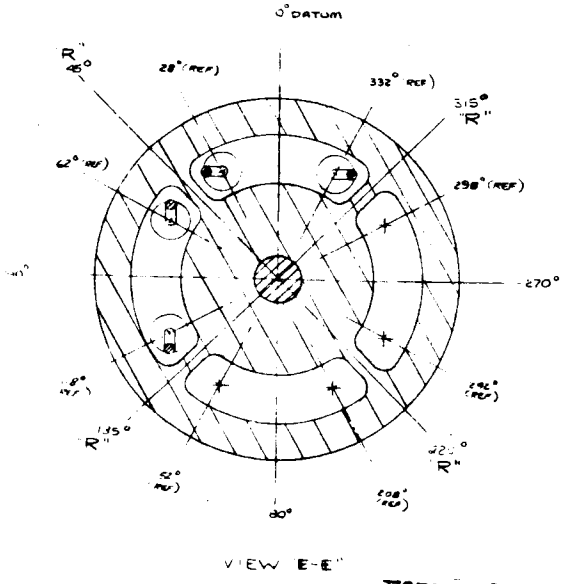

VIEW E-E

PART	SIZE	REQ	LOC	MAT'L	NOTES
			BRAZES		
2001	ND	8			.033 DIA WIRE
2002	ND	9			.030 DIA WIRE

PART	SIZE	REQ	NOTES
			FIXTURES
3090	B	1	TO ALIGN PN 6 AT ASS'Y
3190	B	1	TO BRAZE PN 1 & 2

7 SEE FIXTURE LAYOUTS (3090, 3190 ETC.) FOR FIXTURE INFORMATION.
6 UNK : UNKNOWN ND = NO DRAWING, PROCURE FROM THIS L.O.
5 DOTTED LINES INDICATE ROUGH OR PRELIMINARY MACHINING.
4 ALL MATING CORNERS & FILLETS ARE .015 X 45° CHFR. AND .010 R. RES.
3 MAX PERMISSABLE TAP DRILL DEPTH AND MIN PERMISSABLE FULL THREAD DEPTHS ARE SHOWN.
2 SECTION LOCATIONS DEFINED BY LETTER LOCATION AT END VIEW.
1 NOTES 2 THRU 7 APPLY UNLESS OTHERWISE SPECIFIED.

NOTES

DESIGN FINALIZED	DATE	INIT.	DATE	INIT.	DATE	INIT.	DATE	INIT.

	A	B	C	D	E	F	G	H	J	K	L	M	N	P	R	S	T	U	V	W	Y	Z
I	✓	✓	✓	✓	✓	✓	✓	✓	✓	✓	✓	✓	✓	✓	✓							
2																						
V	✓	✓	✓	✓	✓	✓	✓															
II																						
⊥																						
Ⓜ																						

FIGURE 8.2

PART	SIZE	REV	REQ	MAT'L	NOTES
22	ND		1	S S	#2-56 x .125 LNG SET SCREW
21	B		4	MO	
20	ND		4	S.S.	#8-32 x 375 LNG S.H.C.S
19	ND		3	S.S.	#8-32 x 625 LNG S.H.C.S
18	ND		3	S.S.	#8-32 PLAIN WASHER
17	B		1	S S	
16	ND		3	S.S.	#8-32 x .625 LNG S.H.C.S
15	C		1	S.S.	
14	ND		8	S.S.	#8-32 x .1875 LNG SET SCREW
13	ND		AS REQ'D	Cu	.093 DIA WIRE
12	ND		16	S.S.	#4-40 x .1875 LNG SHCS
11	B		8	S.S.	
10	B		1	Re	
9	B		1	Re	
8	B		1	Re	
7	B		4	W	
6	B		6	Ta	
5	ND		4	S.S.	#2-56 x .1875 S.H.C.S.
4	C		1	Ta	
3	ND		4	S.S.	#2-56 PLAIN WASHER
2	B		8		CERAMASEAL #805B0102-2
1	D		1	Mo	

UNLESS OTHERWISE SPECIFIED

DECIMAL: .X ± .03, .XX ± .01, .XXX ± .005
FILLET RADIUS .010 MAX.
THREADS: CLASS 2
* DIA. CONC. WITHIN ____ T.I.R.
ALL OTHER DIA. CONC. WITHIN .005 ____ T.I.R.
SURFACES TO BE PERP WITHIN .005 ____ T.I.R.
SURFACES TO BE PAR WITHIN .005 T.I.R.
HOLE ANGULAR TOL. 0-2.0 RAD ± 0° 5'
2.0-4.0 RAD ± 0° 5'
ALL OTHER ANGULAR TOL. TO BE ± 0° 30'
REMOVE ALL BURRS AND EDGES

THERMO ELECTRON

DRAWN	CHECKED	ENGINEER
MN 11/65		

TITLE
ELECTRON BOMBARDMENT GUN MODEL II

SCALE: 5X/1 FINISH:

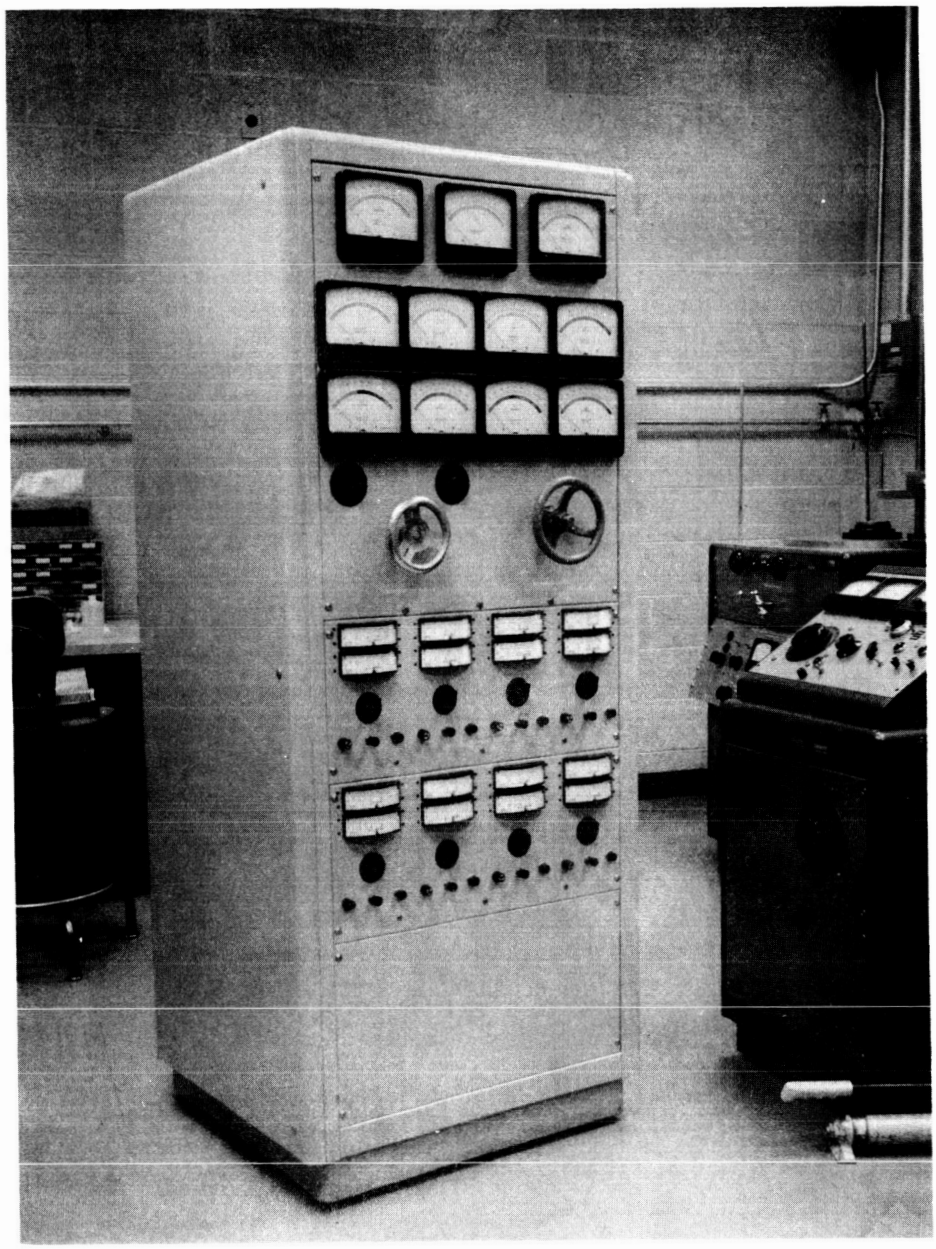

Figure 8.3 Generator Load and Temperature Measurement Setup.

The generator load current is shown in Figure 8.4, and the measuring components are listed in Table 8-1.

Also constructed concurrently was a vacuum system baseplate with enough leadthroughs to accommodate the various connections.

This equipment was used in the initial generator testing. The final tests were conducted at JPL with JPL test equipment.

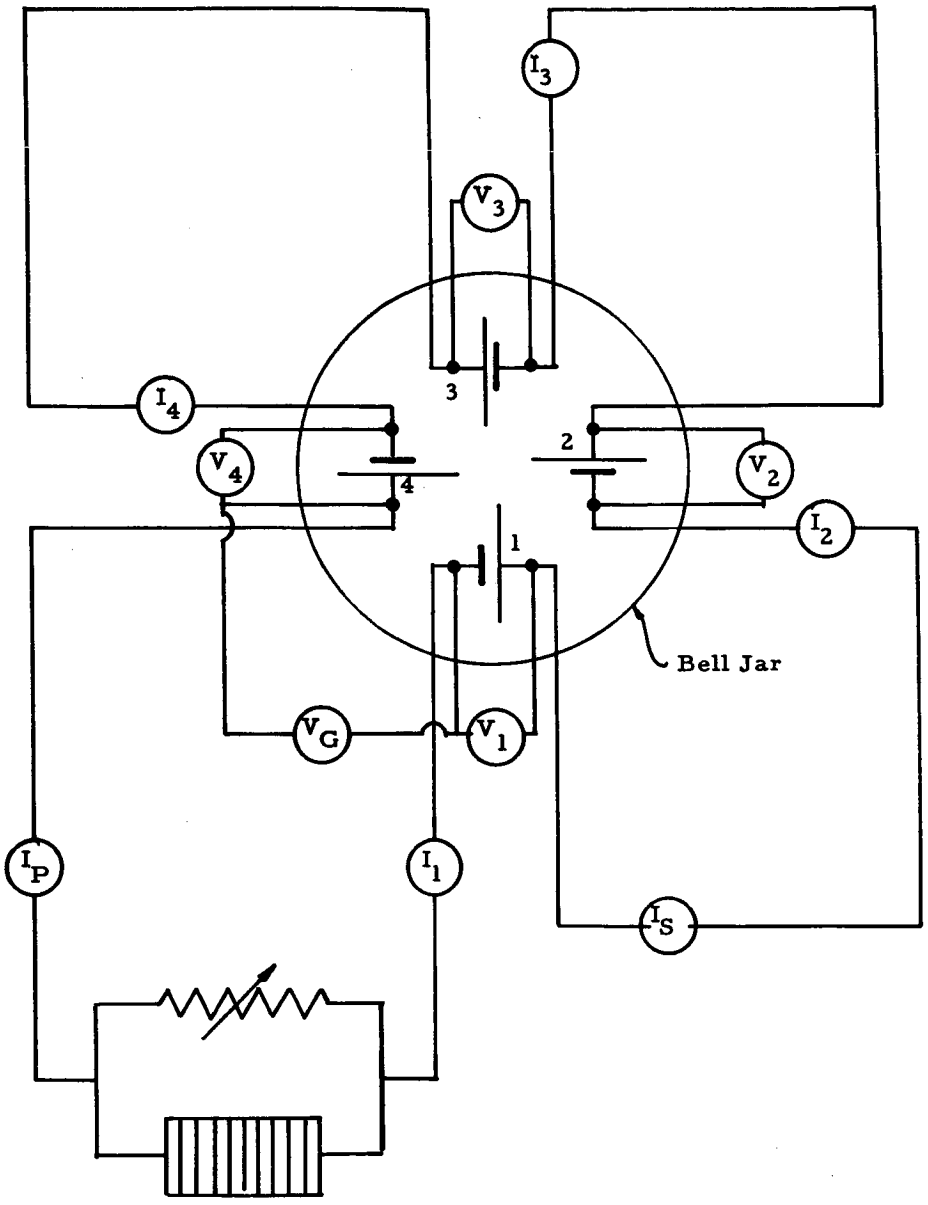

Figure 8.4 Generator Circuit.

TABLE 8-1

GENERATOR TEST CONSOLE – INSTRUMENT SPECIFICATIONS

Instrument	Manufacturer	Range	Accuracy	Size	Quantity
Dc Meters					
Voltmeter - Generator output	Weston	0-6.4 volts	1%	5.6x4.5	1
Ammeter - Converters in parallel	Weston	0-400 amps	1%	5.6x4.5	1
Ammeter - Converters in series	Weston	0-100 amps	1%	5.6x4.5	1
Voltmeter - Converter output	Simpson	0-1.6 volts	2%	4.7x4.0	4
Ammeter - Converter output	Simpson	0-100 amps	2%	4.7x4.0	4
Ac Meters					
Voltmeter - Reservoir and collector heaters	Simpson	0-15 volts	2%	3.25x3.25	8
Ammeter - Reservoir heaters	Simpson	0-10 amps	2%	3.25x3.25	4
Ammeter - Collector heaters	Simpson	0-15 amps	2%	3.25x3.25	4
Rheostats					
Load	Allen-Bradley	.0005-.025 ohm	—	500 watt	1
Load	Jogabi #40	.005-0.5 ohm	—	1000 watt	2
Switches					
Thermocouple switches	J-B-T	14 point	.007 ohm contact resistance	2-1/8 diam	2

CHAPTER 9

GENERATOR ASSEMBLY AND TEST

9.1 ASSEMBLY OF CONVERTERS VIII-S-1 THROUGH VIII-S-6

Following completion of the testing of diode VIII-P-3, the diode design was frozen, and six converters, VIII-S-1 through VIII-S-6, were constructed. The resulting I-V curves at 1700°C observed emitter temperature are shown in Figure 9.1. In Figures 9.2 and 9.3 the power is shown as a function of output voltage at the same emitter temperature. The performance shown on these curves was optimized at each data point shown. The data was taken statically. Of the six converters, VIII-S-1, -3, -5 and -6 produced the highest power and were included in the generator. Converters VIII-S-2 and -4 were used as spares.

9.2 ASSEMBLY OF GENERATOR JG-3

Generator JG-3 was assembled as shown in Figures 6.11, 6.12, and 6.15. The clearances between the four converters were adjusted to be those shown in Chapter 6, with a tolerance of ±1 mil. The completed generator is shown in Figure 9.4. The four converters extend radially to the sides. The entrance to the solar cavity is from the top. The radiator for cooling the block extends downward inside of the generator's support ring.

9.3 GENERATOR TESTING

The generator was mounted on a baseplate, evacuated, and slowly heated with electron bombardment to allow ample time for outgassing of the various parts. The electron-bombardment gun used in this test was shown in Figure 8.1. The gun was driven with a 1000-volt, 4-ampere dc power supply.

Considerable difficulty was experienced in attaining even heating of the four converters, and several mechanical adjustments of the gun were made. After the adjustments, data were taken with total power inputs of 900 and 1000 watts. The data are summarized in Table 9-1, and the power versus voltage is shown in Figure 9.5.

On completion of the 1000-watt input runs, further attempts were made to position the gun in such a way as to heat the diodes more evenly. From Table 9-1 the outputs of the diodes can be seen to vary considerably. During the last such test a sharp instability was observed in the emission current, and before the current could be controlled the generator was severely overheated. On subsequent examination, the converters were found to be damaged. A discussion of the instability can be found in Chapter 8.

The generator was subsequently rebuilt using four new converters supplied by JPL. The current-voltage characteristics of these four converters are shown in Figure 9.6. The converters were designated VIII-S-15, -17, -25 and -26. Looking into the cavity, the clockwise placement order was VIII-S-15, -17, -25, and -26.

When the generator was reassembled, the spacing between converters was increased slightly to reduce the chance that the emitter pieces might touch at high temperatures. The clearances originally used were shown in Chapter 6, while the new clearances are shown in Figure 9.7. The new bombardment gun with four separate filaments, as described in Chapter 8, was used. Tests of the rebuilt JG-3 were conducted at JPL with JPL test equipment and JPL technical support personnel under the direction of a Thermo Electron engineer.

Emitter temperature measurements were made pyrometrically, using a micro-optical pyrometer to view one emitter hohlraum through a bell jar and through a prism. The hohlraum was simulated with a

TABLE 9-1

SUMMARY OF GENERATOR AND CONVERTER TEST DATA

	Run									
	1	2	3	4	5	6	7	8	9	10
Observed Emitter Temperature	1452	1538	1577	1560	1575	1480	1503	1570	1505	1522
Bombardment										
Filament Power - watts	156	150	147	146	142	152	152	149	146	138
Emission Power - watts	750	750	750	750	750	850	850	850	850	850
Total - watts	906	900	897	896	892	1002	1002	999	996	988
Generator Output Current-Amps	32.0	26.3	25.5	22.5	21.0	34.6	34.3	32.2	30.0	25.0
Generator Output Voltage-Volts	1.95	2.50	2.64	2.98	3.25	2.30	2.40	2.43	2.80	3.20
Converter Output Voltage-Volts										
VIII-S-1	0.60	0.73	0.46	0.83	0.88	0.78	0.78	0.48	0.92	1.05
VIII-S-3	0.62	0.72	0.95	0.84	0.96	0.76	0.76	0.96	0.92	1.13
VIII-S-5	0.56	0.68	1.00	0.79	0.84	0.58	0.62	0.98	0.65	0.71
VIII-S-6	0.54	0.69	0.56	0.78	0.78	0.55	0.58	0.52	0.60	0.62
Total Diode Voltage	2.32	2.82	2.97	3.24	3.46	2.67	2.74	2.94	3.09	3.51
Generator Output										
Total	62.5	65.8	67.5	67.0	68.4	79.5	82.3	78.4	84.0	80.0
Based on Diode Voltage	74.2	74.0	75.5	73.0	72.5	92.5	94.0	94.6	92.7	87.9

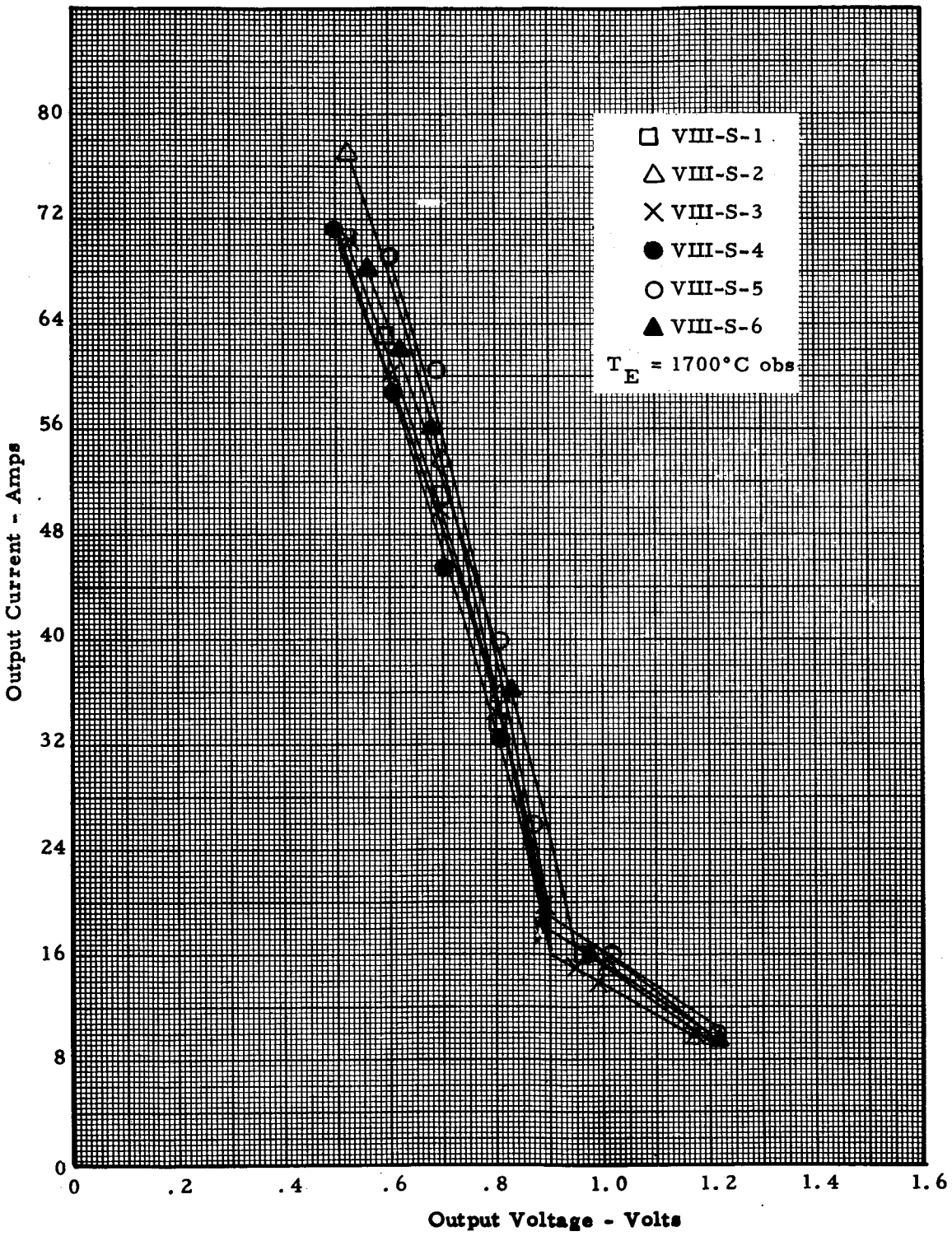

Figure 9.1 Converter Test Data

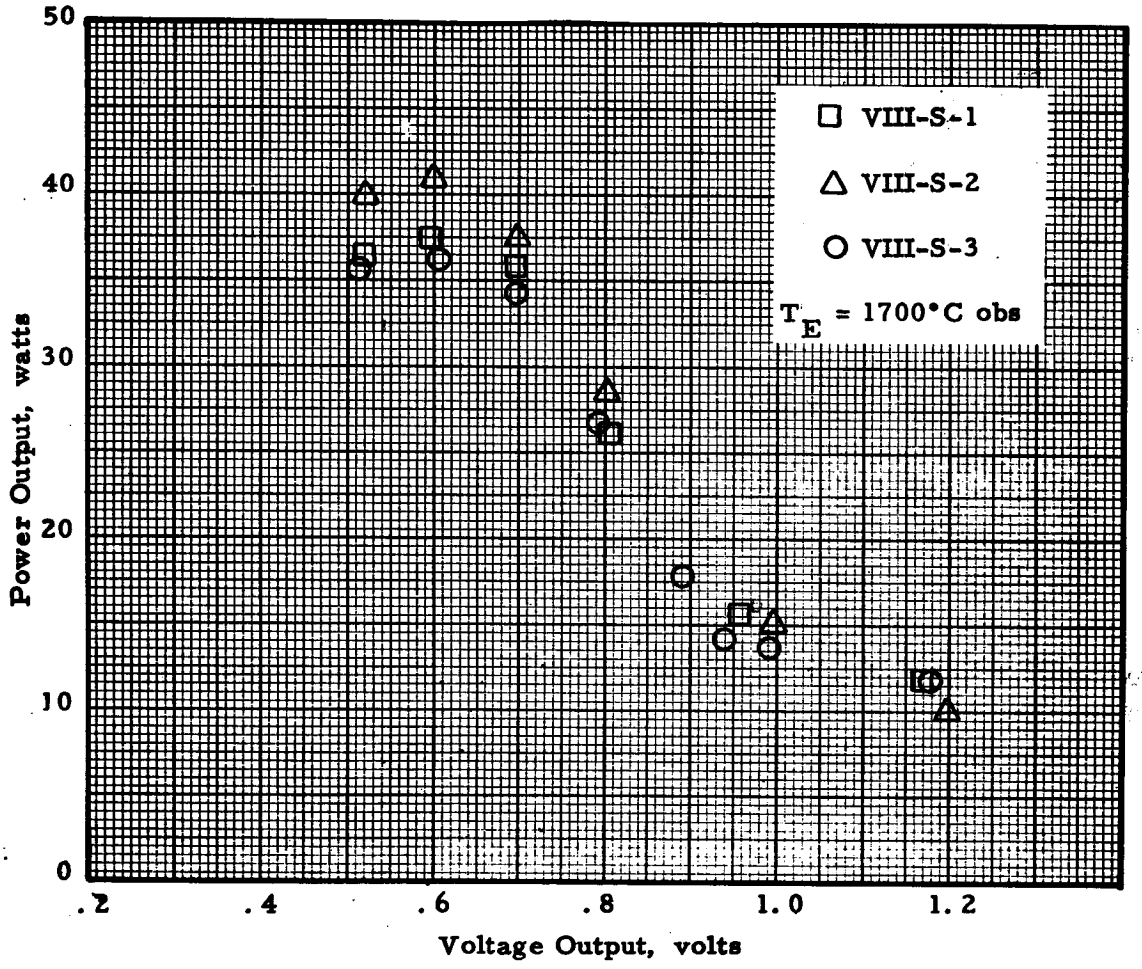

Figure 9.2 Power versus Voltage

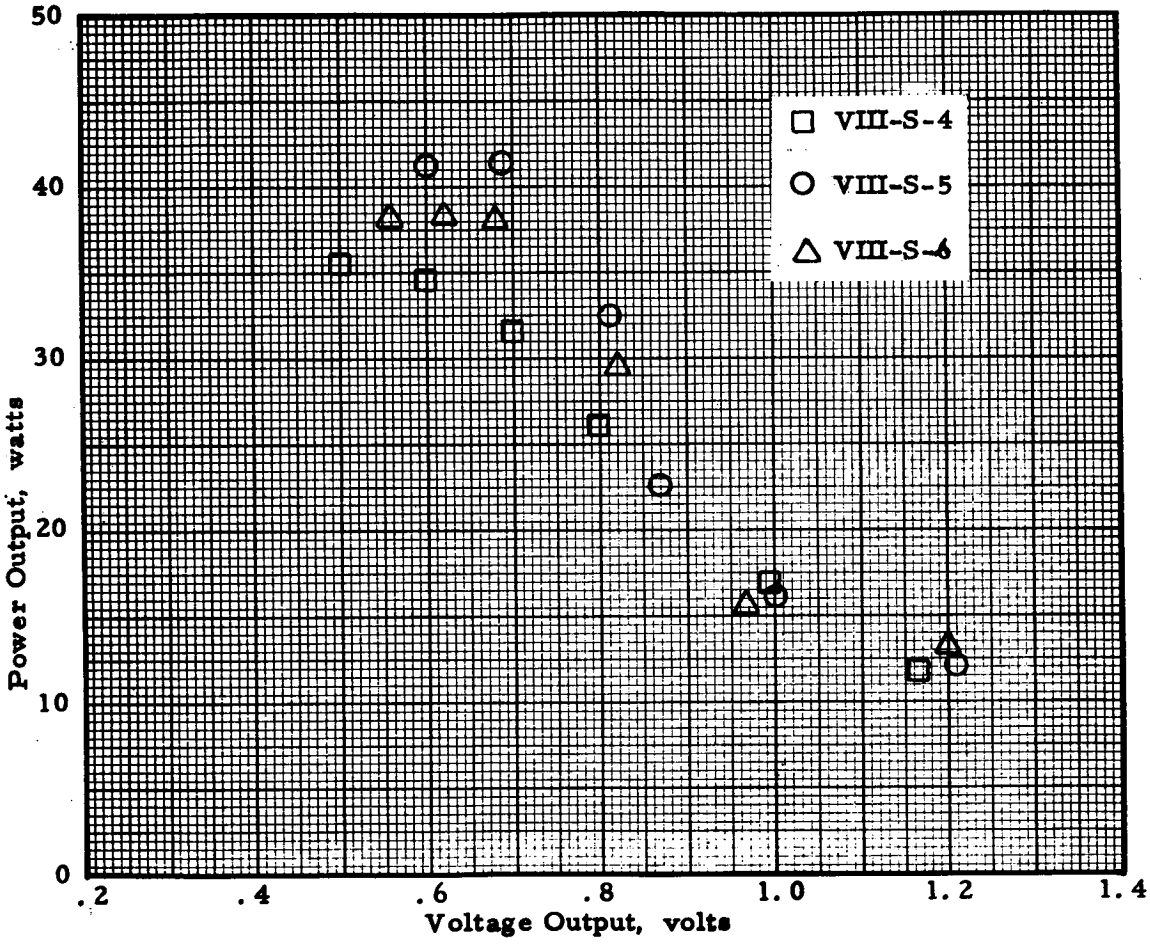

Figure 9.3 Power versus Voltage

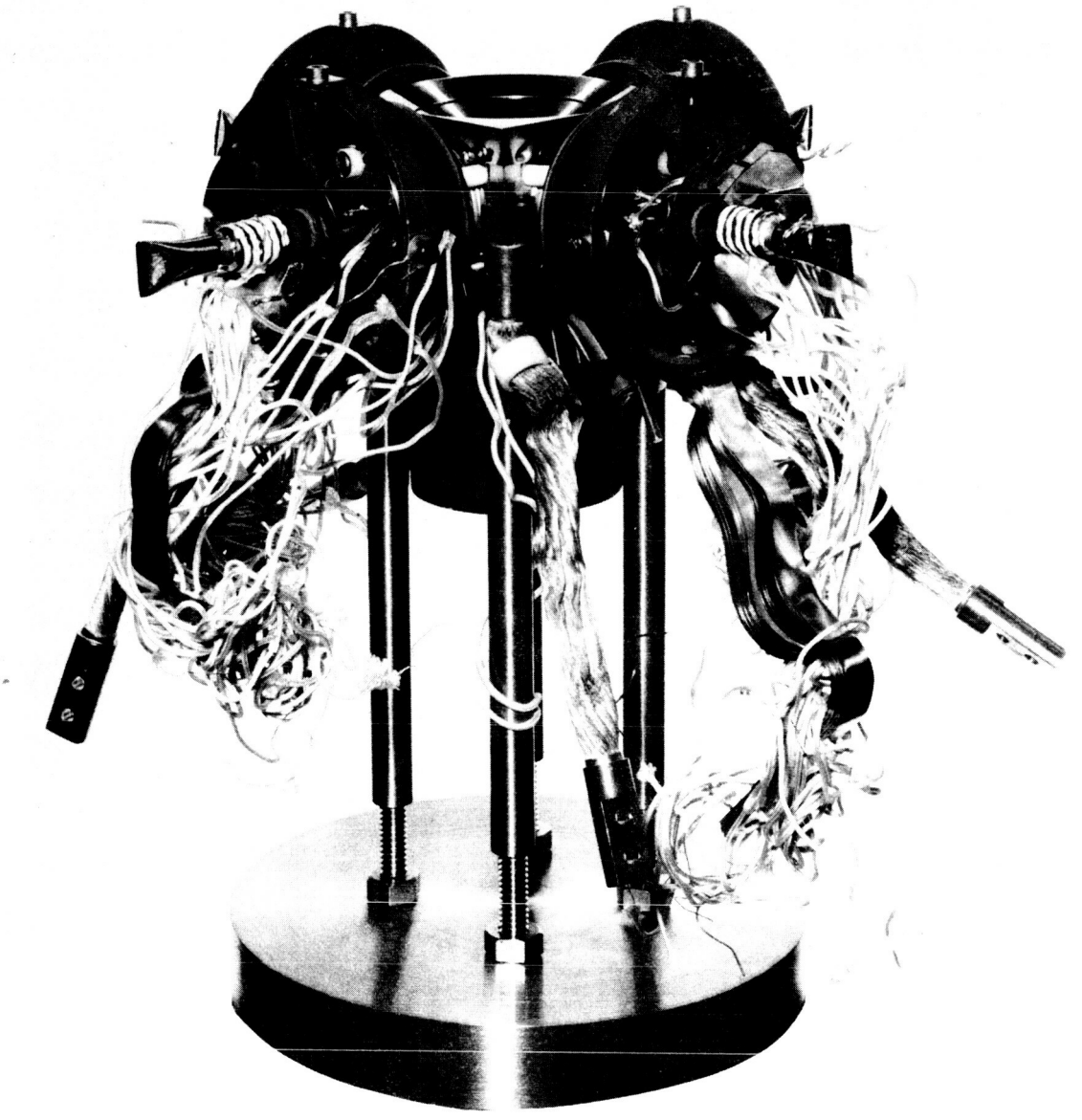

Figure 9.4 Generator JG-3

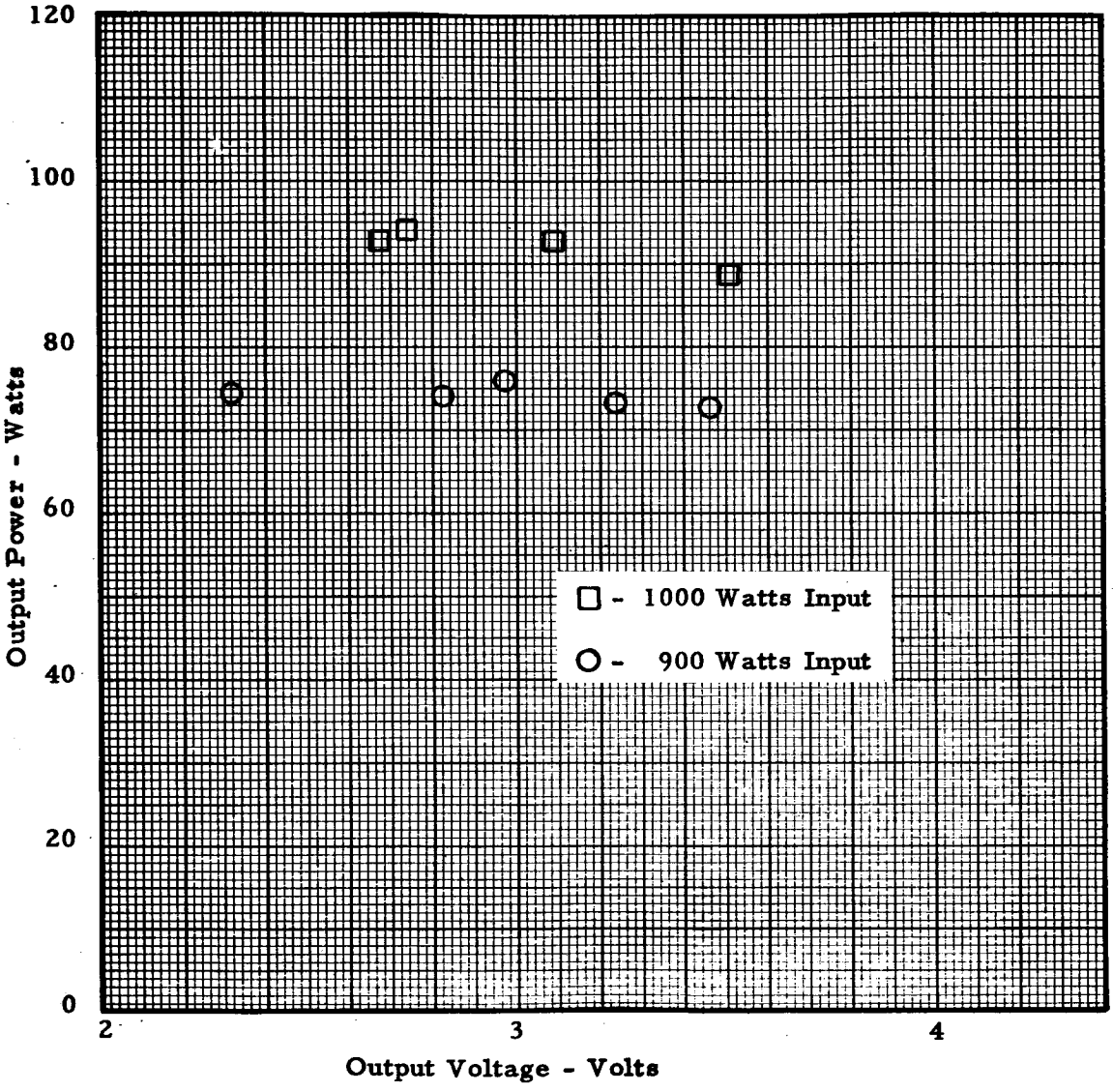

Figure 9.5 Power Output of Generator JG-3 versus Voltage

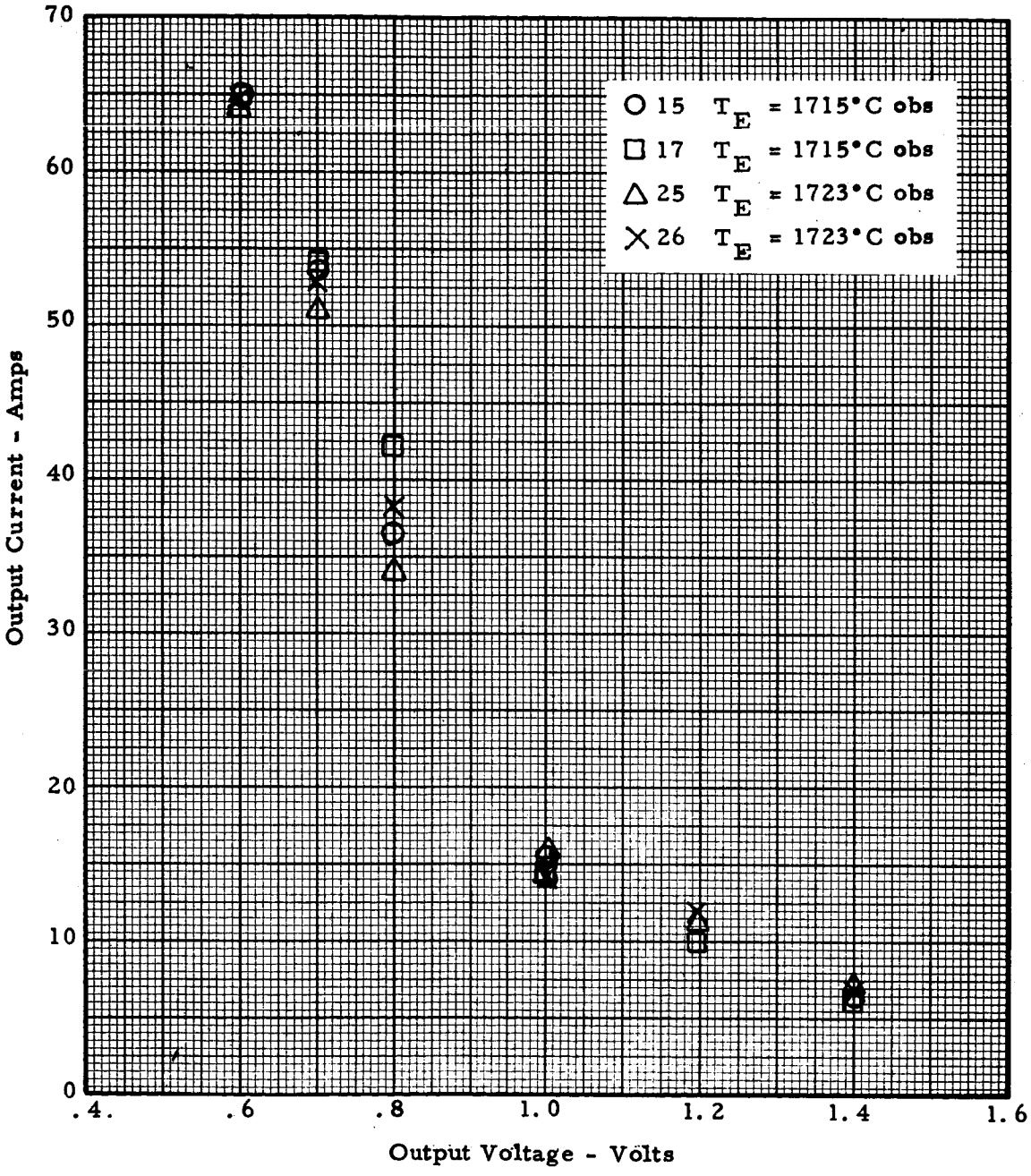

Figure 9.6 Performance of Converters VIII-S-15, -17, -25 and -26

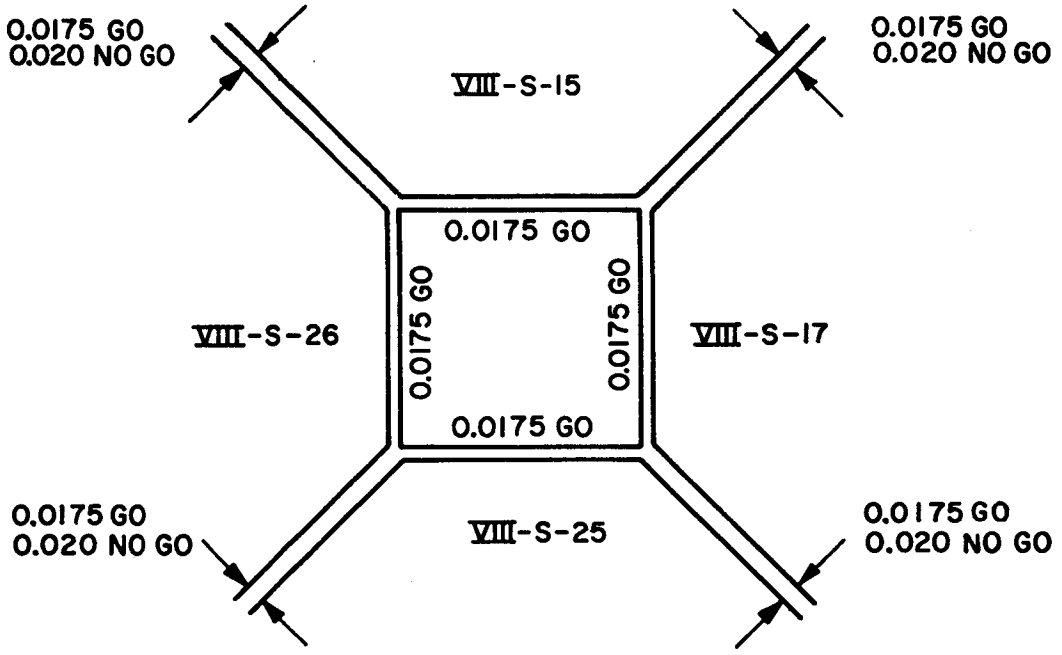

Figure 9.7 Measured Clearances

standard tungsten filament, and the measuring system was calibrated with the results shown in Figure 9.8. All emitter temperatures in the succeeding data are temperatures of the holhraum, with the exception of the curve marked 2000°K. In this case the temperature drop through the emitter from the hohlraum to the emitting surface was calculated as a function of diode current, and the observed temperature was adjusted to achieve an emitter surface temperature of 2000°K.

Figure 9.9 shows the power output with constant power inputs of 900, 1000, 1100 and 1200 watts. The power input is the sum of the bombardment and filament power. Two curves are shown at each power input, one with and one without lead loss. Lead loss will depend on system design and thus will vary between applications.

Figure 9.10 shows the power output at various emitter temperatures, and Figure 9.11 shows the output current versus output voltage.

In Figure 9.12 the generator efficiency, not including lead loss, has been plotted versus power output.

The output voltages of the four diodes have been tabulated in Table 9-2 for the condition of 1100 watts input to show the variation between diodes.

TABLE 9-2

CONVERTER OUTPUT VOLTAGES VERSUS GENERATOR OUTPUT CURRENT WITH 1100 WATTS INPUT

	Generator Current			
	20.0	24.31	25.8	29.63
VIII-S-15	1.125	0.970	0.910	0.780
VIII-S-17	1.075	0.950	0.880	0.810
VIII-S-25	0.925	0.830	0.780	0.700
VIII-S-26	1.040	0.870	0.860	0.740

Table 9-3 summarizes various temperatures that were measured and shows the temperature distribution of the block, the converter collectors, the cesium reservoirs, and the converter seals. These values are shown for various operating points of the generator. For comparison, Tables 9-4, -5, -6 and -7 show the results of earlier tests of each of the converters. The emitter temperature shown in the generator data is that of converter VIII-S-17. This converter was positioned so that its hohlraum could be observed through a hole in the generator block. The other emitters were not visible.

9.4 CONCLUSIONS

A direct comparison between this new generator, JG-3, and the earlier version, JG-2B,* is difficult to make because the electron-bombardment guns used for the tests were quite different. The four-filament type used in JG-3 is certainly less efficient than that in JG-2B. The latter generator used five converters, while the former had four. Figure 9.13 shows a comparison of the two generators at two values of total input power. JG-3, with one less converter, produces equal or slightly more power. More definitive conclusions regarding both power output and efficiency must await solar testing.

With regard to the mechanical structure, both the converters and the entire generator are now capable of withstanding realistic environmental conditions simulating those of a launch vehicle. Only the generator's ability to withstand heating from very low temperatures remains to be evaluated.

The temperature distribution of the various components of the generator is considerably improved. The generator block and converter seal temperatures are maintained within safe limits, unlike JG-2B, where

* "Status Report on Solar Thermionic Power Systems" by Peter Rouklove, AIAA Paper No. 64-734, Third Biennial Aerospace Power Systems Conference, September 1964.

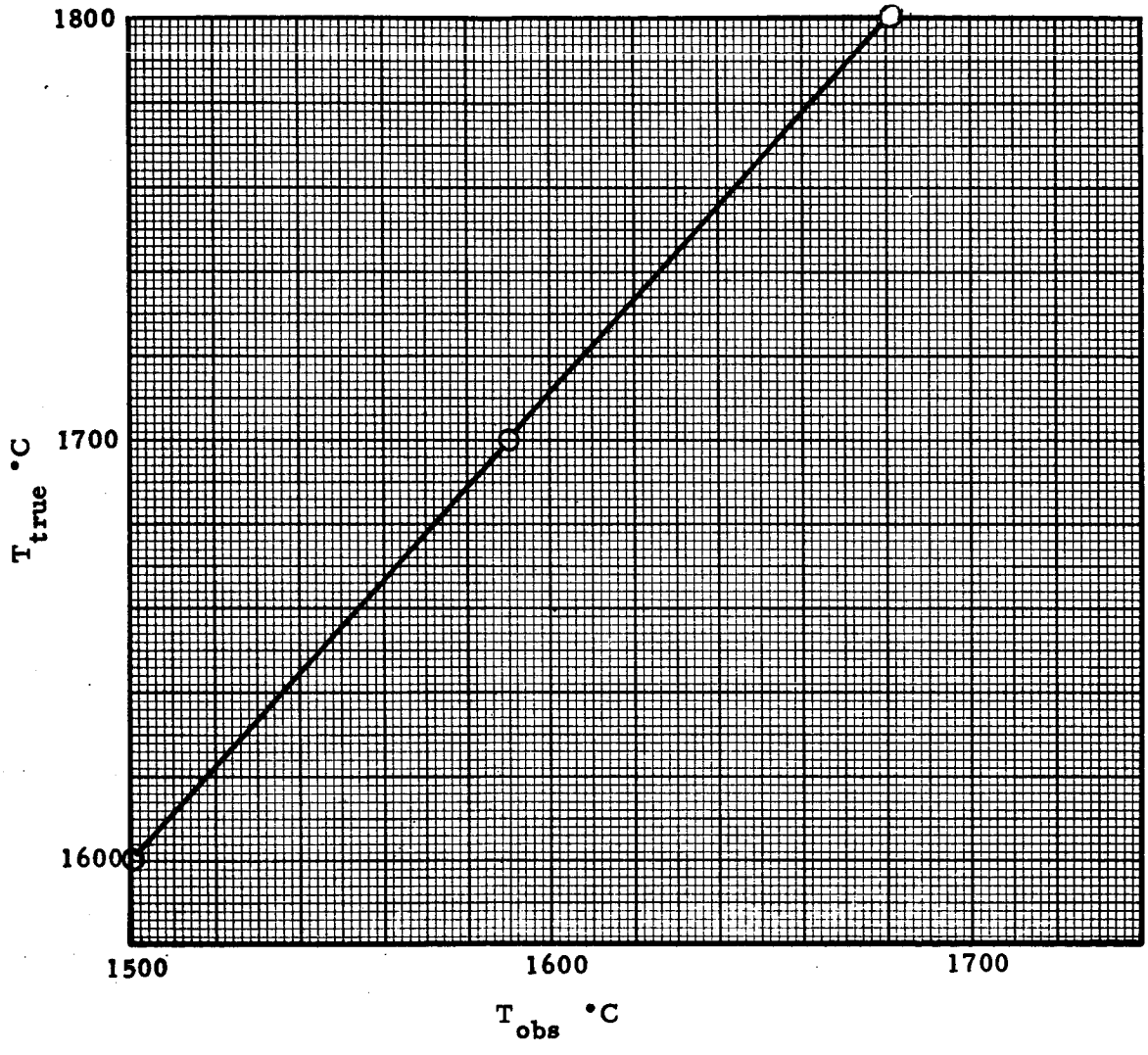

Figure 9.8 Pyrometer, Bell Jar and Prism Calibration

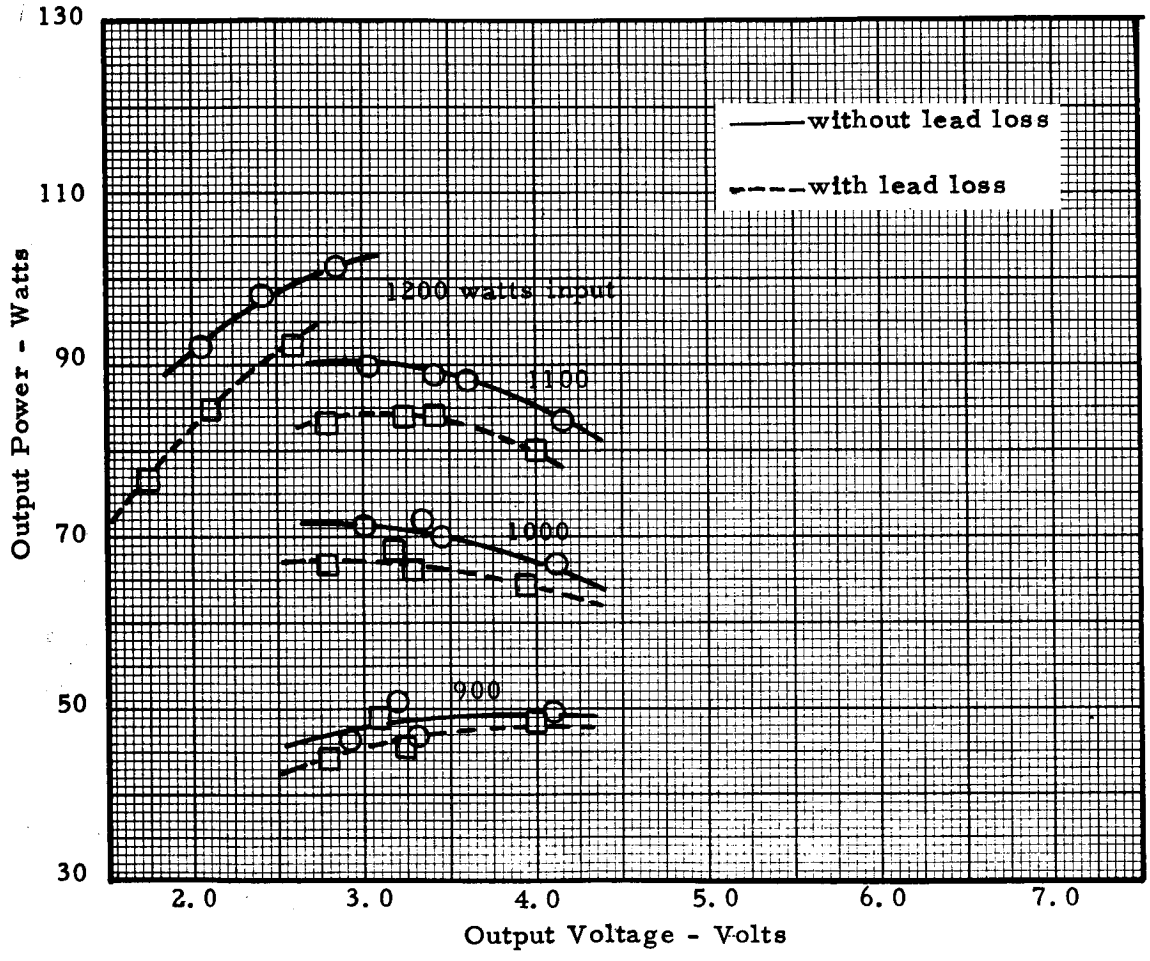

Figure 9.9 Power Output at Constant Power Input

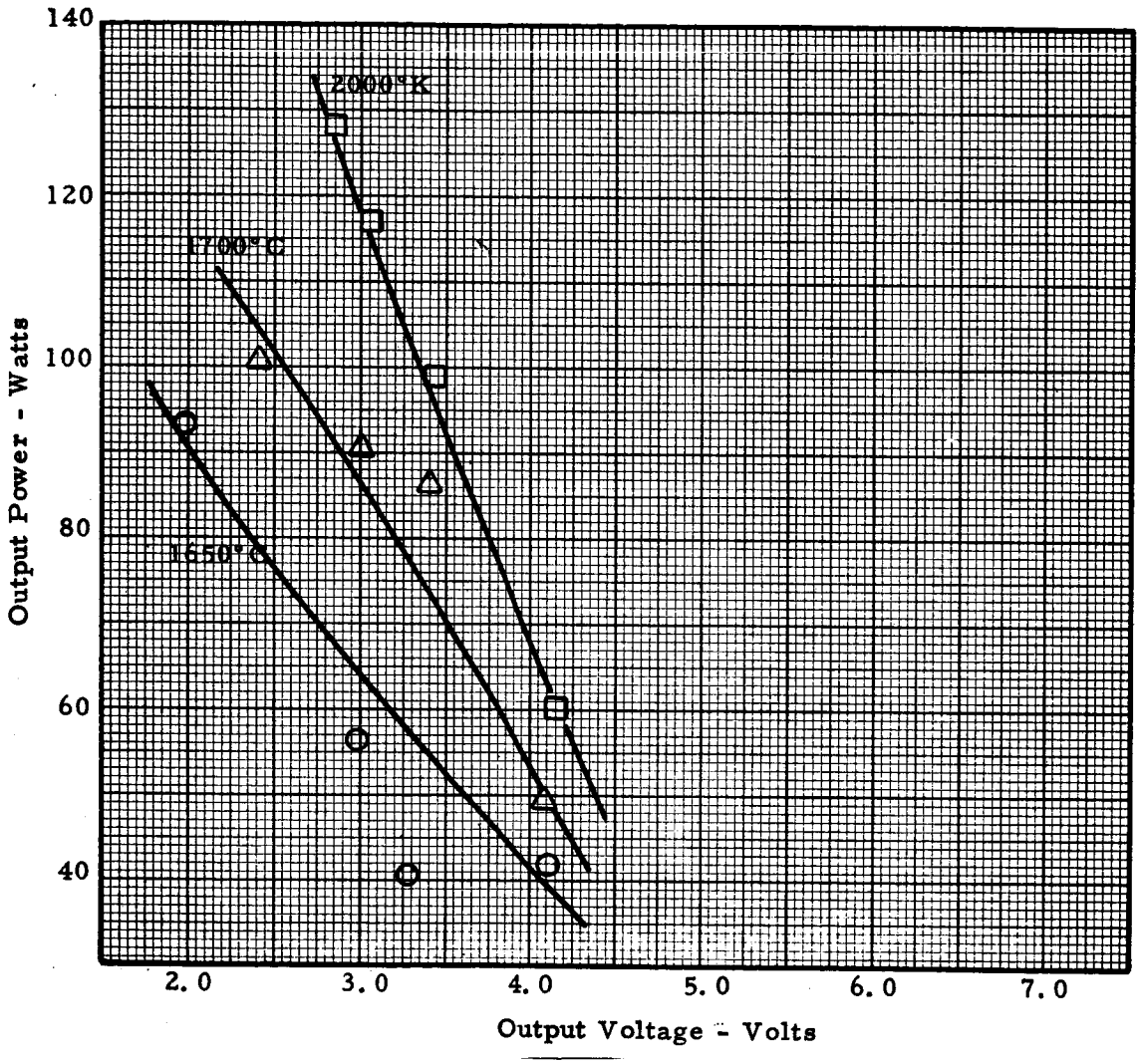

Figure 9.10 Power Output at Constant Emitter Temperature

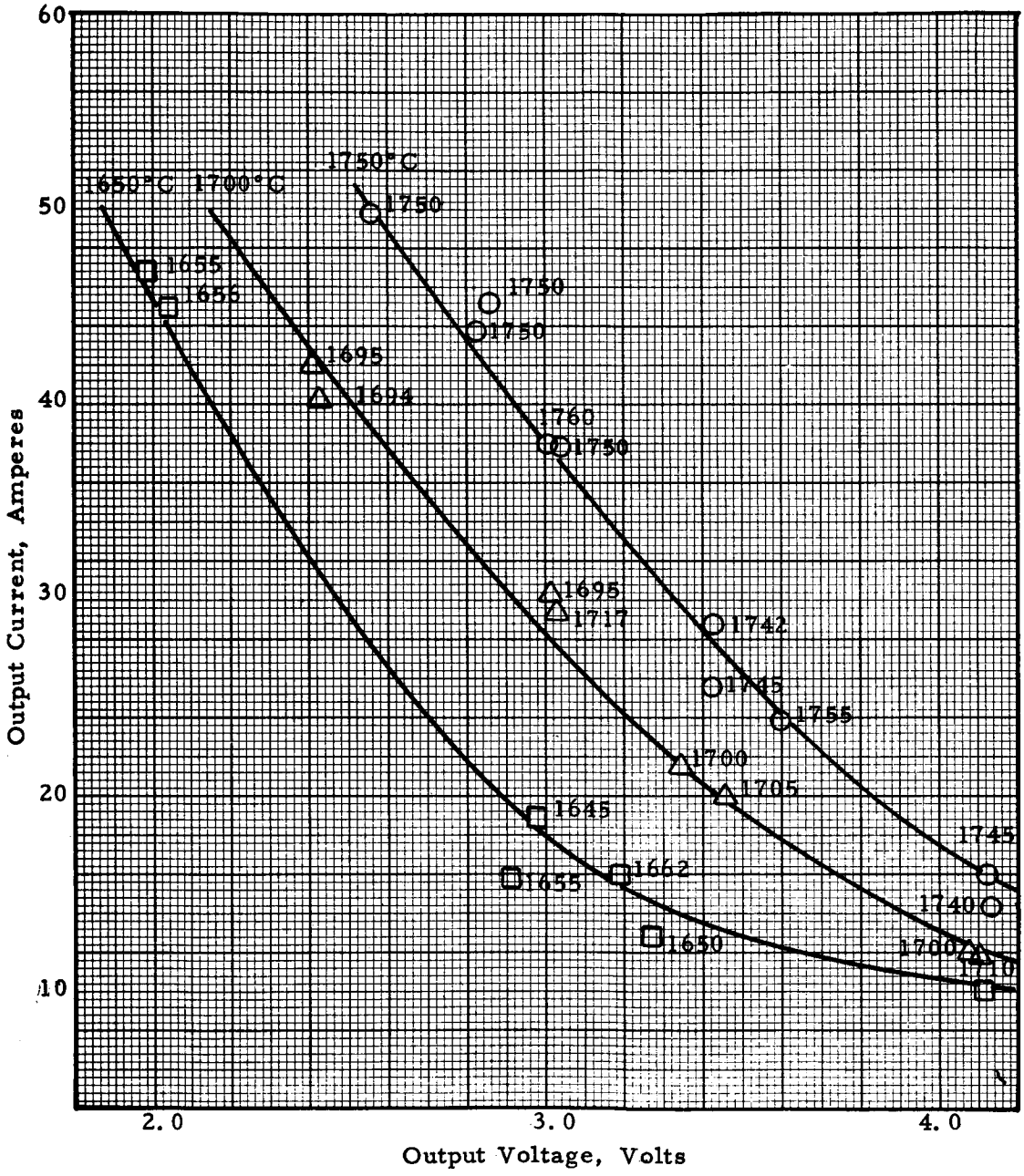

Figure 9.11 Output Current versus Output Voltage at Constant Emitter Temperature

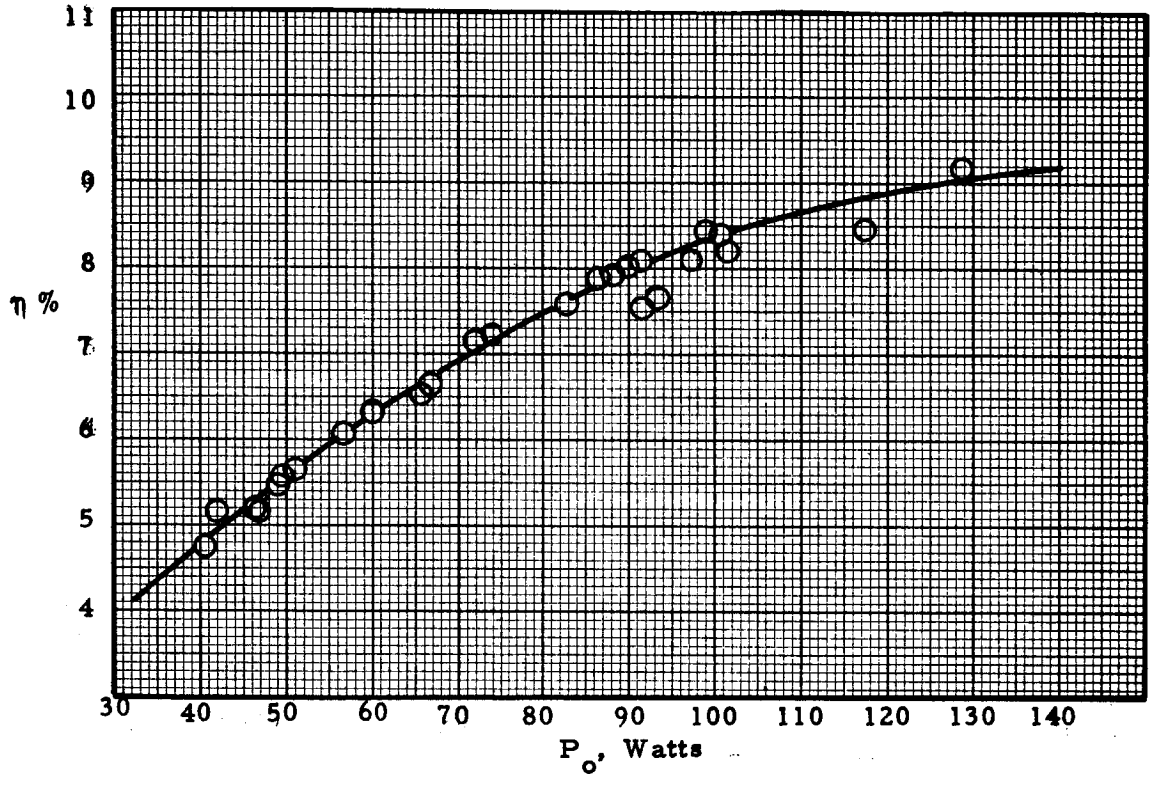

Figure 9.12 Efficiency versus Power

TABLE 9-3

SELECTED GENERATOR AND CONVERTER TEST DATA

Power Input Watts	Generator Current Amps	Holhraum Temperature °C	Block Temperature °C	Cesium Temperature °C				Collector Temperature °C				Diode Voltage volts				Seal Temperature			
				S-17	S-25	S-26	S-15	S-17	S-25	S-26	S-15	S-17	S-25	S-26	S-15	S-17	S-25	S-26	S-15
	12.0	1710	699	314	331	307	309	537	562	546	539	1.02	1.00	1.00	1.08	621	633	630	618
900	14.0	1695	697	317	331	297	312	539	569	551	543	.89	.79	.80	.84	621	633	630	618
	15.8	1655	690	307	317	300	312	537	567	555	546	.77	.73	.67	.75	616	630	630	616
	16.0	1662	685	317	331	312	309	541	567	558	553	.82	.70	.80	.89	626	630	628	621
	16.2	1745	723	326	324	307	317	562	586	574	572	1.02	.95	1.04	1.11	652	654	649	642
1000	21.4	1700	711	326	329	309	317	572	593	581	579	.87	.76	.84	.89	649	654	649	642
	23.8	1678	711	329	331	312	321	576	600	588	586	.78	.65	.74	.80	649	654	654	644
	20.2	1705	718	319	329	309	314	569	593	579	579	.90	.76	.84	.95	649	654	649	644
	20.0	1800	754	326	336	317	321	588	612	597	595	1.08	.92	1.04	1.12	673	678	673	666
1100	25.8	1745	752	324	341	321	319	597	623	609	607	.88	.78	.86	.91	675	682	678	668
	29.6	1717	742	333	343	324	331	602	630	614	612	.81	.70	.74	.78	673	682	678	666
	24.3	1755	754	324	343	321	319	597	623	607	604	.95	.83	.87	.97	673	682	680	668
	35.4	1734	752	338	353	336	338	623	653	640	633	.77	.63	.70	.76	690	697	694	685
1200	40.3	1694	747	343	360	338	343	635	661	647	642	.66	.52	.58	.66	692	697	694	687
	45.0	1656	744	331	362	343	331	642	668	656	649	.56	.43	.49	.56	692	697	702	690

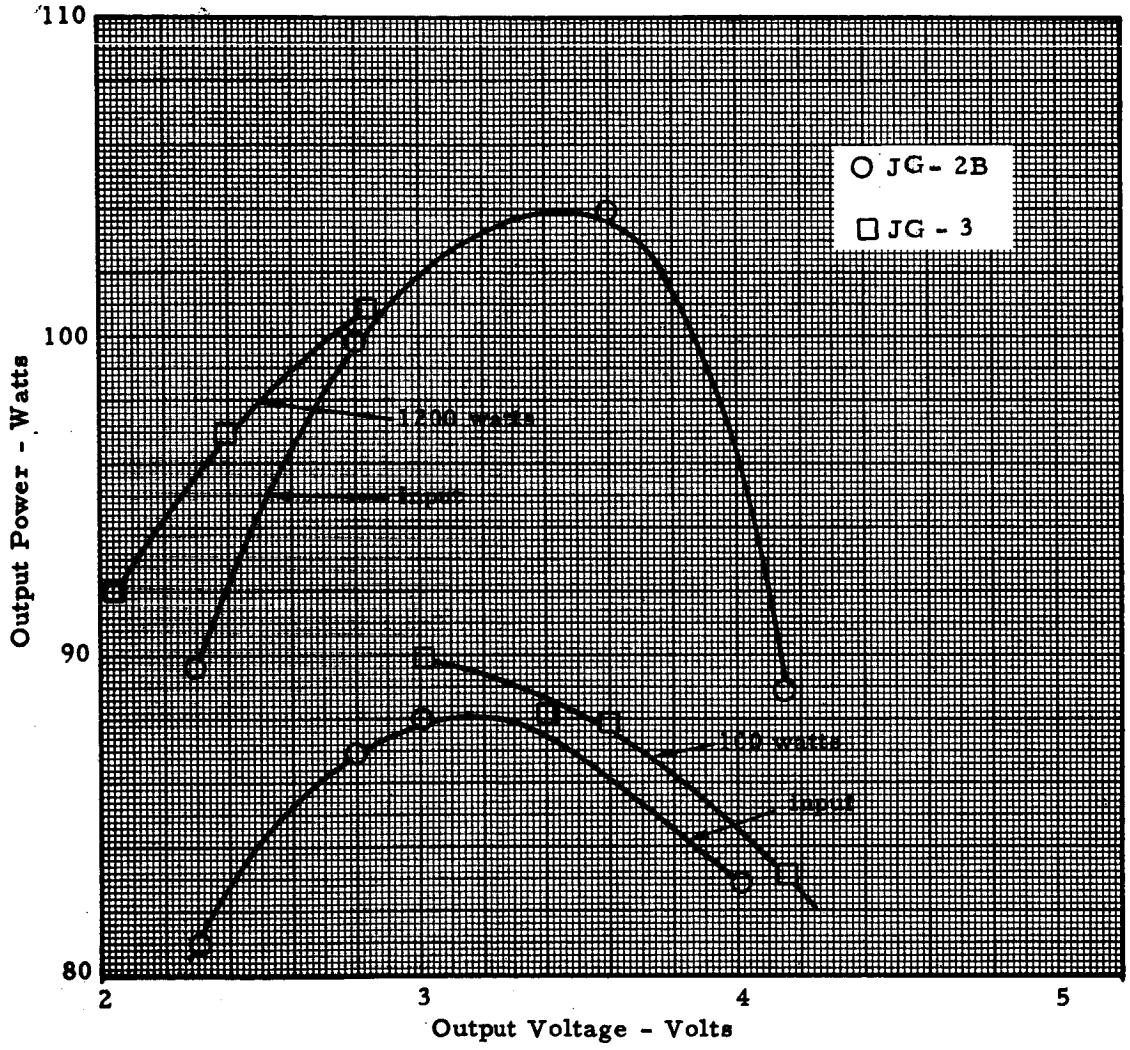

Figure 9.13 Comparison of Generators JG-2B and JG-3

TABLE 9-4

THERMO ELECTRON

ENGINEERING CORPORATION

SHEET 1

CONVERTER NO. VIII -S -15 RUN NO. DATE 6-14-65

	1	2	3	4	5	6	7	8	9	10
TIME	1015	1025	1035	1045	1100	1110	1120	1130	1135	1145
T_o (PYROMETER) °C	1715	1715	1715	1715	1715	1715	1715	1715	1715	1715
T_{ES} (EMITTER) °K										
V_o (OUTPUT VOLTS)	.60	.60	.70	.70	.80	.80	1.0	1.0	1.2	1.2
I_o (OUTPUT AMPS.)	65	65	53.5	54	36.5	36.5	15.5	15.5	11.0	11.0
P_o (OUTPUT WATTS)	39.0	39.0	37.5	37.8	29.2	29.2	15.5	15.5	13.2	13.2
T_R mV	15.15	15.20	14.6	14.55	13.7	13.7	13.0	13.0	12.9	12.85
(RESERVOIR TEMP.) °C	370	372	357	356	336	336	319	319	317	316
T_C mV	33.3 28.4	33.3 28.4	31.0 26.7	31.0 26.7	27.6 24.3	27.6 24.3	23.1 21.0	23.1 20.9	21.8 20.0	21.8 19.9
(COLLECTOR TEMP.) °C	800 682	800 682	744 642	744 642	663 586	663 586	558 508	558 506	527 485	527 483
T_F mV	27.0 25.1	27.0 25.1	25.5 23.9	25.5 23.9	23.3 22.0	23.3 22.0	20.3 19.3	20.2 19.3	19.3 18.5	19.3 18.5
(RADIATOR FIN TEMP.) °C	649 604	649 604	612 576	612 576	562 537	562 537	492 468	489 468	468 450	468 450
T_S mV	29.2	29.2	27.9	27.9	26.0	26.0	23.6	23.6	22.9	22.9
(SEAL TEMP.) °C	702	702	671	671	626	626	569	569	553	553
E_b (BOMB. VOLTS)	1000	1000	1000	1000	1000	1000	1000	1000	1000	1000
I_b (BOMB. mA)	375	375	348	348	301	301	242	242	229	229
P_b (BOMB. WATTS)	375	375	348	348	301	301	242	242	229	229
E_F (FIL. VOLTS)	5.0	5.0	4.9	4.9	4.7	4.7	4.6	4.6	4.5	4.5
I_F (FIL. AMPS.)	35.5	35.5	35	35	34.5	34.5	34	34	34	34
E_C (COL. HEATER VOLTS)	0	0	0	0	0	0	0	0	0	0
I_C (COL. HEATER AMPS.)	0	0	0	0	0	0	0	0	0	0
E_R (RES. HEATER VOLTS)	1.8	1.8	1.95	1.75	1.75	1.75	2.0	2.0	2.0	2.15
I_R (RES. HEATER AMPS.)	—	—	—	—	—	—	—	—	—	—
VACUUM 10^{-6} mm Hg	5	4.5	3.5	3	2.5	2.5	2	2	2	2
OBSERVER	BG									

NOTES:

TABLE 9-4

THERMO ELECTRON

ENGINEERING CORPORATION

SHEET 2

CONVERTER NO. VIII-S-15 RUN NO. DATE 6-14-65

	1	2	3	4	5	6	7	8	9	10
TIME	1155	1205	1220	1230						
T_o (PYROMETER) °C	1715	1715	1715	1715						
T_{ES} (EMITTER) °K										
V_o (OUTPUT VOLTS)	1.4	1.4	.60	.60						
I_o (OUTPUT AMPS.)	6.5	6.5	65	65						
P_o (OUTPUT WATTS)	9.1	9.1	39.0	39.0						
T_R mV	12.3	12.3	15.2	15.2						
(RESERVOIR TEMP.) °C	302	302	372	372						
T_C mV	20.4 18.8	20.4 18.8	33.2 28.3	33.2 28.3						
(COLLECTOR TEMP.) °C	494 457	494 457	798 680	798 680						
T_F mV	18.2 17.5	18.3 17.5	26.9 25.0	26.9 25.1						
(RADIATOR FIN TEMP.) °C	445 426	445 426	647 602	647 609						
T_S mV	22.0	22.0	29.2	29.2						
(SEAL TEMP.) °C	532	532	702	702						
E_b (BOMB. VOLTS)	1000	1000	1000	1000						
I_b (BOMB. mA)	211	211	375	375						
P_b (BOMB. WATTS)	211	211	375	375						
E_F (FIL. VOLTS)	4.45	4.45	4.9	4.9						
I_F (FIL. AMPS.)	33.5	33.5	35	35						
E_C (COL. HEATER VOLTS)	0	0	0	0						
I_C (COL. HEATER AMPS.)	0	0	0	0						
E_R (RES. HEATER VOLTS)	2.0	2.1	1.8	1.8						
I_R (RES. HEATER AMPS.)	-	-	-	-						
VACUUM 10^{-6} mm Hg	1.5	1.5	2	2						
OBSERVER	BG									

NOTES:

TABLE 9-5

THERMO ELECTRON

ENGINEERING CORPORATION

SHEET 1

CONVERTER NO. VIII-S-17 RUN NO. DATE 6-15-65

	1	2	3	4	5	6	7	8	9	10
TIME	1315	1335	1345	1405	1420	1435	1445	1455	1510	1535
T_o (PYROMETER) °C	1715	1715	1715	1715	1715	1715	1715	1715	1715	1715
T_{ES} (EMITTER) °K										
V_o (OUTPUT VOLTS)	.60	.60	.70	.70	.80	.80	1.0	1.0	1.2	1.2
I_o (OUTPUT AMPS.)	65	65	54	54	42	42	14.5	14.5	10	10
P_o (OUTPUT WATTS)	39	39	37.8	37.8	33.6	33.6	14.5	14.5	12	12
T_R mV	15.05	15.1	14.5	14.5	14.0	14.0	13.1	13.1	12.8	12.8
(RESERVOIR TEMP.) °C	368	369	355	355	343	343	321	321	314	314
T_C mV	27.9 28.25	28.0 28.3	26.1 26.6	26.1 26.6	24.3 25.0	24.3 25.0	19.9 21.0	19.8 20.8	18.7 19.8	18.7 19.8
(COLLECTOR TEMP.) °C	671 679	673 680	628 640	628 640	586 602	586 602	483 508	480 504	454 480	454 480
T_F mV	26.7 25.0	26.7 25.0	25.3 23.7	25.3 23.7	24.0 22.5	24.0 22.5	20.2 19.3	20.1 19.2	19.2 18.3	19.2 18.3
(RADIATOR FIN TEMP.) °C	642 602	642 602	609 572	609 572	579 543	579 543	489 468	487 466	466 445	466 445
T_S mV	28.8	28.8	27.5	27.5	26.3	26.3	23.3	23.2	22.5	22.5
(SEAL TEMP.) °C	692	692	661	661	633	633	562	560	543	543
E_b (BOMB. VOLTS)	1000	1000	1000	1000	1000	1000	1000	1000	1000	1000
I_b (BOMB. mA)	371	371	344	343	315	315	240	240	227	227
P_b (BOMB. WATTS)	371	371	344	343	315	315	240	240	227	227
E_F (FIL. VOLTS)	4.8	4.8	4.7	4.7	4.6	4.6	4.5	4.5	4.4	4.4
I_F (FIL. AMPS.)	35	35	35	35	34.5	34.5	33.5	33.3	33	33
E_C (COL. HEATER VOLTS)	0	0	0	0	0	0	0	0	0	0
I_C (COL. HEATER AMPS.)	0	0	0	0	0	0	0	0	0	0
E_R (RES. HEATER VOLTS)	1.9	1.9	1.85	1.85	2.0	2.0	2.3	2.3	2.4	2.4
I_R (RES. HEATER AMPS.)	—	—	—	—	—	—	—	—	—	—
VACUUM 10^{-6} mm Hg	3.5	3	2.5	2	2	2	2	2	1.5	1.5
OBSERVER	R.G.									

NOTES:

TABLE 9-5

THERMO ELECTRON

ENGINEERING CORPORATION

SHEET 2

CONVERTER NO. VIII-S-17 RUN NO. DATE 6-15-65

	1	2	3	4	5	6	7	8	9	10
TIME	1540	1550	1610	1630						
T_o (PYROMETER) °C	1715	1715	1715	1715						
T_{ES} (EMITTER) °K										
V_o (OUTPUT VOLTS)	1.4	1.4	.60	.60						
I_o (OUTPUT AMPS.)	6	6	65.5	65.5						
P_o (OUTPUT WATTS)	8.4	8.4	39.3	39.3						
T_R mV	12.3	12.3	15.2	15.2						
(RESERVOIR TEMP.) °C	302	302	372	372						
T_C mV	17.8 18.9	17.6 18.9	28.0 28.3	28.0 28.3						
(COLLECTOR TEMP.) °C	433 459	433 459	673 680	673 680						
T_F mV	18.4 17.6	18.4 17.6	26.8 25.0	26.8 25.0						
(RADIATOR FIN TEMP.) °C	447 428	447 428	644 602	644 602						
T_S mV	21.8	21.8	28.8	28.8						
(SEAL TEMP.) °C	527	527	692	692						
E_b (BOMB. VOLTS)	1000	1000	1000	1000						
I_b (BOMB. mA)	211	211	372	372						
P_b (BOMB. WATTS)	211	211	372	372						
E_F (FIL. VOLTS)	4.4	4.4	4.8	4.8						
I_F (FIL. AMPS.)	33	33	35	35						
E_C (COL. HEATER VOLTS)	0	0	0	0						
I_C (COL. HEATER AMPS.)	0	0	0	0						
E_R (RES. HEATER VOLTS)	2.3	2.3	2.0	1.9						
I_R (RES. HEATER AMPS.)	—	—	—	—						
VACUUM 10^{-6} mm Hg	1.5	1.5	2	2						
OBSERVER	B.G.									

NOTES:

TABLE 9-6

THERMO ELECTRON

ENGINEERING CORPORATION

SHEET 1

CONVERTER NO. VIII - S - 25 RUN NO. DATE 6-25-65

	1	2	3	4	5	6	7	8	9	10
TIME	1400	1410	1420	1430	1440	1450	1520	1530	1600	1610
T_o (PYROMETER) °C	1723	1723	1723	1723	1723	1723	1723	1723	1723	1723
T_{ES} (EMITTER) °K										
V_o (OUTPUT VOLTS)	.60	.60	.70	.70	.80	.80	1.0	1.0	1.2	1.2
I_o (OUTPUT AMPS.)	64	64	51	51	34	34	16	16	11	11
P_o (OUTPUT WATTS)	38.4	38.4	35.7	35.7	27.2	27.2	16	16	13.2	13.2
T_R mV	14.95	14.95	14.35	14.35	13.70	13.7	12.75	12.75	12.75	12.75
(RESERVOIR TEMP.) °C	365	365	351	351	336	336	313	313	313	313
T_C mV	32.6 28.5	32.6 25.5	30.2 26.6	30.2 26.6	27.0 24.2	27.0 24.2	23.0 21.1	23.0 21.1	21.8 20.1	21.8 20.1
(COLLECTOR TEMP.) °C	783 685	783 685	725 640	725 640	649 583	649 583	555 511	555 511	527 487	527 487
T_F mV	26.7 24.7	26.7 24.7	25.2 23.4	25.2 23.4	23.0 21.6	23.0 21.1	20.3 19.2	20.3 19.2	19.4 18.4	19.4 18.4
(RADIATOR FIN TEMP.) °C	642 575	642 575	607 564	607 564	555 522	555 522	492 468	492 468	471 447	471 447
T_S mV	29.0	29.0	27.6	27.6	25.7	25.7	23.4	23.4	22.7	22.7
(SEAL TEMP.) °C	697	697	663	663	618	618	564	564	548	548
E_b (BOMB. VOLTS)	1000	1000	1000	1000	1000	1000	1000	1000	1000	1000
I_b (BOMB. mA)	377	378	349	349	303	303	254	254	240	240
P_b (BOMB. WATTS)	377	378	349	349	303	303	254	254	240	240
E_F (FIL. VOLTS)	4.8	4.8	4.7	4.7	4.6	4.6	4.4	4.4	4.4	4.4
I_F (FIL. AMPS.)	36	36	35.5	35.5	35	35	34.5	34.5	34	34
E_C (COL. HEATER VOLTS)	0	0	0	0	0	0	0	0	0	0
I_C (COL. HEATER AMPS.)	0	0	0	0	0	0	0	0	0	0
E_R (RES. HEATER VOLTS)	1.2	1.15	1.15	1.20	1.6	1.6	1.75	1.75	2.05	2.0
I_R (RES. HEATER AMPS.)	—	—	—	—	—	—	—	—	—	—
VACUUM 10^{-6} mm Hg	5.5	5	4	4	3.5	3	3	3	3	3
OBSERVER	B.G.									

NOTES:

TABLE 9-6

THERMO ELECTRON

ENGINEERING CORPORATION

SHEET 2

CONVERTER NO. VIII-5-25 RUN NO. DATE 6-25-65

	1	2	3	4	5	6	7	8	9	10
TIME	1620	1630	1645	1700						
T_o (PYROMETER) °C	1723	1723	1723	1723						
T_{ES} (EMITTER) °K										
V_o (OUTPUT VOLTS)	1.4	1.4	.60	.60						
I_o (OUTPUT AMPS.)	7	7	64	64						
P_o (OUTPUT WATTS)	9.8	9.8	38.4	38.4						
T_R mV	12.45	12.45	14.95	14.95						
(RESERVOIR TEMP.) °C	305	305	365	365						
T_C mV	20.8 19.4	20.8 19.4	32.6 28.4	32.7 28.5						
(COLLECTOR TEMP.) °C	504 471	504 471	783 682	786 685						
T_F mV	18.7 17.8	18.7 17.7	26.9 24.7	26.7 24.7						
(RADIATOR FIN TEMP.) °C	454 433	454 431	692 595	642 595						
T_S mV	22.1	22.1	28.9	29.0						
(SEAL TEMP.) °C	531	531	694	697						
E_b (BOMB. VOLTS)	1000	1000	1000	1000						
I_b (BOMB. mA)	228	228	380	380						
P_b (BOMB. WATTS)	228	228	380	380						
E_F (FIL. VOLTS)	4.3	4.3	4.7	4.7						
I_F (FIL. AMPS.)	34	34	35.5	35.5						
E_C (COL. HEATER VOLTS)	0	0	0	0						
I_C (COL. HEATER AMPS.)	0	0	0	0						
E_R (RES. HEATER VOLTS)	1.95	2.0	1.2	1.2						
I_R (RES. HEATER AMPS.)	—	—	—	—						
VACUUM 10^{-6} mm Hg	3	3	3	3						
OBSERVER	BG									

NOTES:

TABLE 9-7

THERMO ELECTRON

ENGINEERING CORPORATION

SHEET 1

CONVERTER NO. VIII - S - 26 RUN NO. DATE 6-28-65

	1	2	3	4	5	6	7	8	9	10
TIME	1635	1645	1655	1705	1715	1725	1735	1745	1755	1805
T_o (PYROMETER) °C	1723	1723	1723	1723	1723	1723	1723	1723	1723	1723
T_{ES} (EMITTER) °K										
V_o (OUTPUT VOLTS)	.60	.60	.70	.70	.80	.80	1.0	1.0	1.2	1.2
I_o (OUTPUT AMPS.)	65	65	53	53	38	38	16	16	11.5	11.5
P_o (OUTPUT WATTS)	39	39	37.1	37.1	30.4	30.4	16	16	13.8	13.8
T_R mV	14.85	14.85	14.4	14.45	13.8	13.8	12.9	12.9	12.85	12.8
(RESERVOIR TEMP.) °C	363	363	353	354	338	338	317	317	315	314
T_C mV	337 28.6	33.7 28.6	31.8 26.9	31.4 26.9	28.5 24.8	28.5 24.8	23.5 21.2	23.6 21.3	22.5 20.4	22.5 20.4
(COLLECTOR TEMP.) °C	810 687	810 687	752 647	754 647	685 597	685 597	587 513	589 516	543 494	543 494
T_F mV	26.9 25.2	26.9 25.2	25.4 23.9	25.4 23.9	23.6 22.3	23.6 22.3	20.4 19.5	20.5 19.5	19.8 18.9	19.8 18.9
(RADIATOR FIN TEMP.) °C	647 607	647 607	612 576	612 576	569 539	569 539	494 473	497 473	480 459	480 459
T_S mV	29.2	29.2	27.9	28.0	26.4	26.4	23.8	23.9	23.3	23.3
(SEAL TEMP.) °C	702	702	671	673	635	635	574	576	562	562
E_b (BOMB. VOLTS)	1000	1000	1000	1000	1000	1000	1000	1000	1000	1000
I_b (BOMB. mA)	388	388	359	359	321	321	260	260	248	248
P_b (BOMB. WATTS)	388	388	359	359	321	321	260	260	248	248
E_F (FIL. VOLTS)	4.8	4.8	4.7	4.7	4.6	4.6	4.5	4.5	4.4	4.4
I_F (FIL. AMPS.)	35.5	35.5	35	35	35	35	34	34	34	34
E_C (COL. HEATER VOLTS)	0	0	0	0	0	0	0	0	0	0
I_C (COL. HEATER AMPS.)	0	0	0	0	0	0	0	0	0	0
E_R (RES. HEATER VOLTS)	1.45	1.45	1.6	1.6	1.7	1.7	1.95	2.05	2.1	2.15
I_R (RES. HEATER AMPS.)	—	—	—	—	—	—	—	—	—	—
VACUUM 10^{-6} mm Hg	7	7	6	5.5	4.5	4.5	4.5	4	4	4
OBSERVER	B.G.									

NOTES:

TABLE 9-7

THERMO ELECTRON

ENGINEERING CORPORATION

SHEET 2

CONVERTER NO. VIII-S-26 RUN NO. DATE 6-28-65

	1	2	3	4	5	6	7	8	9	10
TIME	1810	1820	1830	1840						
T_o (PYROMETER) °C	1723	1723	1723	1723						
T_{ES} (EMITTER) °K										
V_o (OUTPUT VOLTS)	1.4	1.4	.60	.60						
I_o (OUTPUT AMPS.)	7	7	64.5	64.5						
P_o (OUTPUT WATTS)	9.8	9.8	38.7	38.7						
T_R mV	12.4	12.4	14.9	14.9						
(RESERVOIR TEMP.) °C	304	304	364	364						
T_C mV	21.3 / 19.7	21.2 / 19.5	33.6 / 28.6	33.6 / 28.6						
(COLLECTOR TEMP.) °C	516 / 473	513 / 473	687	687						
T_F mV	18.9 / 18.1	18.9 / 18.0	26.9 / 25.2	26.9 / 25.2						
(RADIATOR FIN TEMP.) °C	459 / 440	459 / 438	647 / 607	647 / 607						
T_S mV	22.6	22.6	29.2	29.2						
(SEAL TEMP.) °C	546	546	702	702						
E_b (BOMB. VOLTS)	1000	1000	1006	1000						
I_b (BOMB. mA)	231	231	389	389						
P_b (BOMB. WATTS)	231	231	389	389						
E_F (FIL. VOLTS)	44	44	9.8	9.8						
I_F (FIL. AMPS.)	33.5	33.5	35.5	35.5						
E_C (COL. HEATER VOLTS)	0	0	0	0						
I_C (COL. HEATER AMPS.)	0	0	0	0						
E_R (RES. HEATER VOLTS)	2.0	2.05	1.5	1.4						
I_R (RES. HEATER AMPS.)	—	—	—	—						
VACUUM 10^{-6} mm Hg	4	4	4	4						
OBSERVER	B.G.									

NOTES:

the block severely overheated. Furthermore, the converters' collector temperatures balanced close to those found optimum during converter testing. One problem that arose was an inability to optimize the cesium temperature of VIII-S-25 at 1000 watts input and higher. This effect was attributed to the proximity of large current straps which partially shielded that cesium reservoir. Cesium temperatures ran below or only slightly above optimum.

Insertion of the converters and their attachment to the block was greatly facilitated by the new attachment method, using an accurately jigged flange and bolts rather than the older sleeve and crimp method.

The four-filament electron-bombardment gun proved to be very satisfactory for achieving stable and uniform heating of the converters. After solar testing of JG-3, a useful experiment would be to reduce the clearance between converters to that shown in Chapter 6 and which was used in the first assembly. As can be seen in Figure 9.5, that assembly produced over 90 watts with only 1000 watts input. As shown in Chapter 7, losses through the openings between diodes are a strong function of the clearance and are of significant magnitude.